1986

The reactions of nitric oxide and nitrite with hemerythrin

Judith Mary Nocek
Iowa State University

INFORMATION TO USERS

This reproduction was made from a copy of a manuscript sent to us for publication and microfilming. While the most advanced technology has been used to photograph and reproduce this manuscript, the quality of the reproduction is heavily dependent upon the quality of the material submitted. Pages in any manuscript may have indistinct print. In all cases the best available copy has been filmed.

The following explanation of techniques is provided to help clarify notations which may appear on this reproduction.

1. Manuscripts may not always be complete. When it is not possible to obtain missing pages, a note appears to indicate this.

2. When copyrighted materials are removed from the manuscript, a note appears to indicate this.

3. Oversize materials (maps, drawings, and charts) are photographed by sectioning the original, beginning at the upper left hand corner and continuing from left to right in equal sections with small overlaps. Each oversize page is also filmed as one exposure and is available, for an additional charge, as a standard 35mm slide or in black and white paper format.*

4. Most photographs reproduce acceptably on positive microfilm or microfiche but lack clarity on xerographic copies made from the microfilm. For an additional charge, all photographs are available in black and white standard 35mm slide format.*

*For more information about black and white slides or enlarged paper reproductions, please contact the Dissertations Customer Services Department.

Nocek, Judith Mary

THE REACTIONS OF NITRIC OXIDE AND NITRITE WITH HEMERYTHRIN

Iowa State University PH.D. 1986

The reactions of nitric oxide and nitrite with hemerythrin

by

Judith Mary Nocek

A Dissertation Submitted to the

Graduate Faculty in Partial Fulfillment of the

Requirements for the Degree of

DOCTOR OF PHILOSOPHY

Department: Chemistry
Major: Inorganic Chemistry

Approved:

Signature was redacted for privacy.

In Charge of Major Work

Signature was redacted for privacy.

For the Major Department

Signature was redacted for privacy.

For the Graduate College

Iowa State University
Ames, Iowa

1986

TABLE OF CONTENTS

LIST OF FIGURES

LIST OF TABLES

LIST OF SYMBOLS AND ABBREVIATIONS

Asp	aspartic acid
bpy	bipyridyl
Bpz_3	pyrazolylborate
CD	circular dichroism
CPO I	chloroperoxidase compound I
DAS	dimethylarsine
dmgH	dimethylglyoxime
DMDTC	dimethyldithiocarbamate
EDTA	ethylenediamminetetraacetate
en	ethylenediamnine
EPR	electron paramagnetic resonance
EXAFS	extended X-ray absorption fine structure
Glu	glutamic acid
Hb	hemoglobin
His	histidine
Hr	hemerythrin
LMCT	ligand-to-metal charge transfer
Mb	myoglobin
MCD	magneto-circular dichroism
Mes	2(N-morpholino)ethanesulfonic acid
NLLSQ	nonlinear least squares
NMR	nuclear magnetic resonance
$P_{1/2}$	half-saturation power in mW
phen	o-phenanthroline

PMO	putidamonooxin
salen	N,N'-ethylenebis(salicylideneimine)
TMC	1,4,8,11-tetramethyl-1,4,8,11-tetrazacyclotetradecane
TMP	(3,4,7,8-tetramethylphenanthroline
Tris	tris-hydroxymethylaminomethane
ϵ	extinction coefficient in $M^{-1}cm^{-1}$

I. INTRODUCTION

A. Statement of the Problem

Nearly all forms of animal life have devised a system for concentrating oxygen from the environment and transporting and/or storing it within the organism. These oxygen-carriers are metalloproteins. Some small invertebrates, namely sipunculids and one species of annelid utilize the binuclear, nonheme iron protein, hemerythrin (Hr), to perform these functions.

Uptake of oxygen by Hr (1) is a reversible process and has been described as an oxidative addition reaction wherein the binuclear iron site undergoes a two-electron oxidation with concomitant reduction of O_2 to peroxide (reaction 1.1).

$$\underset{\text{deoxyHr}}{[\text{Fe(II)},\text{Fe(II)}]} + O_2 \rightleftarrows \underset{\text{oxyHr}}{[\text{Fe(III)},\text{Fe(III)}O_2^{2-}]} \qquad (1.1)$$

In its burgundy, oxygenated form this protein is referred to as oxyHr, while the colorless, reduced, deoxygenated state is called deoxyHr.

Physical studies and x-ray crystallography indicate that oxygen coordinates end-on to only one iron (2,3). Therefore, it seems reasonable that when oxygenation occurs, electrons are released sequentially from the iron atoms. Such a mechanism should proceed through a one-electron oxidized species having oxygen bound formally as superoxide, i.e., $[\text{Fe(II)},\text{Fe(III)}O_2^{-}]$. The inability to detect this intermediate apparently stems from the stability of the metal-peroxide complex,

oxyHr, relative to this proposed metal-superoxide derivative and indicates that rapid transfer of the second electron to bound oxygen occurs. On the other hand, iron-nitrosyl complexes having nitric oxide (NO) formally reduced by one electron are known while complexes having a $M\text{-}NO^{2-}$ unit are not likely to be stable entities. Thus, intramolecular transfer of a second electron to NO should not occur, making the product of the reaction between deoxyHr and NO an analog for the hypothesized superoxide intermediate (reaction 1.2).

$$[Fe(II),Fe(II)] + NO \rightleftharpoons [Fe(II),Fe(III)NO^{-}] \nrightarrow [Fe(III),Fe(III)NO^{2-}] \quad (1.2)$$

deoxyNO

Spectroscopic (4,5) as well as structural studies, show that the high-spin Fe(III) atoms in oxyHr are antiferromagnetically coupled leading to a diamagnetic ($S_{eff}=0$) ground state. Whether or not this coupling is maintained upon deoxygenation has not been clearly established, although current thinking favors weak coupling of the high-spin ferrous atoms mediated by a hydroxo bridge (6,7).

Unlike oxygen (a diradical), nitric oxide furnishes a single unpaired electron and upon binding to iron can, thereby, convert an even-electron EPR-silent species into an odd-electron, EPR-observable one. Furthermore, occurrence of electron spin coupling within the binuclear iron site of Hr is expected to affect the ground spin state and/or the orbital angular momentum. As a result, different EPR signals should be observed when NO binds to a spin coupled metal site and when it binds to

an uncoupled site. Thus, a second reason for investigating the reaction between deoxyHr and nitric oxide is to determine whether or not antiferromagnetic coupling is maintained within the binuclear site of deoxyHr.

A second reaction of Hr that occurs intracellularly is the spontaneous conversion of oxyHr to the oxidized derivative, metHr, which no longer binds oxygen (reaction 1.3).

$$\underset{\text{(oxyHr)}}{[Fe(III),Fe(III)O_2^{2-}]} + 2H^+ \rightarrow \underset{\text{(metHr)}}{[Fe(III),Fe(III)]} + H_2O_2 \quad (1.3)$$

This auto-oxidation has a half-time of 18.5 hours at neutral pH in 0.3 M Cl^- and is accelerated by the addition of small anions, including nitrite (7). For most anions, uniphasic kinetics have been reported. However, for azide and cyanate auto-oxiation is biphasic. The first phase, in which the oxyHr color is rapidly bleached, is followed by a slower phase in which the binuclear site is oxidized to metHr. Two possible mechanisms that have been proposed for auto-oxidation of Hr are shown in Scheme 1.1.

Scheme 1.1A: $\quad oxy + L^- \rightarrow metL^- + O_2^{2-}$

Scheme 1.1B:
$$oxy \rightleftarrows deoxy + O_2$$
$$deoxy + L^- \rightleftarrows deoxyL^-$$
$$deoxyL^- + O_2 \rightarrow metL^- + O_2^{2-}$$

The discovery that a mixed-valence intermediate, semi-metHr, was produced during the chemical oxidation of either deoxyHr or oxyHr to metHr with ferricyanide suggests a means for differentiating these proposed mechanisms for auto-oxidation. A mixed-valence intermediate should not be produced if auto-oxidation occurs by direct displacement of peroxide (Scheme 1.1A). On the other hand, if deoxyHr is involved in auto-oxidation (Scheme 1.1B), a mixed-valence intermediate might be detected. For this reason, the reaction of sodium nitrite with deoxyHr was investigated.

In addition, most chemical oxidants of Hr (e.g., ferricyanide) do not react directly at the iron site. Nitrite, because of its smaller size, might provide a contrast to these "outer sphere" oxidations. Indeed, the oxidation of hemoglobin (Hb) by nitrite was reported to occur by an "inner sphere" pathway (8).

Finally, the mixed-valence [Fe(II),Fe(III)] intermediate prepared by oxidation of deoxyHr, $(semi\text{-}met)_O$, exhibits an EPR signal that is different from that of $(semi\text{-}met)_R$, the intermediate that is formed during the reduction of metHr (9). One interpretation of the difference between $(semi\text{-}met)_O$ and $(semi\text{-}met)_R$ is reversal of the iron oxidation states. The x-ray crystal structure of metHr shows that the iron site contains one six-coordinate and one five-coordinate iron. A vacant coordination site, therefore, exists for only one of the two iron atoms. Based on the observation that azide binds to both metHr and semi-metHr, there is probably also one five-coordinate and one six-coordinate iron in semi-metHr.

Since NO reacts more readily with Fe(II) than with Fe(III), reactions of NO with $(semi\text{-}met)_O$ and $(semi\text{-}met)_R$ might determine which, if either, of the semi-metHrs has this vacant coordination site on Fe(II).

Furthermore, stable binuclear compounds having both iron atoms in a pseudo-octahedral environment are relatively rare. This structure has been suggested for the iron sites of several other proteins, namely ribonucleotide reductase (10), methane monooxygenase (11), and the purple acid phosphatases (12-17). The chemistry of the relatively well-characterized site of Hr may provide information about the functioning of such a binuclear site in these less well-characterized proteins.

Thus, studies of the reactions of nitric oxide and nitrite with Hr in its various oxidation states were undertaken with the intention of addressing four problems:

(i) The preparation and characterization of an analog for the putative superoxide intermediate of oxygenation of Hr.

(ii) The magnetic coupling (or lack thereof) between the iron atoms in deoxyHr.

(iii) The mechanism for the auto-oxidation of oxyHr.

(iv) The differences between $(semi\text{-}met)_O$ and $(semi\text{-}met)_R$.

B. Review of Previous Studies on Hemerythrin

1. Molecular properties

The first report of the occurrence of Hr in invertebrates came in 1823 from S. D. Chiaie (18) who was working with the species Sipunculus nudus. Since then, Hr has been isolated from four animal phyla distributed through all parts of the world: Annelida, Sipuncula, Priapula, and Brachiopoda. The majority of the work reported herein involves Hr from the sipunculid, Phascolopsis gouldii, obtained off the coast of Eastern North America. The more common varieties reside near intertidal shores in the substratum, which is usually an oxygen-deficient environment. Some species have been found in the ocean at depths of nearly 7000 m. Average individuals are 3-15 cm long and have a life span of almost 25 years (19).

Hemerythrin is contained within erythrocytes, either nucleated or enucleated (20). It is the major component of these blood cells, present at intracellular concentrations of ~10 mM in dimeric iron. As Fig. 1.1 shows, there are up to three cellular sources of Hr within sipunculan worms: the main body cavity (coelomic Hr), the vascular network, and muscle cells. The only species from which all three forms have been isolated is Themiste zostericola, whereas, for Phascolopsis gouldii, only coelomic Hr has been isolated.

In 1873, fifty years after its discovery, Lankester classified Hr as a respiratory pigment (21). In 1890, Andrews reported the presence of iron in Hr (22) and in 1892, Griffiths showed that despite the implications of its name, the iron in Hr is not coordinated to the

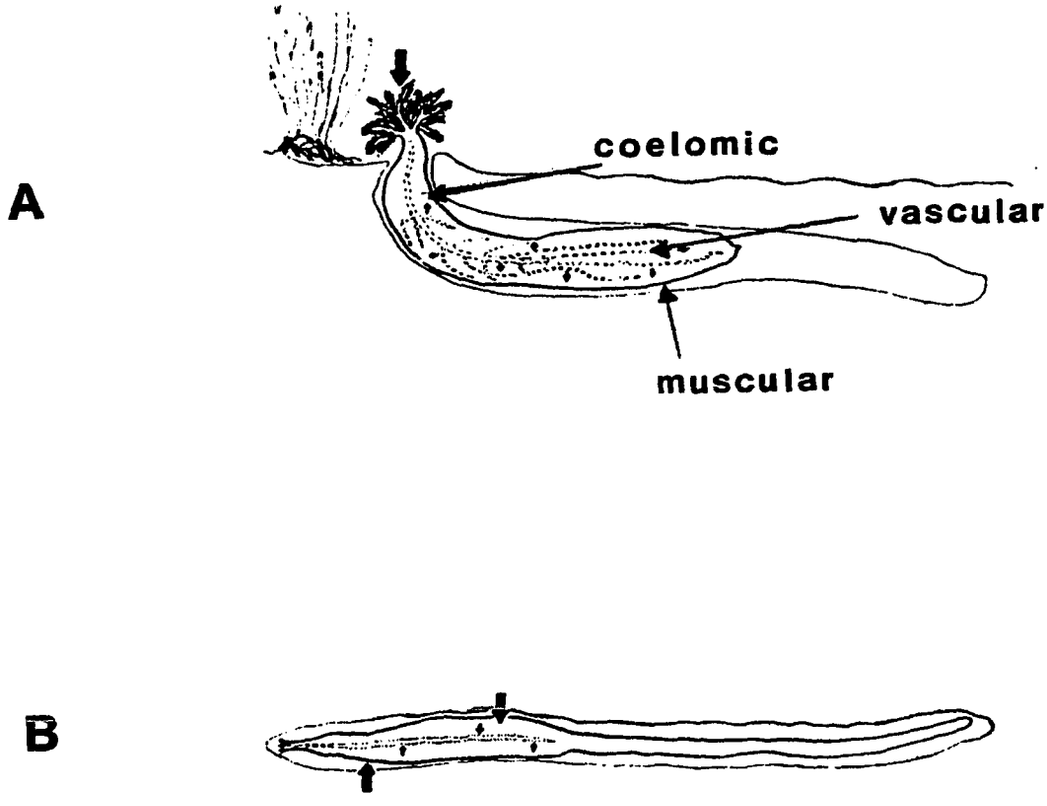

Figure 1.1. Respiratory diagrams for hemerythrin from Themiste zostericola (A) and Siphonosoma ingens (B) (20)

globin unit through a heme prosthetic group (23). Research in this century, prior to solution of the x-ray crystal structure in the late 1970s, focused on three questions:

1. What is the aggregation state of Hr?
2. What is the nature of the Fe-O_2 interaction?
3. Which amino acids ligate the iron to the protein backbone?

To answer the first question, an accurate molecular weight determination was needed. Measurements combining results of sedimentation studies (24) with diffusion coefficient data (25) lead to estimates near 100,000 D. Based on a variety of hydrodynamic measurements, an average value of 107,000 D was reported for the molecular weight of Hr from Phascolopsis gouldii (26). The accepted values for the known octameric Hrs are all between 100 and 120 kD (27).

The oligomeric nature of Hr was first identified by Klotz and Keresztes-Nagy (28). The chemical modification of lysyl residues caused Hr to dissociate into eight smaller units of apparently identical weight and composition. This monomeric form, referred to as meroHr, can also be prepared by chemical modification of cysteinyl (29), carboxylato (30), or tyrosyl residues (31), or by dilution of oxyHr samples to concentrations below ~5 μM (32).

A naturally occurring monomeric form of Hr, referred to as myoHr, was discovered in the retractor muscles of Themiste zostericola by Klippenstein et al. (33). Dimeric (27), trimeric (34), tetrameric (27), and hexameric (35) oligomers have also been reported. All of these oligomers appear to be built up from monomeric units having molecular

weights in the range of 12,500 D to 15,000 D, differing mainly in the relative arrangement of the protomers.

The occurrence of oligomeric forms of Hr suggests that allosteric factors may be of importance in Hr. However, cooperativity in oxygen-binding has been reported for octameric Hrs from only two species of brachiopod (36,37), and no physiologically observed compounds have been reported to affect the binding of oxygen. That is, except for the two brachiopod species, there is essentially no cooperativity in oxygen-binding.

Studies leading to an understanding of the Fe-O_2 interaction began by addressing the question of the stoichiometry of the oxygenation reaction. Using colorimetric analyses in which o-phenanthroline was chelated to the iron liberated by dilute acid treatment, the ratio of bound O_2 to Fe in oxyHr was found to be 1 O_2/2 Fe (38). Klotz and Klotz (1) first suggested that oxygenation involves transfer of two electrons, one from each Fe(II) atom, to O_2 such that oxyHr formally contains 2 Fe(III) atoms per bound peroxide ion.

Prior to x-ray crystallography, identification of the ligands through which the iron atoms are fastened to the protein backbone was approached by two method:

(i) Comparison of the primary structures of Hrs from several species in search of sequence homologies.

(ii) Chemical modification studies.

Octameric Hr from Phascolopsis gouldii was the first to have its amino acid sequence solved (39). Each subunit contains 113 amino acid

residues arranged in a single chain (Fig. 1.2). The molecular weight calculated from this sequence is in good agreement with the subunit molecular weights determined by other methods. Coelomic Hr from Themiste dyscritum also has 113 amino acid residues per subunit (40), whereas myoHr from Themiste zostericola has five additional residues (41). Comparison of the amino acid sequence for Hr from Phascolopsis gouldii with the sequences for Hr from Themiste dyscritum (40) and myoHr from Themiste zostericola (41) shows sequence homology percentages of 79% and 42%, respectively. Since all three forms of Hr bind 2 Fe atoms/subunit and have similar physical and chemical properties, the amino acids that are ligated to the iron are likely to be common to all three species.

Results of chemical modification studies (42) eliminated cysteine, lysine, and methionine, and implicated histidines and tyrosines as the primary candidates for iron ligands. Comparison of the electronic spectra of oxyHr and several ligand adducts of metHr with binuclear iron compounds strongly suggested that a μ-oxo bridge links the iron atoms (43), implying that the two iron atoms are close to each other within a subunit.

Thus, when the first attempts at solving the x-ray crystal structure of Hr were begun, the number, identity and geometric arrangement of the iron ligands were still uncertain. One oxygen molecule was believed to coordinate to a pair of iron atoms, the oxygen being bound as a peroxide ion and the iron atoms being formally trivalent. In addition, a

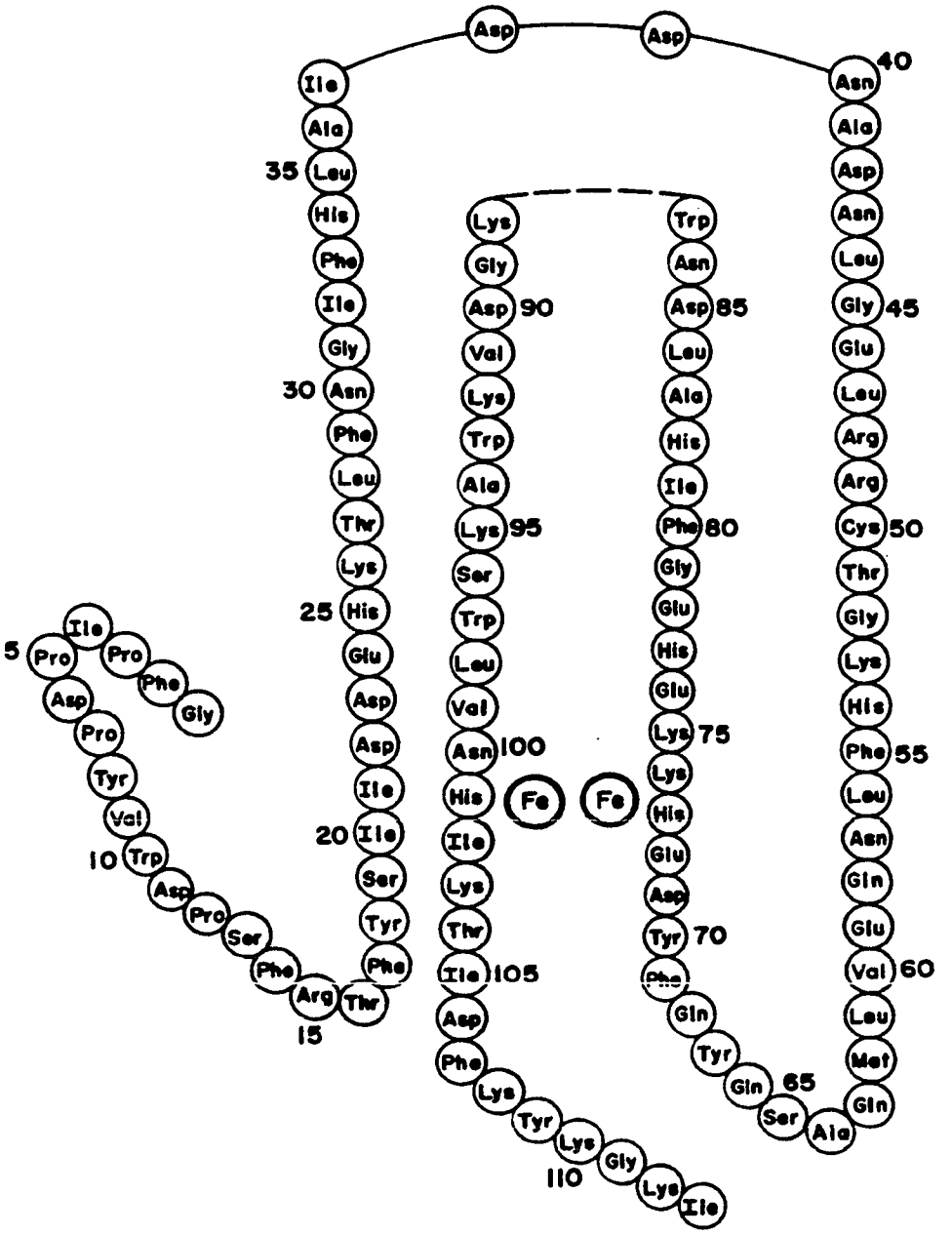

Figure 1.2. Primary structure of hemerythrin from Phascolopsis gouldii (44)

variety of oligomeric arrangements of subunits were known to be possible.

The majority of the crystallographic data on Hr has been compiled for two species: the structure of the octameric Hr from Themiste dyscritum has been resolved to 2.0 Å resolution by Jensen's research group (45) and the structure of myoHr from retractor muscles of Themiste zostericola has been solved to 2.5 Å resolution by the Hendrickson group (46). Less well-refined structures have recently been reported for dimeric Hr from Phascolosoma arcuatum (47) and trimeric Hr from Siphonosoma funafuti (48,49).

With octameric Hr from Phascolopsis gouldii, crystal studies are complicated by the occurrence of molecular variants; differences in primary structure at residues 63 (Glu for Gln), 78 (Asp for Glu), 79 (Gly for Thr), 82 (Asn for His), and 96 (Ala for Ser) occur randomly within the worm population. The 5.5 Å resolution structure (50,51) that has been obtained for variant B from Phascolopsis gouldii is quite similar to that of octameric Hr from Themiste dyscritum.

X-ray crystallography for Hr from Themiste dyscritum (52) verified the amino acid sequence previously determined from sequencing studies (39,53). The structure of octameric Hr from Themiste dyscritum and myoHr from Themiste zostericola show that 70-75% of the amino acid residues are contained in four α-helical segments (Figs. 1.2 and 1.3). Of the remaining amino acids, ~20 are found in the N-terminal peptide, ~10 form a short C-terminal stub, and the rest are involved in connections

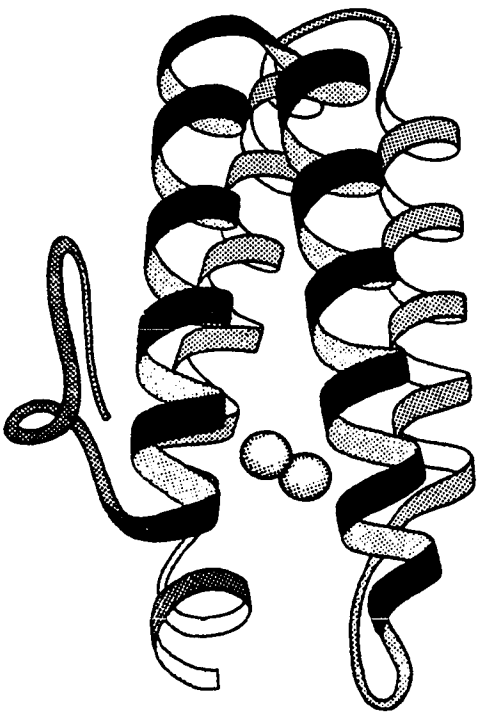

Figure 1.3. Molecular model of the tertiary structure for hemerythrin (46)

between the α-helices. That is, the most prominent feature of the secondary structure is the four helical strands.

Figure 1.3 describes the tertiary structure of Hr. Each subunit approximates an ellipse of dimensions 20 A x 40 A (Fig. 1.4). The four helices run nearly parallel to each other, forming a left-twisted bundle. A pseudo-two-fold axis of symmetry relates helix pairs AB and CD (54).

The Fe-Fe axis lies roughly perpendicular to the four helical axes and the coordination site at which O_2 and other small anions bind is exposed to the center of the subunit. It has been proposed by Stenkamp et al. (55) that access of O_2 to the iron center could occur either via a much smaller tunnel that lies parallel to helices A and B (Fig. 1.4) or through a gap between His-101 and Trp-97 which protrude from the D helix (3). The distances traversed between the surface and the O_2-binding site are 15 A and 10 A, respectively, for the two paths (3).

The quaternary structure of the octamer (Figs. 1.4 and 1.5) has been described as a square doughnut (51,56). Two layers, each containing four subunits, are set back-to-back, forming a square antiprism. Overall, the octamer has dimensions of 75 x 75 x 40 A^3. Within a layer, subunits align in a head-to-tail fashion and are arranged around a central channel ~20 A in diameter, that widens to ~30 A in the core of the doughnut. This cavity is lined by residues from helix B, the majority of which are hydrophobic.

Binding of ClO_4^- induces changes at the active site (see section I.B.3) (57,58). Difference maps reveal two different binding sites for

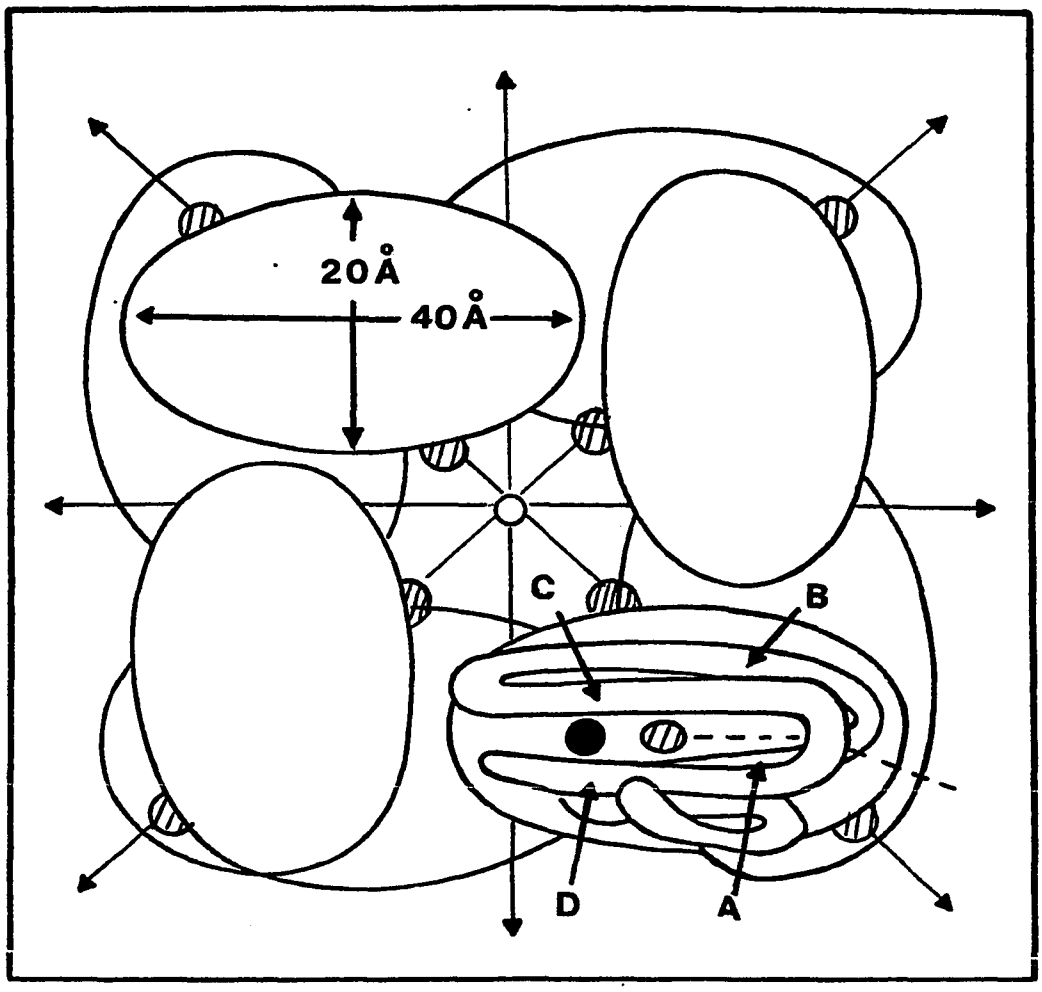

Figure 1.4. Schematic representation of the quaternary structure for hemerythrin from Phascolopsis gouldii (55)

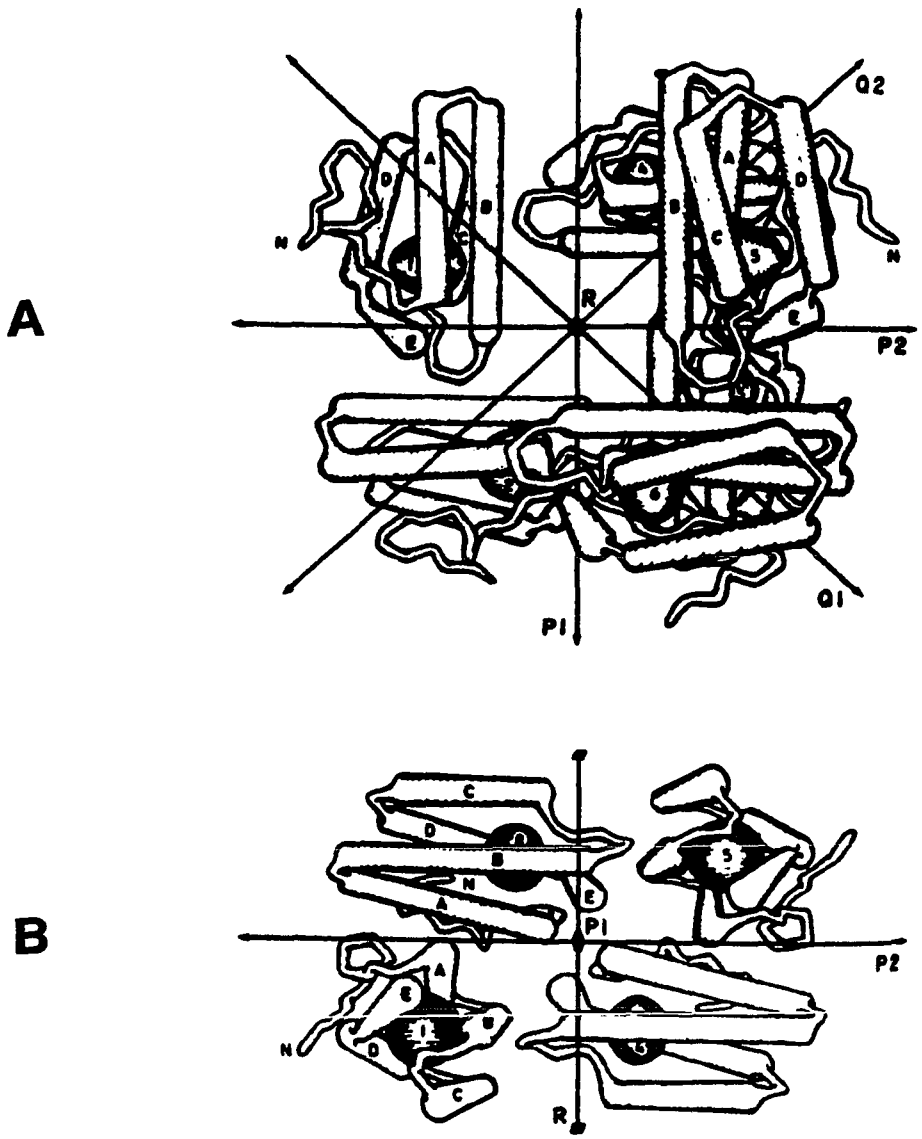

Figure 1.5. Quaternary structure of hemerythrin from Phascolopsis gouldii (41)

ClO_4^- on the surface of the protein, roughly 12 A and 15 A from the Fe center. Both sites lie along the pseudo-two-fold axes that point through the corners of the octamer (Fig. 1.4) (55). The first site is on the outer surface, the ClO_4^- being attached via hydrogen bonds to the peptide amide groups of Asp-30. The second site is on the inner channel and apparently involves electrostatic interactions with Lys residues of adjacent subunits.

Most significantly, crystallographic studies have produced a precise picture of the active site (59). The currently accepted structures for the iron sites of metHr and the azide adduct of metHr ($metN_3^-$) are shown in Fig. 1.6. Azide binds in an end-on fashion to the iron atom that was originally five-coordinate. Shared between the irons are an oxo group, and carboxylate groups from Glu-58 and Asp-106. Histidine residues 25 and 54 complete the coordination sphere around the five-coordinate iron atom, while three histidines (residues 73, 77, and 101) ligate to the second Fe atom, making it six-coordinate. With azide bound, the ligands are arranged in a confacial bioctahedron (Fig. 1.6) with all N-bound ligands situated <u>trans</u> to O-bound ligands. Overall, pseudo C_{2v} site symmetry result.

The distance between the iron atoms (Table 1.1) is too large for metal-metal bonding to occur. While the binding of N_3^- has little effect on the six-coordinate Fe, the carboxylate bonds to the originally five-coordinate Fe are weakened and His-25 shifts its position to accommodate the sixth ligand.

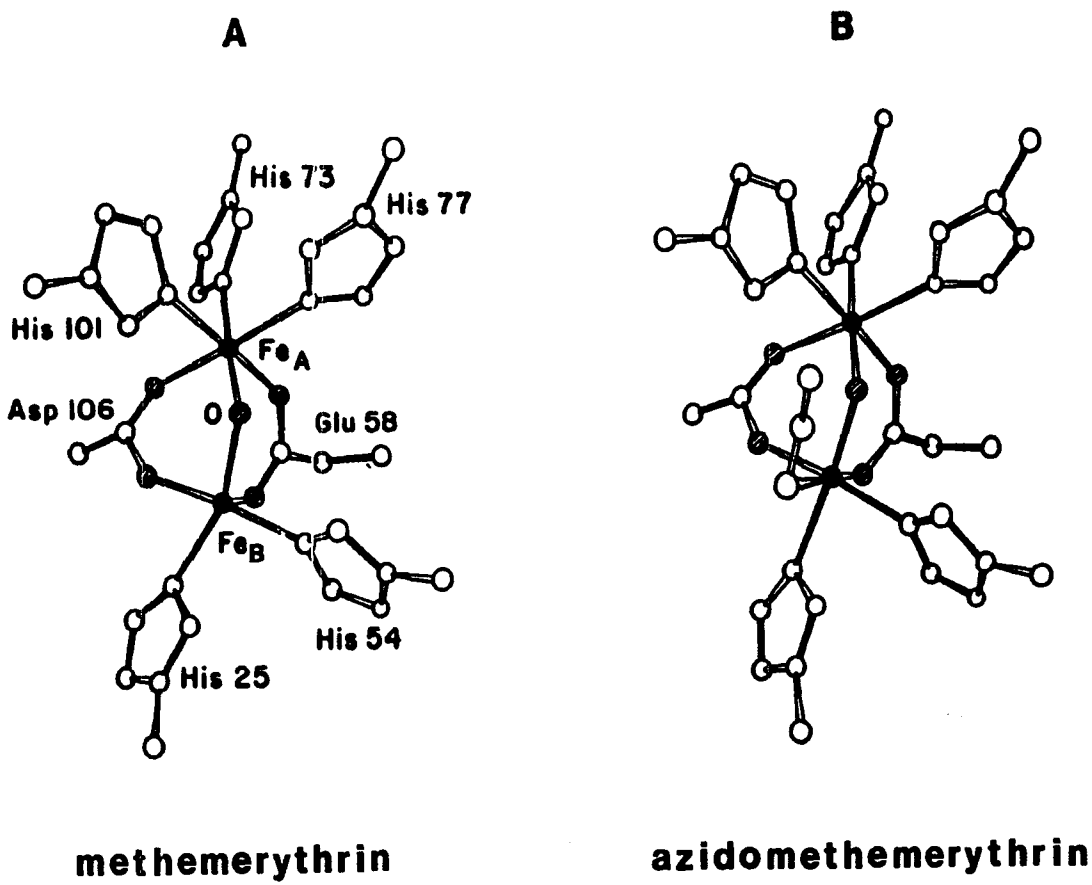

Figure 1.6. Active site structures at 2.0 A resolution for metHr (A) and metN_3^- (B) from Themiste dyscritum (45)

Table 1.1. Bond distances and angles derived from x-ray crystallographic data for derivatives of Hr[a]

	$metN_3$-b,c	met[c]	$metmyoN_3$-b
	Å	Å	Å
Fe_a-O_{oxo}	1.89	1.92	1.80
Fe_b-O_{oxo}	1.64	1.68	1.77
Fe_a--Fe_b	3.25		3.26
Fe_a-O_{Asp}	2.16	2.03	2.12
Fe_b-O_{Asp}	2.20	2.10	2.09
Fe_b-O_{Glu}	2.33	2.04	2.22
Fe_b-$N_{His\ 25}$	2.22	2.15	2.15
Fe_b-$N_{His\ 54}$	2.25	2.19	2.08
Fe_b-N_3	2.34	--	2.01
	deg.	deg.	deg.
Fe_a-O_{oxo}-Fe_b	135	127	132
O_{oxo}-Fe_b-$N_{His\ 25}$	172	143	
O_{oxo}-Fe_b-$N_{His\ 54}$	101	101	
O_{Asp}-Fe_b-$N_{His\ 54}$	154	163	
$N_{His\ 54}$-Fe_b-$N_{His\ 25}$	85	89	
Fe-N-N_2	111	--	
N_3 -Fe-O_{oxo}	93	--	

[a] Fe_a is 6-coordinate; Fe_b is the O_2 (or azide) binding site.

[b] Reference 60.

[c] Reference 45.

Table 1.1 summarizes the bond lengths and angles derived from the crystallographic data (45,60). The corresponding angles and distances for the synthetic models of Armstrong and Lippard (60,61), Wieghardt et al. (62), and Chaudhuri et al. (63) are presented in Table 1.2 and these structures are shown in Fig. 1.7. Compounds with μ-hydroxo bridges have Fe-OH bonds between 1.9 Å and 2.0 Å (64), whereas for μ-oxo bridged compounds the Fe-O bonds are significantly shorter (1.76 Å to 1.82 Å) (64). For the Hr models, the Fe-Fe distance is larger for the μ-hydroxo bridged compounds than for the oxo-bridged compounds. The Fe-O-Fe angle for the compound which has the two ferric ions bridged by an oxo atom is similar to that for the compound having the ferric ions bridged by a hydroxo group. However, the Fe-O-Fe angle is less when hydroxide bridges two ferrous ions than when it bridges two ferric ions.

Weaker van der Waals and hydrogen-bonding interactions near the active site may modulate the functioning of Hr (65). In particular, Tyr-109, once thought to be a ligand to the metal, engages in hydrogen-bonds to the bridging Glu-58 and is in van der Waals contact with His-73 (Fig. 1.8A). His-73 is also stabilized by van der Waals interactions with Met-62 and Ile-105. Hydrogen-bonding with Gln-59 and van der Waals contact with Phe-55 lock His-77 in place. Stacking arrangements of His-101 with the rings of Trp-97, Phe-80, and Tyr-93 form a hydrophobic lining along the hypothesized O_2 tunnel. Both of the histidines of the five-coordinate Fe are involved in hydrogen-bonding networks; His-54 is hydrogen-bonded to Glu-24 and His-25 is hydrogen-bonded, through solvent interactions, to Trp-10, Phe-14, and Asp-22 (Fig. 1.8B). Thus, of the

Table 1.2. Bond angles and distances for the synthetic model compounds of the Hr active site

	$(Fe^{3+})_2(O)$[a]	$(Fe^{3+})_2(OH)$[b]	$(Fe^{3+})_2(O)$[c]	$(Fe^{2+})_2(OH)$[d]
	Å	Å	Å	Å
$Fe\text{-}O_{oxo}$	1.783(2) 1.787(2)	1.960(4) 1.952(4)	1.80 1.77	1.987(8)
$Fe_a\text{--}Fe_b$	3.145(1)	3.439(1)	3.064(5)	3.32(1)
Fe-OAc	2.042(2) 2.042(2) 2.049(3)	1.999	2.03 2.00 2.05	2.142(9)
$Fe_a\text{-}N_{trans}$	2.177(3)	2.102	2.21	2.31(1)
$Fe_a\text{-}N_{cis}$	2.149(3)		2.16	2.257(10) 2.31(1)
	deg.	deg.	deg.	deg.
$Fe_a\text{-}O\text{-}Fe_b$	123.5(1)	123.1(2)	118.3(5)	113.2(2)

[a]Reference 60; $[(HBpz_3)FeO(CH_3CO_2)_2Fe(HBpz_3)]$.

[b]Reference 61; $[(HBpz_3)FeO(CH_3CO_2)_2Fe(HBpz_3)](ClO_4)\cdot CH_2Cl_2$.

[c]Reference 62; $[(tacn)_2Fe_2O(CH_3CO_2)_2]I_2\cdot 0.5\ NaI.3\ H_2O$.

[d]Reference 63.; $[(tacn)_2Fe_2(OH)(CH_3CO_2)_2](ClO_4)\cdot H_2O$.

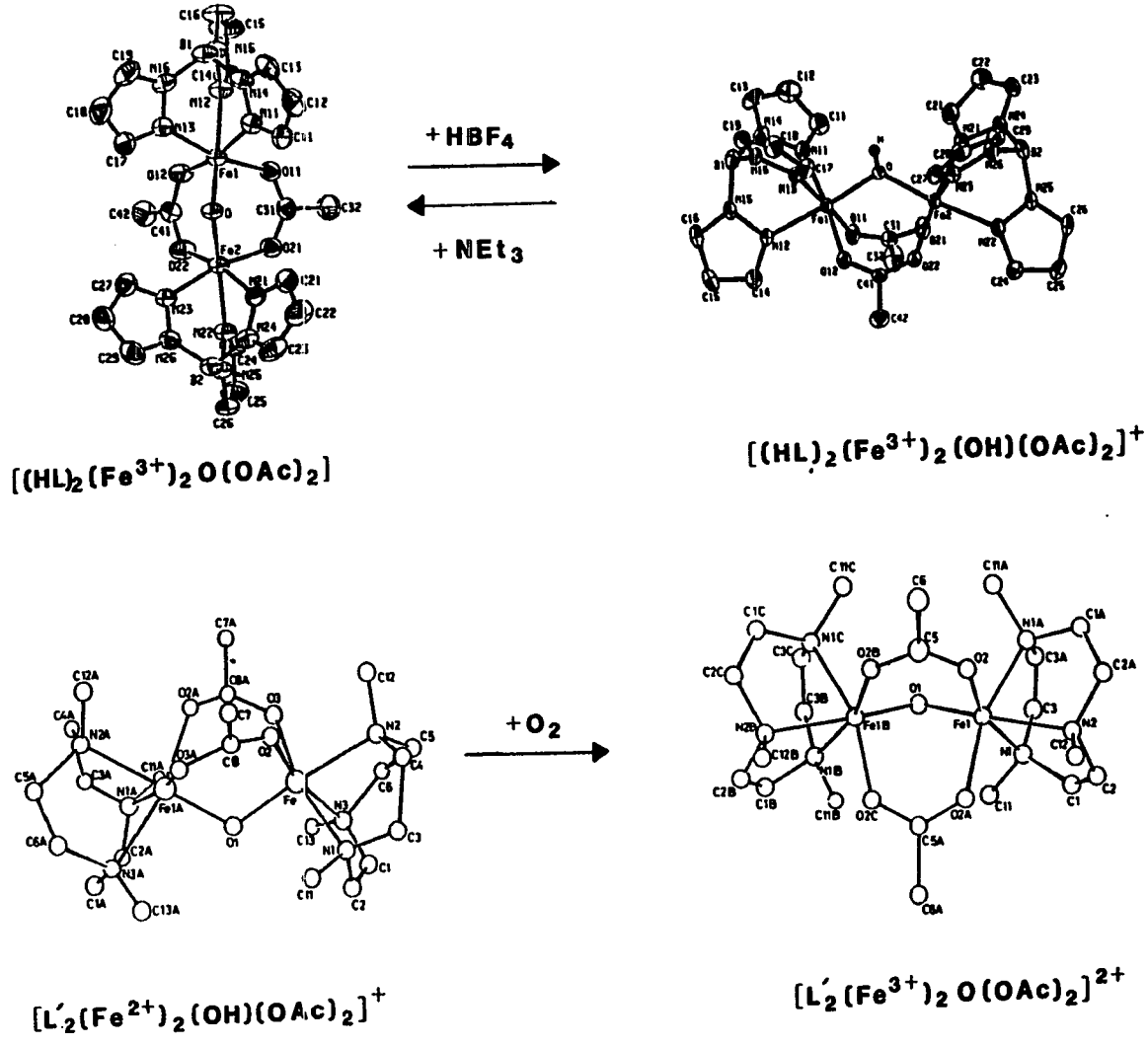

Figure 1.7. Structures of synthetic model compounds for hemerythrin

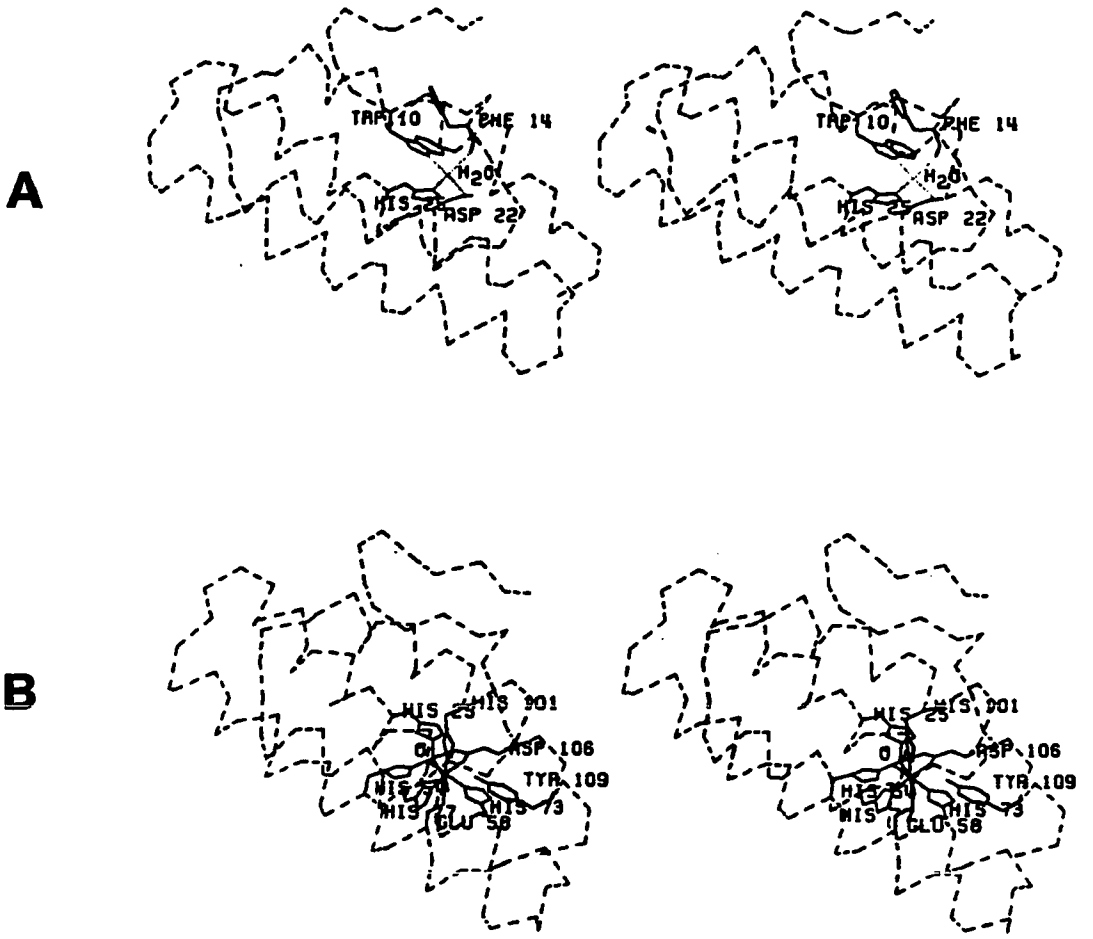

Figure 1.8. Stereodiagrams showing the vicinity of the active site and the locations of H_2O 149 (A) and Tyr 109 (B) (65)

ligands bound to iron, only Asp-106 and the oxo-bridge are free from noncovalent interactions with neighboring residues.

Values for the Fe-Fe separation and the Fe-O-Fe angle have also been determined from extended x-ray absorption fine structure (EXAFS) studies with Phascolopsis gouldii (Table 1.3). From these studies, the average $Fe\text{-}O_{oxo}$ distance for $metN_3^-$ was calculated to be 1.71-1.76 Å (64). This value is within the range observed for oxo-bridged compounds (Table 1.2). The large uncertainties in the distance and angles calculated from the EXAFS data account for the discrepancy between the x-ray crystallographic data and the EXAFS data.

Experimental fits to the EXAFS data, however, agree well with the ligand coordination determined by x-ray crystallography. For oxyHr from Phascolopsis gouldii, EXAFS studies (66) show that the azide ligand has been replaced by the peroxide ion while all the remaining ligands are identical to those of $metN_3^-$.

EXAFS data accumulated at 80 K for deoxyHr indicate an Fe-Fe distance of 3.13 Å (67). At room temperature, the peak arising from Fe-Fe scattering is absent. This was postulated to result from increased thermal motion of the two iron atoms in deoxyHr relative to that in either oxyHr or $metN_3^-$. One interpretation of this result suggests that the bond between iron and the μ-oxo bridge is ruptured.

Subsequent to the EXAFS studies, an electron density difference map between deoxyHr and metHr was obtained for Themiste dyscritum at 3.9 Å resolution (3). This difference map for deoxyHr shows that the same ligands coordinate to the metals in both deoxyHr and metHr. In contrast

Table 1.3. EXAFS data for derivatives of Hr from Phascolopsis gouldii

Derivative	d(Fe-Fe) (Å)	L(Fe-O-Fe) (deg.)	Reference
$metN_3^-$	3.38	165	64
	3.49 ± 0.08	152 (+28/-13)	66
oxy	3.57 ± 0.08	155 (+25/-13)	66
$metOH^-$	3.54 ± 0.08	153 (+27/-13)	66
deoxy	3.13		67

to the EXAFS studies, there is no evidence suggesting that the Fe-O_{oxo} bonds are ruptured upon reduction to deoxyHr. Based on the difference map for deoxyHr, the major structural difference between deoxyHr and metHr is that the Fe-Fe separation is larger for deoxyHr than for metHr. This result is also consistent with the trends observed with model compounds (Table 1.2).

The difference map between oxyHr and metHr (3), obtained at 2.2 Å resolution, shows that oxygen binds at the same site occupied by azide in $metN_3^-$. The peroxide ligand is drawn closer to the Fe-Fe axis than is the azide ligand of $metN_3^-$ and the binding of oxygen alters the electron density associated with the oxo bridge. Based on these results, it was proposed that the ferrous ions of deoxyHr are linked by a hydroxo bridge rather than by an oxo bridge (3). When oxygen binds to deoxyHr, the proton from the hydroxo bridge shifts onto the peroxo anion, leaving a μ-oxo bridge between the ferric ions (Fig. 1.9).

2. Physical properties

Evidence from optical, Mossbauer, electron paramagnetic resonance (EPR), resonance Raman, magnetic susceptibility, nuclear magnetic resonance (NMR), circular dichroism (CD), and magneto-circular dichroism (MCD) studies complements the crystallographic data.

a. Electronic absorption spectra Nearly a full spectrum of colors is observed for the various derivatives of Hr; a semblance of order can be attained by comparing the optical spectra on the basis of oxidation state. As is true for most proteins, the absorbances at wavelengths shorter than 300 nm are dominated by $\pi \rightarrow \pi^*$ transitions arising

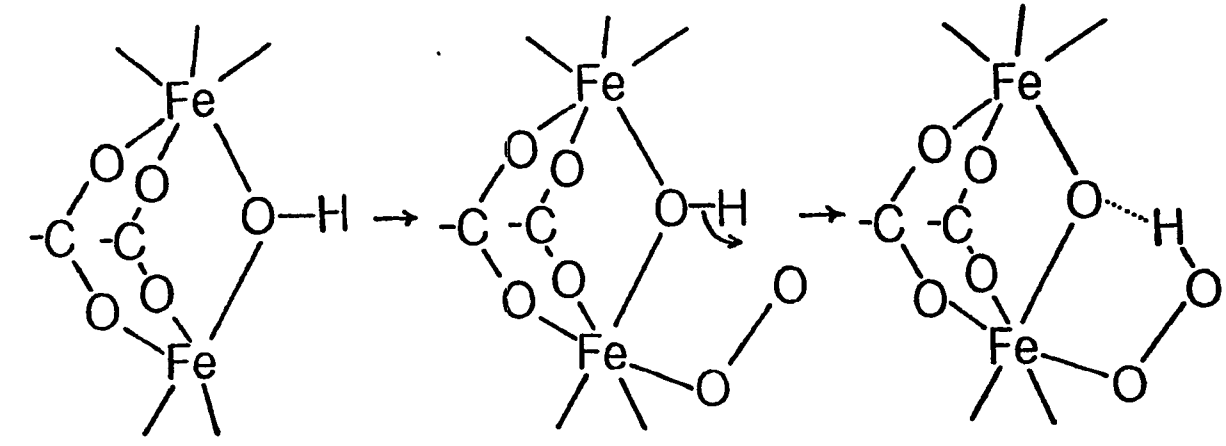

Figure 1.9. Proposed mechanism for the conversion of deoxyHr to oxyHr (3)

from aromatic amino acids. In the visible range, marked differences result from oxidation state changes. Most dramatic is the development of a burgundy color when colorless deoxyHr [Fe(II),Fe(II)] is oxygenated (Fig. 1.10). The visible spectra of the met derivatives [Fe(III),Fe(III)L^-] are similar to that of oxyHr [Fe(III),Fe(III)O_2^{2-}], with the exception that the moderately intense LMCT transition that appears near 500 nm for oxyHr is replaced by the exogenous LMCT transition in the spectra of the met derivatives (Table 1.4). The appearance of two peaks between 300 and 400 nm is characteristic of binuclear Fe(III) μ-oxo complexes (68). The semi-met [Fe(II),Fe(III)L^-] derivatives exhibit LMCT transitions qualitatively similar to those of the corresponding met derivatives and the bands appearing between 300 and 400 nm are about half as intense as those for the metL^- derivatives (Fig. 1.10 and Table 1.4). The band near 330 nm is apparently absent in the semi-metL^- derivatives. Table 1.4 summarizes the assignments that have been made for the electronic transitions.

The spectrum of metHr is pH dependent (Fig. 1.11). For the low pH form, one of the iron atoms is five-coordinate. For the high pH form, the sixth coordination position is occupied by OH^-. The pK_a reported for this effect (reaction 1.4) is 7.8 for Phascolopsis gouldii in the absence of perchlorate, and is raised to 8.7 in the presence of 1 mM perchlorate (69). Such pH effects are not observed for either oxyHr or the ligand adducts of metHr. The spectra of $(semi\text{-}met)_R$ and semi-metN_3^- have also been reported to be sensitive to pH changes, while that of $(semi\text{-}met)_O$ is not.

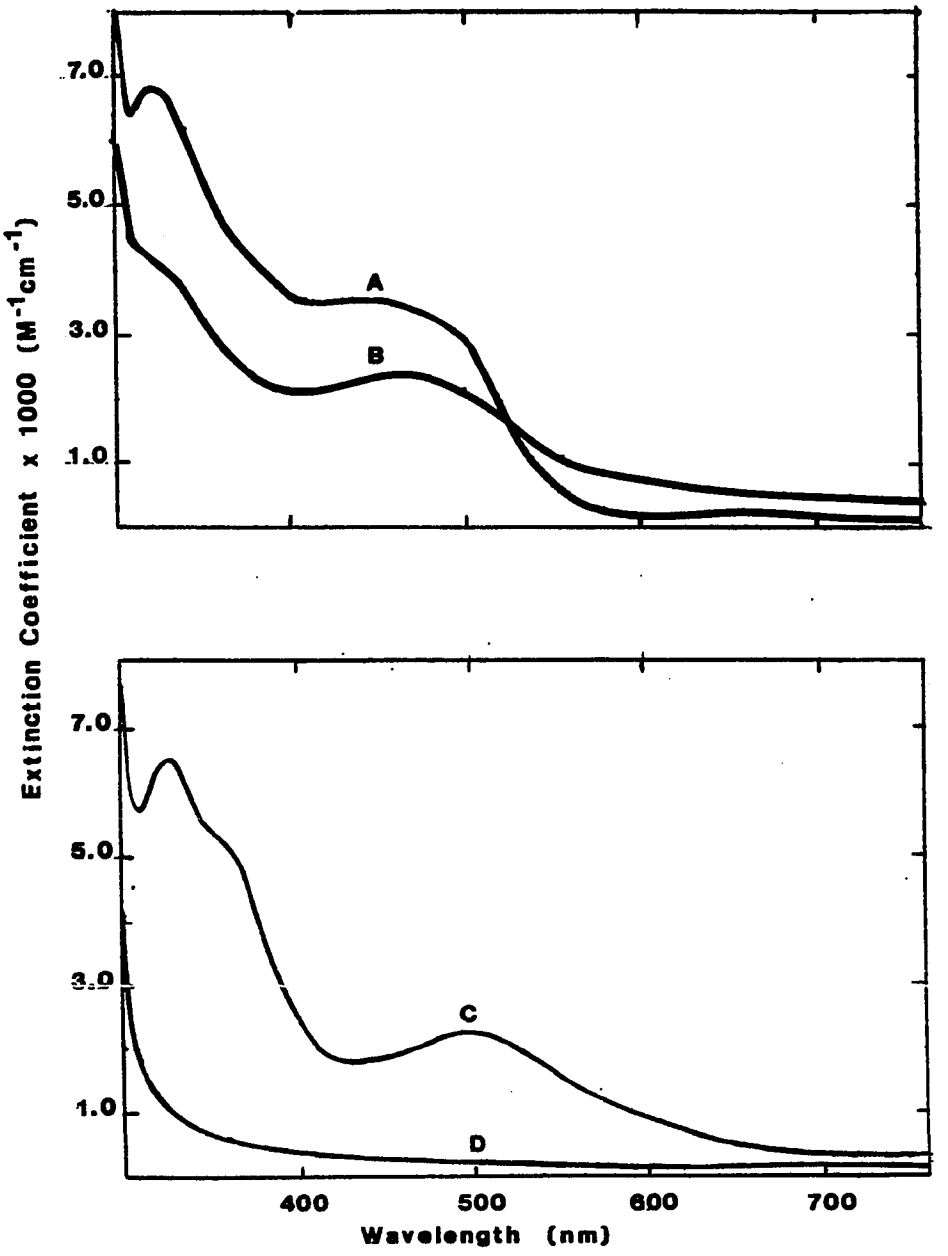

A. $metN_3^-$
B. semi-$metN_3^-$
C. oxyHr
D. deoxyHr

Figure 1.10. Optical spectra for derivatives of hemerythrin

Table 1.4. Optical transitions for derivatives of hemerythrin[a]

Derivatives	λ in nm (ε in $M^{-1}cm^{-1}$)				Reference
	LMCT ($O^{-2}\rightarrow Fe$)	Exogenous LMCT	$^6A_1\rightarrow{}^4T_2(^4G)$	$^6A_1\rightarrow{}^4T_1(^4G)$	
oxy	330 (6800) 360 (5450)	500 (2200)	750 (200)	990 (10)	43,70
$metNO_2^-$	330 (5900) 377 (5400)	480 (770)			7
$metN_3^-$	326 (6750) 380 (4300)	446 (3700)	680 (190)	1010 (10.2)	43,70
$metNCS^-$	327 (7200) 370 (4900)	452 (5100)	674 (200)		43
$metOH^-$ (pH 9.0)	320 (7200) 362 (5900)	480 (550)	610 (140)	990 (8)	43,70
met	355 (6400)	480 (600)	580 (200)		43
semi-$metN_3^-$ (pH 8.2)	315 (4400)	470 (2400)	730 (~80)	910 (~20)	70,71
$(semi\text{-}met)_R$ (pH 6.3)	350 (2000) 400 (880)	450 (400)			70
$(semi\text{-}met)_R$ (pH 8.2)	350 (3000) 400 (1300)	450 (430)	670 (~80)	995 (~8)	70,71

[a]0.1 M Tris-cacodylate; pH 7.0.

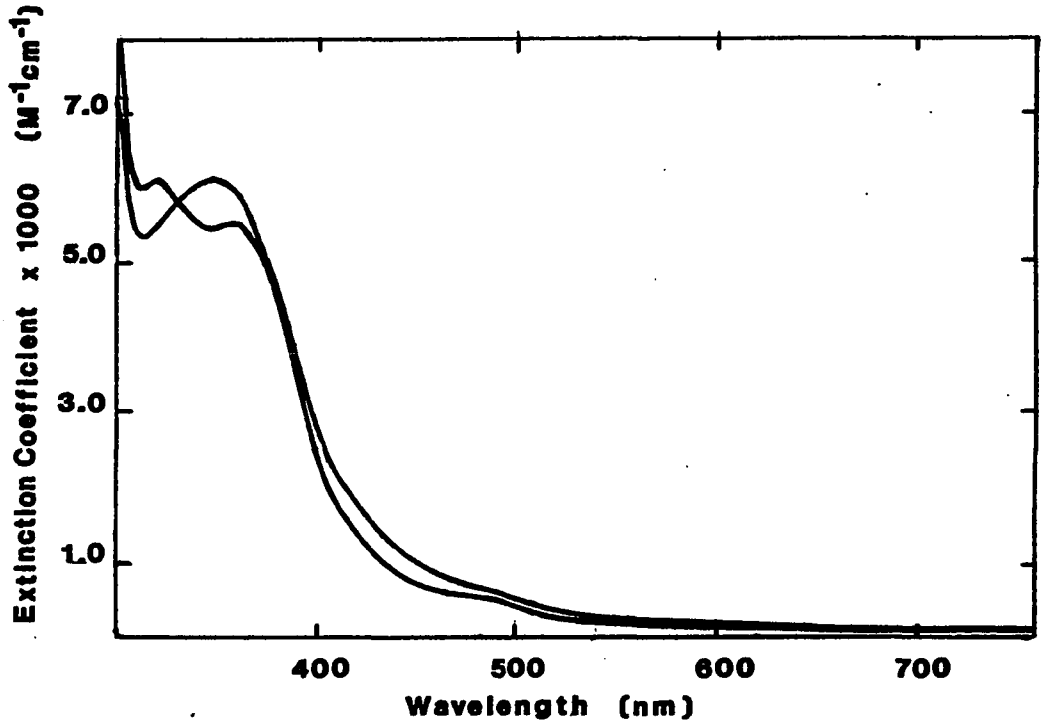

Figure 1.11. Optical spectra of metHr in 50 mM phosphate at pH 6.5 (A) and in 50 mM Tris-sulfate at pH 7.5 (B)

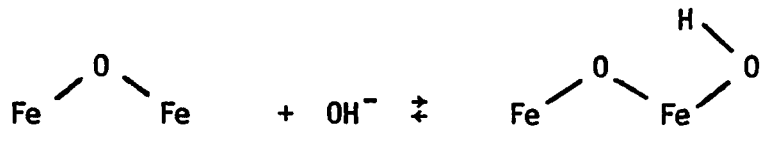

(1.4)

The near-ir d-d transitions (Table 1.4) are weak and, therefore, difficult to observe (70). For deoxyHr, the absorption can be resolved into two bands, one at 855 and the other at 1110 nm. The two components observable in metHr are located at 935 and 1040 nm. For the semi-metHrs, bands from both ferric and ferrous transitions overlap and for semi-metN_3^-, an additional broad transition, whose intensity is proposed to be enhanced by the intervalence character of the excited state, occurs at 1190 nm.

On the basis of polarized single crystal spectra for oxyHr, Gay and Solomon (72) have proposed an energy level diagram for the binding of O_2 to Hr (Fig. 1.12). Their results suggest that O_2 binds to a single iron in an end-on fashion at an angle of nearly 90° relative to the Fe---Fe axis.

b. Mössbauer spectra Formal oxidation states and spin states for the iron atoms were obtained from Mössbauer data (5,73,74). Table 1.5 lists the observed parameters for several derivatives. For oxy and metHrs, doublets attributable to high-spin Fe(III) are observed, whereas for deoxyHr, the doublet is attributable to high-spin Fe(II). The one semi-met derivative that has been examined (75) displays both high-spin Fe(II) and high-spin Fe(III) doublets. With the exception of oxyHr, the iron atoms of the cluster appear equivalent on the Mössbauer time scale

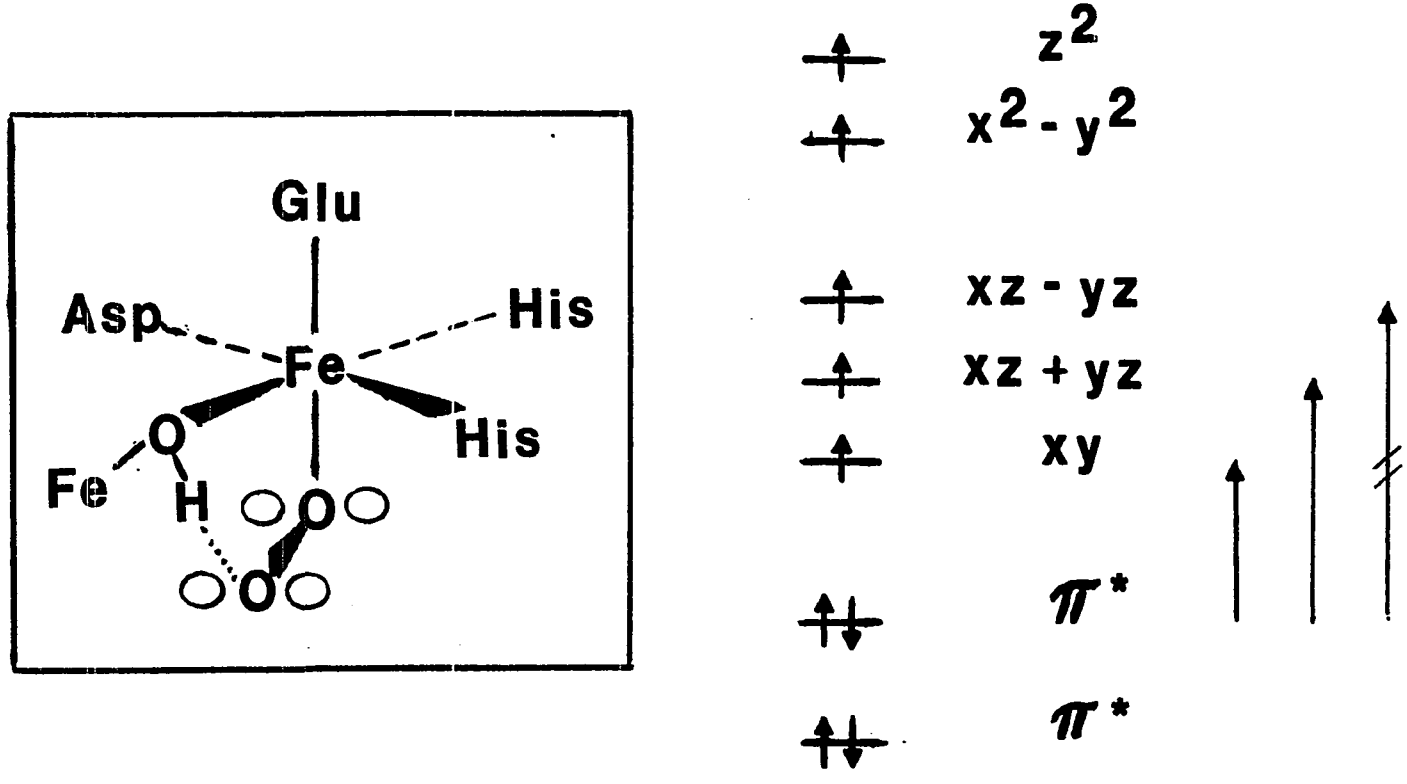

Figure 1.12. Order of the energies of the valence orbitals of the Fe^{3+}-O_2^{2-} center of oxyhemerythrin (72)

Table 1.5. Mössbauer parameters for Hr derivatives and μ-oxo bridged model compounds at 77 K[a]

Derivative	Fe(III) δ (mm/s)	Fe(III) ΔE_q (mm/s)	Fe(II) δ (mm/s)	Fe(II) ΔE_q (mm/s)	Reference
deoxy			1.19	2.81	73
oxy	0.51	1.93			73
	0.48	1.03			73
$metOH_2$	0.46	1.57			73
$metN_3^-$	0.50	1.91			5
μ-S^{2-}-met	0.50	0.99			74
μ-S^{2-}-semi-met	0.58	1.58	1.14	2.43	75
$(FeL)_2O(OAc)_2$	0.52	1.60			76[b]

[a]Isomer shifts are relative to metallic Fe at room temperature.

[b]4.2 K; L = $HBpz_3$.

when they are of identical oxidation state; only one doublet is observed for deoxyHr and for the metHr derivatives. The binding of O_2 to deoxyHr does not produce a spin state change as is observed for the binding of oxygen to Hb.

Information about the magnetic properties of Hr has been obtained from low temperature and magnetic Mössbauer spectra. For oxyHr and metHrs, hyperfine splitting is not observed, even at 4.2 K in magnetic fields of 30 kG. This result strongly suggests that the ground states of these derivatives are diamagnetic and result from antiferromagnetic coupling of the irons. Comparisons to model compounds suggest that this coupling is mediated by an oxo bridge. Line broadening also does not occur at low temperatures and high applied fields in the Mössbauer spectra of deoxyHr. The lack of broadening, in this case, may be due to large zero field splitting (which causes rapid electron spin relaxation) and/or the occurrence of antiferromagnetic coupling. In the Mössbauer spectra of μ-S^{2-}-semi-met, both quadrupole doublets broaden at low temperatures even in the absence of a strong applied field, indicating antiferromagnetic coupling of the irons and a paramagnetic (S=1/2) ground state.

c. EPR spectra Significant EPR signals are not observed either at liquid nitrogen (77 K) or liquid helium (4 K) temperatures for deoxyHr, oxyHr, metHr, or for any of the adducts of metHr. For the semi-met derivatives, distinct EPR signals appear below ~35 K (77). Table 1.6 lists the g-values for several of these derivatives. The average g-value of these signals is less than the free electron value,

Table 1.6. EPR parameters for Hr derivatives [a]

Derivative	g_x	g_y	g_z	Reference
$(semi\text{-}met)_O$	1.71		1.94	77
$(semi\text{-}met)_R$	1.67	1.87	1.95	77
	1.65	1.87	1.95	19
	1.68	1.86	1.93	78
$semi\text{-}metN_3^-$	1.49	1.81	1.90	77
$\mu\text{-}S^{2-}\text{-}semi\text{-}met$	1.40	1.71	1.87	75
$deoxyN_3^-$	--	--	13	6

[a] pH 8.2; Phascolopsis gouldii.

which is consistent with antiferromagnetic coupling of high-spin Fe(III) and high-spin Fe(II) leading to a net spin of 1/2. On an energy level diagram (Fig. 1.13A), it is the transition within the ground state S_{eff} = 1/2 Kramers' doublet that is observed.

On the basis of their EPR spectra (Fig. 1.14 and Table 1.6), two types of semi-metHrs have been identified: $(semi\text{-}met)_O$ prepared via one-electron oxidation of deoxyHr and $(semi\text{-}met)_R$ prepared by one-electron reduction of metHr. The $(semi\text{-}met)_O$ signal is axial, having $g_{\parallel} > g_{\perp}$, while the $(semi\text{-}met)_R$ signal is rhombic with $g_z > g_x, g_y$. The EPR spectrum of semi-metHr is perturbed by the addition of azide, cyanate, bromide, fluoride, cyanide, or thiocyanate (79). Ligand adducts prepared from $(semi\text{-}met)_O$ have EPR signals identical to those prepared from $(semi\text{-}met)_R$. All the ligand adducts of semi-met have rhombic EPR signals (e.g., semi-metN_3^- in Fig. 1.14B).

A third type of EPR signal having g ~ 13 was reported recently for the colorless azide adduct of deoxyHr (Fig. 1.14C) (6). Of the anions known to bind to deoxyHr (namely azide, cyanate, and fluoride), only azide produces this signal.

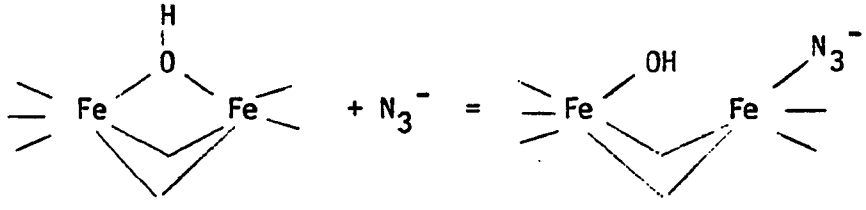

(1.5)

Reem and Solomon (6) have attributed this signal to the forbidden Δm_s = 4 transition from an S = 2 state (Fig. 1.13B) resulting from magnetic uncoupling of the iron atoms (reaction 1.5).

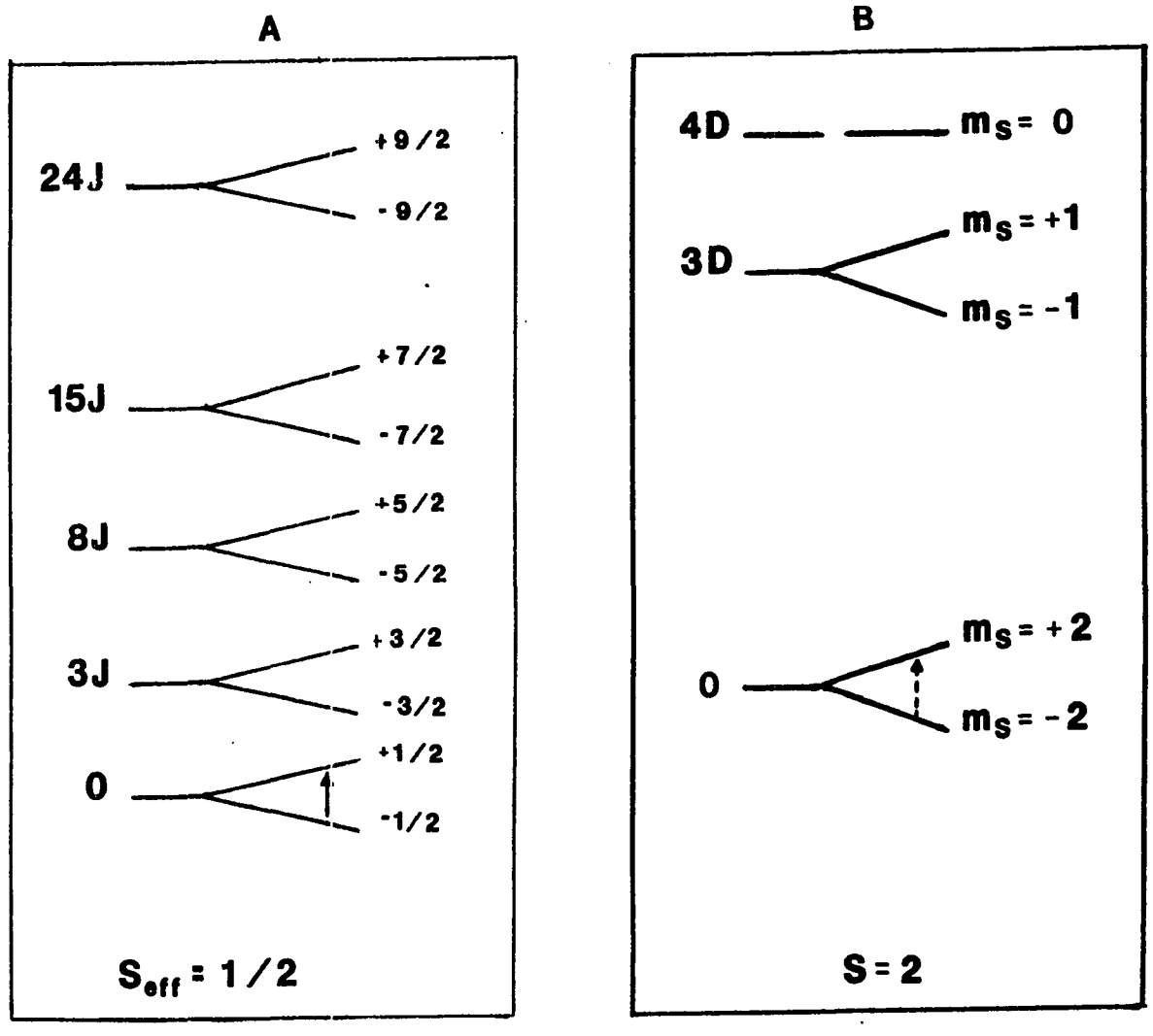

Figure 1.13. Order of the energies of the magnetic states resulting from antiferromagnetic coupling of high-spin Fe^{2+} and high-spin Fe^{3+} ions (A) and from an isolated high-spin Fe^{2+} ion with D > 0 (B)

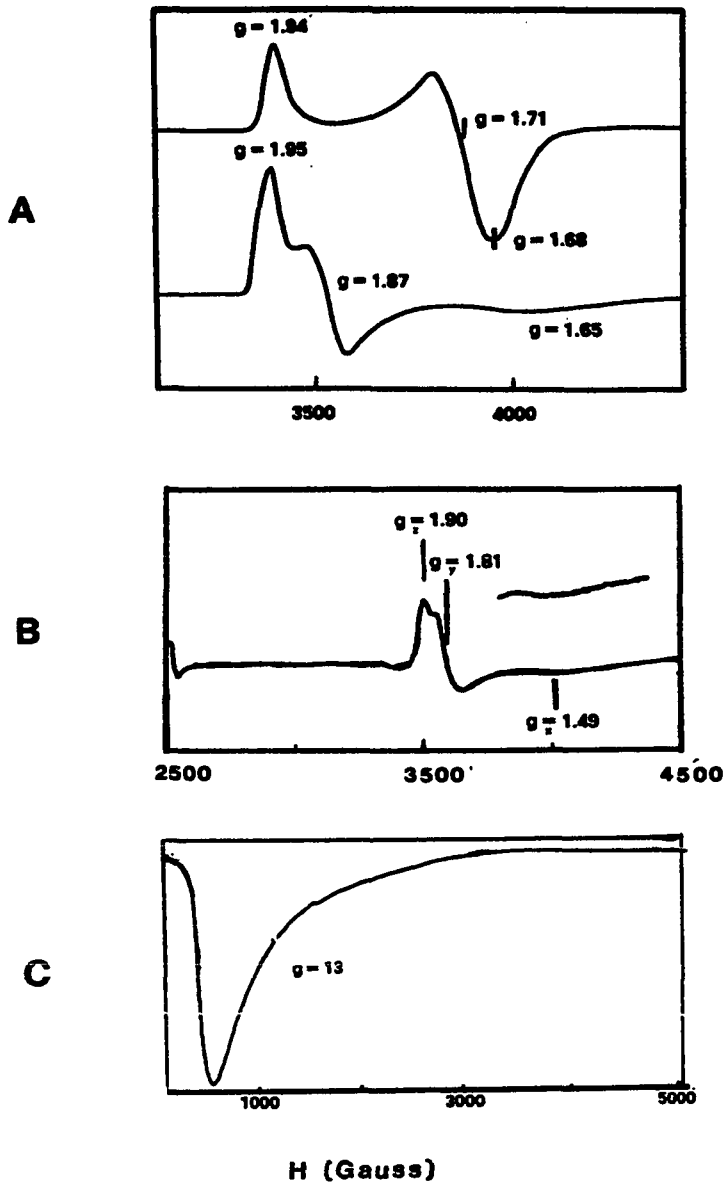

A. $(\text{semi-met})_O$ and $(\text{semi-met})_R$
B. semi-metN_3^-
C. deoxyN_3^-

Figure 1.14. EPR spectra for derivatives of hemerythrin

d. Resonance Raman spectra Resonance Raman spectroscopy has been used to study the mode of binding of ligands at the binuclear site of Hr. Spectra have been obtained for oxyHr, semi-metN_3^-, μ-S^{2-}-semi-met, metHr, and of a number of ligand adducts of metHr.

From resonance Raman data accumulated for oxyHr, it has been shown that the oxygen is at the peroxide oxidation level, that oxygen coordinates in an end-on fashion to one iron of the binuclear pair, that this ligand is apparently protonated, and that the hydroperoxide group is hydrogen-bonded to the μ-oxo bridge (80-83).

The resonance Raman spectrum of oxyHr (Figs. 1.15 and 1.16) contains four bands: ν(O-O) at 844 cm^{-1}, ν_{as}(Fe-O-Fe) at 753 cm^{-1}, ν(Fe-O_2) at 503 cm^{-1}, and ν_s(Fe-O-Fe) at 486 cm^{-1}. Only when the spectrum is obtained using near uv excitation are all four bands observed. With other excitation frequencies, only the bands at 844 and 503 cm^{-1} appear (Fig. 1.17). The excitation profiles for the latter frequencies provide further evidence for assignment of the 500 nm absorption as a $O_2^{2-} \rightarrow Fe^{3+}$ charge transfer transition.

Comparing the frequency observed for the O-O stretching mode of oxyHr (844 cm^{-1}) to that observed for molecular oxygen, superoxide, and peroxide (Table 1.7) shows that the oxygen ligand is at the peroxide oxidation level.

Assignment of the 844 cm^{-1} and 503 cm^{-1} bands as ν(O-O) and ν(Fe-O_2), respectively, was confirmed by isotopic substitution experiments in which either $^{18}O^{18}O$ or $^{16}O^{18}O$ was used to prepare oxyHr. For oxyHr prepared with $^{18}O^{18}O$, the bands at 844 and 503 are shifted to 798

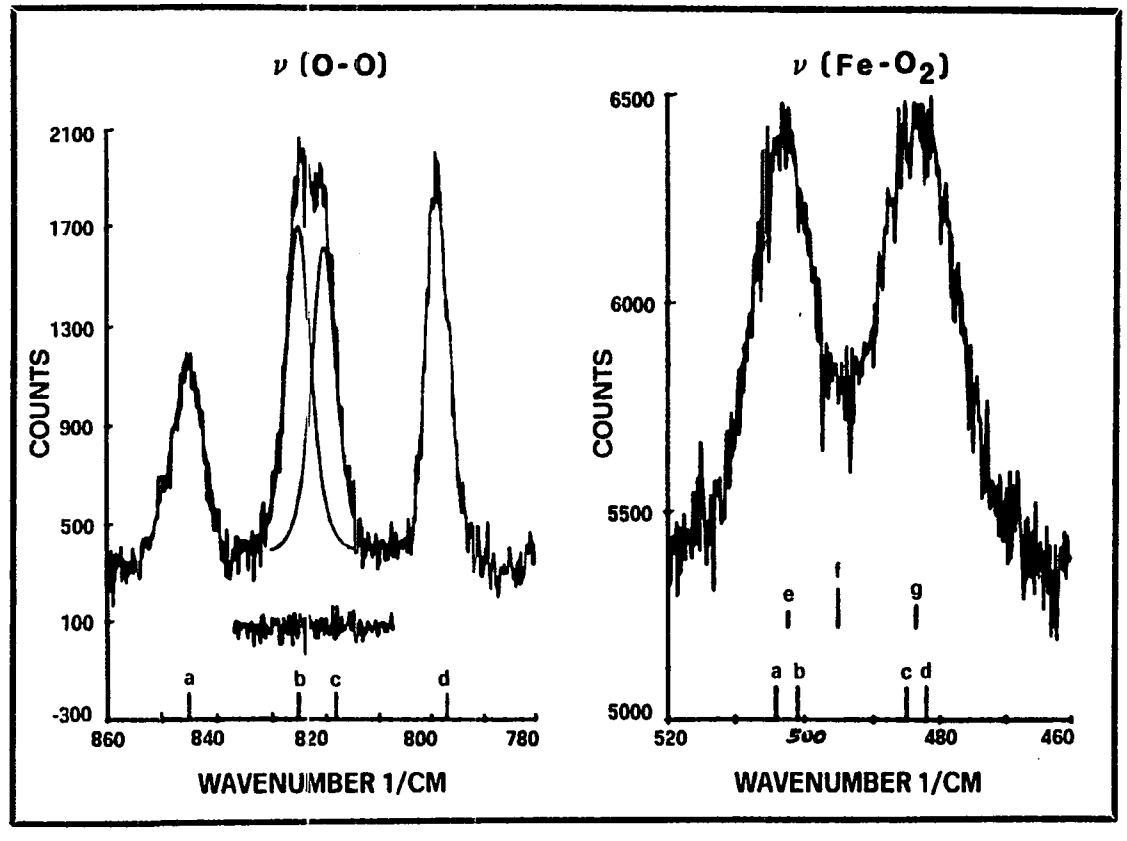

Figure 1.15. Resonance Raman spectra obtained with λ_{ex} = 514.5 nm for oxyhemerythrin prepared with 58 atom % ^{18}O-enriched O_2 gas (82)

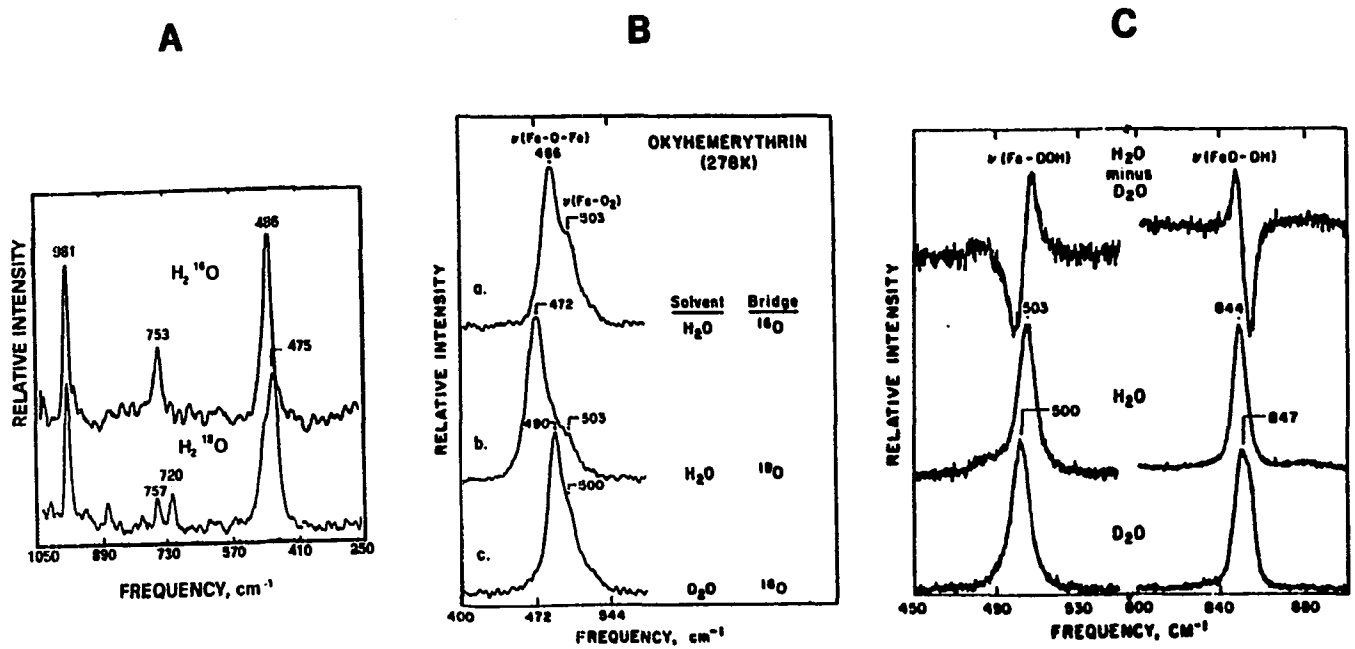

Figure 1.16. Isotopic substitution effects on the resonance Raman spectrum of oxyhemerythrin (80,81,83)

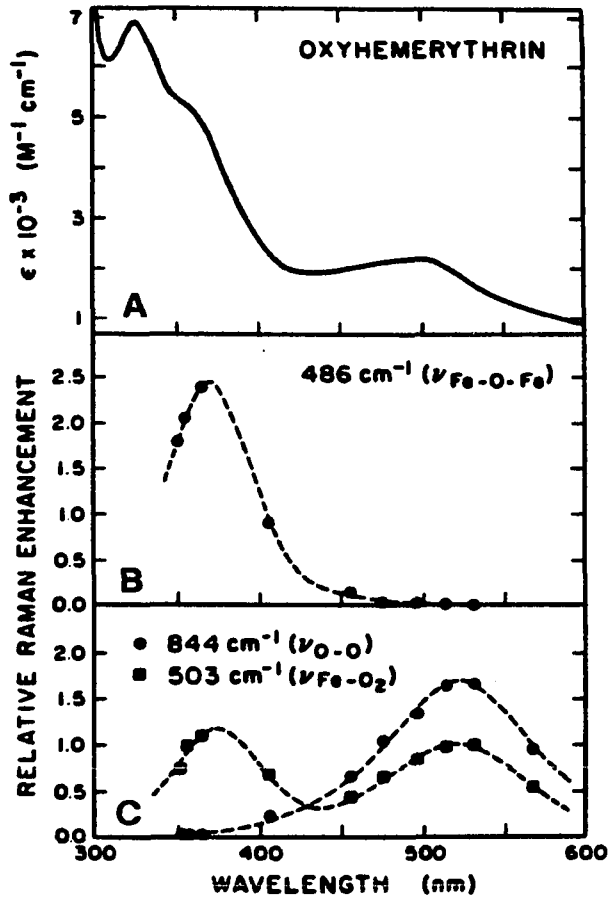

A. Electronic absorption spectrum of oxyhemerythrin
B. Enhancement profile for ν_s(Fe-O-Fe)
C. Enhancement for vibrations of the bound peroxide: ν(O-O) at 844 cm^{-1} and ν(Fe-O_2) at 503 cm^{-1}

Figure 1.17. Resonance Raman enhancement profiles for oxyhemerythrin (80)

Table 1.7. Dependence of $\nu(0\text{-}0)$ on oxidation state

	$\nu(0\text{-}0)$ (cm^{-1})	Reference
O_2	1556	83
KO_2	1145	83
$(NH_4)(HO_2)$	836	83
oxyHr	844	80

and 478, respectively, confirming that they arise from O_2 binding. In the presence of unsymmetrically labeled $O_2(^{16}O^{18}O)$, multiple bands were observed for the O-O stretching vibration and the Fe-O_2 stretching mode (Fig. 1.15) (82). This result indicated that the bound oxygen atoms of O_2 are inequivalent, which supports the structure derived from crystallographic studies (Fig. 1.9).

Metal-ligand vibrations have been observed for several N-bound anion adducts of metHr (Table 1.8). For the azide derivatives, the assignment of these bands as Fe-N stretching modes was confirmed with ^{15}N isotopic substitution experiments.

In addition to the exogenous ligand modes, bands that have been assigned to μ-oxo-bridge vibrations are observed. For C_{2v} symmetry, symmetric (ν_s) and asymmetric stretches (ν_{as}) and a deformation (δ) mode should be Raman active. For oxyHr (Fig. 1.16), these oxo bridge modes occur at 486 cm^{-1} (ν_s) and 753 cm^{-1}(ν_{as}). The deformation mode is apparently too weak to be observed in spectra of oxyHr. However, this mode does appear in spectra of metN_3^- and metNCS$^-$ (Table 1.9).

The preparation of ^{18}O-bridged oxyHr was the first evidence for assignment of these bands as oxo bridge modes. Quantitative incorporation of ^{18}O into the oxo bridge is best achieved by equilibrating deoxyHr crystals in $H_2{}^{18}O$ for several days and then oxygenating the sample (80) (reaction 1.6).

$$\text{deoxy} \xrightarrow{H_2{}^{18}O} {}^{18}\text{O-deoxy} \xrightarrow{O_2} {}^{18}\text{O-oxy} \qquad (1.6)$$

Table 1.8. Iron-exogenous ligand vibrational frequencies for derivatives of Hr

Derivative	ν(Fe-N) (cm^{-1})	$\Delta\nu$(Fe-N)[a]	Reference
metNHCN$^-$	388		81
metN_3^-	374	-8	84
semi-metN_3^-	359	-5	84
metNCS$^-$	298		81
metNCSe$^-$	275		81

[a] $(\Delta\nu) = (Fe\text{-}^{15}N) - (Fe\text{-}^{14}N)$

Table 1.9. Bridging mode vibrations for oxidized derivatives of Hr[a]

L^-	ν_{as}	ν_s (cm^{-1})	δ	Reference
N_3^-	768	507	292	80
SCN^-	780	514	290	80
H_2O	750	510	n.o.	80
OH^-	780	508	n.o.	80
OCN^-	782	509	n.o.	80
CN^-	780	512	n.o.	80
NO_2^-		516		81[b]
F^-		509		81[b]
Cl^-		509		81[b]
Br^-		512		81[b]
I^-		508		81[b]
HCO_2^-		510		81[b]
oxy	753	486	n.o.	80,81,83

[a]n.o. = not observed.

[b]457.9 nm; 60 mW.

^{18}O-oxyHr prepared in this way shows modes at 720 cm^{-1} (ν_{as}) and 475 cm^{-1} (ν_s) (Fig. 1.16). This result confirms that these bands are due to solvent-exchangeable, metal-oxygen vibrations.

^{18}O cannot be incorporated into the μ-oxo bridge by equilibrating metHr in $H_2{}^{18}O$. Thus, two indirect methods were used to prepare ^{18}O-bridged metHr adducts. The first method involves the oxidation of ^{18}O-oxyHr by $Fe(CN)_6{}^{3-}$ followed by ligand addition.

$$^{18}O\text{-oxy} \rightarrow {}^{18}O\text{-met} \rightarrow {}^{18}O\text{-metL}^- \qquad (1.7)$$

With the second method, used for N_3^-, OCN^-, and CN^-, ^{18}O-substitution is achieved by allowing ^{18}O-oxyHr to auto-oxidize in the presence of the ligand and $H_2{}^{18}O$.

$$^{16}O\text{-oxy} + L^- \xrightarrow{H_2{}^{18}O} {}^{18}O\text{-metL}^- + O_2{}^{2-} \quad , \quad L^- = N_3^-, OCN^-, CN^- \qquad (1.8)$$

As with oxyHr, vibrations of the μ-oxo bridge have been observed with the anion adducts of metHr (Table 1.9). For the met derivatives, the μ-oxo bridge modes can be enhanced with excitation in the visible region.

A second argument in support of the assignment of these frequencies to oxo-bridge modes is the appearance of similar isotope-sensitive bands in the IR spectra of oxo-bridged model compounds (Table 1.10).

The spectra obtained when oxyHr is prepared in D_2O provide evidence that the peroxide ligand is protonated and engages in a hydrogen-bonding

Table 1.10. Bridging vibrations for model μ-oxo bridged compounds

Compound	ν_{as}	ν_s (cm^{-1})	δ	Reference
$Fe_2O(OAc)_2(HBpz_3)_2$	751	528	283	76
$Fe_2O(phen)_4(H_2O)_2^{4+}$	827	395	n.o.[a]	85
$Fe_2OCl_6^{2-}$	870	458	203	86
$(Fe^{3+}L)_2(O)^{2+}$[b]	730	n.o.	n.o.	62

[a]Data obtained by IR spectroscopy.

[b]L = 1,4,7-triazacyclononane.

interaction with the oxo bridge (Fig. 1.9). In Figs. 1.16B and 1.16C, it can be seen that in D_2O ν(O-O) and ν_s(Fe-O-Fe) are both shifted upward by 4 cm^{-1} while ν(Fe-O_2) shifts downward by 3 cm^{-1} (80). The magnitude of the shift for ν(Fe-O_2) is close to that expected for deuterium substitution on a hydroperoxide ligand (-3 cm^{-1} vs. -5 cm^{-1}), however, the unusual 4 cm^{-1} increase in frequency for ν(O-O) cannot be accounted for solely on the basis of changes in the mass. Similar increases in frequency for oxyCoHb and oxyCoMb have been rationalized as effects due to hydrogen bonding of the bound O_2 to distal histidine (80,87). In Hr, the most likely source of a hydrogen bond is the bridging oxo group. Thus, the frequency shifts in D_2O suggest that the bound oxygen is protonated and engages in a hydrogen-bonding interaction with the oxo bridge, leading to an Fe-O-O angle that is significantly less than 180°.

The resonance Raman spectrum of metOH$^-$ is temperature-dependent. At 278 K, the broad band that occurs near 500 cm^{-1} which has been assigned as ν_s(Fe-O-Fe), was resolved into two components (ν_1 = 492 cm^{-1} and ν_2 = 506 cm^{-1}). The intensity of the component at 506 cm^{-1} is decreased as the temperature is lowered to 90 K, whereas the intensity of the component at 492 cm^{-1} is enhanced. It was suggested that there are two interconverting conformations in the metOH$^-$ samples (reaction 1.9) (88). Both components shift when ^{18}O is incorporated into the μ-oxo bridge, while only the component at 492 cm^{1} shifts when the sample is prepared in D_2O. It has been suggested that the two species arise from cis-trans isomerization with respect to the Fe-OH bond. The OH^- ligand is hydrogen-bonded to the oxo bridge in the cis isomer but not in the

trans isomer. Thus, only the ν_s(Fe-O-Fe) vibration that arises from the cis conformation is affected by deuterium exchange.

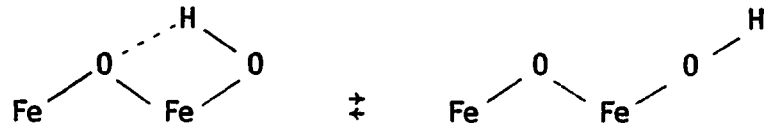

(1.9)

cis ⇌ trans

For semi-metN_3^- (84), attempts to detect oxo bridge vibrations have been unsuccessful. Compared to metN_3^-, the frequencies of the ligand modes are only slightly shifted [15 cm^{-1} and 3 cm^{-1} for ν(Fe-N_3^-) and ν(N-N), respectively]. These results suggest that the coordination mode is the same for metN_3^- and semi-metN_3^- and azide binds to the Fe(III) in the semi-met derivative.

Thus, the resonance Raman data are consistent with the crystallographic model for oxyHr and provide direct evidence for an oxo bridge in oxy and the metHrs.

e. Magnetic properties The magnetic properties of Hr have been explored using magnetic susceptibility, NMR, and MCD. Table 1.11 shows the exchange coupling constants that have been derived with these techniques.

Dawson et al. (4) reported magnetic susceptibility measurements for oxyHr and metHr. From this data, exchange coupling constants (J) of -77 and -134 cm^{-1} were determined for oxyHr and metHr, respectively (Table 1.11), and it was concluded that a μ-oxo bridge mediates the coupling. The values of J measured for synthetic Fe(III) μ-oxo bridged model com-

Table 1.11. Exchange coupling constants for Hr derivatives and synthetic model compounds

Derivative	J (cm^{-1})	Technique	Reference
oxy	-77	Mag. Susc.	4
met	-134	Mag. Susc.	4
semi-metN_3^-	-10	NMR	89
deoxy	-13 ± 5	MCD	6
$(Fe^{3+}L)_2O(OAc)_2$	-122	Mag. Susc.	60[a]
$(Fe^{3+}L)_2(OH)OAc)_2^+$	-17	Mag. Susc.	61[a]
$(Fe^{2+}L')_2(OH)(OAc)_2^+$	-14	Mag. Susc.	63[b]

[a] L = $HBpz_3$.

[b] L' = 1,4,7-triazacyclononane.

pounds support this conclusion. With μ-hydroxo bridged compounds, /J/ tends to be nearly an order of magnitude less than for the μ-oxo bridged compounds. The magnetic susceptibility for deoxyHr is significantly less than for oxyHr suggesting that the iron atoms in deoxyHr are either weakly coupled or uncoupled. No direct measurement of magnetic susceptibility have been reported for the semi-metHrs.

^{1}H-NMR spectroscopy has been used to characterize the magnetic states of several Hr derivatives (Figs. 1.18 and 1.19) (89,90). Working in water, only paramagnetically shifted resonances are readily observable. On the basis of their disappearance in D_2O, the most downfield shifted resonances have been assigned to the N-H protons of the active site His residues. These resonances appear between 12 and 25 ppm for metHr and metN_3^-, and at 73 and 54 ppm for semi-metN_3^-. In mononuclear model compounds, the signals for N-H protons of iron-coordinated imidazoles appear near 65 ppm for high-spin ferrous compounds and near 100 ppm for high-spin ferric compounds (91). The smaller paramagnetic shifts for the histidine N-H protons in the Hr derivatives apparently result from antiferromagnetic coupling between the irons.

For semi-metN_3^-, the histidine resonance at 73 ppm and 54 ppm occur in a 2:3 ratio, as is expected based on the structure of the iron site shown in Fig. 1.6B. The temperature dependence of the chemical shifts has been used to estimate an exchange coupling constant, J, of -10 cm^{-1} (Table 1.11).

For deoxyHr and deoxyN_3^-, the N-H resonances occur approximately in a 3:1:1 ratio. The histidine resonances are very near the values for

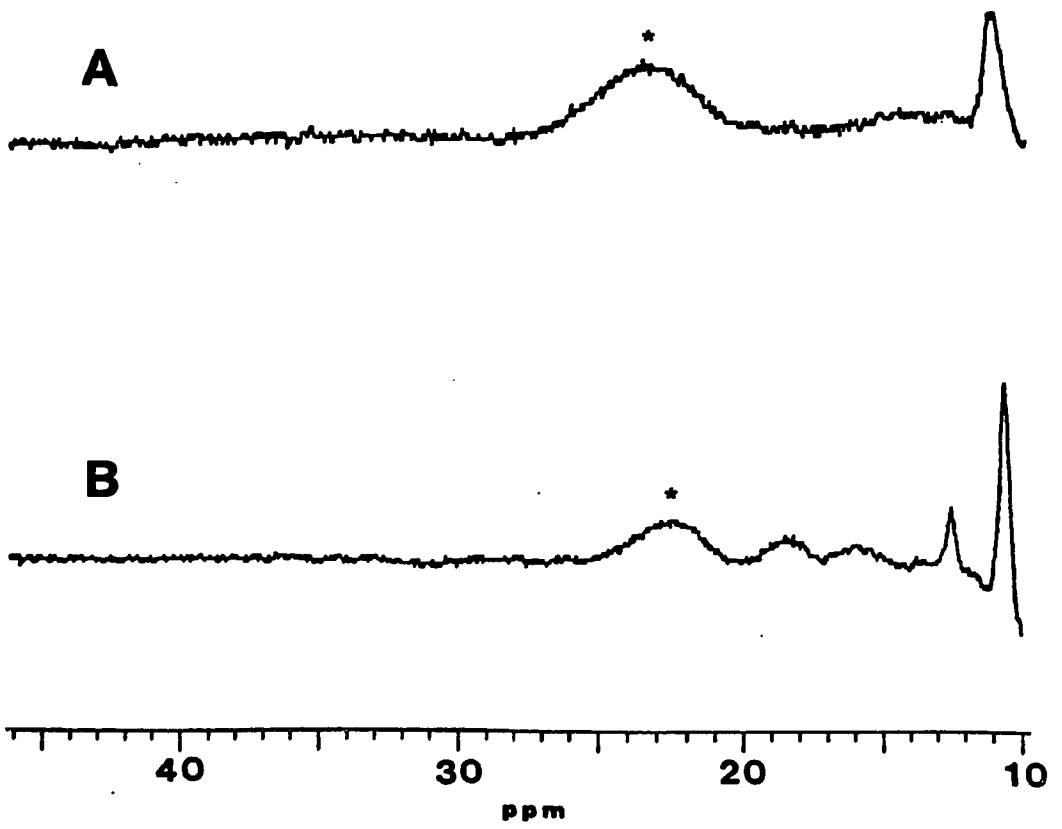

A. $metOH_2$ in 50 mM perchlorate, 300 MHz
B. $metN_3^-$, 300 MHz

Figure 1.18. ^1H-NMR spectra for derivatives of metHr at 30°C (89)

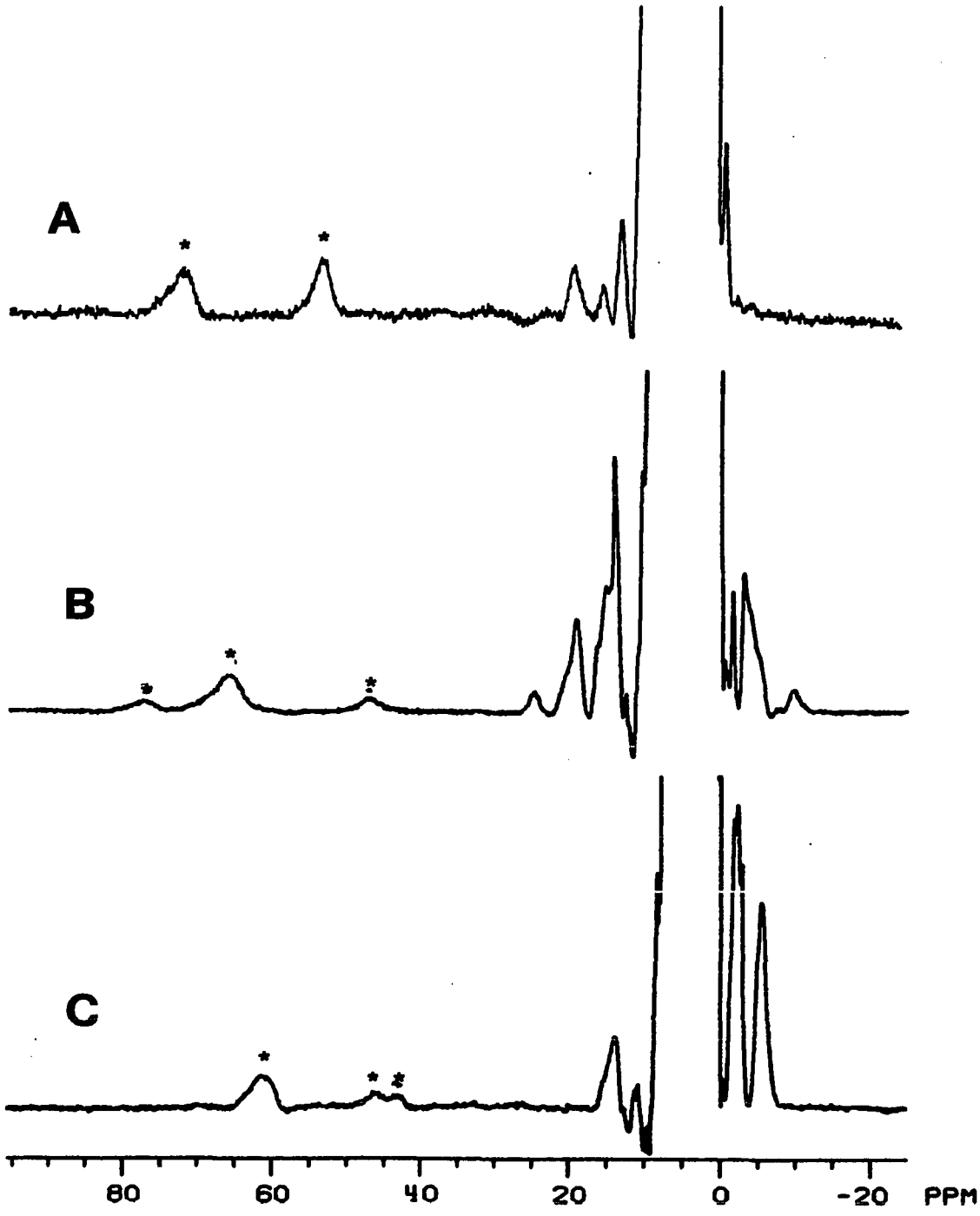

Figure 1.19. ^{1}H-NMR spectra for semi-metN_3^- (A), deoxyN_3^- (B), and deoxyHr (C) (89)

mononuclear iron complexes, indicating very weak antiferromagnetic coupling for these derivatives.

With deoxyHr, an MCD signal is observed near 1050 nm. The intensity of this signal increases as the temperature is raised to 65 K, and decreases above that point. Such behavior occurs for compounds having a singlet ground state. In contrast, the paramagnetic species, deoxyN_3^-, shows signals at 900 nm and 1050 nm that become less intense as the temperature is increased.

For deoxyHr, the variation of the intensity of the MCD signal as a function of temperature was used to estimate limits for the antiferromagnetic exchange coupling constant (J) and the zero field splitting energy (D). In order to determine whether or not exchange coupling is dominant within the binuclear ferrous site, Reem and Solomon point out that two extremes should be considered (Fig. 1.20). For mononuclear high-spin ferrous compounds, zero field splitting constants typically range from 2 to 8 cm^{-1}, with the largest reported value being 12 cm^{-1} (92-94). Neglecting exchange coupling (Model I) leads to D = 35 ± 10 cm^{-1} for deoxyHr, a value larger than that reported for model compounds. Similarly, when the contribution of D to the splitting of the magnetic states is neglected (Model II), an exchange coupling constant can be estimated. For deoxyHr, this leads to J = -20 ± 7 cm^{-1}. If contributions from both D and J are taken into account (a largest reasonable value for D is taken to be 12 cm^{-1}), J is calculated to be -13 ± 5 cm^{-1}. As Reem and Solomon have discussed, this value is reasonable for a structure in which hydroxide bridges and mediates the exchange coupling

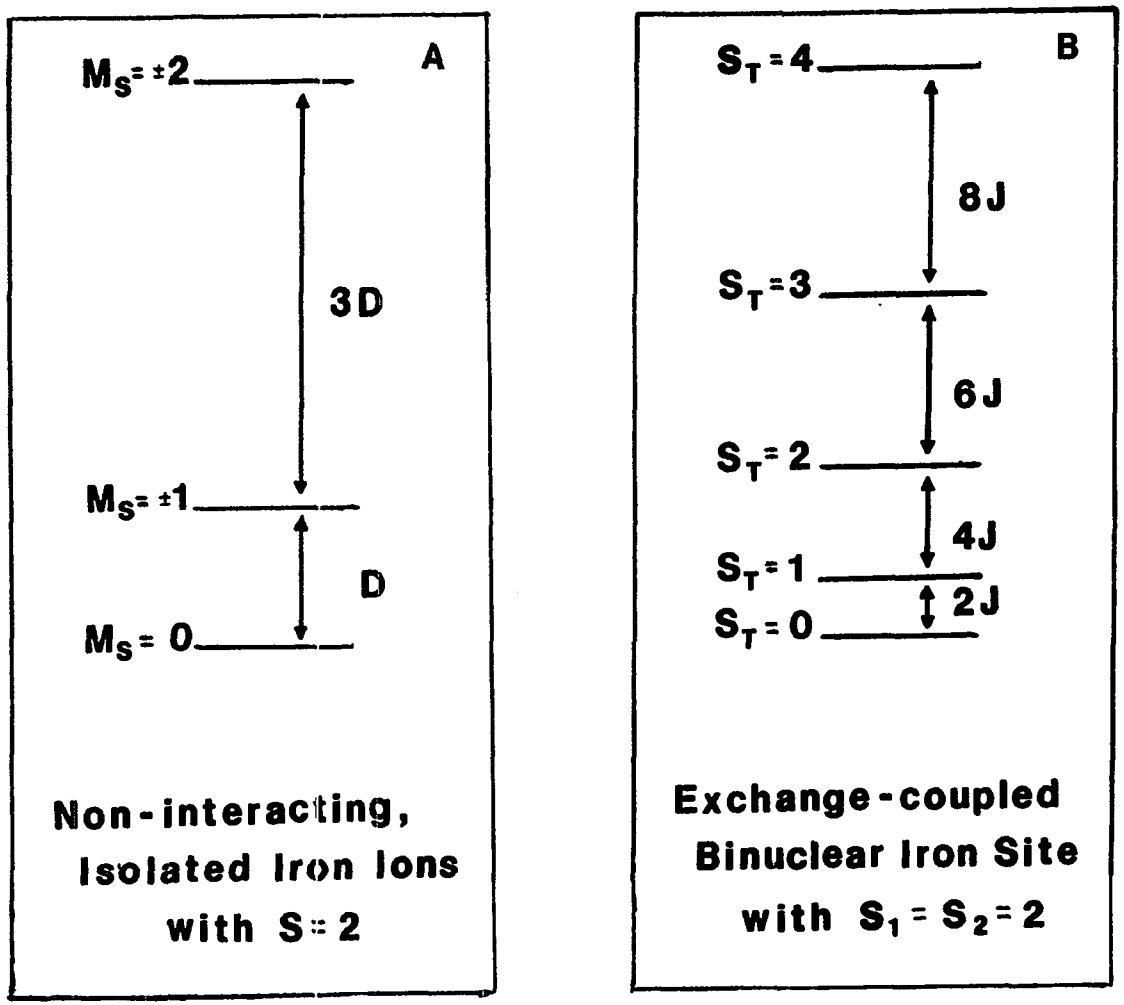

Figure 1.20. Comparison of the ordering of the energies of the magnetic states for two ferrous sites with D >> J (A) and with D << J (B)

although it does not mandate that the bridging unit be a hydroxo group. The magnetic susceptibility measurements reported for the μ-hydroxo bridged synthetic model compound support Solomon's proposal.

A similar treatment of the variable temperature MCD data for deoxyN_3^- has not been reported. The observation of an EPR signal for deoxyN_3^- does, however, suggest that antiferromagnetic coupling is not dominant in the ordering of magnetic states, i.e., D >> J. Structurally, the appearance of the EPR signal in deoxyN_3^- has been attributed to the rupture of the hydroxo bridge (6).

In summary, the results of the spectroscopic and magnetic studies of oxyHr and metHrs are fully consistent with the structural features shown in Figs. 1.6 and 1.9. These studies provide direct evidence for antiferromagnetic exchange coupling between the two high-spin ferric ions, mediated by an oxo bridge. According to Mössbauer data, the deoxyHr active site contains only high-spin Fe(II) and, in combination with MCD, NMR, and EPR results, the existence of weak antiferromagnetic coupling through a hydroxo bridge has been proposed. Addition of N_3^- is thought to labilize this bridge toward Fe-OH bond rupture. NMR spectroscopy shows that weak antiferromagnetic coupling, mediated by either an oxo or hydroxo bridge, occurs between the ferric and ferrous atoms of the semi-metHrs.

3. Chemical properties

Three redox states are accessible to the binuclear iron center in Hr:

(i) deoxyHr, [Fe(II),Fe(II)]

(ii) semi-metHr, [Fe(II),Fe(III)]

(iii) metHr, [Fe(III),Fe(III)]

Figure 1.21 shows chemical reactions that may be conveniently used to prepare derivatives of Hr at each oxidation level.

a. Oxygenation The major physiological function of Hr is the reversible binding of oxygen (reaction 1.10).

$$\text{deoxyHr} + O_2 \underset{k_{-1}}{\overset{k_1}{\rightleftarrows}} \text{oxyHr} \qquad (1.10)$$

The rate constant (k_1) measured by stopped-flow spectroscopy for the binding of oxygen to Hr from Phascolopsis gouldii is 7.4 x 10^6 $M^{-1}s^{-1}$ (58). The rate of dissociation (k_{-1} = 51 s^{-1}) was determined using either $S_2O_4^{2-}$ or deoxyMb to scavenge free O_2 and identical results were obtained with both reagents (58). Using these measurements, the association constant for the binding of oxygen to deoxyHr is 1.5 x 10^5 M^{-1}. This value is in good agreement with the value determined from equilibrium studies [1.3 x 10^5 M^{-1} at 25°C (95)].

Kinetic studies of the oxygen-binding reaction have been reported for Hr from Sipunculus nudus (96,97) and Themiste zostericola (79,98). Measurements of the rate of binding to Sipunculus nudus using laser photolysis (k_1 = 2.9 x 10^7 $M^{-1}s^{-1}$) agree well with the values obtained from temperature-jump studies (k_1 = 2.6 x 10^7 $M^{-1}s^{-1}$). The rate constant for the dissociation reaction, measured by stopped-flow kinetics, is 120 s^{-1}. With Themiste zostericola, stopped-flow measurements (k_1 =

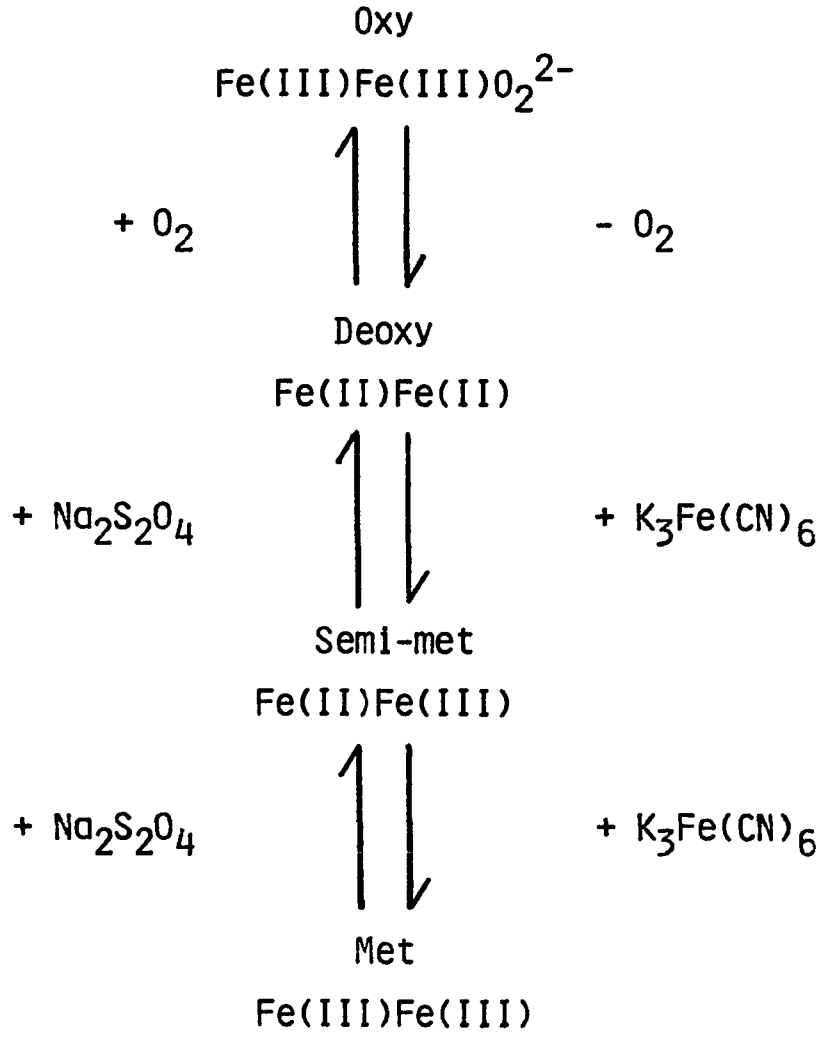

Figure 1.21. Summary of the oxidation levels attainable for hemerythrin

$7.5 \times 10^6\ M^{-1}s^{-1}$; $k_{-1} = 82\ s^{-1}$) were compared to the values obtained by laser photolysis ($k_1 = 9.0 \times 10^6\ M^{-1}s^{-1}$). The oxygen affinity constants determined from kinetic studies range from (0.9-1.5) $\times 10^5\ M^{-1}$. Similarly, the range of values for the association rate constants [(0.74-2.9) $\times 10^7\ M^{-1}s^{-1}$] and dissociation rate constants (51-120 s^{-1}) is narrow.

The on and off rates for the oxygenation of Hr are similar to those for Hb. However, the binding of O_2 to Hr differs from the binding of O_2 to Hb in several important ways. First of all, Hrs generally do not bind O_2 cooperatively; each subunit tends to react independently of its neighbors, thus, showing a Hill coefficient (n) near 1.0. The Hill coefficient for the binding of oxygen to Hb, on the other hand, is ~2.8 (99). Secondly, pH does not affect the oxygen-affinity of Hr within the pH range of ~6.0 to 10. Finally, Hr has a slightly higher affinity for oxygen than does Hb; for Hrs the half-saturation pressures for oxygen range from 1.0 to 15.0 Torr, while for Hb a value of 27 Torr was found.

b. Auto-oxidation A second physiologically relevant reaction of Hr is auto-oxidation, the spontaneous conversion of oxyHr into metHr (7). Auto-oxidation is acid-catalyzed and promoted by monovalent anions, including nitrite. In erythrocytes, Cl^- is a likely catalyst. Rate data for the auto-oxidation promoted by Cl^- and a series of similar monovalent anions are summarized in Table 1.12.

With the exception of N_3^- and OCN^-, uniphasic kinetics were reported. An appealing mechanism invokes simultaneous displacement of peroxide and its replacement in the coordination sphere by the exogenous ligand (reaction 1.11).

Table 1.12. Rate constants for ligand-promoted auto-oxidation of oxyHr to metL-[a]

L-	k ($M^{-1}s^{-1}$) pH 5.3	pH 6.3	pH 7.3	pH 8.3
N_3^-		0.34	0.028[b]	
NO_2^-	3.5	0.31	0.026	0.0022
F^-	2.0	0.12	0.0094	
OCN^-		0.080	0.0062	
HCO_2^-		0.0083		
Imid				0.004[c]
Cl^-		0.00014	0.000033	

[a]Reference 7.

[b]pH 7.5.

[c]pH 8.0.

$$Fe(III)_2O_2^{2-} + L^- \rightarrow Fe(III)_2L^- + O_2^{2-} \quad (1.11)$$

However, bleaching of the burgundy color of oxyHr solutions and the appearance of biphasic kinetics upon addition of N_3^- or OCN^- suggests an alternative pathway. The colorless intermediate implies that these ligands may successfully compete with O_2 for the deoxy site (reactions 1.12 and 1.13).

$$\text{oxy} \rightleftarrows \text{deoxy} + O_2 \quad (1.12)$$

$$\text{deoxy} + L^- \rightleftarrows \text{deoxyL}^- \quad (1.13)$$

The production of $metL^-$ (phase 2) might then occur by oxidation of the $deoxyL^-$ species (reaction 1.14).

$$\text{deoxyL}^- + O_2 \rightarrow \text{metL}^- + O_2^{2-} \quad (1.14)$$

c. Chemical oxidation Kinetics for the conversion of deoxyHr to metHr by $Fe(CN)_6^{3-}$ have been reported by Bradic et al. (100). A biphasic reaction is observed and the mechanistic interpretation of this is shown in Scheme 1.2. This mechanism indicates that a sequential removal of electrons occurs. The rapid first phase shows a first order dependence on [Hr] and $[Fe(CN)_6^{3-}]$ at pH 6.3 and 8.2, with the rates for Themiste zostericola being 1000 times greater than those for Phascolopsis gouldii (Table 1.13).

Table 1.13. Rate constants for the outer-sphere oxidation of deoxyHr to metHr[a]

Oxidant	pH	k_1 ($M^{-1}s^{-1}$)	k_2 (s^{-1})	k_3 (s^{-1})	I (M)
		Phascolopsis gouldii			
$Fe(CN)_6^{3-}$	6.3	1.2×10^3	0.17×10^3[b]	--	0.15
	6.3	1.0×10^3	0.10×10^3[b]	--	0.30
	8.0	1.7×10^2	1.1×10^{-3}	--	0.30
	8.2	1.5×10^2	1.7×10^{-3}	--	0.15
$Co(terpy)_2^{3+}$	8.2	0.6[c]			
		Themiste zostericola			
$Fe(CN)_6^{3-}$	6.3	$>10^5$	0.55×10^{-3}	1.1×10^{-3}	
	8.2	10^5	1.2×10^{-3}	2.6×10^{-3}	

[a]Reference 100.

[b]$M^{-1}s^{-1}$.

[c]Reference 101.

Scheme 1.2:

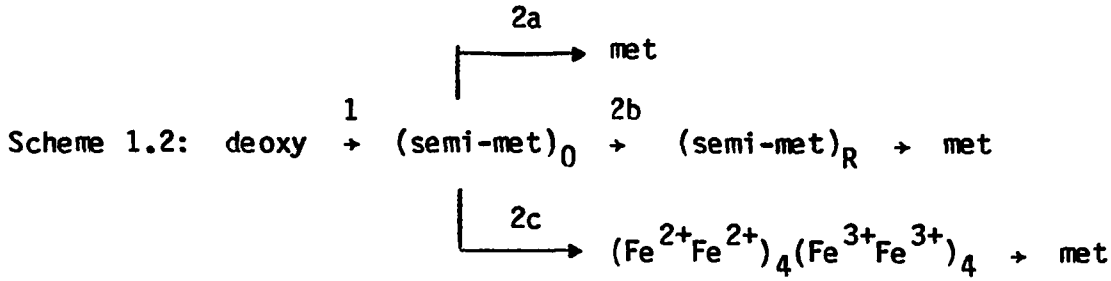

The product of the first phase of this reaction is $(semi\text{-}met)_0$. In the presence of excess oxidant, further oxidation leads to the production of metHr. Under most conditions, the second phase is independent of [oxidant], which leads to the suggestion that the second phase occurs either via conversion of $(semi\text{-}met)_0$ to $(semi\text{-}met)_R$ (path 2b) or via a disproportionation-controlled reaction (path 2c). In contrast, at pH 6.3 with Phascolopsis gouldii, this step shows a first order dependence on [oxidant]; conversion to metHr, therefore, occurs by "direct" oxidation (path 2a).

When only one oxidative equivalent of ferricyanide is added, the EPR signal of $(semi\text{-}met)_0$ still decreases with time. This result has been attributed to the occurrence of the intramolecular disproportionation reaction (reaction 2c). With Themiste zostericola, this reaction occurs nearly to completion, but with Phascolopsis gouldii disproportionation accounts for only ~20% of the decomposition perhaps due to a conformational change - the o→r conversion (path 2b) - that occurs at a rate comparable to that for disproportionation (k_3 in Table 1.14). Conversion of $(semi\text{-}met)_0$ to $(semi\text{-}met)_R$ is most easily followed by EPR spectroscopy (Fig. 1.22) (19); detection of $(semi\text{-}met)_R$ is best achieved

Table 1.14. Rate constants for the conversion of $(semi\text{-}met)_0$ to $(semi\text{-}met)_R$[a]

	pH	k (s^{-1})	k_{-1} (s^{-1})
P.g.	8.2	1.7×10^{-3}	-
T.z. (Monomer)	8.2	1.0×10^{-2}	$<10^{-3}$

[a]Reference 101; Phascolpsis gouldii (P.g); Themiste zostericola (T.z).

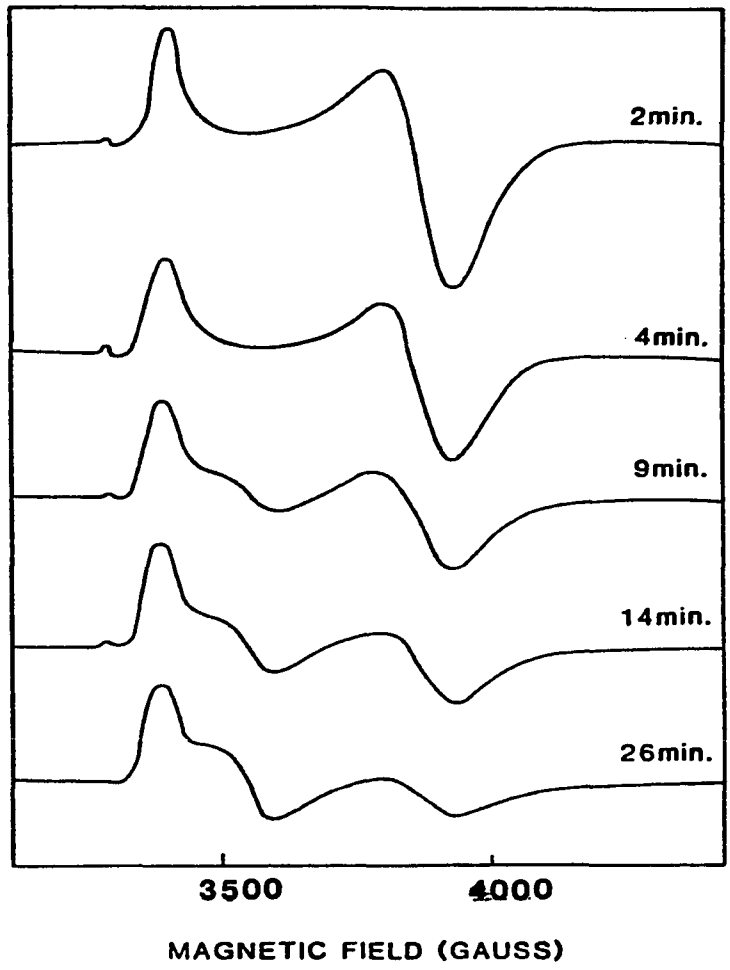

Figure 1.22. EPR spectra for the conversion of $(\text{semi-met})_O$ to $(\text{semi-met})_R$

at higher pHs in the absence of anions such as ClO_4^-, which tend to stabilize $(semi\text{-}met)_O$.

The reaction of oxyHr with ferricyanide also produces metHr. Again, biphasic kinetics are observed. The rate law describing the first phase is shown in Eq. 1.15,

$$R = \{k_1/(K[O_2]) + k_4\}[Fe(CN)_6^{3-}][Hr] \qquad (1.15)$$

and a mechanism from which this rate law derives is shown in Scheme 1.3. From a plot of $k/[Fe(CN)_6^{3-}]$ versus $1/[O_2]$ and using a value of 2×10^5 M^{-1} for K_{HrO_2}, values of 0.1 $M^{-1}s^{-1}$ and 116 $M^{-1}s^{-1}$ were obtained for k_4 and k_1, respectively, at pH 8.2. Since $k_4 << k_1$, it was suggested that deoxyHr is an intermediate of the reaction. The rates for the second phase are similar to those for the second phase of ferricyanide oxidation of deoxyHr.

Scheme 1.3:

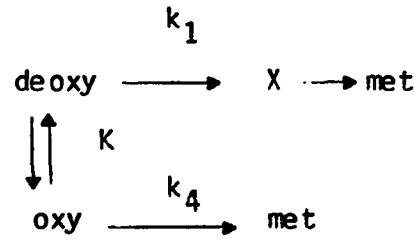

d. Reduction reactions Just as with oxidation, the reduction of metHr to deoxyHr involves the intermediacy of a mixed valence derivative, $(semi\text{-}met)_R$. It has been established that the immediate product of the reduction reaction is $(semi\text{-}met)_R$. However, the kinetics for the

further reduction to deoxyHr are complex and the mechanism is the subject of current debate (102-104).

The reduction potentials for the met/$(semi\text{-}met)_R$ and $(semi\text{-}met)_O$/deoxy couples (Table 1.15) have been reported (105,106). The values obtained for Themiste zostericola show that intramolecular disproportionation is a thermodynamically feasible reaction.

An important distinction can be made between $(semi\text{-}met)_O$ and $(semi\text{-}met)_R$ on the basis of their relative rates of reaction with oxidants and reductants (Table 1.16). $(Semi\text{-}met)_O$ is rapidly reduced and only slowly oxidized, while $(semi\text{-}met)_R$ behaves in an exactly opposite fashion.

e. Reactions with anions The anions that interact with Hr have been grouped into two categories on the basis of whether or not the anion is capable of binding directly to the active site iron. The monovalent anions that perturb the iron active site but do not directly bind to iron are typified by ClO_4^-. The sites where these anions bind have been identified by x-ray crystallography (see section I.B.1). Among them are BF_4^-, PF_6^-, $B(Ph)_4^-$, NO_3^-, $H_2PO_4^-$, borate, and HCO_3^-. Ligands of the second type bind directly to the iron. These ligands alter the visible spectrum of metHr, promote the auto-oxidation of oxyHr, and the met adducts frequently exhibit metal-ligand stretching modes in their resonance Raman spectra (see section I.B.2).

Association constants (Table 1.17) for the binding of ligands directly at the iron site (reaction 1.16) have been derived from kinetic measurements.

Table 1.15. Reduction potentials in volts for hemerythrin derivatives[a]

	P.g.	T.z.	T.z. (mono)
met + e^- → $(semi\text{-}met)_R$	0.11	0.11	0.07
$\mu\text{-}S^{2-}$met + e^- → $\mu\text{-}S^{2-}$-semi-met	0.295	-	-
$(semi\text{-}met)_O$ + e^- → deoxy	-	0.31	0.35

[a]References 105 and 106; Phascolopsis gouldii (P.g.); Themiste zostericola (T.z.).

Table 1.16. Rate constants for redox reactions of $(semi\text{-}met)_O$ and $(semi\text{-}met)_R$[a]

	pH	k ($M^{-1}s^{-1}$)	I (M)
	$\underline{(semi\text{-}met)_O}$		
$Fe(CN)_6^{3-}$	8.2	1.7×10^{-3}	0.15[b]
		1.3×10^{-3}	
$S_2O_4^{2-}$	8.2	4×10^5	
	$\underline{(semi\text{-}met)_R}$		
$Fe(CN)_6^{3-}$	8.2	340	0.15[b]
	6.3	$>>10^5$	
	8.2	4×10^5	
$S_2O_4^{2-}$	6.3	7.0×10^{-4}[c]	
	8.2	1.1×10^{-3}[c]	

[a] *Themiste zostericola*; Reference 71; 20°C.

[b] *Phascolopsis gouldii*; Reference 100.

[c] s^{-1}.

Table 1.17. Rate and equilibrium constants for the binding of ligands to metHr[a]

L^-	pH	k_f ($M^{-1}s^{-1}$)	k_d(s^{-1})	K(M^{-1})
N_3^-	6.3	7.6	$<0.5 \times 10^{-4}$	$>1.5 \times 10^5$
	8.2	1.9	v. small[b]	--
NCS^-	6.3	82	69×10^{-4}	1.2×10^4
	7.5	11	62×10^{-4}	1.8×10^3
NCO^-	6.3	0.520	1.3×10^{-4}	4000[c]
	8.5	0.15	0.4×10^{-4}	3750[c]
F^-	6.3	0.035	3.9×10^{-4}	90
Cl^-	6.3	0.006	0.75×10^{-4}	80
Br^-	6.3	0.016	15×10^{-4}	10.7[c,d]
HCO_2^-	6.3	0.012	15×10^{-4}	8.0[c,e]

[a]Reference 107; 25°C; I = 0.1 M.

[b]Reference 101.

[c]Reference 108.

[d]I = 0.30 M.

[e]I = 0.25 M.

$$met + L^- \rightleftarrows metL^- \qquad (1.16)$$

Direct measurements were made of the association rates (k_f). The values of the dissociation rates (k_d) were determined by indirect methods. The three reactions used were the anation reaction (reaction 1.17),

$$met + L^- \rightleftarrows metL^- \qquad (1.17)$$

azide displacement reactions (reactions 1.18 and 1.19),

$$metL^- \rightleftarrows met + L^- \qquad \text{(rate determining)} \qquad (1.18)$$

$$met + N_3^- \rightleftarrows metN_3^- \qquad (1.19)$$

and the reduction of the ligand complex by dithionite (reactions 1.20 and 1.21) (107,108).

$$metL^= \rightleftarrows met + L^- \qquad \text{(rate determining)} \qquad (1.20)$$

$$met + S_2O_4^{2-} \rightarrow product \qquad (1.21)$$

The list of ligands capable of binding to deoxyHr is considerably smaller and binding is much weaker (Table 1.18).

Although a number of anionic ligands are known to bind to semimetHr (CN^-, N_3^-, SCN^-, Br^-, F^-, and NCO^-) (79), only the binding con-

Table 1.18. Rate and equilibrium constants for the binding of ligands to deoxyHr[a]

L^-	k_1 ($M^{-1}s^{-1}$)	k_{-1} (s^{-1})	K_{kin} (M^{-1})	K_{MCD} (M^{-1})
N_3^-	50	0.70	71	70[b]
OCN^-	7.7	0.30	26	70[b]
F^-	-	-	-	7[b]
O_2[c]	7.4×10^6	51	1.5×10^5	-

[a]Reference 7; Phascolopsis gouldii.

[b]Reference 6.

[c]Reference 58.

stant for the azide derivative has been reported (Table 1.19). The association constants are intermediate between those for deoxyN_3^- and metN_3^-.

f. Bridge substitution reactions Two examples of reactions in which the oxo bridge has been ruptured have been reported for Hr. The first of these involves the incorporation of sulfide or selenide in place of the oxo bridge and may be achieved either by addition of excess chalcogenide to $(semi\text{-}met)_R$ or by the anaerobic reaction of metHr with excess chalcogenide (109). In these reactions, bridge exchange appears to occur at the semi-met rather than the met oxidation level (reaction 1.22). For the latter method, the chalcogenide serves to both reduce the binuclear site by one electron and to replace the oxo bridge.

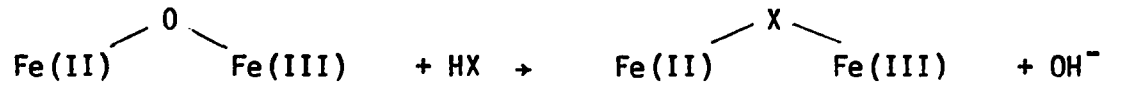

(X = S or Se) (1.22)

Exchange reactions have also been reported to occur at the deoxyHr oxidation level (80), where the bridging hydroxo group is replaced by oxygen derived from the solvent (reaction 1.23).

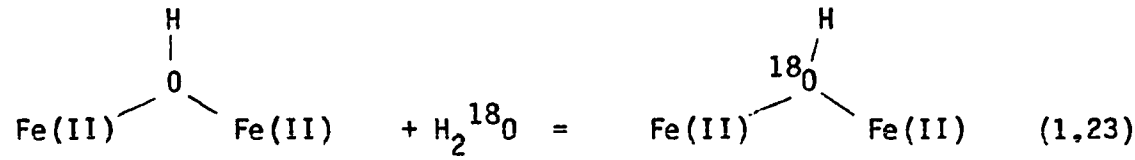

(1.23)

Table 1.19. Rate and equilibrium constants for the binding of azide to $(semi\text{-}met)_O$ and $(semi\text{-}met)_R$[a]

pH	k_1 ($M^{-1}s^{-1}$)	k_{-1} (s^{-1})	k_{kin} (M^{-1})
		$(semi\text{-}met)_O$	
6.3	1100	0.30	3600
8.2	320	0.20	1600
		$(semi\text{-}met)_R$	
6.3	2800	~0.15	~2 x 10^4
8.2	33	0.01	3300

[a]Reference 71; Themiste zostericola.

With synthetic binuclear, oxo-bridge ferric compounds exchange with $H_2{}^{18}O$ is quite facile (69). In contrast, the iron site of metHr is inert to solvent exchange.

C. Aqueous Chemistry of NO and NO_2^-

Numerous studies of the reactions of NO and NO_2^- with Fe^{2+} and Fe^{3+} complexes have been conducted. A brief summary of some of the more pertinent aspects of this work and a description of the physical properties of NO and NO_2^- in aqueous solutions follow.

1. Physical properties

Nitric oxide has no absorption in the visible region of the spectrum. In the near-uv region, however, an intense, solvent-dependent band appears that has been attributed to charge transfer between NO and the solvent (110).

Nitric oxide exists as a free radical. At room temperature, the association of gaseous NO to diamagnetic N_2O_2 (reaction 1.27) is extremely small.

$$2NO \rightleftarrows ON\text{-}NO \qquad (1.24)$$

The EPR signal observed for an aqueous buffer solution of NO has $g \sim 1.97$ (Fig. 1.23) (111).

Gaseous nitric oxide is sparingly soluble in water (1.9 mM at 25°C) (112) compared to oxygen (0.316 mM at 25°C) (113). It has recently been suggested (114) that in aqueous solution, NO disproportionates, forming N_2O and HONO (reaction 1.28).

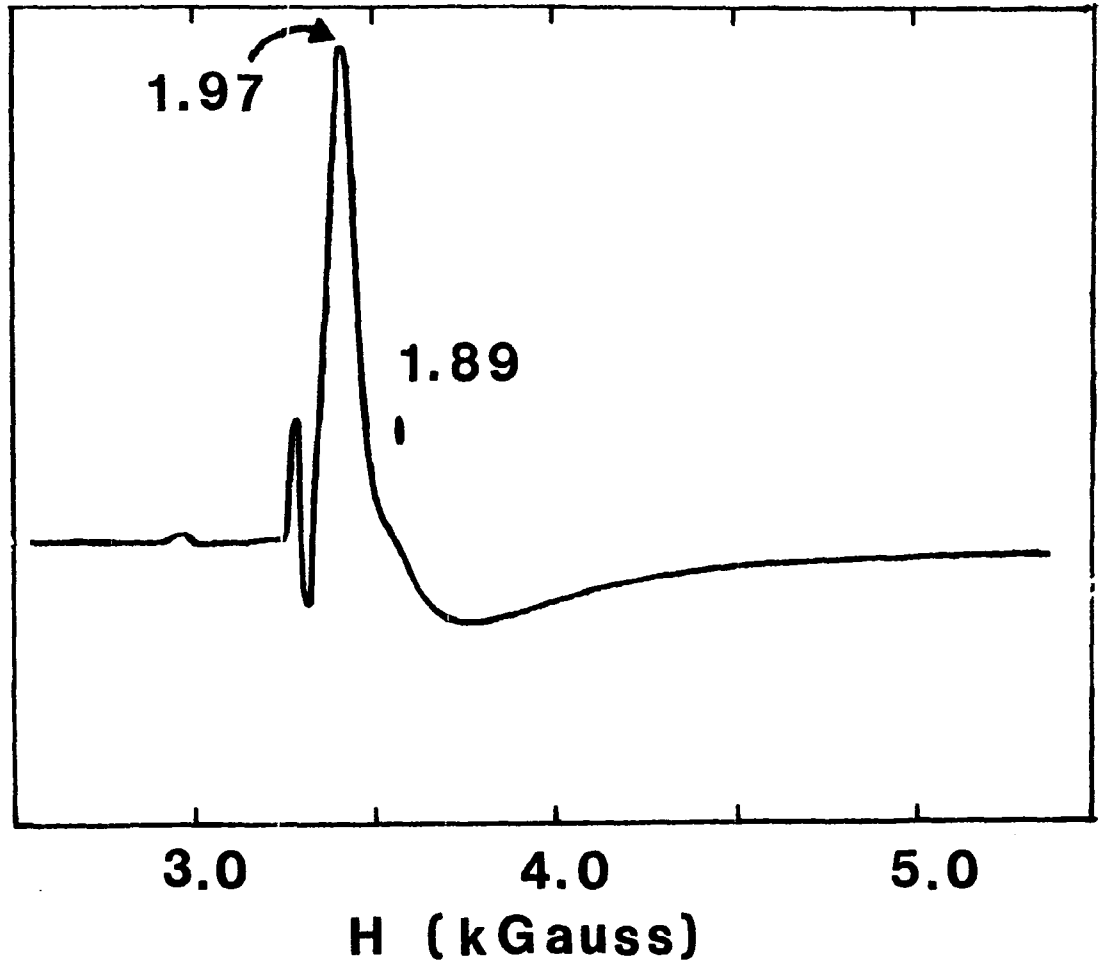

Figure 1.23. EPR spectrum of NO in phosphate buffer at pH 6.5

$$4NO + H_2O = N_2O + 2HONO \qquad (1.25)$$

Aqueous solutions of sodium nitrite are a very pale yellow color (ϵ_{354} = 22.5 $M^{-1}cm^{-1}$; ϵ_{287} = 9.4 $M^{-1}cm^{-1}$; ϵ_{210} = 5380 $M^{-1}cm^{-1}$ (115). At physiological pHs, solutions of sodium nitrite are stable for several days. Nitrous acid is weakly acidic (pK_a = 2.94 at 25°C and μ = 0.50 M) (116), and only a small percentage of HONO is present at the pHs employed for the experiments described in this dissertation. In strongly acidic media, further protonation of nitrous acid occurs. The pK_a for this reaction is -6.5 (reaction 1.26) (117).

$$H_2ONO^+ \rightleftarrows HONO + H^+ \qquad (1.26)$$

Dehydration of H_2ONO^+ leading to formation of NO^+ (reaction 1.30) occurs rapidly.

$$HONO + H^+ \rightleftarrows [H_2ONO^+] \rightleftarrows NO^+ + H_2O \qquad (1.27)$$

Thus, the equilibrium constant for the conversion of HONO to NO^+ is 3 x 10^{-7} or $1/K_a$.

2. Oxidation of Fe^{2+} compounds by nitrous acid

In Table 1.20, the reduction potentials of several oxides of nitrogen are listed. Combining the value of 0.99 V for the standard reduction potential of nitrous acid with the value of the pK_a (2.94) for HONO, one obtains a value of 0.366 V for the reduction potential of the NO_2^-/NO

Table 1.20. Reduction potentials for NO_x compounds[a]

Reaction	E^o (volts)
$HONO + H^+ + e^- = NO + H_2O$	0.99
$2HONO + 4H^+ + 4e^- = N_2O + 3H_2O$	1.27
$2HONO + 4H^+ + 4e^- = H_2N_2O_2 + 2H_2O$	0.80
$NO_2 + e^- = NO_2^-$	0.993[b]
$NO_2^- + H_2O + e^- = NO + 2OH^-$	-0.46
$2NO_2^- + 2H_2O + 4e^- = N_2O_2^{2-} + 4OH^-$	-0.18
$2NO_2^- + 3H_2O + 4e^- = N_2O + 6OH^-$	0.15
$2NO + H_2O + 2e^- = N_2O + 2OH^-$	0.76
$2NO + 2e^- = N_2O_2^{2-}$	0.10
$2NO + 2H^+ + 2e^- = N_2O + H_2O$	1.59
$NO_3^- + H_2O + 2e^- = NO_2^- + 2OH^-$	0.01
$NO_3^- + 3H^+ + 2e^- = HONO + H_2O$	0.94

[a]Reference 118.

[b]Reference 112.

couple at pH 7.0. The reduction potential of the NO/N_2O couple at pH 7.0 that is obtained using the Nernst equation and the value of 0.76 V for the standard reduction potential (Table 1.20) is 1.17 V.

The oxidation of Fe(II) complexes by nitrous acid has been investigated in strongly acidic solutions. These reactions proceed by an outer sphere transfer of one electron (reaction 1.28).

$$Fe^{2+}(aq) + HONO + H^+ \rightarrow Fe^{3+}(aq) + NO + H_2O \qquad (1.28)$$

Two mechanisms have been proposed to explain these reactions (Schemes 1.4 and 1.5). Scheme 1.4 requires a first order dependence of the rate upon $[H^+]$, while Scheme 1.5 requires that the rate be independent of pH.

The mechanism shown in Scheme 1.4 was proposed for the oxidation of $Fe(CN)_6^{3-}$ (119), $Fe(phen)_2(CN)_2$ (120), and $Fe(bpy)_2(CN)_2$ (120) by nitrous acid. Observation of a first order dependence of the rate upon $[H^+]$ was interpreted as arising from protonation of nitrous acid. Subsequent loss of H_2O produces NO^+, which is proposed to be the redox active species. The second order rate constants for these reactions are in the range of $5\text{-}7 \times 10^9\ M^{-1}s^{-1}$.

Scheme 1.4: $HONO + H^+ \rightleftarrows NO^+ + H_2O$

$$Fe^{2+} + NO^+ \rightarrow Fe^{3+} + NO \qquad \text{(rate determining)}$$

The mechanism shown in Scheme 1.5 was proposed by Ram and Stanbury (112) for the oxidation of $Fe(TMP)_3^{2+}$ by nitrous acid. Two phases were reported (Schemes 1.5A and 1.5B), and both were found to be independent of $[H^+]$ between pH 1 and pH 2. The rate limiting step of the slow phase was ascribed to the direct oxidation of Fe^{2+} by nitrous acid. One mole of H^+ is consumed when the "HONO⁻" radical is converted to NO. This conversion is proposed to occur subsequent to the rate limiting step, which accounts for the lack of an observed pH dependence for the slow phase.

Scheme 1.5A: $Fe^{2+} + HONO \rightarrow Fe^{3+} + \text{"}HONO^-\text{"}$ (rate limiting step)

$\text{"}HONO^-\text{"} + H^+ \rightarrow NO + H_2O$

The fast phase was found to be second order in [HONO] and independent of $[H^+]$ between pH 1 and 2. The pathway described in Scheme 1.5A is not consistent with the second order dependence of [HONO]. Rather, Ram and Stanbury suggest that NO_2 is the principal oxidant (Scheme 1.5B). Production of both NO_2 and NO from the disproportionation of HONO accounts for the second order dependence on [HONO]. In this mechanism, nitric oxide does not result from a direct redox reaction with iron.

Scheme 1.5B: $2HONO \rightleftarrows NO + NO_2 + H_2O$

$Fe^{2+} + NO_2 \rightarrow Fe^{3+} + NO_2^-$ (rate limiting step)

$NO_2^- + H^+ \rightarrow HONO$

Bonner and Pearsall (121) have examined the oxidation of $Fe^{2+}(aq)$ by nitrite in acetate-buffered aqueous solutions. Their results indicate that nitrite is sequentially reduced to NO (reaction 1.29), N_2O (reaction 1.30), and eventually N_2.

$$Fe^{2+}(aq) + NO_2^- + 2H^+ \rightarrow Fe^{3+}(aq) + NO + H_2O \qquad (1.29)$$

$$2Fe^{2+}(aq) + 2NO + 2H^+ \rightarrow 2Fe^{3+}(aq) + N_2O + H_2O \qquad (1.30)$$

N_2O is not produced below pH 4 and the threshold for production of N_2 was found to occur at pH 8.

Production of N_2O involves N-N bond formation which Bonner and Pearsall (121) found involves dimerization of the monomeric precursor (HNO) (reaction 1.31).

$$2HNO \rightarrow NNO + H_2O \qquad (1.31)$$

In a later study (122), it was suggested that the oxidation of Fe^{2+} by NO involves a ferrous intermediate having linear and bent nitrosyl groups arranged in a <u>cis</u> geometry (Scheme 1.6).

Scheme 1.6: $Fe^{2+}(aq) + 2NO \rightarrow$ 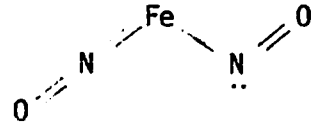

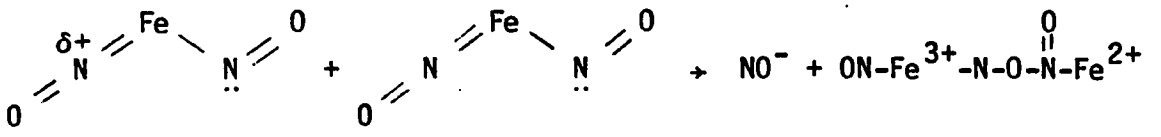

$$ON\text{-}Fe^{3+}\text{-}N\text{-}O\text{-}\overset{O}{\overset{\|}{N}}\text{-}Fe^{2+} \rightarrow (FeNO)^{2+} + Fe^{3+} + 2NO$$

$$2NO^- + 2H^+ \rightarrow N_2O + H_2O$$

Kinetic studies of the reaction of nitrite with hemoglobin were reported by Doyle et al. (123). Treatment of deoxyHb (Hb) with nitrite under strict anaerobic conditions yielded a mixture containing 72% metHb (Hb^+) and 28% HbNO. The reaction rate exhibits a first order dependence on $[NO_2^-]$ and a first order dependence on $[H^+]$. At pH 7 and 25°C, the observed second order rate constant has a value of 2.69 $M^{-1}s^{-1}$. Scheme 1.7 describes the mechanism that was proposed for the oxidation of deoxyHb by nitrite.

Scheme 1.7: $H^+ + NO_2^- \rightleftarrows HONO$

$Hb + HONO \rightarrow Hb^+ + NO + OH^-$ (rate-determining)

$Hb + NO \rightarrow HbNO$

According to Scheme 1.7, equal amounts of Hb^+ and HbNO should be produced. Two possible explanations were offered to rationalize the observed yields of metHb and HbNO. First of all, conversion of NO to N_2O would reduce the amount of nitric oxide available to bind to deoxyHb. A

second explanation, summarized in Scheme 1.8, is that the dimer of NO oxidizes deoxyHb to metHb.

Scheme 1.8: $2NO \rightleftarrows (NO)_2$

$$2Hb + (NO)_2 + 2H^+ \rightarrow 2Hb^+ + N_2O + H_2O$$

3. Iron-nitrosyl compounds

Nitric oxide adducts have been prepared with nearly all of the first period transition metal elements. To systematize the structural types, Enemark and Feltham introduced a notation which classifies complexes according to the number of valence electrons (124). According to this system, the nitrosyl complexes of iron(II) are designated as $\{FeNO\}^7$ and those of iron(III) as $\{FeNO\}^6$. For iron(II), both low-spin (S=1/2) and high-spin (S=3/2) nitrosyl compounds are known, while for iron(III), only diamagnetic, low-spin (S=0) compounds have been prepared. To establish the oxidation and spin state for these compounds, EPR and ^{57}Fe= Mossbauer spectroscopy have been used (Tables 1.21 and 1.22).

Low-spin (S=1/2) $\{FeNO\}^7$ complexes have g-values ranging between 2.1 and 1.8, whereas S=3/2 $\{FeNO\}^7$ complexes have g-values near 4.0 and 2.0. Nitric oxide complexes with iron(III) are EPR-silent (Table 1.21). The first five compounds listed in Table 1.22 belong to the class of S=3/2 $\{FeNO\}^7$ compounds. All of these compounds exhibit isomer shifts between 0.44 mm/s and 0.68 mm/s. The S=1/2 $\{FeNO\}^7$ class of compounds have isomer shifts between -0.07 and 0.28 mm/s.

Table 1.21. EPR g-values for S = 1/2 and S = 3/2 $\{FeNO\}^7$ compounds[a]

Compound	g_x	g_y	g_z	Reference
		S = 3/2		
Fe(EDTA)NO	4.1	3.95	2.0	125
$Fe(TMC)NO^{2+}$	3.87		2.09	92
PMO.NO	4.16 4.09	3.89 3.98	2.0 2.0	126
4,5-PCD.NO	4.09	3.91	2.00	127
SLO.NO	4.0	3.75	2.0	128
		S = 1/2		
Fe(II)Blm.NO	2.04	2.008	1.976	129
Hb(II)NO	2.065	2.005	2.01	130
cyt P450.NO	2.073	2.009	1.976	131
HRP.NO	2.08	2.004	1.955	132
CPO.NO	2.082	2.004	1.955	133
catalase.NO	2.050	2.003	1.970	132
LPO.NO	2.070	2.004	1.958	132

[a]Putidamonooxin (PMO); protocatechuate dioxygenase (PCD); soybean lipoxygenase (SLO); bleomycin (Blm); horseradish peroxidase (HRP); chloroperoxidase (CPO); lactoperoxidase (LPO); tetramethylcyclam (TMC).

Table 1.22. Mossbauer parameters for S = 1/2 and S = 3/2 $\{FeNO\}^7$ compounds[a]

Derivative	δ (mm/s)	ΔE_q (mm/s)	T (K)	Reference
	S = 3/2			
Fe(salen)NO	0.440	0.352	275	134
$Fe(TMC)(NO)^{2+}$	0.46	0.53	300	135
Fe(5-Cl-salen)NO	0.653	0.575	77	134
Fe(EDTA)NO	0.66	1.67	4.2	127
PMO.NO	0.68	1.40	4.2	136
	S = 1/2			
$Fe(CN)_5NO^{3-}$	-0.07	-1.25	195	137
$Fe(Me_2[14]tetraenatoN_4)NO$	0.14	2.14	r.t.	138
Hb(II)NO	0.2	1.5	4.2	139
$Fe(Me_2[15]tetraenatoN_4)NO$	0.21	1.86	r.t.	138
$Fe[S_2C_2(CN)_2]_2NO$	0.21	0.97	77	137
$Fe(S_2CNMe_2)_2NO$	0.28	0.89	~300	137
Fe(salen)NO	0.281	1.950	4.2	134

[a]Putidamonooxin (PMO); room temperature (r.t.).

Solid samples of the nitrosyl adducts of $Fe(TMC)^{2+}$ (135) and Fe(salen) (134) undergo a reversible, temperature-induced spin-state transition which was followed by Mössbauer spectroscopy. For both compounds, an abrupt transition occurs near 175 K that corresponds to conversion from the high-spin (S=3/2) compound to the low-spin (S=1/2) derivative. X-ray crystal structures show that the salen compound is five-coordinate with a bent MNO unit in both spin states (LMNO is 147° in the S=3/2 form and 127° in the S=1/2 state). In contrast, the TMC derivative has a nearly linear MNO unit (LMNO is 177° at 298 K). Upon lowering the temperature to 35 K, only slight broadening of the ν(N-O) band is observed, which indicates that the nearly linear geometry is retained in the S=1/2 spin state.

NO ligands having linear and bent MNO geometries are often described as NO^+ and NO^- ligands, respectively. Valence bond representations of these two modes of coordination are shown below and a molecular orbital description is shown in Fig. 1.24.

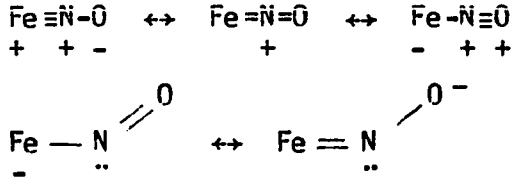

For a linear metal-nitrosyl (Fig. 1.24A), the σ-bonding interaction arises from overlap of an sp hybrid orbital of NO^+ with the d_{z2} metal orbital. Back-donation from the d_{yz} metal orbital into one of the vacant π^* orbitals of NO^+ results in a π-interaction. A second π-bond may

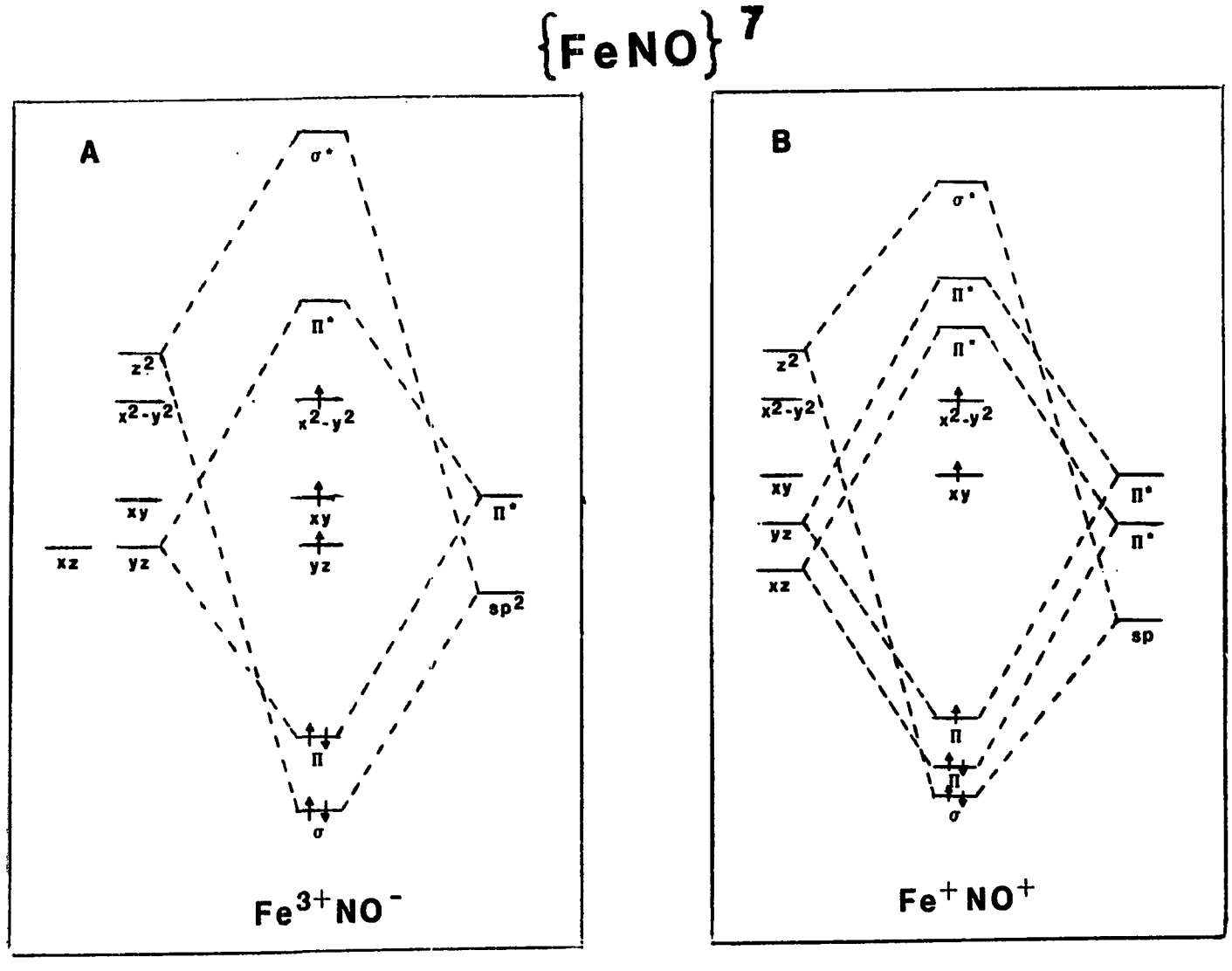

Figure 1.24. Molecular orbital diagrams for the binding of NO to iron in a linear geometry (A) or a bent geometry (B)

be formed by overlap of the metal d_{xz} orbital with the second π^* orbital. Bending of the MNO unit decreases the extent of the π-interactions. Thus, for a bent metal-nitrosyl compound (Fig. 1.24B), there is a σ-bond formed from the overlap of an sp^2 hybrid orbital on NO^- with the metal d_{z2} orbital and a π-bond formed from overlap of the empty π^* orbital of NO^- with the metal d_{yz} orbital.

Linear M-N-O groups exhibit N-O stretching frequencies in the range of 1650-1900 cm^{-1} and, based on x-ray crystallography, these have MNO angles ranging between 165° and 180° (Table 1.23) (140). The N-O stretching frequencies for compounds having bent M-N-O moieties range between 1525 cm^{-1} and 1690 cm^{-1} and have MNO angles between 120° and 140° (Table 1.23) (140).

While the N-O stretching frequency is most often used to differentiate linear and bent geometries (124), the valence bond representations shown above indicate that ν(M-NO) and δ(M-N-O) should also be sensitive to the coordination geometry of the MNO unit. The MNO stretching and bending modes are considerably less intense in the infrared spectra than the N-O stretching mode and these appear in a frequency region where strong bands of other ligands are often found. For these reasons, values for ν(M-NO) and δ(M-N-O) have been reported for only a few compounds (Table 1.23).

By IR and NMR spectroscopies, a facile equilibrium (reaction 1.32) has been observed between linear and bent geometries for solutions of $Ir(NO)(\eta^3\text{-}C_3H_5)(PPh_3)_2^+$ in either CH_2Cl_2 or CH_3CN (141).

Table 1.23. ν(M-NO) and δ(M-N-O) modes for linear and bent {MNO}^{6} and {MNO}^{7} compounds[a]

Compound	ν(M-NO)	$\Delta\nu$ (cm^{-1})	δ(M-N-O)	$\Delta\delta$	L(MNO) (deg.)	Reference
		{FeNO}^{7}				
$Fe(DMDTC)_2NO$	563	-4	106 46	-4 -3	173	142
$Fe(DAS)_2(NO)Br^+$	455	-3	570	-15	148	142
$Fe(DAS)_2(NO)(NCS)^+$	463	-5	580	-15	159	142,143
MbNO	n.o.[b]		554	-9	145	144
Fe(Por)NO	480					145[c]
		{FeNO}^{6}				
$Na_2[Fe(CN)_5NO]$	496		663		177	146
$K_2[Fe(CN)_5NO]$	652 548		665 716			147[d] 147[e]
$Fe(DMDTC)_2(NO)I$	621 550	-4 -4	565 542	-14 -12	175	142
Mb^+NO	595	-6	573	-11		144

[a]Horseradish peroxidase (HRP); dimethyldithiocarbamate (DMDTC); o-phenylenebis(dimethylarsine) (DAS); ferric myoglobin (Mb^+); ferrous myoglobin (Mb); frequency difference between the ^{15}N-enriched compound and the ^{14}N-compound for the M-NO stretching mode ($\Delta\nu$) and the M-N-O bending mode ($\Delta\delta$).

[b]n.o. = not observed.

[c]Five-coordinate nitrosyl heme ester.

[d]Band at 462 cm^{-1} is assigned as $\nu(Fe-C_{ax})$; ground state assignments.

[e]Excited state in which, based on the value of ν(N-O), the M-N-O group is presumed to be bent.

Table 1.23. Continued

Compound	ν(M-NO)	$\Delta\nu$ (cm^{-1})	δ(M-N-O)	$\Delta\delta$	L(MNO) (deg.)	Reference
$HRP^{+}NO$	604	-6	574	-10		144
$HbA^{+}NO$	594		~554			144
NO adducts with metals other than Fe						
$Co(NO)(en)_2(ClO_4)^{+}$	494		568		138	142
$Co(NO)(DAS)_2Br^{2+}$	371		542		132	142
$Co(NO)(DAS)^{2+}$	491		506		178	142
$K_2[RuCl_5(NO)]$	340		583			146
$K_2[RuBr_5(NO)]$	300		569			146
$K_2[RuI_5(NO)]$	291		558			146
$K_2[Ru(CN)_5(NO)]$	420		633			146

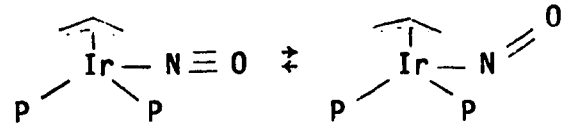

(1.32)

The isomer with the bent MNO unit crystallizes when BF_4^- is the counterion [LIrNO = 129(1)°]. From the N-O stretching frequency (1763 cm^{-1}), the isomer that crystallizes when PF_6^- is the counterion was shown to have a linear MNO group. The crystal structure of the linear isomer was not reported.

In addition to the five and six coordinate nitric oxide adducts, a number of four coordinate M-NO compounds have been prepared (148). Compounds having more than one NO ligand per metal are also known (148). However, in light of the discussion of the active site structure of Hr (section I.B.1), it is not likely that Hr would form a nitrosyl complex having either of these structural types.

Binuclear iron nitrosyl complexes, on the other hand, may be structurally relevant for Hr. For the known examples, both bridging and terminal NO geometries have been observed (Fig. 1.25). The mercaptide bridged dimer (149,150) formally contains a metal-metal single bond and two low-spin ferric ions. The cyclopentadienyliron dimer (151), on the other hand, has two bridging NO ligands, a metal-metal double bond, and is a neutral compound. The thioester derivative (152) has two terminally bound NO ligands per metal, a metal-metal single bond, and pseudotetrahedral coordination around each metal.

The ability of NO to bind to a metal in either a linear or a bent geometry is important to understanding the reactivity exhibited by

A

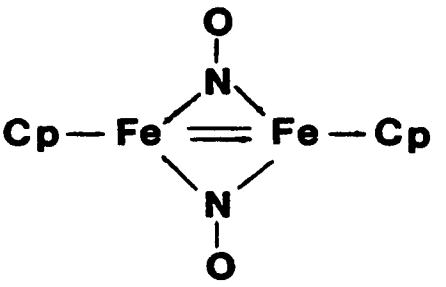

B

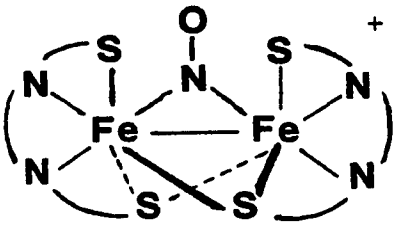

C

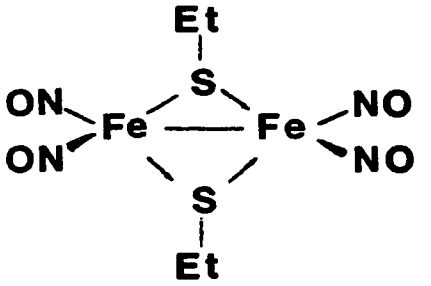

A. $[Fe(cp)NO]_2$
B. $[(FeL)_2NO]^+$ where L = N,N'-diethyl-N,N'-bis(β-mercaptoethyl)ethylenediamine
C. $[Fe(SEt)(NO)_2]_2$

Figure 1.25. Structures of binuclear iron nitrosyl compounds

metal-nitrosyl compounds. The linear nitrosyl group readily undergoes nucleophilic attack at the nitrogen center while compounds with bent nitrosyl ligands frequently undergo electrophilic attack at nitrogen.

Metal-nitrosyl complexes are stable with respect to "free" NO. For the mononitrosyl compound, $Fe(H_2O)_5NO^{2+}$ the stability constant was reported to be 0.634 atm^{-1} (25°C, pH 0.5-3.3, μ = 2.20 M) which compares favorably with the value of 0.63 atm^{-1} that was determined from kinetic studies (k_{on} = 6.2 x 10^5 $M^{-1}s^{-1}$; k_{off} = 1.4 x 10^3 s^{-1}; K_{assoc} = 440 M^{-1} (122). For comparison, the association constant (K_{assoc}) for the binding of NO to sperm whale Mb is 1.4 x 10^{11} M^{-1} (153).

4. Coordination of nitrite to metal complexes

A variety of coordination geometries have been observed for metal-nitrite compounds (154). Nitrite can coordinate either via nitrogen to form a nitro complex or via oxygen to form a nitrito complex. The nitrito form is usually less stable and tends to isomerize to the nitro form (reaction 1.33). For example, in chloroform an equilibrium is established between the nitro and nitrito isomers of Ni(N,N-dimethyl ethylenediamine)$_2$(NO_2)$_2$ (155).

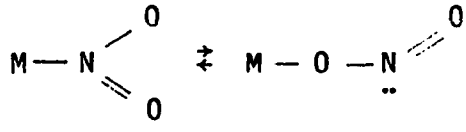

nitro nitrito

Both the cis and trans isomers of $Fe(NO)(NO_2)[S_2CNMe_2]_2$, compounds in which nitric oxide and nitrite simultaneously coordinate to iron,

were prepared by Ileperuma and Feltham (156). By x-ray crystallography, it was shown that nitrite is coordinated through nitrogen in the cis isomer. By infrared and ^{1}H-NMR spectroscopies, it was established that nitrite also coordinates through the nitrogen atom in the trans isomer.

Complexes in which nitrite is a bidentate ligand have also been reported. These compounds may be either mononuclear (structure I) or polynuclear (structures II through V in Fig. 1.26). The type III structure is the only one of these for which no examples have yet been characterized.

The complexes having the overall composition of $[Ni(en)_2(NO_2)]X$ demonstrate the great versatility in the coordination mode adopted by the nitrite ligand. Merely changing the counterion produces distinctly different coordination complexes. Thus, complexes with X^- = Cl^-, Br^-, I^-, or NO_3^- have been shown to have type I coordination (157). With X^- = ClO_4^-, BF_4^-, PF_6^-, or I_3^-, linear chains occur within which type II coordination is observed for nitrite (158). With X^- = BPh_4^-, discrete binuclear clusters form rather than linear chains (157). One nitrite ligand exhibits type IV coordination in which a single oxygen atom bridges the metals. The second oxygen then chelates to one nickel center. A second nitrite ligand is coordinated as a monodentate nitrito group.

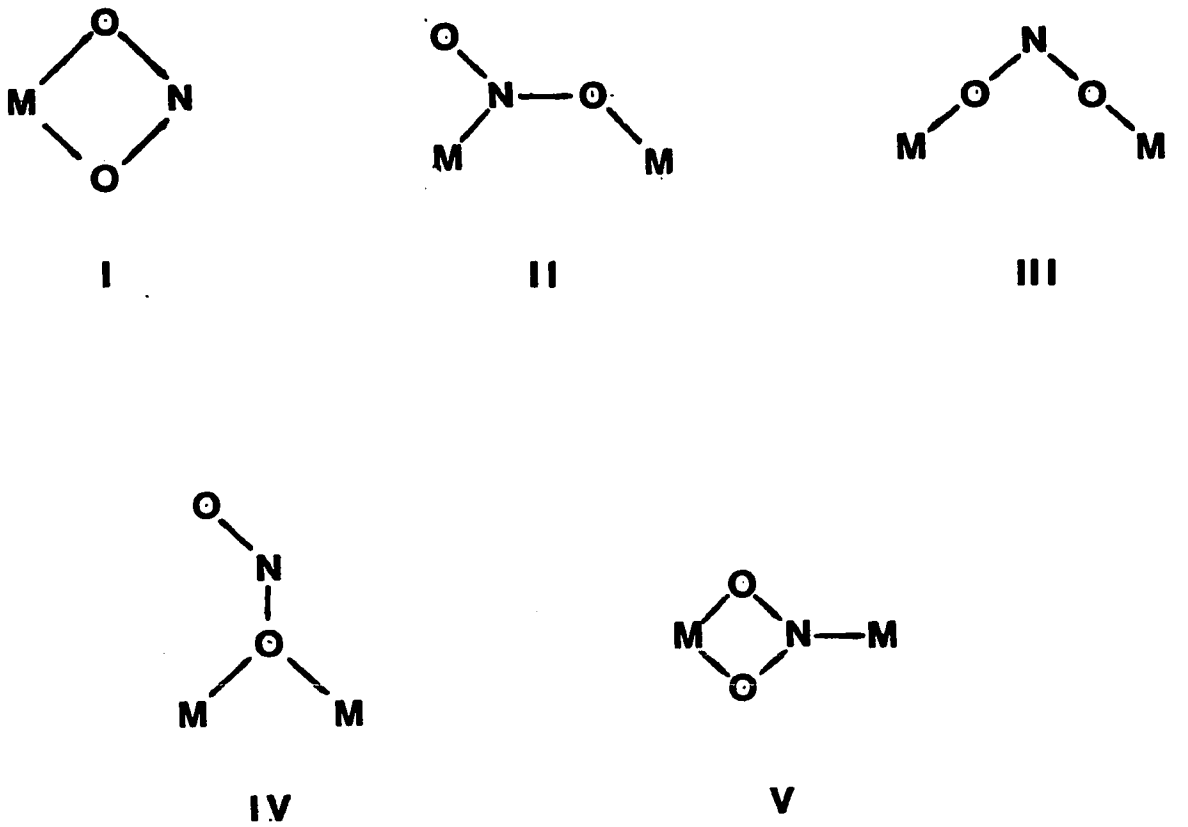

Figure 1.26. Bidentate coordination modes for the nitrite ligand

II. EXPERIMENTAL WORK

A. Instrumentation

1. Optical spectra

Optical spectra were obtained using either a dual-beam Perkin-Elmer 554 spectrophotometer or a single-beam Perkin-Elmer Lambda-Array 3840 UV/Visible spectrophotometer. For air-stable samples, 1 cm pathlength quartz cells were used. A 1 cm pathlength quartz cell equipped with a teflon-stoppered vacuum attachment was used for anaerobic work. Samples (1 ml) were added under argon via gas-tight syringes through the double-septum seals (159). Typical concentrations were 0.1-0.3 mM for metHr samples, or 0.2-0.5 mM for deoxyNO samples, where concentrations are based on dimeric iron sites.

2. EPR spectra

A Bruker ER-220D spectrometer equipped with an Oxford Instruments ESR-10 helium flow system was used to obtain X-band EPR spectra. Early work employed a dual cavity set-up as a single cavity. Later studies used a single cavity. Except for improved sensitivity, no differences were observed between spectra obtained with the two cavities.

All samples were contained in quartz tubes (Heraeus-Amersil, Inc., in Sayreville, NJ) with a 4 mm outer diameter and 3 mm inner diameter. Minimum tube lengths of 8 inches were required. The samples (100-200 µl) were injected into the septum-capped tubes under argon via gas-tight syringes. After freezing the samples in liquid nitrogen, the tubes were evacuated, flame-sealed under vacuum, and then stored at 77 K. Sample concentrations typically ranged from 1.0 to 2.0 mM.

Spectra were collected at 4.5 ± 0.5 K, unless otherwise stated. A modulation amplitude of 16 G at 100 kHz was used for semi-met samples and 40 G for the nitric oxide derivatives. Nonsaturated signals were obtained with power inputs of 100 μW (semi-met derivatives) and 40 μW (nitric oxide derivatives). Scan times were typically 200 sec with the time constant set at 0.10 or 0.20 sec.

Power saturation curves were obtained prior to quantitation of the signals. The variation of the signal intensity as a function of the power input is described by Eq. 2.1.

$$\log(S/P^{1/2}) = a - b/2 \log(P_{1/2} + P) \qquad (2.1)$$

Here, S represents the normalized signal intensity and P is the power expressed in mW (160-162). The signal intensity is the measured height from peak to trough at a single g-value (Fig. 2.1). This intensity, measured for a series of spectra recorded with a range of powers, is normalized and then divided by $\sqrt{P}$. The half-saturation point, $P_{1/2}$ is then obtained by plotting $\log(S/P^{1/2})$ versus log P. When the signal is not saturated (i.e., $P < P_{1/2}$), Eq. 2.1 takes the form of a line with zero slope. The signal saturates when the input power exceeds the half-saturation limit (i.e., $P > P_{1/2}$) and, in this case, Eq. 2.1 plots as a line whose slope is -b/2. The intersection of these two lines yields the value for $P_{1/2}$. To determine $P_{1/2}$, the points in the saturated region were fit by least-squares analysis to the best line. Points lying

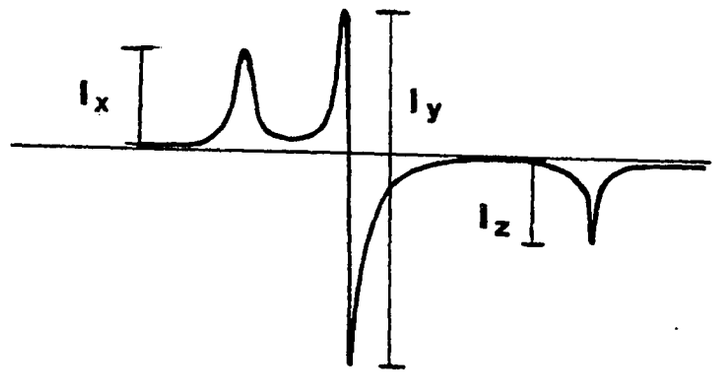

Figure 2.1. EPR spectrum for an S = 1/2 center having rhombic symmetry

in the nonsaturating region were averaged. Finally, the point of intersection of these two lines, $P_{1/2}$, was calculated.

For relaxation by an Orbach process (163), Eq. 2.2 describes the temperature dependence of the saturation behavior of an EPR signal.

$$\ln P_{1/2} = \ln A - (\Delta/k)(1/T) \tag{2.2}$$

The value of Δ is a measure of the energy separation between the ground state and the first excited state. For a binuclear center, this energy difference is a function of both the zero-field splitting energy, D, and the antiferromagnetic exchange coupling energy, J. Experimentally, the value of Δ was determined from the slope of a plot of $\ln P_{1/2}$ vs. $1/T$.

Signals to be quantitated were recorded with nonsaturating powers. Quantitation was achieved by comparing the signal intensity to that of a $CuSO_4 \cdot 5\ H_2O$ standard of similar concentration recorded with identical instrumental settings. Equation 2.3 was used for this purpose.

$$N_x = \frac{[(G_s)(P_s)^{1/2}(M_s)(W_s)(g_p)_s](A_x)(h_x)(2^{is})_x}{[(G_x)(P_x)^{1/2}(M_x)(W_x)(g_p)_x](A_s)(h_s)(2^{is})_s} N_s \tag{2.3}$$

Here, x represents values for the sample and s represents values for the standard. N is the molar concentration, G is the receiver gain, P is the input power expressed in Watts, M is the modulation amplitude in Gauss, W is the sweep width in Gauss used to calculate the integrated area, A is the integrated area (generated by the EPR spectrometer's

computer), h is the measured height of the integral, and IS is a scaling factor representing the number of times that the data was divided by two in order for the computer to calculate the integrated area. The g_p term (164) accounts for the difference in the weighted-average g-value of the sample compared to the standard and it is determined according to Eq. 2.4.

$$g_p = 2/3[1/3(g_x^2 + g_y^2 + g_z^2)]^{1/2} + 1/9(g_x + g_y + g_z) \quad (2.4)$$

Typically, each signal was integrated 3-5 times and the average value was reported. Reproducibility of the integrated areas was within 10-15% for most samples.

3. ^{57}Fe-Mössbauer spectra

^{57}Fe-Mössbauer spectra were collected in the laboratory of Professor Peter Debrunner in the Department of Physics at the University of Illinois in Champaign-Urbana. A constant acceleration spectrometer equipped with a variable temperature cryostat was used. Velocities are reported relative to Fe metal at 300 K. Due to the low abundance of ^{57}Fe in the samples, scans were accumulated for several days at either 100 K or 4.0 K. A small magnetic field (320 G) was routinely applied.

Spectra were recorded of deoxyNO prepared both as crystalline suspensions and as frozen solutions. Either oxyHr or deoxyHr was used as the starting material for preparing the samples of deoxyNO. Samples were drawn up into a gas-tight syringe and transferred to cylindrical nylon cups (1/2" or 5/8" diameter), frozen immediately in liquid nitro-

gen and shipped either on dry ice or in a biological shipper at liquid nitrogen temperature.

For deoxyHr, crystalline samples were used to obtain the ^{57}Fe-Mössbauer spectra. A concentrated frozen solution was used to obtain the Mössbauer spectrum of deoxyF$^-$NO. The sample was prepared as described in section II.C.3, then concentrated using an Amicon cell equipped with a PM-30 membrane.

4. Resonance Raman spectra

Resonance Raman spectra were obtained at the Oregon Graduate Center in Beaverton, Oregon. The instrument used was a computer-interfaced Jarrell-Ash spectrometer. A Spectra-Physics 164-05 argon ion laser was used to produce monochromatic red light (647.1 nm). The scattered light was detected on an RCA C31034 photomultiplier tube and processed in an ORTEC Model 9302 amplifier/discriminator. 180° back-scattering geometry was used.

Spectra were collected at 77 K, unless stated otherwise. To maintain this temperature, the samples were kept in a liquid nitrogen cold-finger having a transparent window (10). The incident light (70-120 mW) was focused through a slit width of 0.25 mm upon samples (50 μl) in open-ended capillary tubes (1.5-1.8 x 90 mm) sealed with either Apiezon-N grease or Dow-Corning sealant. An excitation frequency of 647.1 nm was chosen because of the high degree of sample fluorescence at shorter wavelengths and because this frequency is within an absorption band of the samples. Multiple scans were collected at a rate of 2 cm^{-1}/s. Sulfate was used as an internal frequency marker [$\nu(S-O) = 448\ cm^{-1}$].

The temperature dependence of the resonance Raman spectrum of deoxyNO in D_2O was investigated. Spectra were accumulated at several temperatures between 77 K and 249 K.

A curve-fitting procedure was used to determine the peak positions and areas in the resonance Raman spectra. Unless otherwise stated, the peaks were fit with widths at half-height of 18 cm^{-1} using a 10% Gaussian/90% Lorentzian shape model.

The integrity of a deoxyNO sample subjected to laser irradiation was tested by obtaining the EPR spectrum both before and after the sample was exposed to intense monochromatic irradiation. For this experiment, an EPR tube containing the sample was immersed in a liquid nitrogen bath. Red light (619.5 nm) from an argon ion laser was focused through a quartz window onto the sample for 65 min at a power output of 70 mW.

To determine theoretical isotopic shifts for the ν(Fe-NO) stretching vibration, the diatomic oscillator model was used (165).

B. Preparation of Reagents and of Hemerythrin and Myoglobin in Their Various Oxidation Levels

1. Preparation of nitric oxide

Four methods were used in the delivery of nitric oxide into reaction mixtures:

(i) Direct addition of purified NO(g).

(ii) Addition of aliquots of a saturated aqueous stock solution of nitric oxide.

(iii) Generation of NO by reduction of sodium nitrite.

(iv) *In situ* dissociation of NO from metal-containing nitrosyl transfer agents.

Nitric oxide (99.0% minimum purity) was obtained from Matheson Gas Products. This was passed through a 1.0 M sodium hydroxide solution to remove trace impurities (NO_2 and N_2O_3). Aliquots of gas were withdrawn from above the OH^- solution with a gas-tight syringe and injected into the reaction mixture.

Saturated stock solutions of NO were prepared by bubbling the purified gaseous NO through buffered aqueous solutions for at least 30 minutes. The buffer had previously been made anaerobic by bubbling argon through it for a minimum of 30 minutes. Solutions were buffered using phosphate (pH 6-7), Tris-sulfate or Tris-perchlorate (pH 7.5-8.5), or acetate (pH 3-5). At 20°C, NO has a solubility of 1.9 mM (112).

The third method was used when preparing ^{15}N-enriched samples of NO. Sodium ^{15}N-nitrite from MSD Isotopes had a chemical purity of 91% and contained 99 atom-% ^{15}N. Sodium dithionite, hydroxylamine sulfate, or an acidic solution of ferrous sulfate can be used to reduce nitrite. However, with these reductants, a mixture of NO and N_2O results. Contamination with N_2O was minimal with L-ascorbic acid and, thus, this reducing agent was used most frequently.

In a typical experiment, 3 ml of a 0.1 M anaerobic solution of L-ascorbic acid in 50 mM phosphate (pH 6.5) was transferred with a gas-tight syringe to a degassed vial containing a measured amount of solid sodium nitrite (21 mg). Nitrite was employed as the limiting reagent and the amount used was such that the solubility limit of NO would be

exceeded. The gas above the solution was used, without purification, immediately after adding the ascorbate solution in order to keep the production of contaminating gases at a minimum.

With the fourth method, the nitrosyl transfer agents used were $Co(dmgH)_2NO{\cdot}MeOH$ and $[Co(NH_3)_5NO]Cl_2$. The dimethyl-glyoximate compound was provided by Mike Doyle. The pentammine reagent was prepared according to the method of Moeller and King (166). Black crystals of the product were obtained in a 12.2% yield. The reactions of these compounds that result in release of NO are described in section III.D.1.

2. Assay of aqueous solutions of NO

To ascertain the stability of the saturated NO solutions, the stock solution was reacted with an acidic (pH 3-6.5) solution of Fe^{2+}(EDTA) after various decomposition periods. Fe^{2+}(EDTA) was prepared by dissolving $FeSO_4{\cdot}7\ H_2O$ or $FeCl_2{\cdot}4\ H_2O$, and Na_2(EDTA) (1 mol Fe^{2+}:10 mol EDTA) in degassed buffer under argon. Stock solutions of nitric oxide were prepared as described above. To assay the solution, aliquots of the Fe^{2+}(EDTA) and NO(aq) solutions were combined to give a final solution that was equimolar in iron and NO. Samples were frozen immediately for observation by EPR. The incubation time of the NO(aq) solution was varied from less than one minute to approximately one hour.

Control experiments were performed in which Fe^{2+}(EDTA) was reacted separately with gaseous NO and with sodium nitrite. By one method, gaseous NO was injected directly into an anaerobic solution of Fe^{2+}(EDTA) (5.0 mM). In the second method, NO(g) was injected into anaerobic phosphate buffer (50 mM, pH 6.5). An aliquot of this solution

was mixed with an aliquot of a 5.0 mM solution of Fe^{2+}(EDTA) such that equimolar amounts of NO and Fe^{2+} were present and that the concentration of NO was less than 1.9 mM (the aqueous solubility limit for NO). The reaction of nitrite with Fe^{2+}(EDTA) was initiated by diluting an anaerobic stock solution of 5.0 mM Fe^{2+}(EDTA) with an anaerobic stock solution of 50 mM sodium nitrite. A two-fold molar excess of nitrite over Fe^{2+} was employed. The products of both reactions were characterized by their optical and EPR spectra.

3. Isolation and purification of hemerythrin

The procedure used in the isolation and purification of cellular Hr was adapted from the original procedure of Klotz et al. (167). Live worms of the species Phascolopsis gouldii were obtained from Marine Biological Laboratories in Woods Hole, Massachusetts. Three hundred worms were slit lengthwise and the coelomic fluid was collected in a porcelain evaporating dish, kept cooled on ice. From this point on, the preparations were carried out in a cold box refrigerated at 4°C. After settling overnight, the coelomic fluid was filtered through cheesecloth. The sediment was rinsed with artificial sea water (aquarium salts equilibrated in deionized water). Next, the filtrate was centrifuged and the fatty layer was removed with a Pasteur pipette. This step was repeated several times, each time resuspending the cells in sea water, until the fatty layer was no longer visible.

To isolate Hr, the cells were lysed overnight in 2.5 times their volume of deionized water. The cell debris was removed by two one-hour centrifugations at 15,000 rpm. Dialysis against several changes of a

15% ethanol/H_2O mixture produced burgundy-colored crystals of oxyHr which were stored in glass containers at 4°C. With the more recent preparations, the crystals were centrifuged, the mother liquor was discarded and the crystals were frozen and stored in liquid N_2 until needed. Storage in liquid nitrogen did not alter the reactivity of Hr, although it does impede the auto-oxidation process.

OxyHr isolated from Themiste dyscritum was provided as a 1.68 mM solution by Professor Joann Sanders-Loehr at the Oregon Graduate Center in Beaverton, Oregon.

4. Preparation of hemerythrin in its various oxidation levels

a. DeoxyHr Solutions of deoxyHr were prepared from oxyHr by scavenging O_2 with sodium dithionite (BDH Laboratories, 85% minimum purity). Crystals of oxyHr were dissolved in buffer, usually at pH 7.5, to a final concentration near 1-2 mM. These solutions were dialyzed against 5-15 mM $S_2O_4^{2-}$ in deaerated buffer. OxyHr is reduced to deoxyHr within an hour under these conditions. However, because oxyHr solutions are rarely free of metHr, dialysis was allowed to proceed overnight to assure complete reduction of the slower reacting metHr. Occasionally, the solution retained a pale yellow color, which even prolonged dialysis against dithionite at room temperature would not completely remove. Excess dithionite was removed by anaerobic dialysis against several changes of buffer. Once deoxygenated, the dialysis bags of deoxyHr could be stored at 4°C for several weeks in rigorously deaerated buffer.

When concentrations of deoxyHr in excess of 2 mM were desired, the ionic strength of the buffer solution was increased to 0.3 M by adding

Na_2SO_4 or H_2SO_4 prior to adjustment of the pH. Higher ionic strength enhances the solubility of both oxyHr and deoxyHr.

After removing the excess dithionite, crystals of deoxyHr could be prepared by dialyzing the deoxyHr solution (>2 mM and containing 0.3 M SO_4^{2-}) against deionized water. This lowering of the ionic strength of the solution usually lead to formation of white needle-like crystals of deoxyHr. Sometimes lowering the pH facilitated crystallization, owing to the decreased solubility of deoxyHr below pH 7. Best results were obtained when dialysis was allowed to proceed without stirring of the dialysate.

Solutions of deoxyHr were transferred anaerobically from the dialysis bag into 2-dram glass vials using the following procedure. The glass vial was placed in a 50 ml 24/40 Schlenk-type flask. The flask, sealed with a rubber septum, was then alternately degassed and flushed with argon several times. The septum was removed and, with a steady stream of argon flowing in from the sidearm, the dialysis bag was cut open and drained into the glass vial. The vial was then quickly capped with a septum and placed under argon on the vacuum line.

The concentration of deoxyHr was determined spectrophotometrically by air oxidizing an aliquot of the stock solution. The optical spectrum of oxyHr has ε_{330} = 6800 $M^{-1}cm^{-1}$, ε_{360} = 5450 $M^{-1}cm^{-1}$, and ε_{500} = 2200 $M^{-1}cm^{-1}$ (43). The concentrations determined from all three wavelengths were usually within 5% of each other and the average value was used.

b. OxyHr OxyHr was either used as isolated or prepared by oxygenating solutions of deoxyHr.

c. MetHr MetHr was prepared according to a procedure adapted from that of Keresztes-Nagy and Klotz (168). A slight molar excess of potassium ferricyanide was added to a buffered solution of oxyHr. Reaction was allowed to proceed at room temperature for several hours. Excess ferricyanide and ferrocyanide produced during the reaction were removed by dialysis against several changes of buffer at 4°C.

Concentrations of metHr solutions were determined spectrophotometrically from the absorption spectrum of metN$_3^-$ (ε_{326} = 6750 $M^{-1}cm^{-1}$, ε_{380} = 4300 $M^{-1}cm^{-1}$, and ε_{446} = 3700 $M^{-1}cm^{-1}$) (43). A 10-fold or greater molar excess of recrystallized sodium azide (Eastman Kodak) was added to metHr either as a solid or from a concentrated stock solution. Approximately 15 minutes (several hours when ClO_4^- was present) were allowed for the reaction with azide to be completed.

d. (Semi-met)$_R$ (Semi-met)$_R$ was prepared by the one-electron reduction of metHr with sodium dithionite. First, a stock solution of sodium dithionite was prepared by dissolving a weighed amount of $Na_2S_2O_4$ in argon-saturated buffer. MetHr was made anaerobic by several cycles of evacuating and flushing with argon. After the dithionite was standardized (as described below), one reducing equivalent was added to metHr, producing (semi-met)$_R$ within 1-2 minutes. Because of its instability with respect to disproportionation, (semi-met)$_R$ was used within 5 minutes after preparation.

To standardize the dithionite solution, a limiting amount of dithionite was reacted with $Fe(CN)_6^{3-}$. From the difference in the absorbance at 419 nm [ε_{419} = 1030 $M^{-1}cm^{-1}$ for ferricyanide (84)] before and

after addition of dithionite, the concentration of the dithionite was determined. Stock solutions of sodium dithionite ranged in concentration from 50-100 mM and 20.0 mM for potassium ferricyanide.

e. $(Semi\text{-}met)_0$ $(Semi\text{-}met)_0$ was prepared by the one-electron oxidation of deoxyHr with $Fe(CN)_6^{3-}$. Stock solutions of $Fe(CN)_6^{3-}$ were prepared from a measured amount of solid potassium ferricyanide dissolved in argon-saturated buffer and concentrations were determined either by weight or from the absorbance at 419 nm. One equivalent of ferricyanide was added via gas-tight syringe to deoxyHr of known concentration. Production of $(semi\text{-}met)_0$ was complete within 3-5 minutes and solutions of $(semi\text{-}met)_0$ were used within 5 minutes of preparation.

5. Preparation of myoglobin in its various oxidation levels

a. MetMb A 1.0 mM solution of myoglobin was made by dissolving crystalline myoglobin from sperm whale skeletal muscles (Sigma Chemicals) in 50 mM phosphate buffer (pH 7) containing 0.15 M sulfate [molecular weight = 17,800 D (169)]. Since the crystalline sample is a mixture of oxyMb and metMb, the oxyMb was converted to metMb by adding a slight stoichiometric excess of potassium ferricyanide to the buffered solution. The oxidation was allowed to proceed for 3-4 hrs at room temperature. Dialysis against several changes of buffer at 4°C removed the ferrocyanide and the unreacted ferricyanide from the Mb solution.

The concentrations of metMb were determined spectrophotometrically using $\varepsilon_{409.5} = 157\ mM^{-1}cm^{-1}$, $\varepsilon_{505} = 9{,}470\ M^{-1}cm^{-1}$, and $\varepsilon_{635} = 3{,}555\ M^{-1}cm^{-1}$ (169). Alternatively, addition of a 10-fold or greater excess

of solid sodium cyanide yields $Mb^{+}CN^{-}$ within several minutes, which has ε_{423} = 109.7 $mM^{-1}cm^{-1}$ and ε_{540} = 10.7 $mM^{-1}cm^{-1}$ (169).

b. DeoxyMb DeoxyMb was prepared from metMb by reduction with sodium dithionite. Sodium dithionite was standardized as described above. An aliquot of a stock solution of metMb was mixed with a 1-5 fold molar excess of sodium dithionite immediately before it was used. Concentrations of deoxyMb were determined from the absorbance readings at 434 nm (ε = 115 $mM^{-1}cm^{-1}$) and 556 nm (ε = 11.8 $mM^{-1}cm^{-1}$) (169).

c. NitrosylMb MbNO was prepared from deoxyMb by the addition of either limited amounts of gaseous NO or aliquots of a saturated solution of NO buffered at pH 7 with 50 mM phosphate. With a 1-2 fold molar excess of NO over Mb, quantitative production of MbNO occurs within less than 1 min. However, when larger quantities of NO are added, oxidation to metMb competes with the binding of NO to deoxyMb. Sample concentrations were determined using ε_{420} = 127 $mM^{-1}cm^{-1}$, ε_{548} = 11.3 $mM^{-1}cm^{-1}$, and ε_{579} = 10.1 $mM^{-1}cm^{-1}$ (131).

C. Preparation of Nitric Oxide and Nitrite Derivatives of Hemerythrin

1. Preparation of deoxyNO

The best preparations of deoxyNO were achieved by the direct addition of gaseous NO to solutions of deoxyHr, to solutions of oxyHr, or to crystalline suspensions of deoxyHr.

For most experiments, gaseous nitric oxide was added directly with a gas-tight syringe, in several aliquots and with rigorous shaking, to deoxyHr (1-2 mM) in 50 mM phosphate at pH 6.5. Gas volumes were estimated using the ideal gas equation and usually the mole ratio of NO to

Hr was between 1.5 and 5.0 (0.1-0.5 ml NO/1.0 ml Hr solution). Complete formation of deoxyNO was achieved within 5 minutes when the reaction was performed at room temperature.

DeoxyNO was also prepared from oxyHr in 50 mM phosphate. Prior to adding NO, the oxyHr solutions were alternately evacuated and flushed with argon to reduce the amount of free oxygen in the solution. During this procedure, only partial deoxygenation of oxyHr occurs. Nitric oxide was then added as described above. This method was convenient for preparing concentrated samples of deoxyNO, since oxyHr is more soluble than deoxyHr.

Crystalline samples of deoxyNO were prepared under argon from a crystalline slurry of deoxyHr (prepared as described above) in 50 mM phosphate (pH 6.5). One to two ml of gaseous NO was bubbled into one ml of the crystalline slurry. The slurry was then incubated for 5 to 10 minutes at room temperature before being frozen.

In addition, the following methods could be used to prepare deoxyNO from deoxyHr:

(i) Addition of an aliquot of an aqueous stock solution of NO.

(ii) Transfer of NO from either $[Co(NH_3)_5NO]Cl_2$ or $Co(dmgH)_2NO$ to deoxyHr.

(iii) Reaction with $NO^+BF_4^-$.

The reaction of deoxyHr with an aqueous solution containing NO was conducted with a slight molar excess of NO over Hr. An aliquot of the saturated stock solution of NO was mixed with a solution of deoxyHr in phosphate buffer (pH 6.5). After 1-2 minutes of mixing, EPR samples

were frozen. Samples were prepared after incubating the stock solution of NO for 1, 3, 7, 11, and 20 minutes.

DeoxyHr was combined under argon with either $[Co(NH_3)_5NO]Cl_2$ or $Co(dmgH)_2NO{\cdot}MeOH$ in phosphate buffer (pH 7.5). With the dimethylglyoximate compound, reactions were conducted with a 1.5-fold or a 3.0 fold molar excess of the nitrosylating agent which was added as an aliquot of a concentrated (5.3 mM) stock solution to a diluted solution of deoxyHr (34 μM). Slow decomposition of the dimethylglyoximate compound in aqueous solutions produces NO which then reacts with Hr. The pentaammine compound, however, decomposes rapidly in aqueous solutions. A cobalt-containing precipitate and gaseous NO are produced. For this reason, deoxyHr was added to a weighed sample of the black solid. A 40-fold excess of $[Co(NH_3)_5NO]Cl_2$ over Hr was employed. However, since the solubility of the free NO that is released is minimal (1.9 mM), the ratio of dissolved NO to Hr was only 1.8. The precipitate was separated by centrifugation and the optical spectrum of the supernatant was recorded.

Using nitrosyl tetrafluoroborate, $NO^+BF_4^-$, as a nitrosylating reagent, the reaction was carried out by the direct addition of protein to the solid reagent. A 40-50 fold molar excess of NO^+ was employed.

Reactions using protein isolated from Themiste dyscritum were conducted in 0.2 M Tris-sulfate at pH 8.0.

2. Attempts to prepare a nitric oxide adduct of deoxyHr containing magnetically uncoupled iron sites

The first attempt made to produce a magnetically uncoupled iron site involved the gradual addition of 25 μl aliquots of a 1.0 M solution

of sodium hydroxide to a stock solution of deoxyNO (1.66 mM) in pH 6.5 phosphate buffer until the pH of the solution was ~10. The contents of the reaction mixture were examined by optical spectroscopy and EPR spectroscopy.

The second method attempted to uncouple the iron site prior to adding NO. Nitric oxide was added as a tool for detecting the uncoupled sites. The reagents used in attempting to uncouple the iron site included:

(i) Protein denaturing reagents.

(ii) Anions that bind to the active site.

(iii) Anions that bind to Hr at a site other than the active site.

(iv) H^+ or OH^-.

To denature deoxyHr, either urea or guanidine hydrochloride were used. Experiments were performed at low (1.5 M) and high (6.0 M) denaturant concentrations. The deoxygenated protein was dialyzed overnight at 4°C in 1 liter of denaturant in 50 mM phosphate (pH 6.5) containing 0.3 M sulfate. To test whether or not magnetically uncoupled sites had been formed, gaseous nitric oxide was added. Samples were frozen for observation by EPR spectroscopy before and after the addition of NO.

Several additional experiments were conducted with the deoxyHr sample prepared in 6.0 M urea. The first of these involved the anaerobic addition of azide as a solid to the deoxygenated form. In the second experiment, nitric oxide was added first, followed by the anaerobic

addition of azide. In a third experiment, oxygen was bubbled into a portion of the deoxygenated solution.

Azide, cyanate, and fluoride are ligands known to promote the uncoupling of the irons within the deoxyHr site. One ml of deoxyHr in 50 mM phosphate (pH 6.5) was added to the solid reagents (0.1 mmol). After a short incubation time (typically 30 minutes to 1 hour), NO(g) was added in a 5-10 fold molar excess over Hr.

Using fluoride, the effect of incubation time was studied. For this experiment, a 45.8-fold excess of fluoride was used. The solution of deoxyF^- was equilibrated for either 8, 43, or 202 minutes prior to the addition of NO.

Azide was used to determine whether or not the production of magnetically uncoupled sites is affected by the ratio of azide to nitric oxide. One-half ml of deoxyHr (2.92 mM) was added to either 77, 172, 380, 574, or 763 µmol of solid sodium azide. After a 5 minute incubation period, a 2.7-fold molar excess of nitric oxide was added to each solution of deoxyN_3^-. Samples were frozen for observation by EPR spectroscopy both before and after the addition of nitric oxide.

An attempt was made to use sulfide to facilitate the uncoupling of the iron atoms. DeoxyHr was incubated at room temperature with a 23-fold molar excess of sulfide for either 15, 75, or 277 minutes prior to addition of NO. Sodium sulfide ($Na_2S \cdot 9\ H_2O$) was prepared as a 0.1 M stock solution in 0.5 M phosphate (pH 6.5).

For comparison, the effects of anions that have not been shown to induce magnetic uncoupling of the iron site of deoxyHr were examined.

Included among these were NaCl, NaBr, NaCN, NaNCS, and NaI. The salt of the monovalent anion (0.1 M final concentration) was added to deoxyHr in 50 mM phosphate buffer at pH 6.5. After a one-hour incubation at room temperature, gaseous NO (2 to 5 fold excess over Hr) was injected with a gas-tight syringe.

In a third experiment, anions that bind at a site other than the active site were used to attempt to magnetically uncouple the iron site of deoxyHr. The reagents studied were sodium salts of perchlorate, hexafluorophosphate, tetrafluoroborate, and tetraphenylborate. Samples were prepared by adding an appropriate volume of deoxyHr (50 mM phosphate at pH 6.5) to make the solution 0.1 M in the anion. To each of these solutions, a 2-5 fold molar excess of NO(g) was added, and samples were frozen for observation by EPR spectroscopy.

In a fourth experiment, the effects of pH on the preparation of deoxyNO was examined. Nitric oxide was added to deoxyHr prepared at pH 6.0 (50 mM Mes), pH 6.5 (phosphate), and pH 8.5 (Tris-sulfate).

3. Preparation of deoxyF⁻NO

To prepare deoxyF⁻NO, a solution of deoxyHr at pH 6.5 in phosphate buffer was added to a weighed amount of sodium fluoride to make the solution 0.1-1.0 M in fluoride. After incubating this solution at room temperature for one hour, gaseous NO was injected as it was when preparing deoxyNO. At room temperature, the reaction was complete within 5 minutes as judged by the absence of further changes in the visible absorbance. Samples could be concentrated under nitrogen using an Amicon cell equipped with a PM-30 membrane.

4. Preparation of semi-metNO_2^-

Routine preparation of semi-metNO_2^- involved addition of a 20-fold or greater molar excess of sodium nitrite to an anaerobic solution of deoxyHr in phosphate buffer at pH 6.5. Nitrite was added either via gas-tight syringe as an aliquot from a concentrated anaerobic stock solution or the degassed protein stock solution was added to a measured amount of solid sodium nitrite in a degassed vial. The reaction was allowed to proceed for at least 5 hours, at which time the completeness of the reaction was checked by the anaerobic addition of sodium azide to an aliquot of the reaction mixture. Within 5 minutes, displacement of nitrite by azide occurs. From the extinction coefficient of semi-metN_3^- at 470 nm (ε = 2400 $M^{-1}cm^{-1}$) (71), a product yield was determined. Semi-metNO_2^- prepared in this fashion is stable for at least 24 hrs. Storage at 4°C for ~1 week, however, results in production of significant amounts of metNO_2^-.

Two other reactions that result in production of semi-metNO_2^- are:

(i) the reaction of nitrite with $(\text{semi-met})_O$

(ii) the reaction of nitrite with $(\text{semi-met})_R$.

The preparation of $(\text{semi-met})_O$ and $(\text{semi-met})_R$ was described in section II.B.4. An aliquot of an anaerobic solution of sodium nitrite was injected with a gas-tight syringe into stock solutions of either $(\text{semi-met})_O$ or $(\text{semi-met})_R$ such that nitrite was present in a 20- fold molar excess. Samples were withdrawn and frozen with liquid nitrogen for observation by EPR spectroscopy.

5. Preparation of (semi-met$_R$)NO

The preparation of (semi-met)$_R$NO was best accomplished by the direct addition of a 2 to 10 fold molar excess of NO(g) via gas-tight syringe to an anaerobic stock solution of (semi-met)$_R$ in 50 mM phosphate (pH 6.5). Because of the inherent instability of (semi-met)$_R$, NO was added within 1 minute after reducing metHr with dithionite (as described above). The solution was rapidly inverted to facilitate dissolution of NO. The reaction was considered complete after 5 minutes, since no further changes in the visible absorbance occurred.

A second attempt at preparation of (semi-met)$_R$NO involved the reduction of metHr and trapping of the product with NO according to the method used by Brudvig et al. (170) with oxidized cytochrome oxidase. A 4.7-fold molar excess of NO was injected into an anaerobic solution of metHr and incubated for 10 minutes. Then, a 67-fold molar excess of sodium azide was added and the reaction was followed at room temperature for three hours.

The third preparative method, which involved the oxidative decomposition of deoxyNO, was used to prepare samples for resonance Raman spectroscopy. A stock solution of deoxyNO was allowed to auto-oxidize overnight at room temperature under argon. Addition of a 20-fold molar excess of sodium nitrite decreases the decomposition time to 10-15 minutes but increases the production of semi-metNO_2^-.

6. Preparation of (semi-met)$_0$NO

(Semi-met)$_0$ was prepared as described in section II.B.4. Three to five minutes after its preparation, a 5 to 10-fold molar excess of NO(g)

was injected. The reaction was usually performed at room temperature in 50 mM phosphate (pH 6.5) containing 0.1 M sodium perchlorate. The presence of 0.1 M ClO_4^- slows down the decomposition of $(semi\text{-}met)_O$. Five minutes after the addition of NO, no further absorbance changes occurred.

7. Preparation of $metNO_2^-$

$MetNO_2^-$ was prepared either by auto-oxidation of oxyHr with a 20-fold or greater excess of sodium nitrite or by addition of a measured excess of solid sodium nitrite to a stock solution of metHr. The latter method was used most frequently.

8. Attempts to prepare metNO

Four attempts were made to prepare a nitrosyl adduct of metHr:

(i) Direct addition of NO

(ii) Transfer of NO from $Co(dmgH)_2NO$ or $[Co(NH_3)_5NO]Cl_2$ to metHr

(iii) Reduction of $metNO_2^-$ with ascorbate

(iv) Oxidation of $(semi\text{-}met)_ONO$ with potassium ferricyanide.

NO, prepared as an aqueous stock solution or as a gas, was added to an anaerobic solution of metHr in either a stoichiometric amount or as much as a ten-fold molar excess.

The second method involved the release of NO from either $Co(NH_3)_5NO^{2+}$ or $Co(dmgH)_2NO$. Reactions were conducted with either a 1:1 ratio of nitrosyl transfer agent to metHr or with the nitrosyl transfer agent in 10 to 100 fold molar excess over metHr.

For the third method, $metNO_2^-$ was prepared by adding an anaerobic solution of metHr to a 20-fold or greater molar excess of sodium ni-

trite. After incubating the solution at room temperature for a minimum of 30 minutes, the stock solution of metNO_2^- was added in aliquots to a measured amount of L-ascorbic acid such that the reducing agent was present in excess over protein but not nitrite.

With the fourth method, a 5 to 10 fold molar excess of ferricyanide stock solution was added from a stock solution to (semi-met)$_0$NO. Samples, frozen periodically over the course of three hours, were frozen for observation by EPR spectroscopy, as described in section II.A.

D. Isotopic Enrichment of Samples

1. ^{15}N-enriched samples

^{15}N-enriched samples of the nitrite derivatives were prepared using $Na^{15}NO_2$.

^{15}N-labeled nitric oxide was prepared from $Na^{15}NO_2$ by reduction with L-ascorbic acid (reaction 2.7) as described below. The gas evolved was drawn into a gas-tight syringe and added to the solution of protein.

$$^{15}NO_2^- + \text{L-Asc} \rightarrow {}^{15}NO + \text{dehydroascorbate} \qquad (2.7)$$

2. ^{18}O-enriched samples

Incorporation of ^{18}O into the iron site was achieved at the Oregon Graduate Center by dissolving crystals of deoxyHr in $H_2{}^{18}O$ (80). Exchange takes place according to reaction 2.8, which takes several days at room temperature.

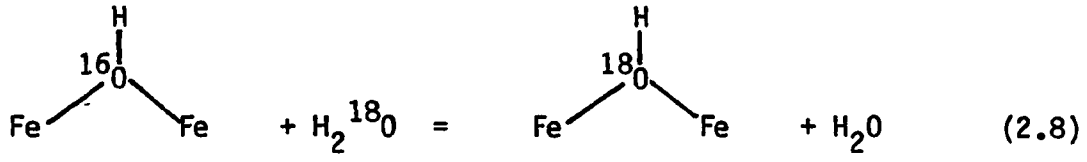

(2.8)

A sample in which ^{18}O was present in the bound nitrosyl group but not in the bridge position was prepared by adding NO to oxyHr in $H_2{}^{18}O$. Exchange with the bridging oxygen does not occur to an appreciable extent as long as the solutions of deoxy or oxyHr are used within several hours after the crystalline protein is dissolved in $H_2{}^{18}O$. Trace amounts of O_2 lead to production of NO_2. This, after being hydrolyzed, catalyzes the exchange of ^{18}O between NO and $H_2{}^{18}O$ (171) according to reactions 2.9 and 2.10.

$$NO + O_2 \rightleftarrows NO_2 \qquad (2.9)$$

$$NO + H_2{}^{18}O \rightleftarrows N^{18}O + H_2O \qquad (NO_2 \text{ catalyzed}) \qquad (2.10)$$

This sample of deoxy$N^{18}O$ prepared in $H_2{}^{18}O$ was chemically oxidized to metHr by the aerobic addition of an excess of $K_3Fe(CN)_6$. Azide was then added and the resonance Raman spectrum was checked to verify that ^{18}O was not incorporated into the μ-oxo bridge.

3. Preparation of samples in D_2O

Deuterium substitution into deoxyNO was achieved by replacing the solvent H_2O with D_2O prior to the addition of nitric oxide. A starting solution of oxyHr in phosphate buffered H_2O was concentrated in an

Amicon cell equipped with a PM-30 membrane and rediluted with buffered D_2O. This process was repeated three or four times until the solvent was greater than 95% D_2O. A second sample of deoxyNO was prepared in D_2O using crystalline deoxyHr as the starting material. After centrifuging the crystalline slurry and discarding the supernatant solution, the crystals were dissolved in buffered D_2O containing 0.3 M Na_2SO_4. The sample was equilibrated for one hour prior to reaction with nitric oxide.

For deoxyF⁻NO, replacement of solvent H_2O with D_2O was also performed before nitric oxide was added to the protein. Crystals of deoxyHr were dissolved in unbuffered D_2O and equilibrated for 20 hours. Fluoride and nitric oxide were then added as described in section II.C.3.

For the more stable derivatives, semi-metNO_2^- and metNO_2^-, the deuterium exchange was performed after the desired product had been prepared. The stock solution (in H_2O) was concentrated in an Amicon cell (PM-30 membrane) and diluted with unbuffered D_2O. This procedure was repeated 3 or 4 times until the solvent was greater than 95% D_2O.

E. Reactivity Studies with the Nitric Oxide and Nitrite Derivatives of Hemerythrin

1. Oxidation of deoxyHr by nitrite

Kinetic studies of the oxidation of deoxyHr by sodium nitrite were performed at Hope College in Holland, Michigan and the data were analyzed at Iowa State. Reactions were initiated by injection of aliquots of a concentrated anaerobic solution of sodium nitrite (50 mM phosphate

buffer) into 40-120 μM deoxyHr at 25.0°C. Pseudo-first-order reaction conditions were maintained by using nitrite concentrations 10 to 100 times in excess over the protein concentration.

Changes in the absorbance at 380 nm as a function of time were measured using a Pye Unicam SP8-200 spectrophotometer. Contributions to the absorbance from both reactants are minimal at this wavelength. To determine the rate constants, the data were fit by computer to two exponential processes using an iterative nonlinear least squares program, NLLSQ. For most fits, the value of the absorbance at infinite time was held fixed at the experimental value while the two first-order rate constants and their pre-exponential factors were allowed to vary. The reported rate constants are the averages of 2-6 replicate runs.

The effect of variation of the pH was studied within the range of 6.5 to 7.5 using phosphate buffered media. For a few of the higher pH runs, Tris-sulfate was used.

To follow the reaction by EPR spectroscopy, sodium nitrite (20-50 fold molar excess over protein) was added from a concentrated stock solution to deoxyHr (>1.0 mM) in 50 mM phosphate (pH 6.5 or 7.5). Aliquots were transferred with a gas-tight syringe to EPR tubes, which were then immediately frozen with liquid nitrogen.

The reaction of sodium nitrite with deoxyHr in the presence of sodium azide was monitored by optical spectroscopy. The sample (~0.20 mM in Hr) was prepared in phosphate buffer (pH 6.5) with a 1:20:50 ratio of Hr to nitrite to azide. DeoxyHr was incubated with azide for 5 minutes before nitrite was added.

2. Oxidation of oxyhemerythrin with nitrite

OxyHr was reacted with sodium nitrite in 50 mM phosphate at pH 6.5. Prior to the addition of a 21-fold molar excess of nitrite to a solution of oxyHr, excess dissolved oxygen was removed by repeatedly evacuating the sample and flushing it with argon. Aliquots were withdrawn with a gas-tight syringe periodically over the course of three hours and after allowing the reaction to proceed overnight. These aliquots were transferred to EPR tubes, and frozen with liquid nitrogen for observation by EPR spectroscopy.

3. Intracellular reactions with nitrite

Oxygenated erythrocytes were suspended in sea water (pH 7.2) containing 50 mM sodium nitrite and stirred at 0°C. After centrifugation, samples of the packed cells were transferred to EPR tubes, and frozen in a liquid nitrogen bath. The EPR samples were prepared after reaction times of either 45, 196, or 377 minutes.

Deoxygenated erythrocytes were prepared by bubbling a slow stream of argon through a suspension of cells in sea water for 45 minutes. After centrifugation and removal of the supernatant with a gas-tight syringe, the cells (~0.50 ml) were stirred in 5.0 ml of sea water containing 50 mM sodium nitrite (pH 7.2). Samples were transferred to EPR tubes and frozen in a liquid nitrogen bath after 40, 193, and 375 minutes.

4. Auto-oxidation of oxyhemerythrin in the presence of azide

The optical changes accompanying the auto-oxidation of oxyHr in the presence of azide were monitored in order that a comparison could be

made to the auto-oxidation of deoxyNO. OxyHr (0.063 mM) was reacted with a 74-fold excess of sodium azide at room temperature in phosphate (pH 7.5) in air. Spectra were recorded at 30 minute intervals for 4 hours.

Since it has been proposed that deoxyN_3^- is an intermediate of the auto-oxidation when azide is present, the reaction of deoxyN_3^- with oxygen was also monitored by optical spectroscopy. To prepare deoxyN_3^-, a solution of deoxyHr (0.86 mM) in 50 mM phosphate buffer (pH 6.5) was incubated with an 1800-fold molar excess of sodium azide at room temperature for two hours. After diluting the protein to 0.17 mM, oxygen was bubbled into the sample with a Pasteur pipette. Optical spectra were recorded at 15 minute intervals and a final spectrum was recorded after the reaction had proceeded overnight.

5. Reactivity of deoxyNO

a. Stability of deoxyNO The stability of deoxyNO was examined by EPR spectroscopy. A stock solution of deoxyNO (1-2 mM) was prepared as described above. Aliquots were withdrawn and frozen in liquid nitrogen immediately after preparation and intermittently after incubation for up to 24 hours at room temperature. To the final sample, a 10-fold or greater molar excess of sodium azide was added and both the EPR and optical spectra of the product were observed.

These stability experiments were performed under the following conditions:

(i) 50 mM phosphate at pH 6.5.

(ii) 50 mM phosphate at pH 6.5, 0.1 M ClO_4^-.

(iii) 50 mM phosphate at pH 6.5, 1.0 M ClO_4^-.

Samples containing perchlorate were prepared by adding an appropriate volume of deoxyHr to a weighed amount of solid sodium perchlorate such that the perchlorate was either 0.1 M or 1.0 M. After an hour-long incubation period, nitric oxide was added as described above. Samples for EPR spectroscopy were prepared after various decomposition times.

b. Reactions with oxidants The reaction of deoxyNO with oxygen was performed by bubbling air through a Pasteur pipette into a stock solution of deoxyNO for 1-3 minutes. OxyHr was identified as the product from its optical spectrum.

The reactions with sodium nitrite was initiated by dissolving a weighed amount of solid sodium nitrite in a solution of deoxyNO (0.88 mM) in 50 mM phosphate (pH 6.5) such that nitrite was present in a 52-fold molar excess over the protein. This experiment, performed at room temperature and pH 6.5, was monitored by EPR spectroscopy for nearly three hours by freezing aliquots of the reaction mixture at several points during the time course of the reaction.

Oxidation by ferricyanide was carried out by adding the oxidant to a stock solution of deoxyNO such that the mole ratio of oxidant to protein was 1:1. Portions were withdrawn and EPR samples were prepared over the course of two hours, at which time the reaction appeared complete. At this point, the optical spectrum of the product was checked both in the presence and in the absence of a 29-fold molar excess of sodium azide.

c. Reactions with anions Azide, cyanate, fluoride, chloride, bromide, iodide, thiocyanate, sulfide, and cyanide were used for these experiments. Sodium azide and sodium cyanide were recrystallized from ethanol/water before being used. With the exception of sulfide, all the reactions were carried out by adding a portion of the solution of deoxyNO via gas-tight syringe to a measured amount of the sodium salt of the anion such that the concentration of the anion was 0.1 M, 0.5 M, or 1.0 M. Sulfide was added from a concentrated stock solution (0.1 M) prepared in 0.5 M phosphate (pH 6.5). Samples were prepared for observation by either optical or EPR spectroscopy immediately following mixing and ~30 minutes after mixing.

d. Reaction with dithionite A stock solution of sodium dithionite was prepared and standardized as described in section II.B.4. An aliquot of this solution, containing 3.6 reducing equivalents, was added to the solution of deoxyNO in 50 mM phosphate (pH 6.5) and the reaction allowed to proceed for 1 1/2 hours. The progress of the reaction was followed by freezing aliquots for EPR spectroscopy. The optical spectrum of the final product was recorded in the presence and absence of oxygen.

6. Reactivity of deoxyF^-NO

Both ligand substitution reactions and oxygen-reactivity were investigated. These were conducted similarly to the deoxyNO reactions described above.

7. Reactivity of Semi-metNO_2^-

Unless stated otherwise, all reactions were conducted in 50 mM phosphate at pH 6.5 and a 20-fold molar excess of nitrite over Hr was present in all solutions. Samples for optical and EPR spectroscopies were prepared as previously described.

a. Redox reactions For oxidation by ferricyanide, one mole of ferricyanide was added per mole of semi-metNO_2^- and the reaction was monitored by optical and EPR spectroscopies.

Reactions with ascorbate and dithionite were also investigated. Dithionite was added from a standardized aqueous stock solution in a 4-fold molar excess over semi-metNO_2^-. For the ascorbate reduction, a 10-fold molar excess of reductant was used. Visible spectra were used to characterize the products and EPR spectroscopy was used to follow the time course of the reactions.

b. Ligand substitution experiments Ligand substitution experiments employed 0.1 M anion. Samples were frozen for observation by EPR after either a 15-20 min reaction period or after the reaction had proceeded for 4 hrs at room temperature. Reactions were initiated by injecting Hr under argon into a vial containing a measured amount of the sodium salt of the anion.

8. Reactivity of semi-metNO

All reactions were performed in 50 mM phosphate buffer at pH 6.5.

a. Oxidation by ferricyanide Ferricyanide was added from a stock solution in a 2.5 to 3.0-fold molar excess over the protein. Excess ferricyanide was kept to a minimum so that the absorbance changes

between 300 and 400 nm that are characteristic of oxidation of Hr would not be obscured by absorbances from the oxidant. The final product was identified from the EPR and optical spectra of the product obtained after addition of sodium azide.

b. Reduction by ascorbate Semi-metNO was added under argon to solid L-ascorbic acid with the latter present in a 40 to 50-fold molar excess. Samples were withdrawn and immediately frozen for analysis by EPR spectroscopy.

c. Reduction by dithionite A 4.5-fold molar excess of dithionite, standardized against $Fe(CN)_6^{3-}$, was added to Hr under argon. The progress of the reaction was monitored by EPR spectroscopy. After three hours, the optical spectrum of the product was recorded. After oxygenating this sample, its optical spectrum was again recorded.

d. Reaction with sulfide A portion of an aqueous stock solution of sodium sulfide (buffered in 0.5 M phosphate to pH 6.5) was diluted into a sample of semi-metNO in a 5 to 20-fold molar excess. Samples were frozen for EPR measurement before and immediately after the addition of sulfide.

e. Ligand substitution reactions Azide was added either from a concentrated stock solution or directly as a solid in a 20-fold or greater molar excess over semi-metNO. Optical spectra were recorded and samples for EPR were frozen both immediately after addition and 5 hours or more after azide was added.

For cyanate, fluoride, cyanide and thiocyanate, a 50 to 100-fold molar excess of ligand was added to solutions of semi-metNO.

III. RESULTS AND DISCUSSION

A. Oxidation of Hemerythrin by Nitrite

1. Kinetics of the reaction of deoxyhemerythrin with nitrite

In anaerobic phosphate buffer, excess sodium nitrite added to deoxyHr generates a brown-colored product within minutes. Over the course of several hours, this product converts to an amber-colored derivative that is stable at 4°C for several days. Figure 3.1 displays the changes in absorbance for such a reaction. From semi-log plots of the absorbance changes as a function of time (Fig. 3.2), the biphasic nature of the reaction is clearly seen. The absorbance changes were computer fit using a nonlinear least squares program, NLLSQ, to a biphasic reaction in which both phases exhibit first order behavior. In Fig. 3.3, it is seen that the absorbance values determined from such an analysis are in agreement with the experimental values.

Tables 3.1 and 3.2 present the concentration dependence for the two phases. The rate of the rapid first phase shows first order concentration dependences on Hr, nitrite, and H^+ (also plotted in Fig. 3.4), while the slower phase is dependent only upon the concentration of Hr. By analogy to the nitrite oxidation of Hb (123), the first order dependence upon H^+ is interpreted as an acid/base equilibration between HONO and NO_2^- [pK_a is 2.94 at 25°C, I = 0.5 M (116)]. The two phases are most readily discerned below pH 7.

When the progress of the reaction is followed by EPR spectroscopy (Fig. 3.5), only a single product is observed. This species exhibits a rhombic signal having g-values at 1.93, 1.87 and 1.66. Build-up of the

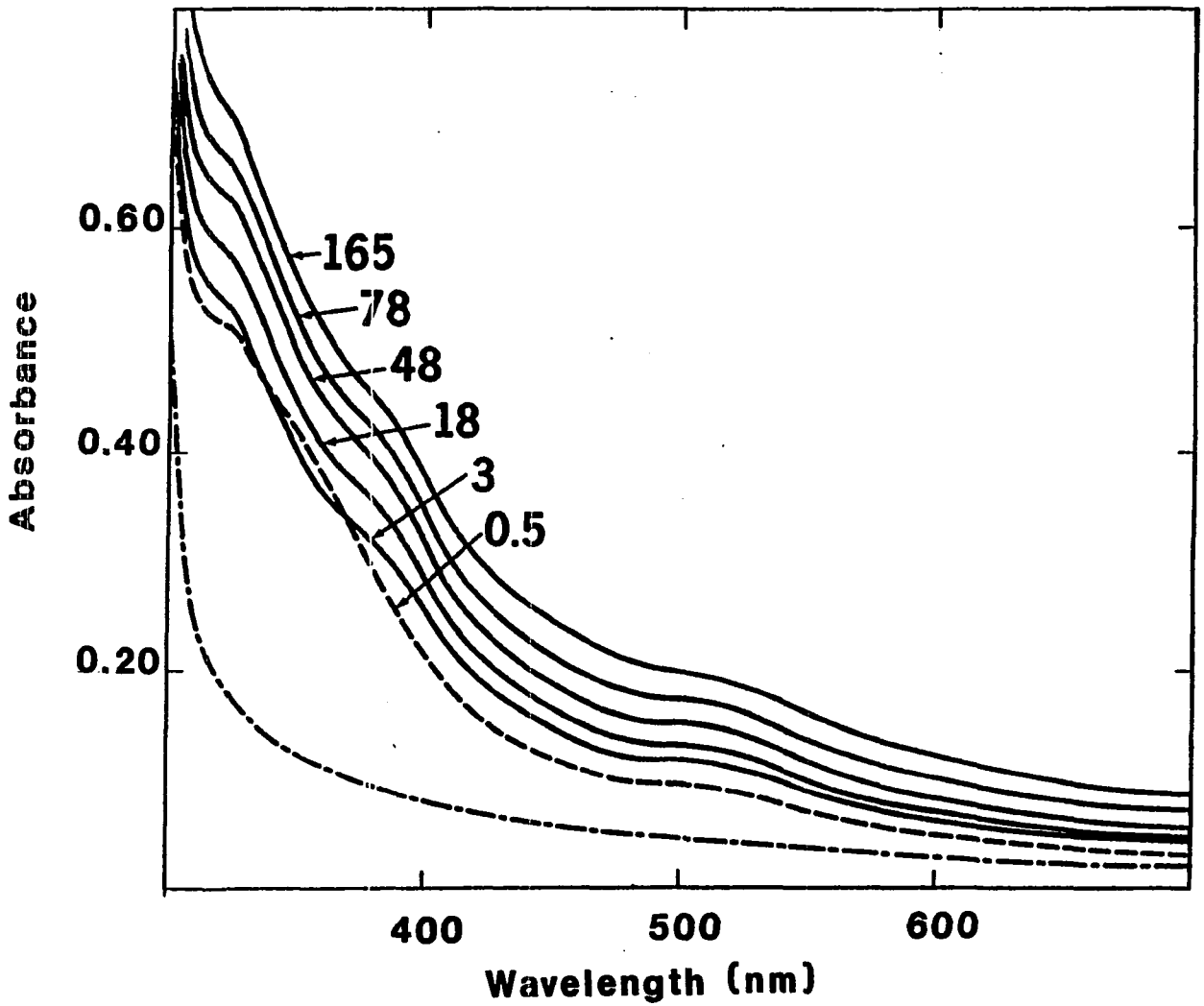

Figure 3.1. Spectral time course for the oxidation of deoxyHr with excess nitrite

0.128 mM Hr; 2.65 mM $NaNO_2$; 50 mM phosphate, pH 6.5; numbers refer to time in minutes after the addition of $NaNO_2$

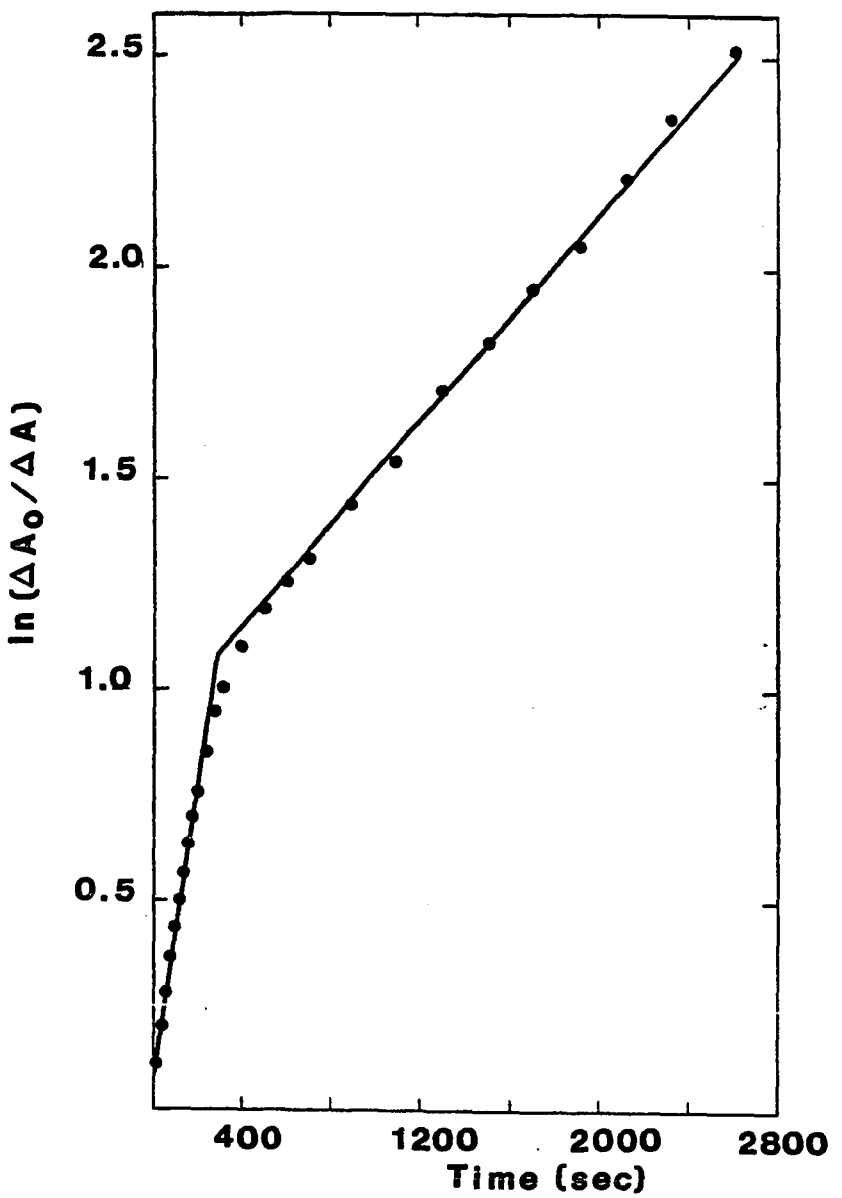

Figure 3.2. Semi-log plot of the absorbance changes at 380 nm as a function of time for the oxidation of 0.0682 mM deoxyHr with 6.91 mM $NaNO_2$ in 50 mM phosphate (pH 7.05)

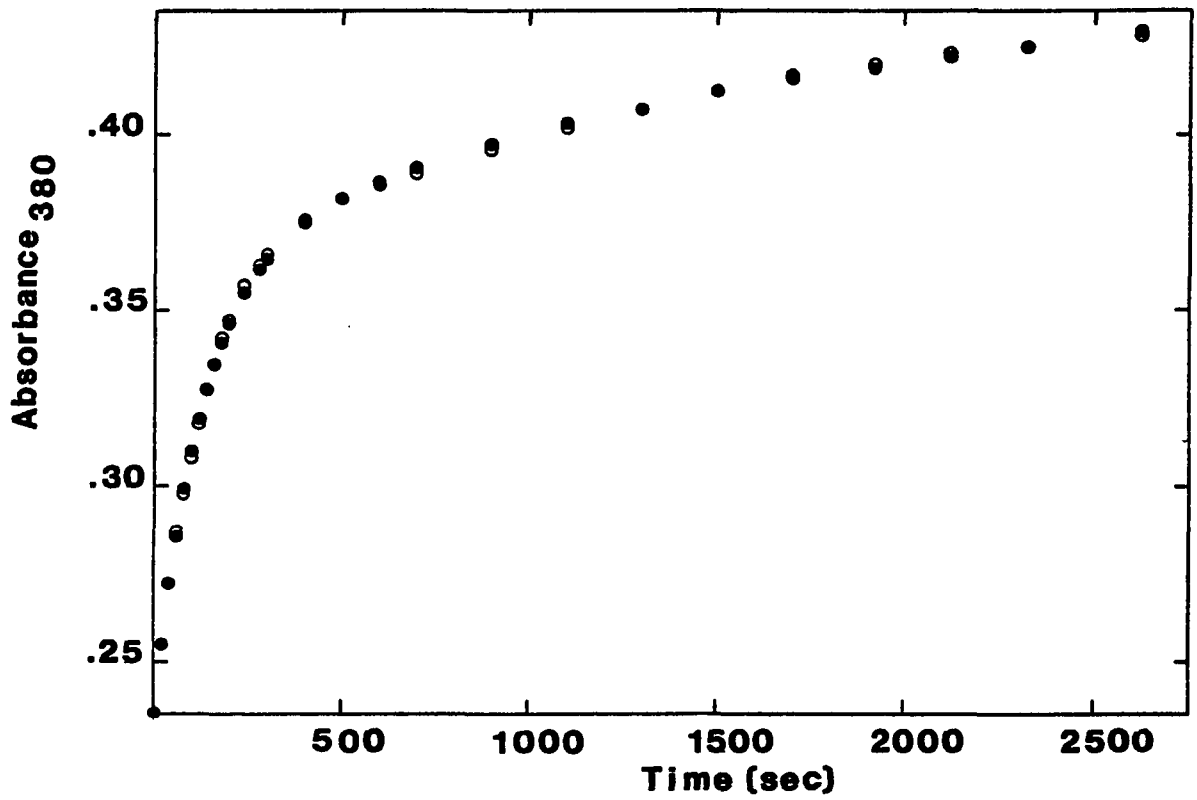

Figure 3.3. Comparison of the absorbance changes at 380 nm calculated from an NLLSQ fit with the experimental absorbance changes

0.0682 mM Hr; 6.91 mM $NaNO_2$; 50 mM phosphate, pH 7.05; 25.0°C; open circles are the experimental values; filled circles are calculated from an NLLSQ fit where k_{obs} = 7.79 x 10^{-3} s^{-1} and k'_{obs} = 4.99 x 10^{-4} s^{-1}. Calculated A_∞ = 0.453; observed A_∞ = 0.446

Table 3.1. Rate constants for the first phase of the oxidation of deoxyHr by nitrite[a]

[Hr] (mM)	$[NO_2^-]$ (mM)	pH	$10^3\ k_{obs}$ (s^{-1})	$k_{obs}/[NO_2^-]$ ($M^{-1}s^{-1}$)
0.0618	1.50	6.58	3.18	2.12
0.0618	3.08	6.58	6.50	2.11
0.0618	6.18	6.58	12.92	2.09
0.0682	1.73	7.05	0.910	0.526
0.0682	3.46	7.05	1.81	0.523
0.0682	6.91	7.05	3.60	0.521
0.0697	3.48	7.48	0.588	0.169
0.0697	6.97	7.48	1.164	0.167
0.0727	3.62	7.74	0.340	0.0930
0.0727	7.25	7.74	0.683	0.0942

[a]25.0°C; 50 mM phosphate; pH 6.5; rate constants are average values for two kinetic determinations (±0.06); NLLSQ fit.

Table 3.2. Rate constants for the second phase of the oxidation of deoxyHr by nitrite[a]

[Hr] (mM)	$[NO_2^-]$ (mM)	pH	$10^3 k_{obs}$ (s^{-1})
0.0618	1.50	6.58	0.635
0.0782	3.83	6.58	0.651
0.0618	6.18	6.58	0.548
0.0795	1.95	6.83	0.640
0.0795	3.90	6.83	0.602
0.0491	2.45	7.00	0.534
0.0491	4.91	7.00	0.655
0.0682	3.46	7.05	0.552
0.0682	6.91	7.05	0.632
0.0697	6.97	7.48	0.554

[a]25.0°C; 50 mM phosphate; pH 6.5; rate constants determined from 2-4 kinetic runs; average ±0.05; NLLSQ fit.

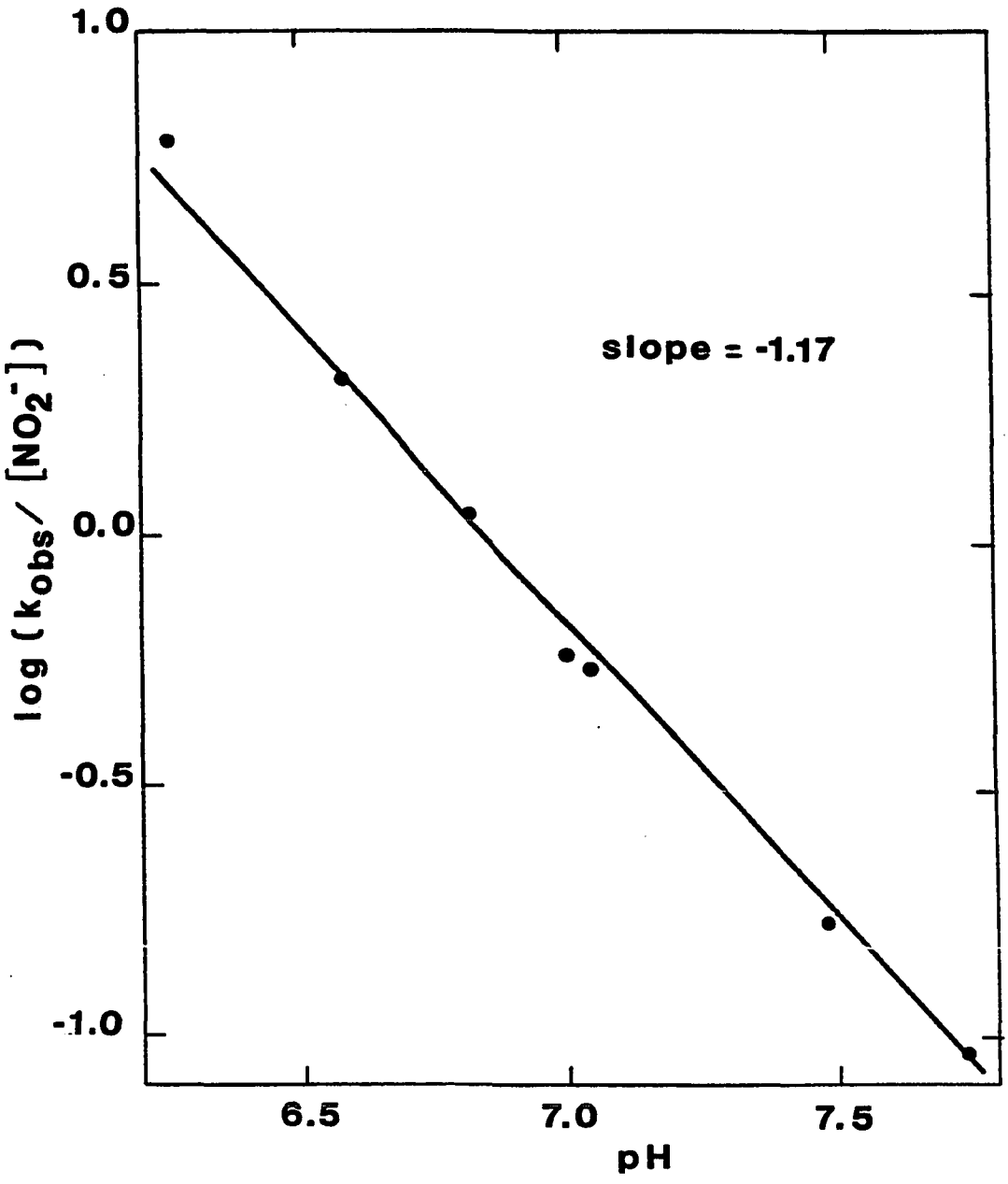

Figure 3.4. pH dependence of the second-order rate constant for the initial fast phase of the oxidation of deoxyHr by excess nitrite

[$NaNO_2$]/[Hr] = 10-100; 50 mM phosphate; 25.0°C; plotted values are the average of 2-6 kinetic determinations and have a maximum range of ±6%; slope = -1.17

Figure 3.5. Time course for the oxidation of deoxyHr by excess nitrite followed by EPR spectroscopy

Spectral parameters: temperature, 4.2 K; frequency, 9.57 GHz; power, 100 μW; modulation, 16 G; time constant, 0.1 s; gain, 3.2×10^4; double integration of the spectrum obtained at 187 min yields 1.2 spins/Hr; 1.3 mM Hr; 24 mM $NaNO_2$; 50 mM phosphate, pH 6.5

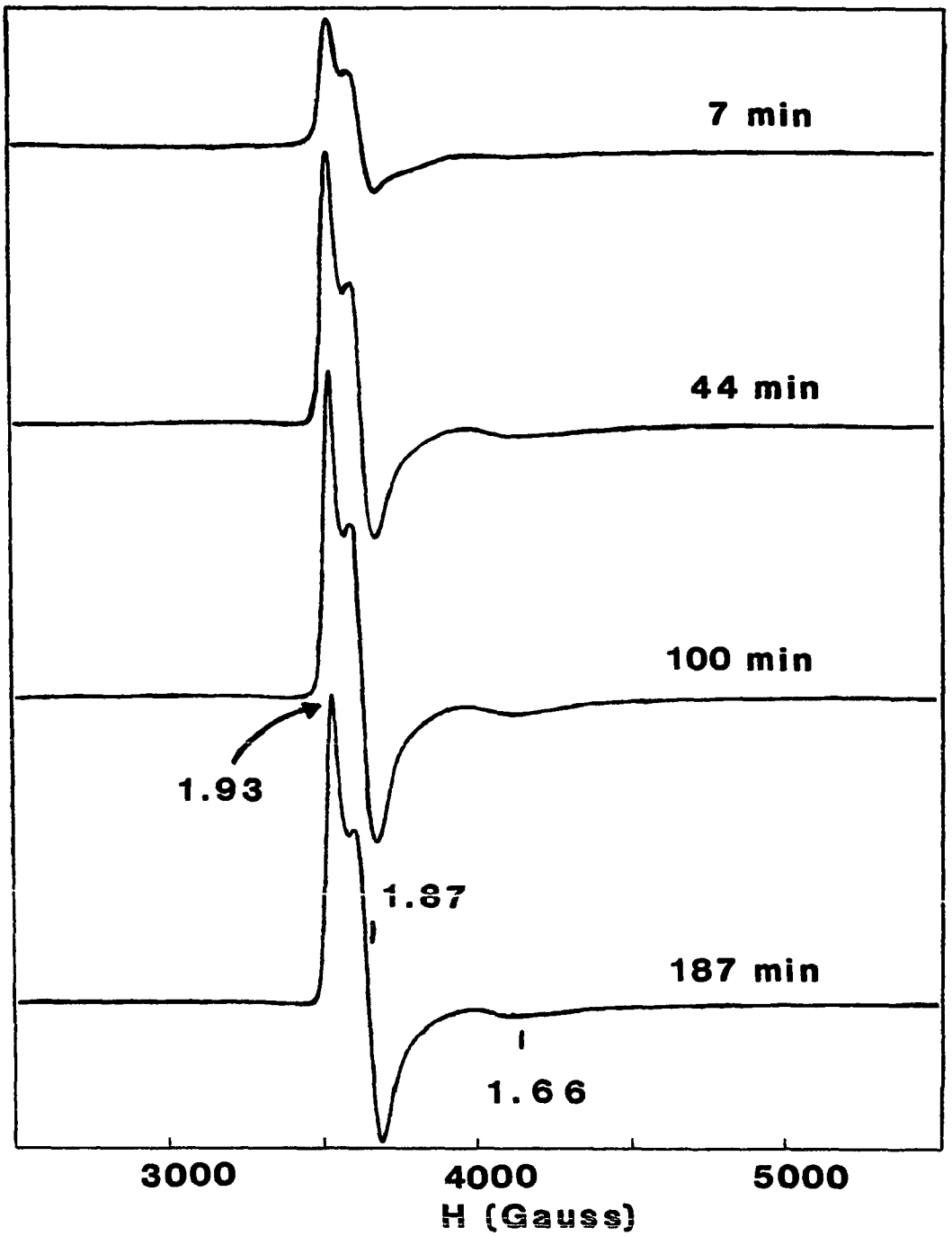
7 min
44 min
100 min
1.93
1.87
187 min
1.66
3000
4000
5000
H (Gauss)

signal coincides with the slow absorbance changes occurring during the second phase of the reaction. Double integration of this signal after a ~3-4 hour reaction period (Table 3.3) accounts for >95% of the protein. Thus, the product of the first phase is not detectable by EPR spectroscopy, while the final product is paramagnetic.

An EPR-silent intermediate could result from either a one-electron oxidation (shown in reaction 3.1) or a two-electron oxidation (shown in reaction 3.2).

$$\text{deoxy} + \text{HONO} \rightarrow \text{semi-metNO} + OH^- \qquad (3.1)$$

$$\text{deoxy} + \text{HONO} \rightarrow \text{met} + NO^- + OH^- \qquad (3.2)$$

In order to determine the oxidation state of the product, nitrite was added to a solution of deoxyHr containing sodium azide (Fig. 3.6). The rate of binding of azide to both metHr (Table 1.17) and semi-metHr (Table 1.19) exceeds the rates measured for the second phase of the nitrite oxidation. Thus, azide should trap any metHr or semi-metHr formed during the nitrite oxidation reaction. In addition, the optical spectrum of semi-metN_3^- is easily distinguished from that of metN_3^-. Even early in the reaction, metN_3^- is not formed. Rather, semi-metN_3^- builds up at a rate that is similar to that of the second phase of the nitrite oxidation. Thus, the product of the first phase is at the semi-met oxidation level.

Table 3.3. Quantitation by double integration of the EPR spectra of the product of nitrite oxidation[a]

[Hr] (mM)	$[NO_2^-]$ (mM)	Time (min)	% pmag
0.797	13.7	148	110.0[b]
1.30	24.1	187	125.0[b]
1.52	30.4	240	98.2
1.52	30.4	24 hrs	106
1.03	1.03	75	69.4[c]
1.90	1.90	60	80.6
0.874	15.6	120	33.6[b,d]
1.57	32.2	38	23.9[b,d]

[a]pH 7.5; 50 mM phosphate; % pmag = [spins]/[Hr] x 100.

[b]pH 6.5.

[c]124.1 mM sodium azide added after 75 min.

[d]OxyHr, deaerated prior to nitrite addition.

Figure 3.6. Spectral time course of the oxidation of deoxyHr by excess nitrite in the presence of NaN_3

0.0968 mM Hr; 1.94 mM $NaNO_2$; 40 mM NaN_3; 50 mM phosphate, pH 7.5; numbers refer to time in minutes after the addition of $NaNO_2$

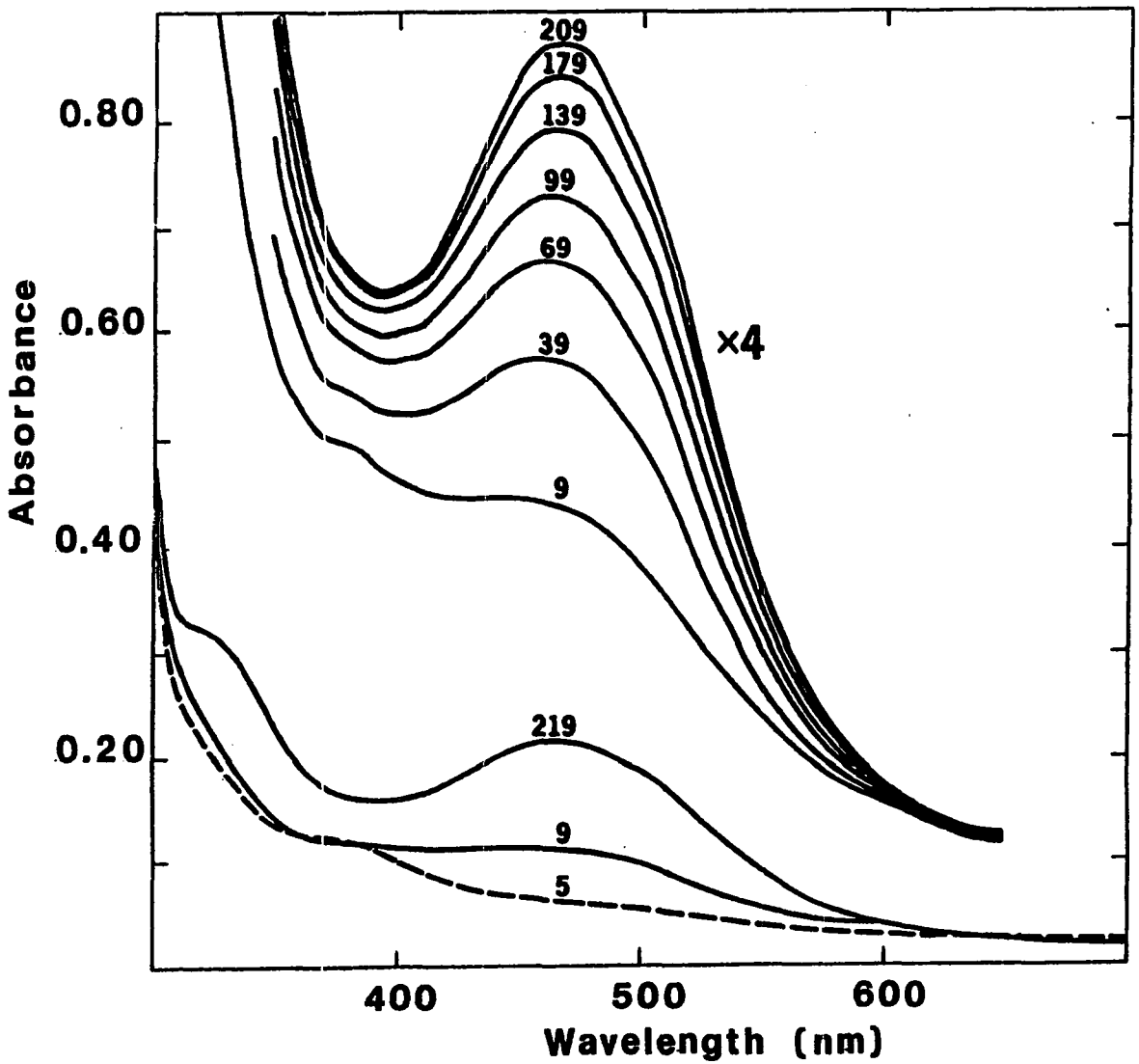
209
179
139
99
69
39
9
×4
219
9
5
0.80
0.60
0.40
0.20
Absorbance
400
500
600
Wavelength (nm)

Furthermore, semi-metNO has been independently prepared by addition of NO to dithionite-generated $(semi\text{-}met)_R$ (see section III.C). Its optical spectrum is strikingly similar to the spectra generated during the early stages of the nitrite reaction and the EPR signal of $(semi\text{-}met)_R$ disappears in the presence of NO. The EPR- silent, brown-colored product of the first phase of the nitrite oxidation of deoxyHr is, thus, identified as $(semi\text{-}met)_R NO$.

In the second phase of the nitrite oxidation of deoxyHr, a paramagnetic derivative is produced (Fig. 3.5). The g-values and general shape of this spectrum are similar but not identical to those of other known Hr derivatives. In particular, they are different from those of $(semi\text{-}met)_O$ (Fig. 1.14A), the intermediate resulting from outer sphere oxidations of deoxyHr. Neither are they identical to those of $(semi\text{-}met)_R$ (Fig. 1.14A). In fact, signals attributable to either $(semi\text{-}met)_O$ or $(semi\text{-}met)_R$ are never observed during the course of the oxidation of deoxyHr by <u>excess</u> nitrite.

Two products, both of which are expected to be paramagnetic, that might conceivably result from this reaction are semi-metNO_2^- and metNO. The first of these could result from the following reaction:

$$\text{semi-metNO} + NO_2^- \rightarrow \text{semi-met}NO_2^- + NO \qquad (3.3)$$

On the other hand, the reaction that could lead to a metNO derivative is:

$$\text{semi-metNO} + \text{HONO} \rightarrow \text{metNO} + \text{NO} + \text{OH}^- \qquad (3.4)$$

To distinguish these two alternatives, several attempts (section III.E) were made to prepare a metNO derivative. All were unsuccessful.

Secondly, and more convincingly, sodium azide was added at the completion of the oxidation reaction. Within less than 5 minutes, the optical spectrum characteristic of semi-metN_3^- (as opposed to that of metN_3^-) develops (Fig. 3.7). In addition, an EPR sample frozen after addition of azide to the paramagnetic product has g-values at 1.91, 1.83, and 1.51. These are very close to the g-values previously reported for semi-metN_3^- [1.90, 1.81, and 1.49 (77)]. Thus, the ultimate product of the nitrite oxidation of deoxyHr is a semi-met derivative.

As previously mentioned, the g-values of the EPR signal of this semi-met derivative differ from those of other Hr derivatives. As Table 3.3 shows, at pH 7.5, this product is stable for at least 24 hours. Ligand-binding of monovalent anions, such as azide, is known to stabilize the semi-met oxidation level of Hr (78). Thus, it is likely that the stability of the product of the nitrite oxidation of deoxyHr derives from binding of a ligand to the semi-met site. Since the most abundant anionic ligand present in the reaction mixture is nitrite, the product is most likely the nitrite adduct of semi-metHr, i.e., semi-metNO_2^-.

To confirm that semi-metNO_2^- was the product of the oxidation by nitrite, excess sodium nitrite was reacted with $(\text{semi-met})_O$ and with $(\text{semi-met})_R$. EPR samples frozen within minutes after mixing (Fig. 3.8) showed the EPR signals characteristic of semi-metNO_2^-.

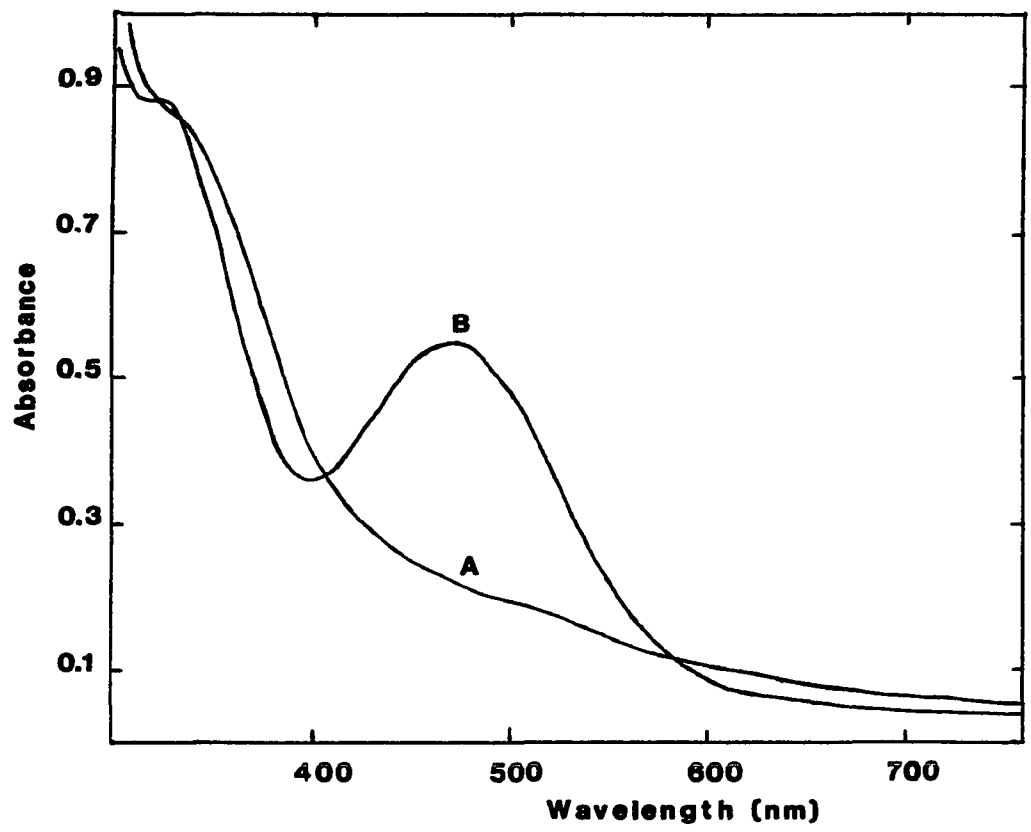

Figure 3.7. Optical spectra before (A) and after (B) the addition of excess NaN_3 at 3 1/2 hours after mixing deoxyHr with nitrite

0.239 mM Hr; $[NO_2^-]/[Hr]$ = 96.9; azide added in excess as a solid; 50 mM phosphate, pH 6.5; 0.3 M sulfate

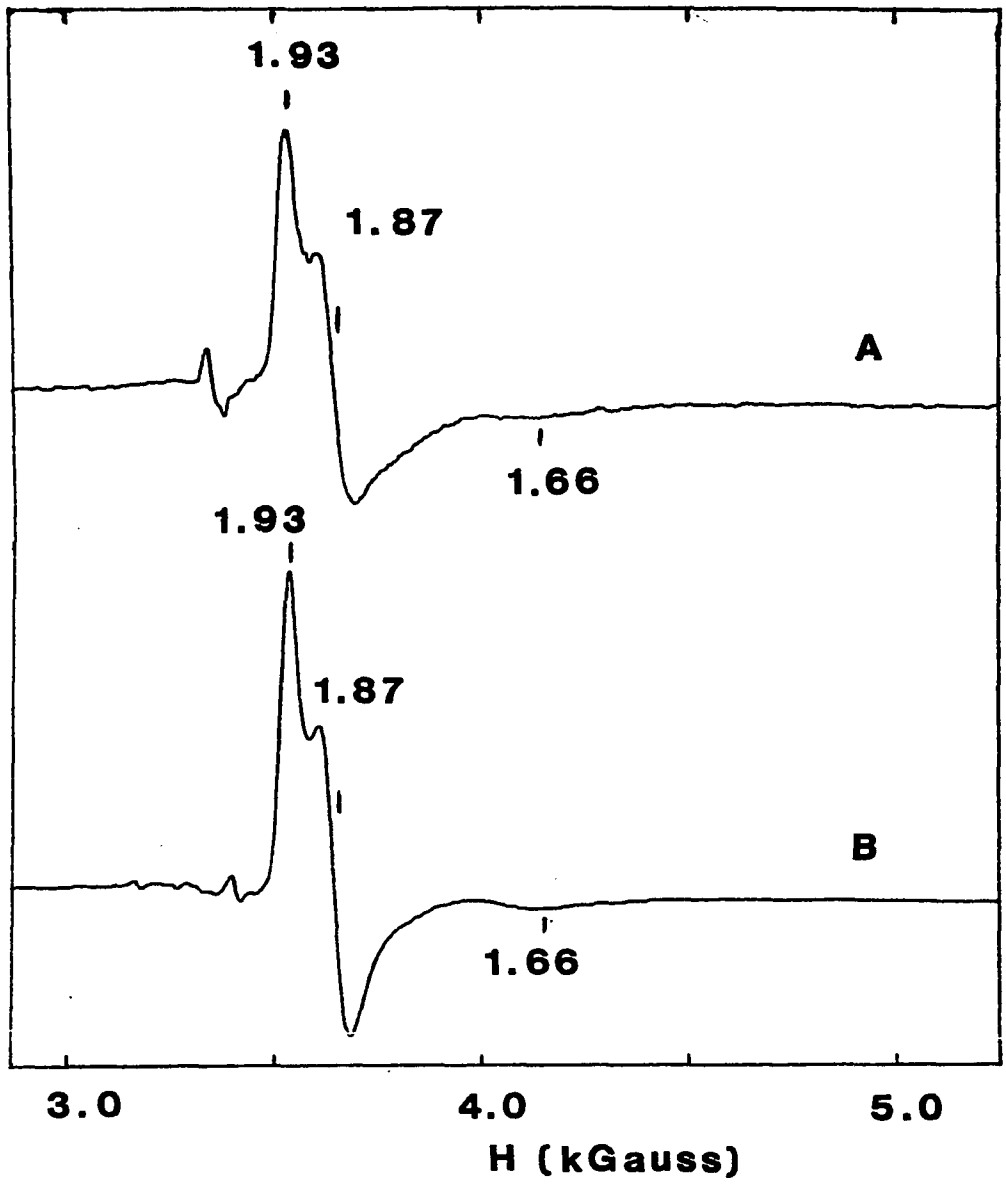

Figure 3.8. EPR spectra obtained after addition of excess $NaNO_2$ to $(semi\text{-}met)_O$ (A) and $(semi\text{-}met)_R$ (B)

Spectral parameters: temperature, 4.2 K; frequency, 9.57 GHz; power, 100 μW; modulation, 16 G; gain, 8.0×10^4; time constant, 0.2 s; 50 mM phosphate, pH 6.5

A. 0.986 mM Hr; 0.966 mM ferricyanide; 22.2 mM nitrite; 6 minutes after adding nitrite

B. 1.00 mM Hr; 0.966 mM dithionite; 17.8 mM nitrite; 4 minutes after adding nitrite

The appearance of semi-metN_3^- when azide is added to the final product of the nitrite oxidation reaction, thus, occurs via displacement of nitrite by azide (reaction 3.5).

$$\text{semi-met}NO_2^- + N_3^- \rightarrow \text{semi-met}N_3^- + NO_2^- \qquad (3.5)$$

MetHr has a much higher affinity for azide than for nitrite, and so it is not surprising that semi-metHr should exhibit similar affinities.

The paramagnetic product was further characterized by resonance Raman spectroscopy. Vibrational bands are observed at 433 cm^{-1} and 422 cm^{-1}. No other bands were observed using an excitation of 647.1 nm. Table 3.4, which presents the effects of isotopic substitutions on these vibrations, shows that both vibrations are affected by substitution of $^{14}NO_2^-$ with $^{15}NO_2^-$. By analogy to the assignments made for deoxyNO (see section 3.D), ν_1 is attributed to ν(Fe-NO) and ν_2 is assigned as δ(Fe-N-O).

Observation of ν(Fe-NO) indicates that nitrite is ligated to iron via nitrogen forming a nitro complex rather than via oxygen to form a nitrito complex. The absence of an Fe-O stretching band argues against the occurrence of nitro-nitrito isomerism (reaction 3.6).

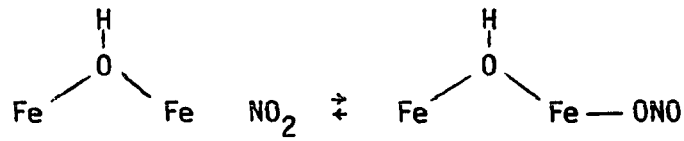

nitro nitrito (3.6)

Table 3.4. Isotopic substitution effects on the resonance Raman modes of semi-metNO_2^-[a]

Isotope	ν_1 (cm^{-1})	ν_2 (cm^{-1})
$^{14}NO_2^-$	433	422
$^{15}NO_2^-$	428	416
D_2O[b]	432	439

[a]77 K; 647.1 nm excitation; 100 mW; 0.25 mm slit width; 2 cm^{-1}/min.

[b]120 mW.

In D_2O, ν_2 is shifted upward from its position in H_2O by 17 cm^{-1}, whereas the frequency of ν_1 is not altered. Both the direction and the magnitude of the shift contrast with the effects observed with deoxyNO and deoxyF$^-$NO (section III.D). Upward shifts in D_2O of 4 cm^{-1} and 26 cm^{-1} have been observed for the ν_s(Fe-O-Fe) modes of oxyHr and cis- metOH$^-$, respectively (172). These shifts have been interpreted as effects due to hydrogen-bonding between the ligand and the μ-oxo bridge. By analogy to these derivatives, the structure shown in Fig. 3.9 is proposed for semi-metNO_2^-.

Further examination of the second phase raises a question about the pathway for converting semi-metNO to semi-metNO_2^-. Does this conversion occur in a concerted manner (reaction 3.7)

$$\text{semi-metNO} + NO_2^- \rightarrow \text{semi-met}NO_2^- + NO \qquad (3.7)$$

or is the rate dependent upon the dissociation of nitric oxide (reactions 3.8 and 3.9)?

$$\text{semi-metNO} \rightarrow (\text{semi-met})_R + NO \quad \text{(rate-determining)} \qquad (3.8)$$

$$(\text{semi-met})_R + NO_2^- \rightarrow \text{semi-met}NO_2^- \qquad (3.9)$$

One experimental result favoring the dissociation of NO as the rate limiting step of the second phase is that the reaction between (semi-met)$_R$ and nitrite occurs within the time of mixing. This reaction,

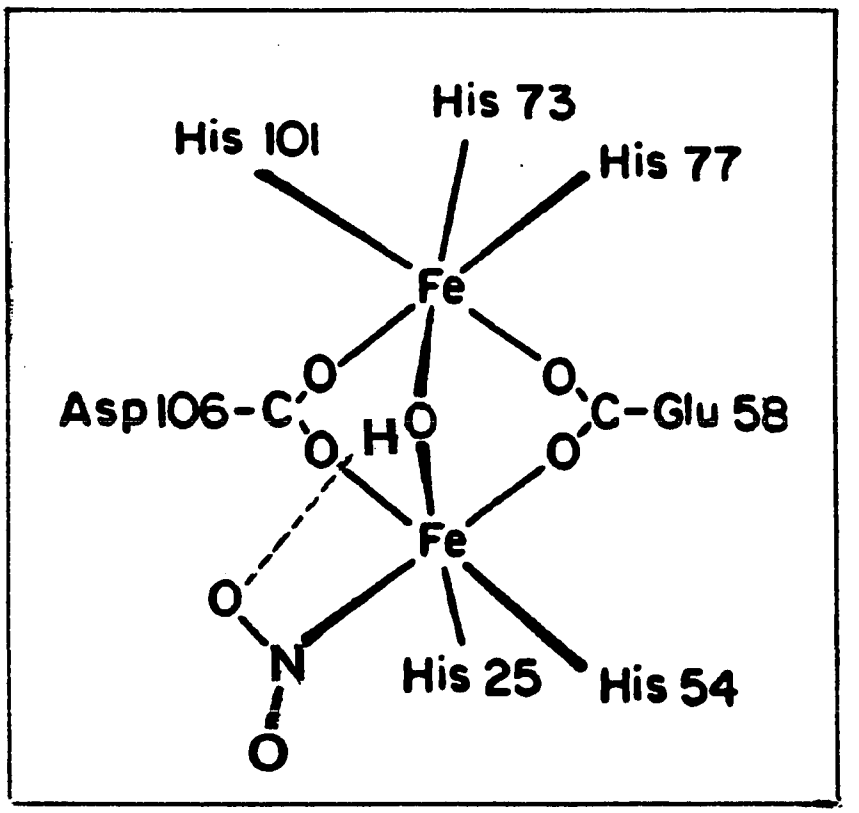

Semi-met NO_2^-

Fe(II)Fe(III)NO_2^-

Figure 3.9. Proposed structure for semi-metNO_2^-

being much faster than the rate of the second phase, could occur subsequent to the dissociation of NO.

Secondly, when azide is present in excess over nitrite (Fig. 3.6), semi-metN_3^- is obtained as a product. The rate of formation of semi-metN_3^- (9.5×10^{-5} s^{-1} for 0.0705 mM Hr, 1.37 mM NO_2^-, 23.6 mM N_3^-, pH 7.5) is nearly identical to that for the formation of semi-metNO_2^- in the second phase. If the conversion to semi-metNO_2^- occurs in a concerted fashion (reaction 3.7), one would expect the rates for the two ligands to be quite different. The invariance of the rates suggests that dissociation of NO from semi-metNO is the rate limiting step of the second phase with the subsequent binding of nitrite being more rapid. Similarly, the displacement of NO from $(\text{semi-met})_R$NO prepared from dithionite-generated $(\text{semi-met})_R$ by azide requires several hours for completion (see section III.C). Reactions 3.10 and 3.11 depict a possible route leading to formation of semi-metN_3^-.

$$\text{semi-metNO} \rightarrow (\text{semi-met})_R + \text{NO} \qquad (3.10)$$

$$(\text{semi-met})_R + N_3^- \rightarrow \text{semi-met}N_3^- \qquad (3.11)$$

Results of an experiment conducted at pH 7.5 with a 1:1 molar ratio of nitrite to deoxyHr indicate that dissociation of NO leads to production of $(\text{semi-met})_R$ rather than $(\text{semi-met})_O$ (Fig. 3.10). At this pH, the first and second phases occur on the same time scale. When a stoichiometric amount of nitrite (with respect to dimeric iron) is added to

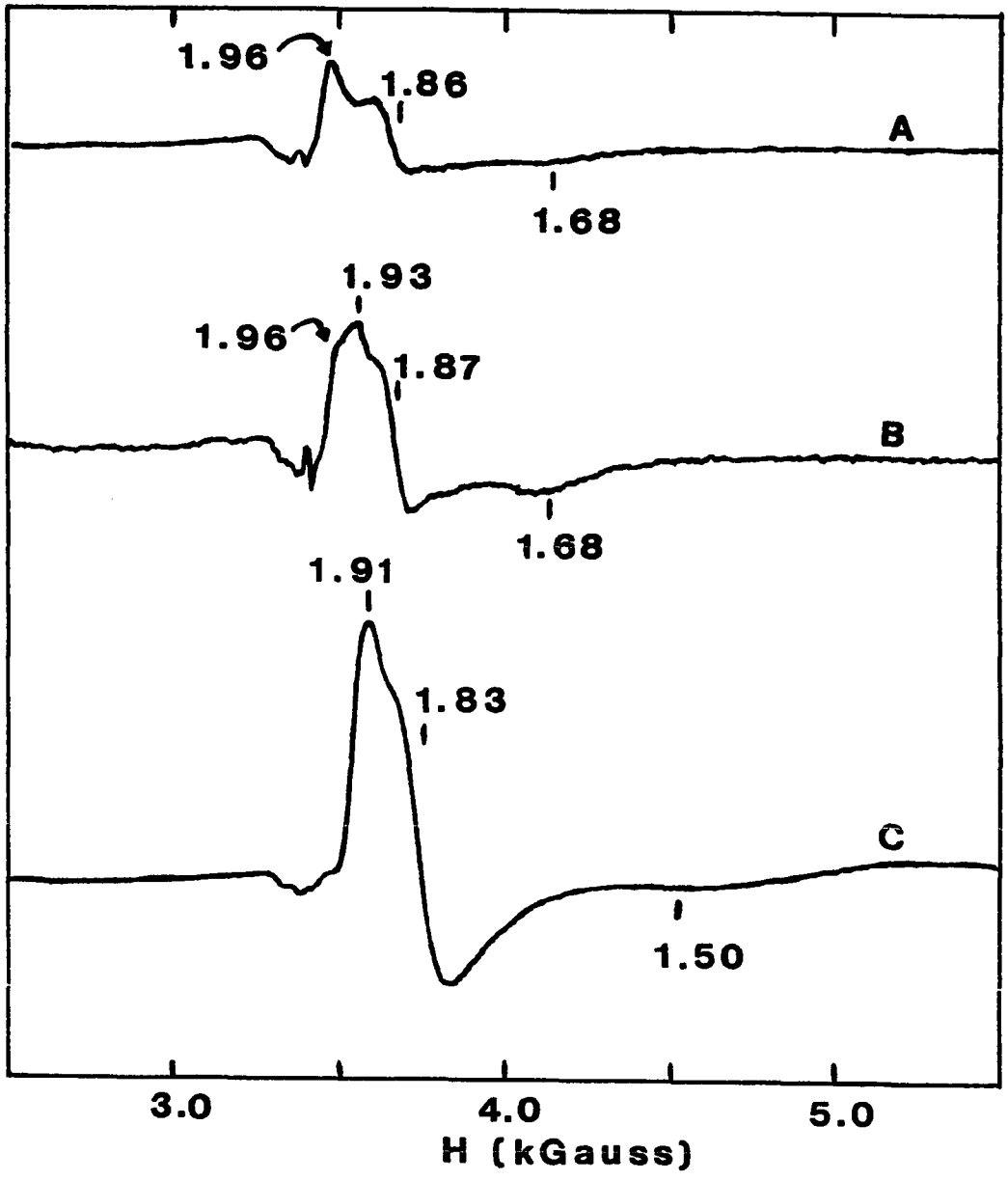

Figure 3.10. Time course for the 1:1 reaction of deoxyHr with $NaNO_2$ followed by EPR spectroscopy

Spectral parameters: temperature, 4.2 K; frequency, 9.57 GHz; power, 100 μW; modulation, 16 G; gain, 1.5 x 10^5 (A and B) and 6.3 x 10^4 (C); time constant, 0.2 s; 1.90 mM Hr; 1.90 mM $NaNO_2$; 50 mM phosphate, pH 7.5; the sample for spectrum C contains 1.42 mM Hr, 1.42 mM $NaNO_2$, and 123 mM NaN_3

deoxyHr, less than quantitative formation of semi-metNO_2^- is expected. In addition, the low concentration of nitrite is expected to allow semi-metHr to accumulate in the solution. Therefore, a mixture of semi-metHr, semi-metNO, and semi-metNO_2^- should result. By EPR spectroscopy, only semi-met and semi-metNO_2^- will be detected. Thus, the paramagnetic component of the sample should not account for all of the Hr. The results shown in Table 3.3 show that ~75% of the protein is detectable by EPR. The EPR spectra obtained from this experiment are shown in Fig. 3.10. A signal, attributable to $(\text{semi-met})_R$, appears at g = 1.96 along with the semi-metNO_2^- signal. This result is consistent with production of $(\text{semi-met})_R$ followed by the binding of nitrite.

Based on all of these observations, the mechanism shown in Scheme 3.1 is proposed for the oxidation of deoxyHr by nitrite.

Scheme 3.1:

Phase 1: $H^+ + NO_2^- \rightleftarrows HONO$

$\text{deoxy} + HONO \rightarrow \text{semi-metNO} + OH^-$

Phase 2: $\text{semi-metNO} \rightarrow (\text{semi-met})_R + NO$ (rate determining)

$(\text{semi-met})_R + NO_2^- \rightarrow \text{semi-met}NO_2^-$

2. Reaction of oxyhemerythrin with nitrite

Bradíc et al. (7) reported that when a solution of Hr is saturated with O_2, oxyHr is quantitatively oxidized to metNO_2^- (reaction 3.12).

$$\text{oxy} + NO_2^- + 2H^+ \rightarrow \text{met}NO_2^- + H_2O_2 \qquad (3.12)$$

During the course of this work, it has been found that when a solution of oxyHr is degassed to remove dissolved O_2 prior to the addition of nitrite, as much as 35% conversion to semi-metNO_2^- is observed (Table 3.3 and Fig. 3.11). Since degassing does not completely remove the bound oxygen, the suppression of the yield of semi-metNO_2^- is probably due to competition between auto-oxidation of oxyHr to metNO_2^- (reaction 3.12) and oxidation of deoxyHr to semi-metNO_2^- (Scheme 3.1). A similar result was reported for the oxidation of oxyHr to metHr by ferricyanide (Scheme 1.3), where competition occurs between direct oxidation of oxyHr to metHr and oxidation via deoxyHr.

3. Intracellular reactions with nitrite

Nitrite is able to penetrate the cell membrane and oxidize Hr intracellularly. Figure 3.12 shows that production of semi-metNO_2^- can occur within O_2-depleted cells. Similar results are obtained when nitrite is added to oxygenated cells. In contrast to the extracellular reaction, semi-metNO_2^- produced intracellularly can undergo further redox transformations. This is evidenced by the slow decrease in the intensity of the EPR signal for nitrite-treated cells that occurs over the course of 24 hours.

B. Assay of Aqueous Solutions of Nitric Oxide

Prior to examining the reactions between gaseous nitric oxide and aqueous protein-containing solutions, the stability of nitric oxide in aqueous solutions was investigated. In Fig. 3.13, the EPR spectra of assay mixtures containing Fe^{2+}(EDTA) and either gaseous NO (A), a 2-fold

Figure 3.11. Time course for the reaction of oxyHr with excess $NaNO_2$ followed by EPR spectroscopy

Spectral parameters: temperature, 4.2 K; frequency, 9.57 GHz; power, 100 μW; modulation, 16 G; gain, 5×10^4; time constant, 0.2 s; 0.874 mM oxyHr; 15.6 mM $NaNO_2$; 50 mM phosphate, pH 6.5

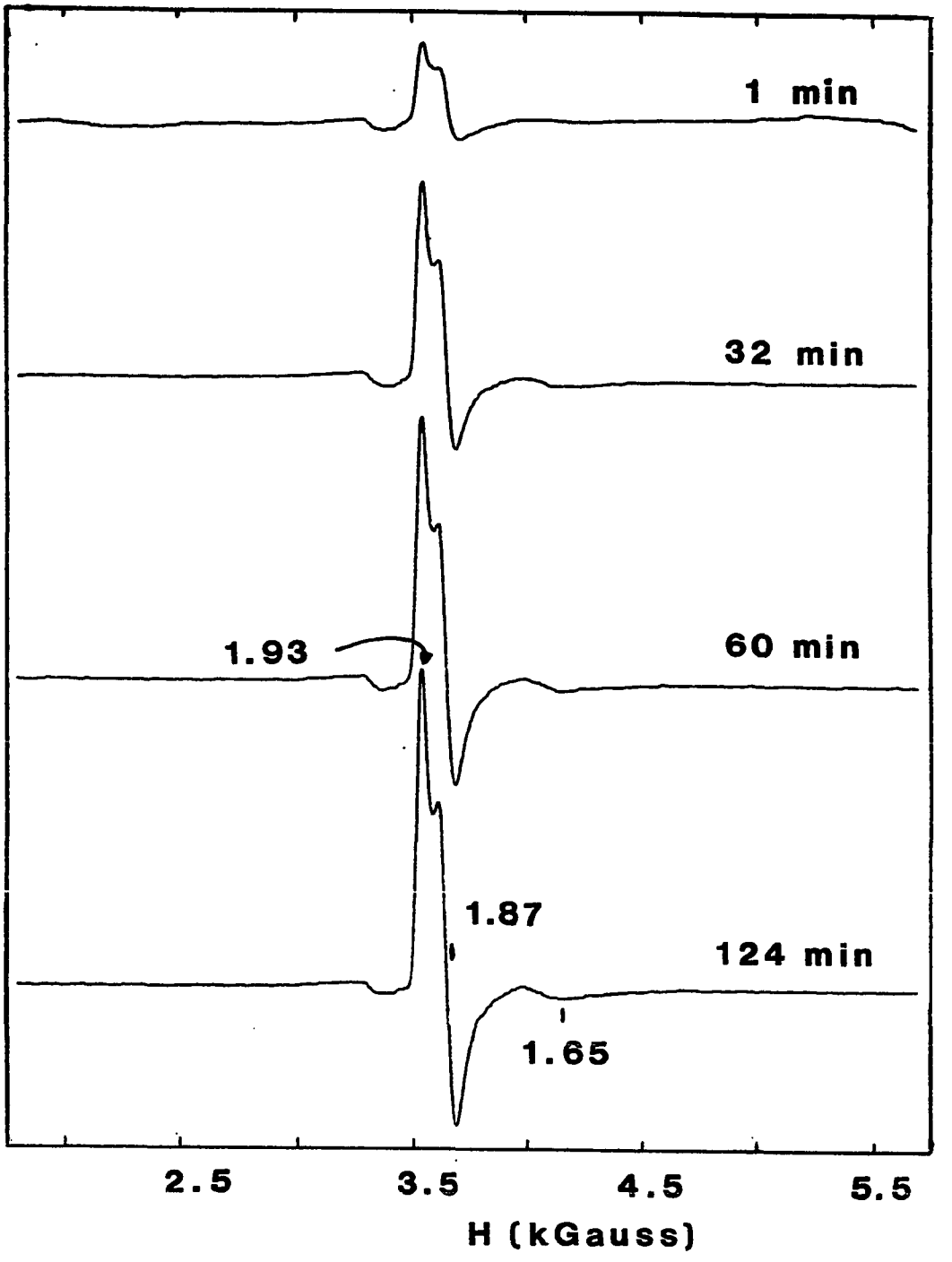
1 min
32 min
1.93
60 min
1.87
124 min
1.65
2.5
3.5
4.5
5.5
H (kGauss)

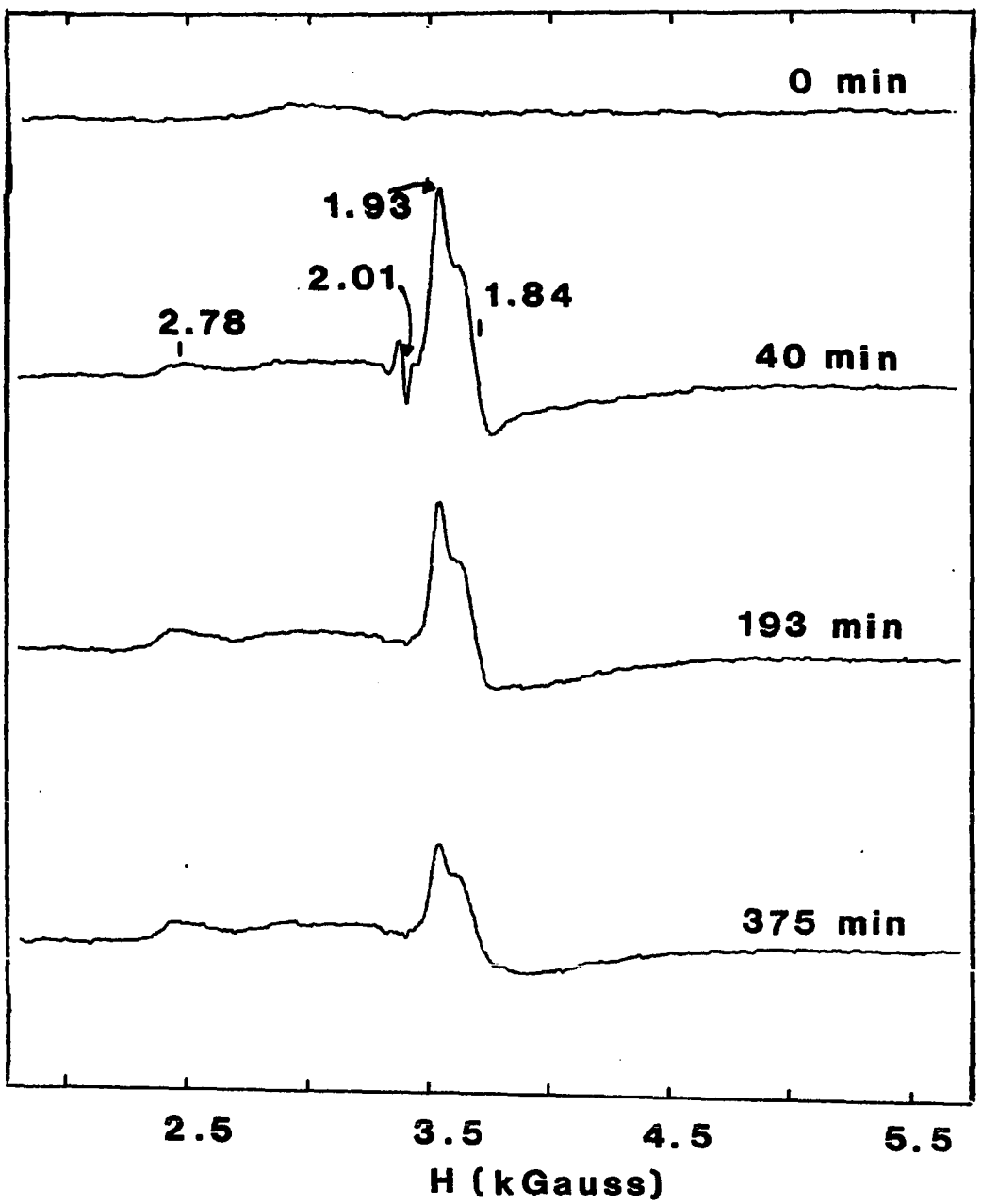

Figure 3.12. Time course for the intracellular oxidation by nitrite of O_2-depleted erythrocytes from Phascolopsis goudlii

Spectral conditions: temperature, 4.2 K; frequency, 9.57 GHz; power, 100 μW; modulation, 16 G; gain, 8 x 10^4; time constant, 0.2 s; 50.4 mM $NaNO_2$; sea water adjusted to pH 7.2; equilibration conducted at 0°C

Figure 3.13. EPR spectra of assay mixtures containing Fe^{2+}(EDTA) and either gaseous NO (A), a 2-fold excess of $NaNO_2$ (B), or a saturated aqueous solution of NO (C)

Spectral parameters: temperature, 4.2 K; frequency, 9.57 GHz (A and B), 9.42 GHz (C); power, 100 μW; modulation, 16 G; gain, 6.3×10^3 (A), 2.5×10^4 (B), 1×10^4 (C); time constant, 0.2 s

A. 5.57 mM Fe^{2+}; 49.7 mM EDTA: $[NO]/[Fe^{2+}] = 4.20$; 50 mM phosphate, pH 6.5; 0.3 M sulfate

B. 2.02 mM Fe^{2+}; 23.2 mM EDTA: 4.35 mM $NaNO_2$; 50 mM phosphate, pH 6.5

C. 1.38 mM Fe^{2+}; 12.4 mM EDTA; 1.42 mM NO; 50 mM phosphate, pH 6.5

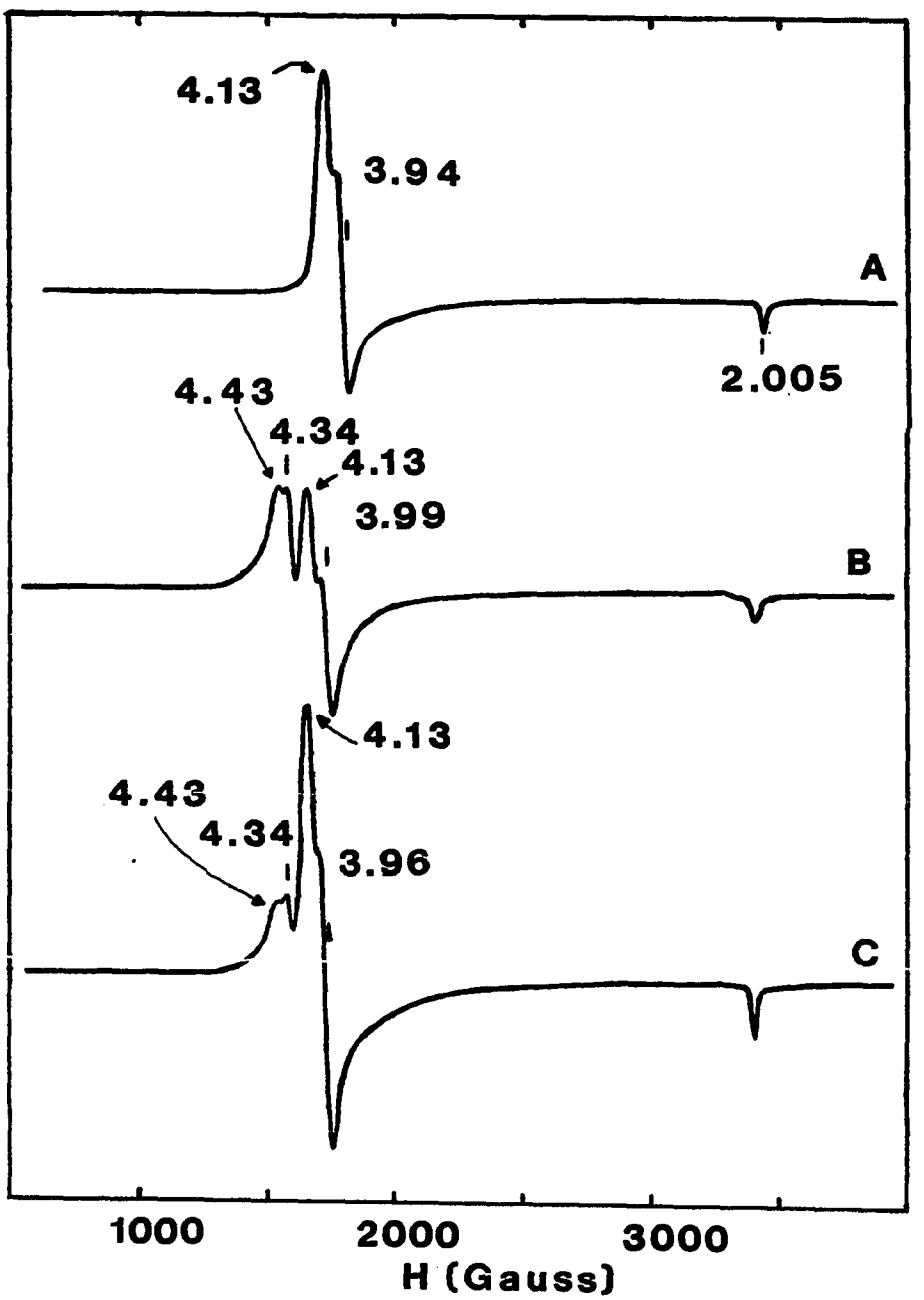
4.13
3.94
A
2.005
4.43
4.34
4.13
3.99
B
4.13
4.43
4.34
3.96
C
1000
2000
3000
H (Gauss)

excess of sodium nitrite (B), or a saturated aqueous solution of NO (C) are shown.

Rich et al. (125) have shown that a nitric oxide adduct having g-values of 4.1, 3.95, and 2.0 forms when nitrite is added to a solution containing Fe^{3+}(EDTA) and dithionite. This spectrum is typical of monomeric S = 3/2 $\{FeNO\}^7$ compounds. The identical spectrum is obtained when gaseous NO is injected into a solution of Fe^{2+}(EDTA) (Fig. 3.13A).

Figure 3.14 depicts the optical spectrum obtained from such a solution. A shoulder occurs at 340 nm with peaks at 430 nm and 640 nm. Estimates of the extinction coefficients at each of these wavelengths are tabulated in Table 3.5.

Oxidation of Fe^{2+}(EDTA) with nitrite leads to a mixture containing approximately equal amounts of high spin Fe^{3+}(EDTA) which has its principal g-value at 4.3, and this NO adduct (Fig. 3.13B):

$$2Fe^{2+}(EDTA) + HONO \rightarrow Fe^{3+}(EDTA) + Fe^{2+}(EDTA)NO + OH^- \quad . \quad (3.13)$$

The optical changes accompanying the reaction are shown in Fig. 3.15. In contrast to the binding of nitric oxide to Fe^{2+}(EDTA), the reaction of nitrite with Fe^{2+}(EDTA) is not complete within the time of mixing. Thus, nitric oxide is generated during the nitrite oxidation of Fe^{2+}(EDTA) and is trapped as Fe^{2+}(EDTA)NO.

When NO, that was prepared as a saturated stock solution, was added to the Fe^{2+}(EDTA) assay mixture (Fig. 3.13C), signals attributable to the NO adduct were invariably accompanied by features at g = 4.3. The

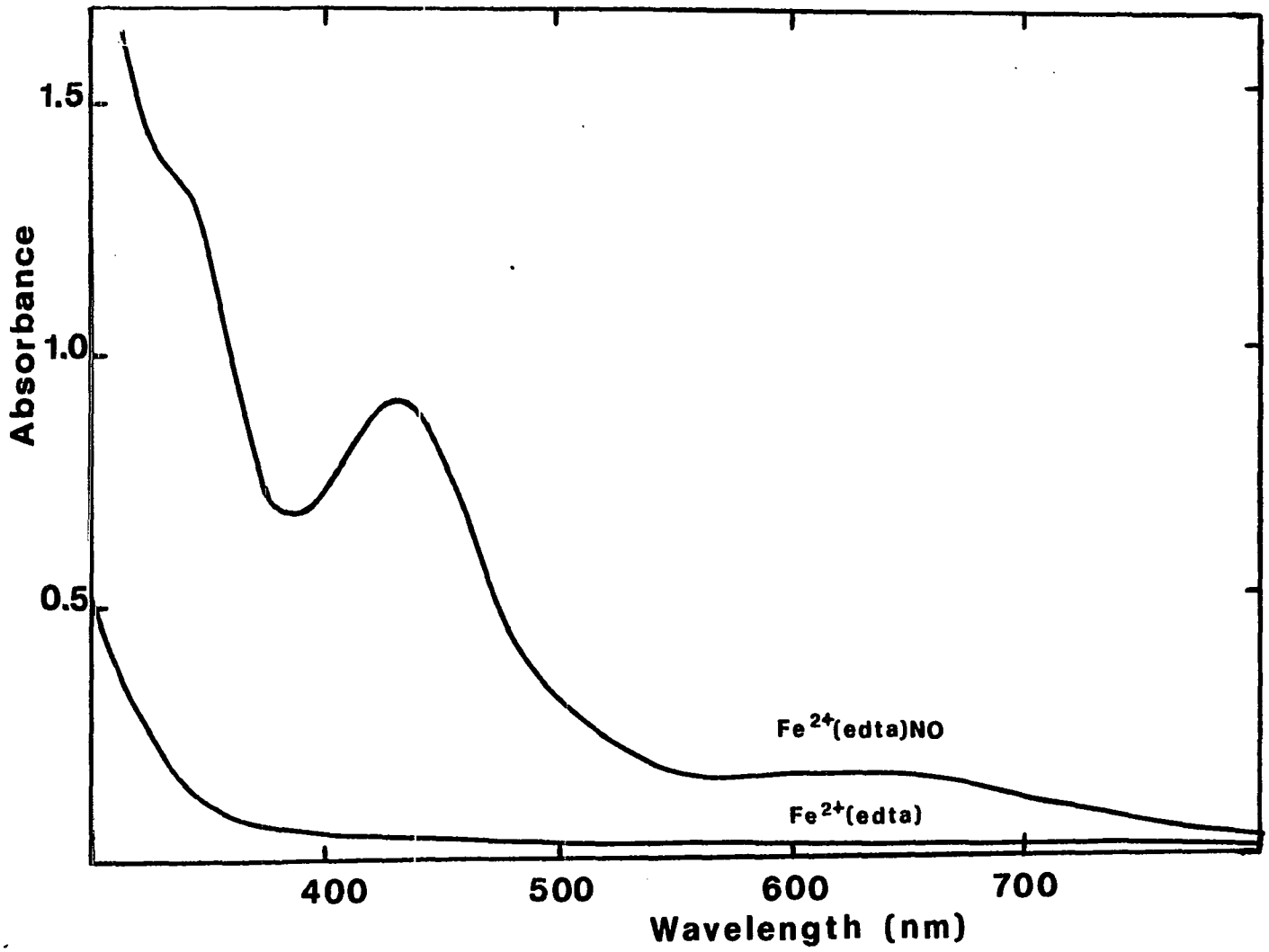

Figure 3.14. Optical spectra of Fe^{2+}(EDTA) and Fe^{2+}(EDTA)NO

1.40 mM Fe^{2+}; 12.4 mM EDTA; [NO]/[Fe^{2+}] = 4.20; 50 mM phosphate, pH 6.5; 0.3 M sulfate

Table 3.5. Estimates of the extinction coefficients for $Fe^{2+}(EDTA)NO$[a]

$[Fe^{2+}]$ (mM)	[EDTA] (mM)	$[NO]/[Fe^{2+}]$	ε ($M^{-1}cm^{-1}$) 340 nm	430 nm	640 nm
1.21	12.5	4.80	1100	763	141[b]
1.49		3.90	--	572	101[c]
1.40		4.20	891	650	107
1.38	12.4	1.03	--	522	68[d]
1.33	15.2	0.99	900	564	89[d]
		average =	960	610	100
			±96	±85	±24

[a] 50 mM phosphate; pH 6.5; 0.3 M Na_2SO_4.

[b] ^{15}NO.

[c] D_2O.

[d] No sulfate present.

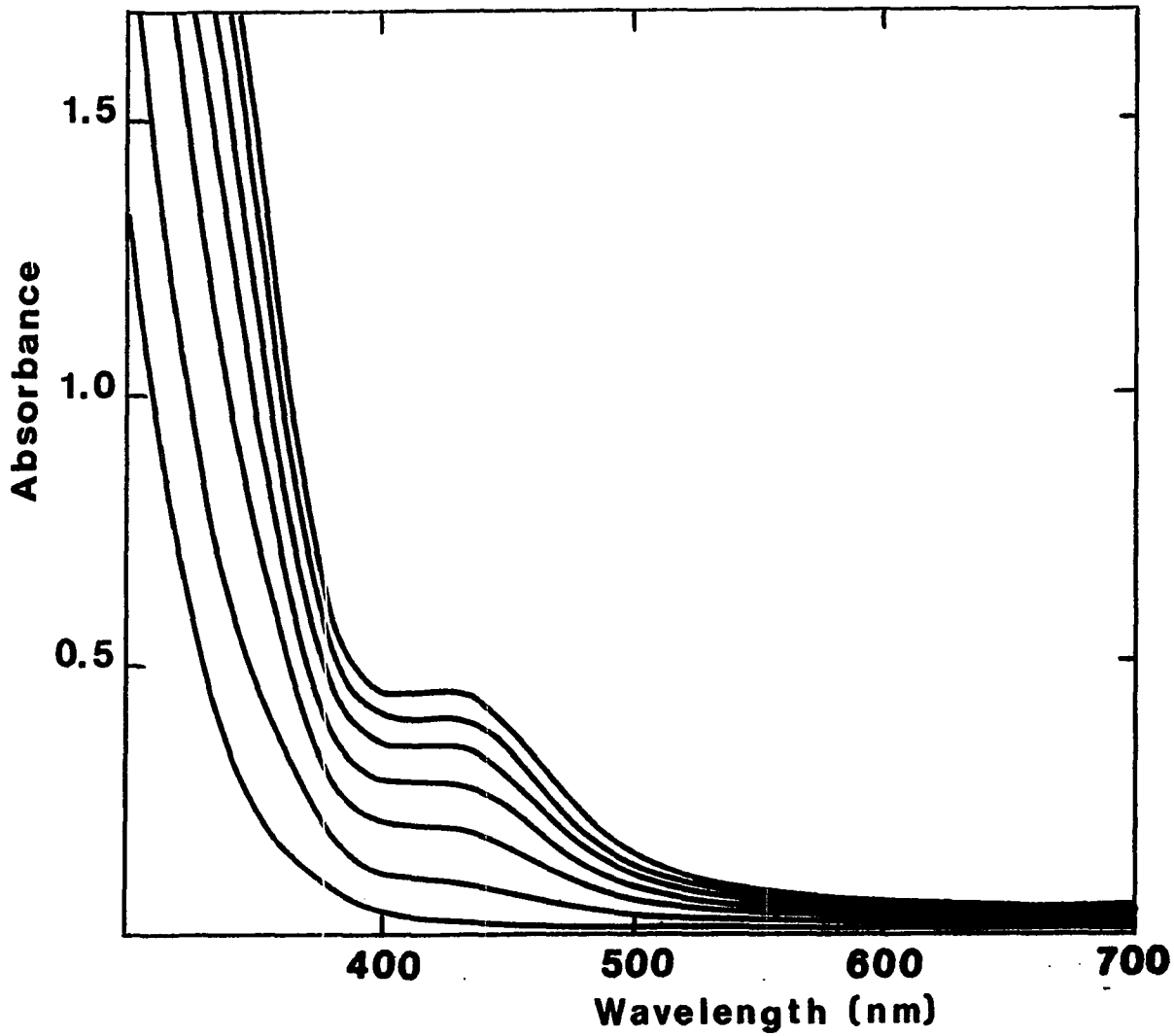

Figure 3.15. Spectral time course for the oxidation of Fe^{2+}(EDTA) with sodium nitrite

2.03 mM Fe^{2+}; 23.3 mM EDTA: 4.08 mM $NaNO_2$; 50 mM phosphate, pH 6.5

presence of signals due to oxidized iron suggests that oxidizing equivalents, probably in the form of sodium nitrite, are generated when preparing the stock solutions of NO. For this reason, preparation of NO derivatives by the direct addition of gaseous NO is preferred. This result suggests that examining the reactions of nitrite may assist in interpreting results of reactions with nitric oxide.

C. Preparation and Characterization of NO Adducts of $(Semi\text{-}met)_O$ and $(Semi\text{-}met)_R$

Disproportionation leading to a mixture of deoxyHr and metHr has been reported to occur with semi-metHr in anaerobic solutions (reaction 3.14) (71).

$$2\ \text{semi-metHr} \rightarrow \text{deoxyHr} + \text{metHr} \qquad (3.14)$$

Under aerobic conditions, the observed products are oxyHr (resulting from the binding of oxygen to deoxyHr) and metHr. This result implies that oxygen reacts only indirectly with semi-metHr. In contrast, the mechanism proposed for the oxidation of deoxyHr by nitrite invokes the formation of an EPR-silent nitric oxide adduct of semi-metHr as an intermediate. This suggests that nitric oxide should react directly with the binuclear iron center of semi-metHr to produce an EPR-silent derivative. To test this proposal, the reactions of nitric oxide with $(semi\text{-}met)_O$ and $(semi\text{-}met)_R$ were investigated.

1. Preparation and characterization of $(semi\text{-}met)_R NO$

Addition of a 1 to 10-fold molar excess of nitric oxide to an anaerobic solution of $(semi\text{-}met)_R$ produces a dark brown-colored adduct. The optical spectrum of this product (Fig. 3.16) has peaks at 330 and 380 nm and a shoulder at 510 nm. Table 3.6 shows the extinction coefficients calculated for several preparations of $(semi\text{-}met)_R NO$.

The values for the extinction coefficients at 330 nm and 380 nm are typical of those for semi-met adducts, being ~50% of the metHr values (Table 1.4). However, the appearance of two peaks in this range is unique for semi-met adducts [e.g., compare the spectra of semi-metN_3^- and $(semi\text{-}met)_R NO$ in Fig. 3.16]. In addition, the feature near 600 nm that occurs for the S = 3/2 $\{FeNO\}^7$ unit of deoxyNO, deoxyF^-NO, and Fe^{2+}(EDTA)NO is absent (see section III.D).

The EPR spectrum of $(semi\text{-}met)_R$ has g-values at 1.95, 1.87, and 1.67 (77). A sample frozen five minutes after a 4.5-fold molar excess of NO(g) was added to $(semi\text{-}met)_R$ (Fig. 3.17B) accounts for only 14% of the Hr, and the paramagnetic component resembles that of deoxyNO (see section III.D) rather than $(semi\text{-}met)_R$. The sample of $(semi\text{-}met)_R$ frozen prior to the addition of NO accounted for 89% of the Hr. Thus, addition of NO to $(semi\text{-}met)_R$ results in the disappearance of the $(semi\text{-}met)_R$ EPR signal.

Kinetic measurements of the rate of reduction of metHr with excess dithionite have shown that $(semi\text{-}met)_R$ is unstable, being ultimately reduced to deoxyHr (102-104). To ascertain that the loss of the EPR signal is indeed the result of a reaction of NO with $(semi\text{-}met)_R$ and not

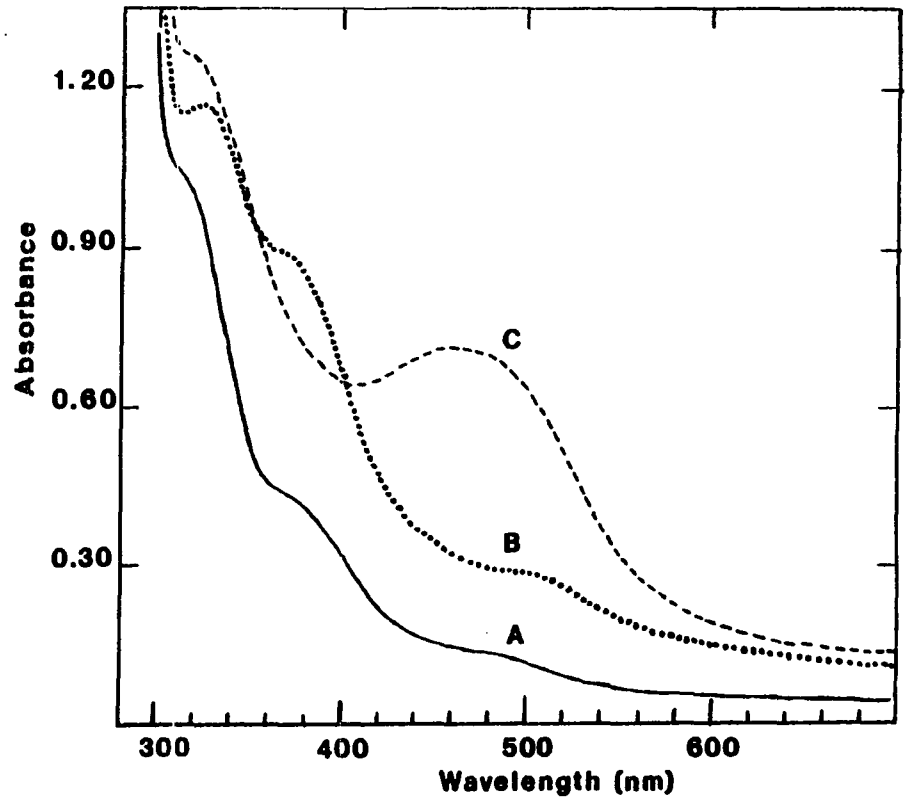

Figure 3.16. Optical spectra of $(semi\text{-}met)_R$ (A), $(semi\text{-}met)_RNO$ (B), and $semi\text{-}metN_3^-$ (C) in 50 mM phosphate (pH 6.5)

A. 0.240 mM Hr; 0.119 mM dithionite
B. 0.240 mM Hr; 0.119 mM dithionite; 1.08 mM NO
C. 0.215 mM Hr; 4.15 mM azide; 4 3/4 hrs after adding azide to sample B

Table 3.6. Extinction coefficients for (semi-met)$_R$NO[a]

[Hr] (mM)	[$S_2O_4^{2-}$] (mM)	[NO]/[Hr]		ε ($M^{-1}cm^{-1}$) 330 nm	380 nm	510 nm
0.240	0.238	4.54		4870	3520	1120
0.190	0.188	2.61		4980	3400	1140
0.198	0.209	5.80		5040	3490	1280
			average =	4960	3470	1180
				±70	±51	±71

[a]pH 6.5; 50 mM phosphate.

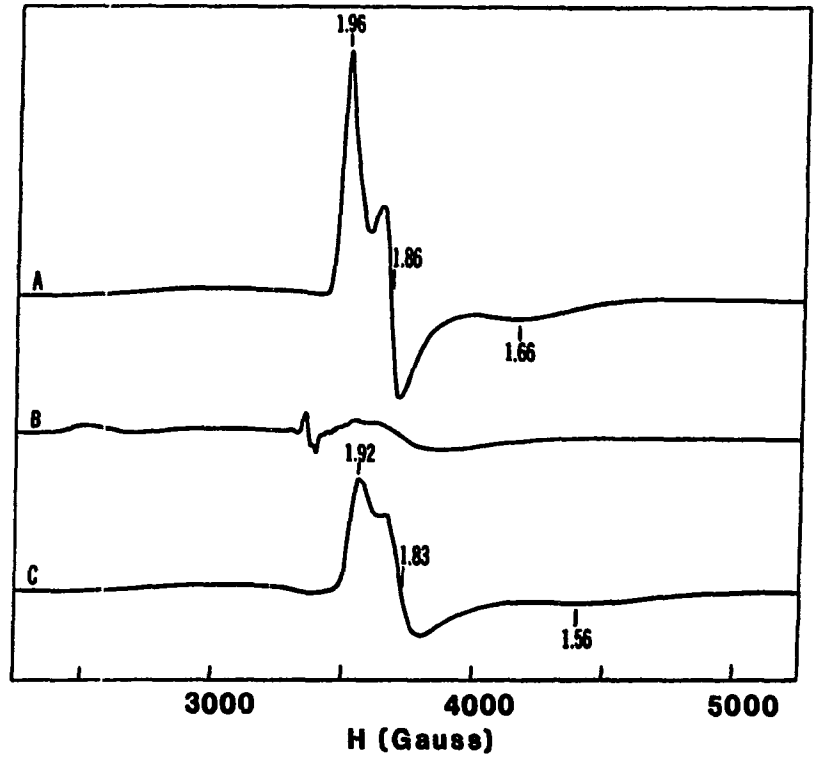

Figure 3.17. EPR spectra showing the disappearance of the EPR signal upon addition of NO to $(\text{semi-met})_R$

Spectral parameters: temperature, 4.2 K; frequency, 9.57 GHz; power, 100 μW; modulation, 16 G; gain, 4×10^4; time constant, 0.2 s

A. 1.44 mM Hr; 1.43 mM dithionite; 50 mM phosphate, pH 6.5; 5 minutes after addition of dithionite

B. NO added 7 minutes after adding dithionite to metHr; [NO]/[Hr] = 4.55

C. N_3^- (22-fold excess over Hr) added to the remainder of sample B at 20 minutes and aliquot frozen at 5.5 hrs; $[Hr]_{total}$ = 1.27 mM

the result of this inherent instability, aliquots of a $(semi\text{-}met)_R$ stock solution were withdrawn and EPR samples were frozen at various times after the preparation of $(semi\text{-}met)_R$. In order to minimize the decomposition, only one reducing equivalent of dithionite was used to prepare $(semi\text{-}met)_R$. The results of this experiment are shown in Fig. 3.18 and the double integrations of these signals are summarized in Table 3.7.

After 36 minutes, 24% of the Hr remains as $(semi\text{-}met)_R$ when NO is absent from the solution. When NO is present, only 14% of the Hr is in a paramagnetic form five minutes after the preparation of $(semi\text{-}met)_R$. It is clear that the EPR signal for $(semi\text{-}met)_R$ disappears more rapidly when NO is added to the reaction mixture. If one is to obtain quantitative formation of $(semi\text{-}met)_RNO$, one must add NO within minutes after preparing $(semi\text{-}met)_R$.

There are three possible reactions that could lead to the disappearance of the EPR signal (reactions 3.15 to 3.17).

Disproportionation of $(semi\text{-}met)_R$:

$$2(semi\text{-}met)_R \rightarrow deoxyHr + metHr \qquad (3.15)$$

Binding of NO to $(semi\text{-}met)_R$:

$$(semi\text{-}met)_R + NO \rightarrow (semi\text{-}met)_RNO \qquad (3.16)$$

Oxidation of $(semi\text{-}met)_R$ to metHr by NO:

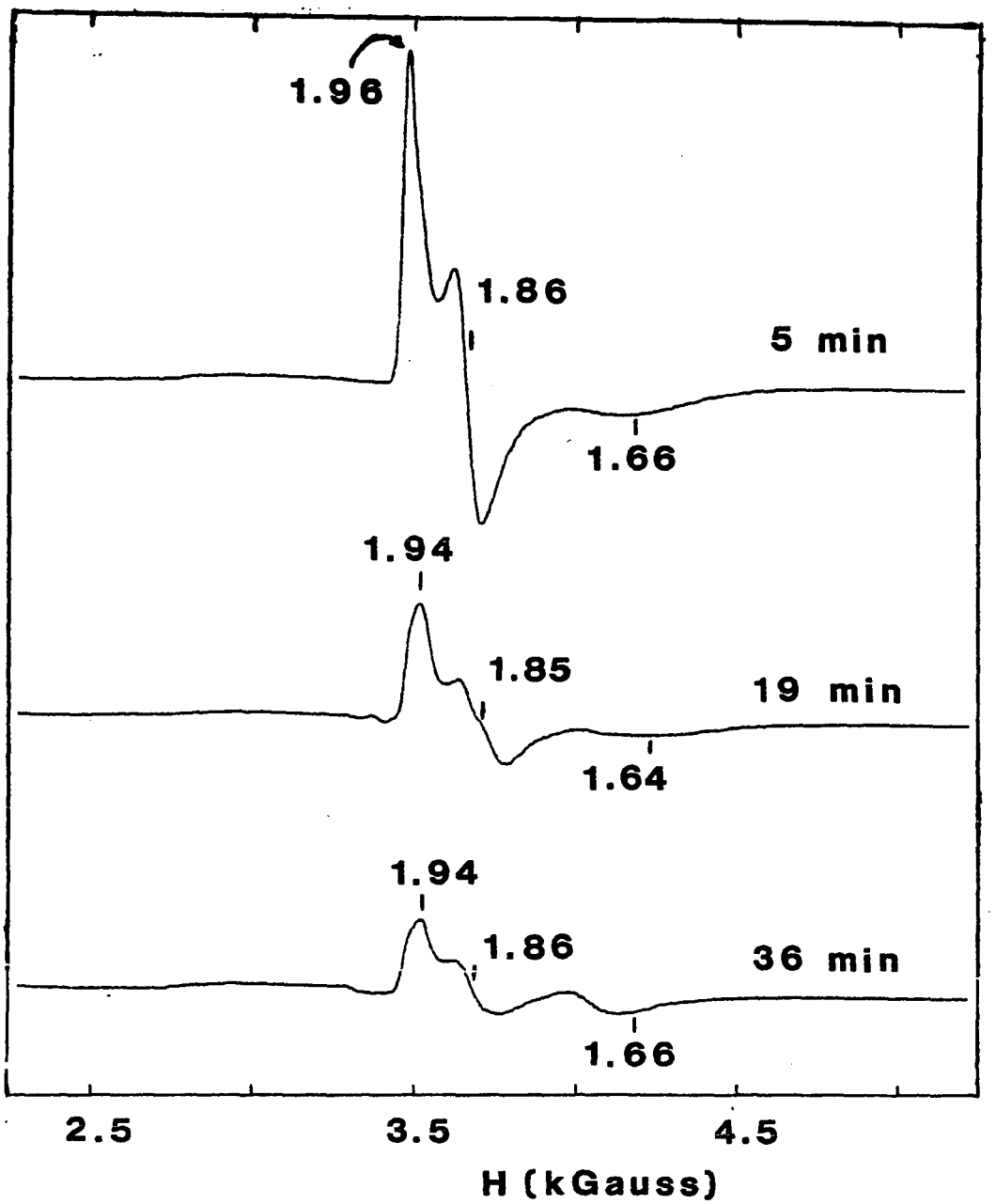

Figure 3.18. Time course for the disappearance of the EPR signal of $(semi\text{-}met)_R$ prepared with one equivalent of dithionite

Spectral parameters: temperature, 4.2 K; frequency, 9.57 GHz; power, 100 μW; modulation, 16 G; gain, 4 x 10⁴; time constant, 0.2 s; 1.44 mM Hr; 0.713 mM dithionite; 50 mM phosphate, pH 6.5

Table 3.7. Double integration of the EPR signals observed during the decomposition of $(semi\text{-}met)_R$[a]

Time (min)[b]	% pmag
5	89
19	80
36	24

[a]% pmag = [spins]/[Hr] x 100%; [Hr] = 1.44 mM; [dithionite] = 0.713 mM; pH 6.5; 50 mM phosphate.

[b]Measured relative to the time at which dithionite was added to metHr.

$$(\text{semi-met})_R + NO \rightarrow \text{met} + NO^-(N_2O) \qquad (3.17)$$

The first of these, the disproportionation of $(\text{semi-met})_R$, should produce a mixture of deoxyHr and metHr. In the presence of NO, deoxyHr would be converted to deoxyNO. Thus, if disproportionation were occurring, equimolar amounts of deoxyNO and metHr should be obtained. Detection of only 14% deoxyNO indicates that reaction 3.15 is not occurring to any appreciable extent. It is more likely that the presence of 14% deoxyNO resulted from the presence of deoxyHr in the original $(\text{semi-met})_R$ sample, rather than from the reduction of $(\text{semi-met})_R$ by NO.

Binding of NO to the paramagnetic mixed valence derivative, $(\text{semi-met})_R$ (reaction 3.16) or oxidation of the iron site by NO (reaction 3.17) could also result in an EPR-silent product. To differentiate between these two possibilities, sodium azide was added to a portion of the EPR-silent reaction mixture. The optical spectrum obtained from the sample containing NO and azide exhibits a peak at 470 nm (Fig. 3.16C), showing that the product is semi-metN_3^- rather than metN_3^-. Furthermore, the EPR spectrum obtained for the azide-containing sample (frozen five hours after the addition of azide) exhibits g-values at 1.92, 1.83, and 1.56 (Fig. 3.17C). These parameters are similar to those reported previously for semi-metN_3^- (77). Quantitation of the EPR signal for this sample by double integration accounts for 84% of the Hr. Since 89% of the Hr was originally present as $(\text{semi-met})_R$, the nearly quantitative production of semi-metN_3^- indicates that NO binds to $(\text{semi-met})_R$ (reaction 3.16) without oxidizing or reducing $(\text{semi-met})_R$.

Table 3.8 enumerates the spin-coupling schemes that could explain the absence of an EPR signal when NO binds to semi-metHr. It is assumed that nitric oxide binds to only one of the irons of the binuclear site, and that only the iron to which NO binds may change its spin state. The integer ground states, $S_{eff} = 1$ and $S_{eff} = 2$, usually do not exhibit EPR signals owing to large zero-field splittings and rapid spin relaxation.

Of the possible coupling schemes, case 3 is preferred. Nitric oxide does not react with metHr (section III.E), indicating that NO prefers to bind to Fe(II). On this basis, case 2 and case 4 are deemed less likely. In addition, one would expect the FeNO moiety to be a better electron acceptor than the Fe(II) site. Thus, an [Fe(III),{FeNO}^{7}] center is more probable than an [Fe(II),{FeNO}^{6}] center. In the two remaining schemes, case 3 and case 5, NO is coordinated to the Fe(II) site. By analogy to deoxyNO (section III.D), binding of NO to the Fe(II) site results in an S = 3/2 spin state rather than an S = 1/2 spin state (section III.D). Thus, model 3 in which an S = 5/2 Fe(III) site is antiferromagnetically coupled to an S = 3/2 {FeNO}^{7} site is the most likely explanation for the absence of an EPR signal for $(semi\text{-}met)_R NO$.

2. Preparation and characterization of $(semi\text{-}met)_O NO$

The EPR spectrum of $(semi\text{-}met)_O$ is axial with g-values at 1.94 and 1.71 (77). If one freezes an EPR sample within 5 minutes after adding one equivalent of ferricyanide to deoxyHr, quantitative oxidation to $(semi\text{-}met)_O$ is observed. However, from the EPR spectrum obtained for a sample frozen ~30 min after the reaction was initiated, it is found

Table 3.8. Possible spin-coupling schemes for $(semi\text{-}met)_R NO$[a]

Case	Site A	Site B	S_{eff}
1	semi-met, S = 1/2	NO, S = 1/2	0
2	Fe(II), S = 2	$\{FeNO\}^6$, S = 2	0
3	Fe(III), S = 5/2	$\{FeNO\}^7$, S = 3/2	1
4	Fe(II), S = 2	$\{FeNO\}^6$, S = 0	2
5	Fe(III), S = 5/2	$\{FeNO\}^7$, S = 1/2	2

[a] S_{eff} was determined by assuming antiferromagnetic rather than ferromagnetic coupling between the two sites.

that only 18% of the Hr remains in a paramagnetic state. Figure 3.19 shows the time course for the disappearance of the EPR signal of (semi-met)$_0$ and Table 3.9 summarizes the results of the double integration of these signals.

Changes in the optical spectrum of a (semi-met)$_0$ solution accompany the disappearance of the EPR signal (Fig. 3.20). An isosbestic point is observed at 410 nm. The final spectrum, obtained after three hours, resembles that of the low pH form of metHr. When sodium azide was added anaerobically to this solution after allowing the reaction to proceed overnight, it was found that 80% of the Hr had been converted to metN_3^-. Similarly, when oxygen was added instead of azide, the development of a peak at 500 nm verified the presence of deoxyHr. Thus, the decrease of the (semi-met)$_0$ EPR signal results from the disproportionation of (semi-met)$_0$ (reaction 3.14).

Addition of a 4 to 5-fold molar excess of NO(g) to an anaerobic solution of (semi-met)$_0$ (within 3-5 minutes after its preparation) leads to subtle changes in the optical spectrum. Within 1-2 minutes, the pale yellow (semi-met)$_0$ solution turns a golden-brown color. The optical spectrum resulting ~5 minutes after the addition of NO (Fig. 3.21) exhibits a broad feature at 620 nm and a shoulder near 350 nm.

For comparison, Fig. 3.21 also shows the optical spectrum of (semi-met)$_R$NO. Distinct differences in the optical spectra indicate that the adduct of (semi-met)$_0$ is not the same as that formed with (semi-met)$_R$. The feature at 620 nm in the spectrum of (semi-met)$_0$NO is not observed for (semi-met)$_R$NO. On the other hand, this feature is observed in the

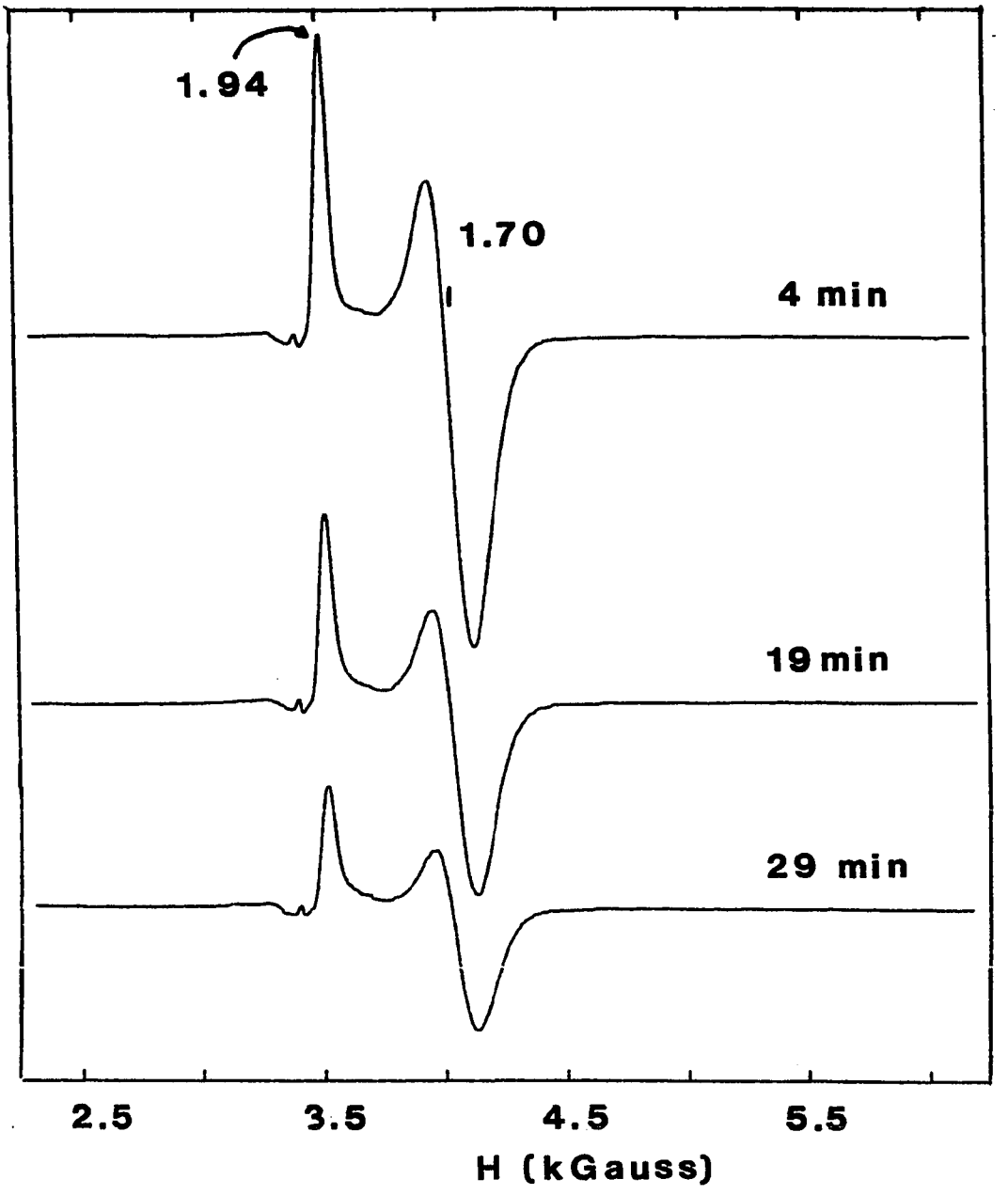

Figure 3.19. Time course for the disappearance of the EPR signal of $(semi\text{-}met)_O$ prepared with one equivalent of ferricyanide

Spectral parameters: temperature 4.2 K; frequency, 9.57 GHz; power, 100 μW; modulation, 16 G; gain, 4 x 10^4; time constant, 0.2 s; 1.04 mM Hr; 1.05 mM ferricyanide; 50 mM phosphate, pH 6.5

Table 3.9. Double integration of the EPR signals observed during the decomposition of $(semi\text{-}met)_0$[a]

Time (min)[b]	% pmag[c]
4	108
10	87.7
29	17.9

[a]50 mM phosphate; pH 6.5; [Hr] = 1.04 mM; [ferricyanide] = 1.05 mM.

[b]Measured relative to the time at which ferricyanide was added to deoxyHr.

[c]% pmag = [spins]/[Hr] x 100.

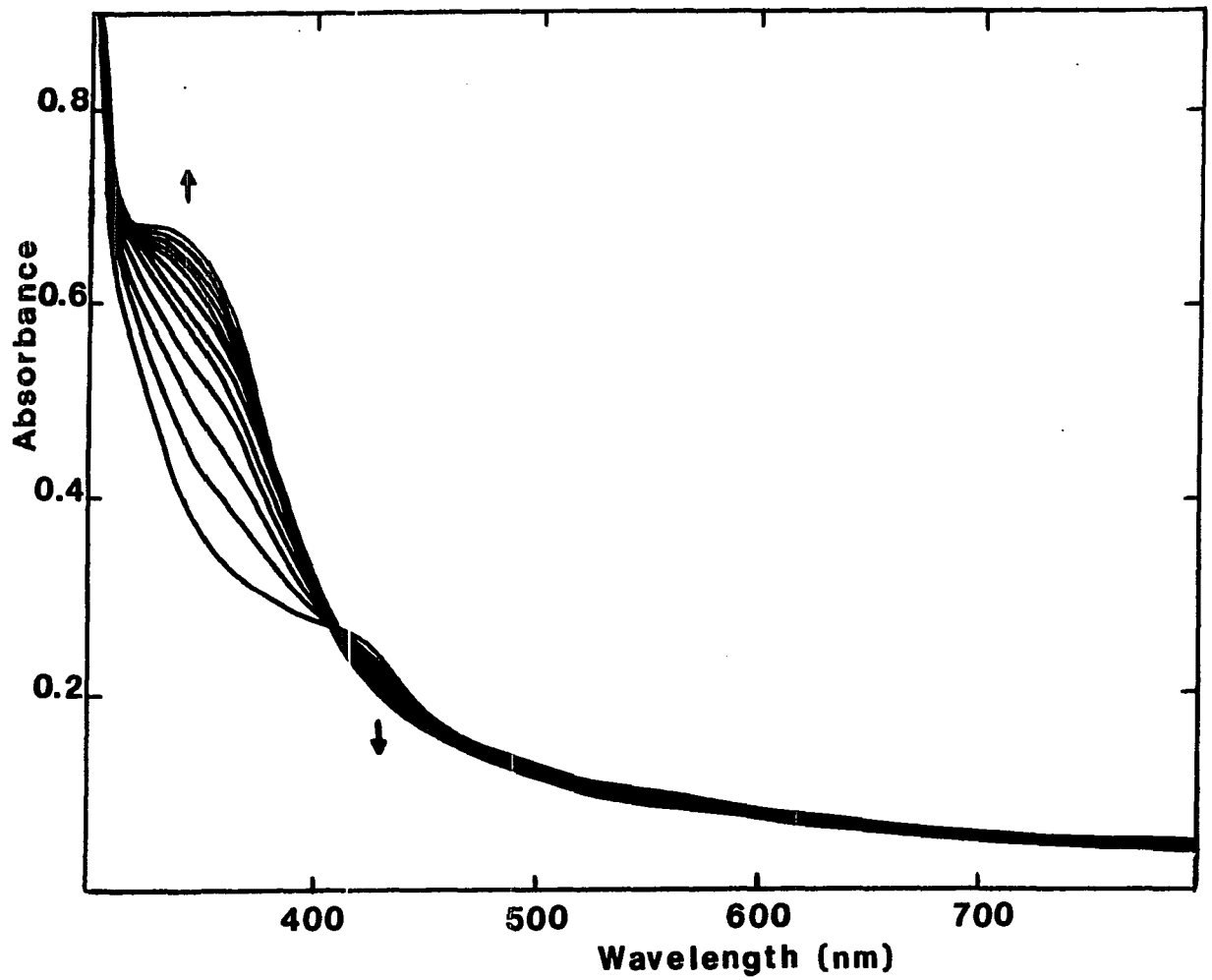

Figure 3.20. Spectral time course for the decomposition of (semi-met)$_0$ prepared with one equivalent of ferricyanide

0.116 mM Hr; 0.110 mM ferricyanide; 50 mM phosphate, pH 6.5; 0.1 M perchlorate; spectra recorded at 10 minute intervals; last three spectra are at 30 minutes intervals

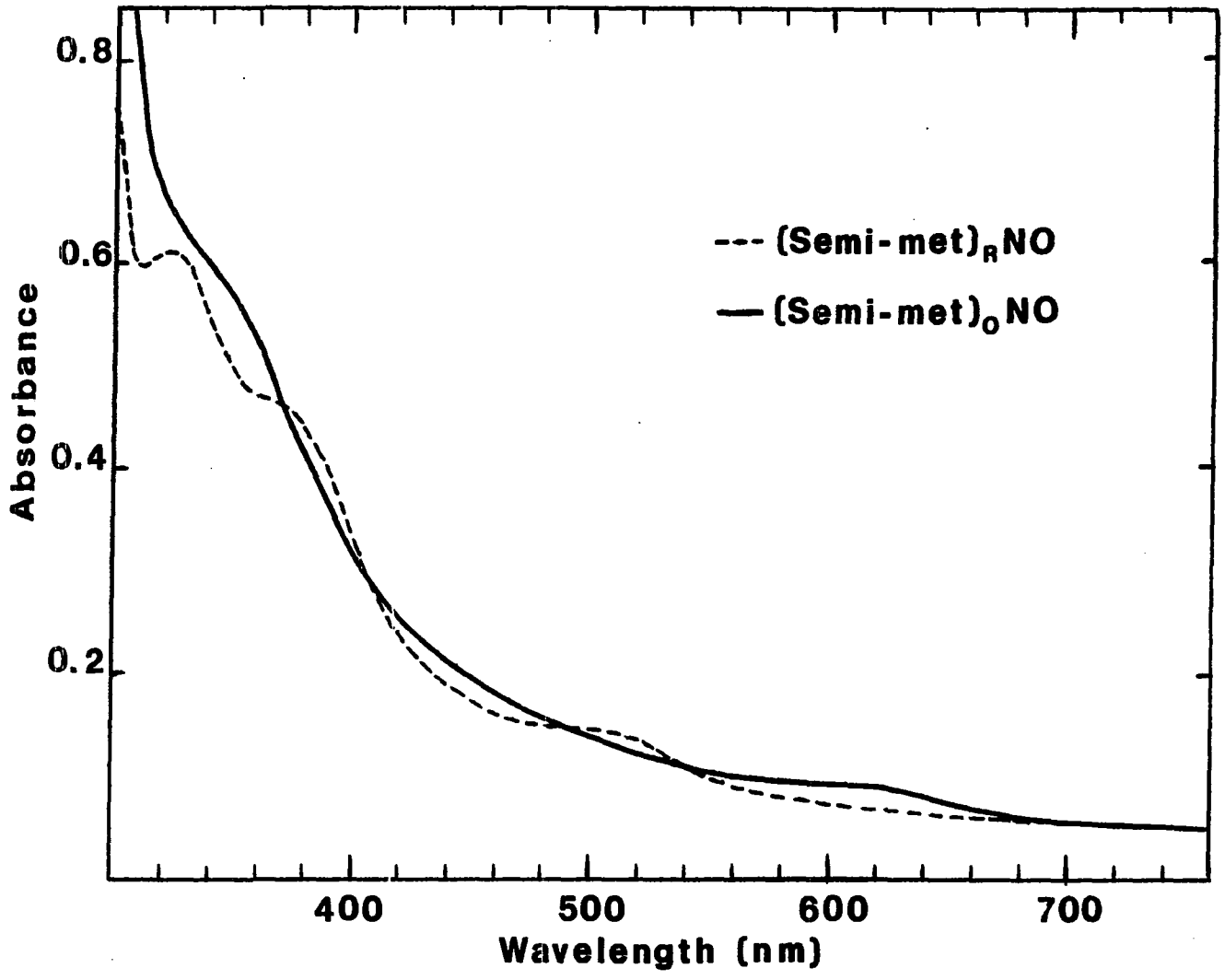

Figure 3.21. Optical spectra for (semi-met)$_O$NO and (semi-met)$_R$NO

0.125 mM Hr; 50 mM phosphate, pH 6.5; [NO]/[Hr] = 8.54 for (semi-met)$_O$NO and 4.55 for (semi-met)$_R$NO; sample of (semi-met)$_O$NO contains 0.3 M sulfate

optical spectra of deoxyNO and deoxyF⁻NO (section III.D). Thus, the coordination geometry of the FeNO moiety in $(semi\text{-}met)_0NO$ may be more "deoxy-like" than in $(semi\text{-}met)_RNO$.

Like the reaction between $(semi\text{-}met)_R$ and NO, the addition of NO to $(semi\text{-}met)_0$ leads to loss of the EPR signal for semi-metHr (Fig. 3.22). Figure 3.22 shows that the EPR signal associated with $(semi\text{-}met)_0$ disappears more quickly when NO is present.

Table 3.10 summarizes the results of the double integrations of the EPR signals before and after the addition of NO. These results demonstrate that the reaction between NO and $(semi\text{-}met)_0$ is nearly quantitative.

The EPR-silent nature of this adduct also is not the result of oxidation or reduction since a semi-metN_3^- EPR signal appears when azide is added in a 50-fold molar excess.

3. Resonance Raman spectra of semi-metNO

Semi-metNO may also be prepared by the spontaneous auto-oxidation of deoxyNO. This method, discussed in section III.F, was used to prepare the samples of semi-metNO from which resonance Raman spectra were obtained.

As with most of the other nitric oxide derivatives, two vibrational bands are observed (Table 3.11). For semi-metNO, these appear at 431 cm^{-1} and 423 cm^{-1}. By analogy to the assignments made for deoxyNO (section III.D), the band at higher energy is assigned as ν(Fe-NO) and the low energy band is assigned as δ(Fe-N-O), providing direct evidence that for semi-metNO, nitric oxide is bound to the binuclear center.

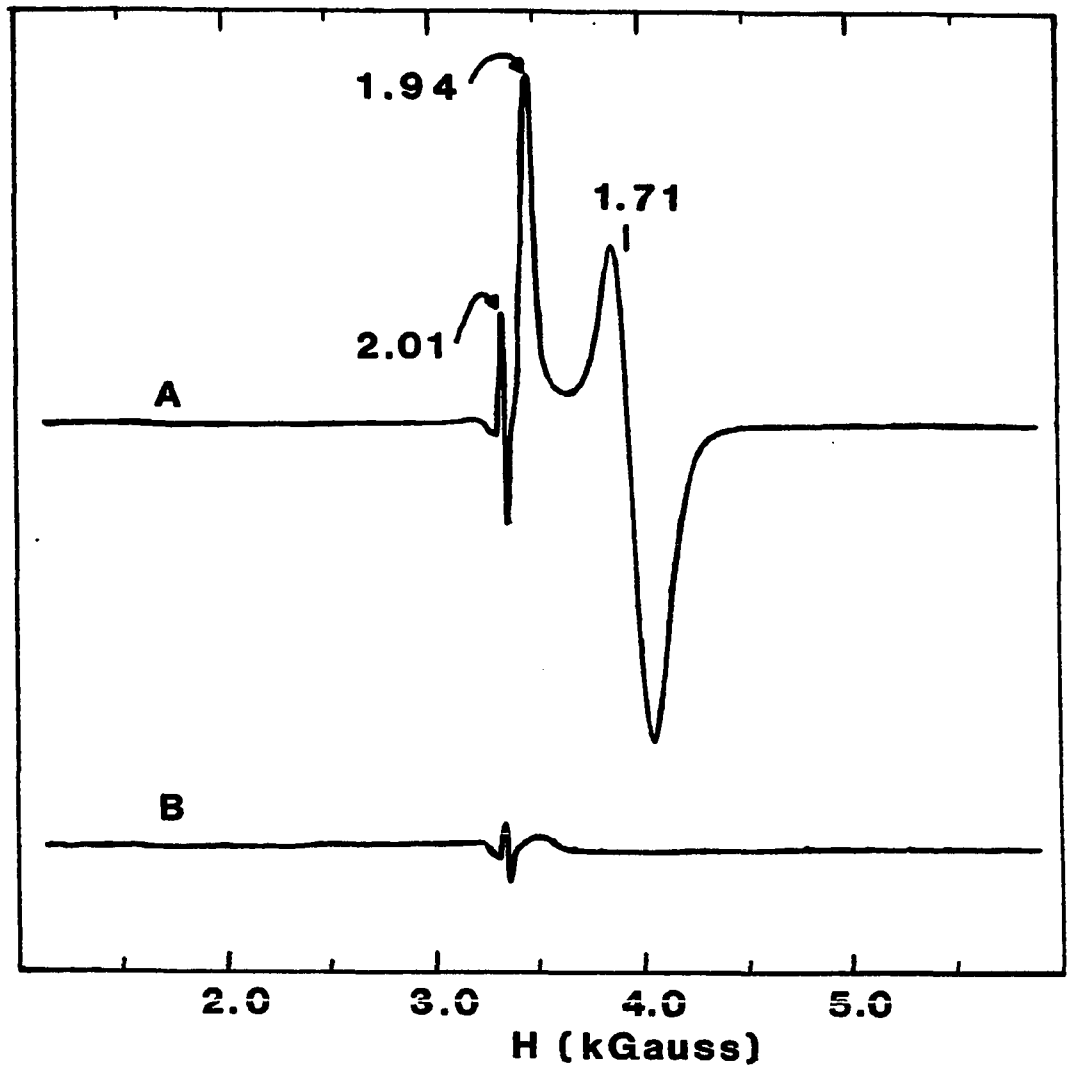

Figure 3.22. EPR spectra showing the disappearance of the EPR signal for $(\text{semi-met})_0$ upon addition of NO

Spectral parameters: temperature, 4.2 K; frequency, 9.42 GHz; power, 100 μW; modulation, 16 G; gain, 4×10^4; time constant, 0.2 s; 1.77 mM Hr; 1.74 mM ferricyanide; [NO]/[Hr] = 4.7; 50 mM phosphate, pH 6.5; 0.3 M sulfate; samples frozen 3 minutes after adding ferricyanide (A) and 2 minutes after adding NO (B)

Table 3.10. Double integration of the EPR signals before and after the addition of nitric oxide to $(\text{semi-met})_0$[a]

[Hr] (mM)	[ferricyanide] (mM)	[NO]/[Hr]	[spins] (mM) before	after
1.77	1.74	4.68	1.01	0.02
1.28	1.21	8.09	1.30	0.145[b]
1.41	1.25	8.54	0.658	0.066[c]

[a]pH 6.5; 50 mM phosphate.

[b]0.1 M perchlorate.

[c]0.3 M sulfate.

Table 3.11. Resonance Raman vibrational data for semi-metNO[a]

Isotope	ν_1 (cm^{-1})	ν_2 (cm^{-1})
$^{14}N^{16}O$[b]	431	423
$^{15}N^{16}O$[c]	423	416

[a]647.1 nm; 77 K; 0.25 mm slit width; 2 cm^{-1}/s scan rate.

[b]80 mW.

[c]120 mW.

D. Preparation and Characterization of NO Adducts of DeoxyHr and DeoxyF⁻Hr

1. Preparation of deoxyNO

The reaction of deoxyHr with NO is of particular interest owing to the function of NO as an analog for the physiological substrate, O_2. Unlike O_2, it is expected that NO will formally accept no more than one electron from the binuclear center, thereby, mimicking the hypothesized superoxide intermediate.

Gradual addition of a 1.5 to 5.0-fold molar excess of gaseous nitric oxide to an anaerobic solution of either oxyHr or deoxyHr results in formation of a pine-green-colored adduct, deoxyNO (Fig. 3.23).

The same product is obtained, although the yields are somewhat less, when NO is added from an aqueous stock solution. The amount of deoxyNO produced by this method decreases as the incubation time of the stock solution of NO is increased prior to adding deoxyHr (Fig. 3.24).

A third method for producing deoxyNO is to generate NO by the *in situ* decomposition of nitrosyl transfer agents: $[Co(NH_3)_5NO^{2+}]$ or $Co(dmgH)_2NO$. The pentaammine complex decomposes upon being dissolved in aqueous solutions according to reaction 3.18.

$$Co(NH_3)_5NO^{2+} \rightarrow Co^{2+} + 5NH_3 + NO \qquad (3.18)$$

The dimethylglyoximate compound, on the other hand, is stable in aqueous solutions. It was proposed (173) that the release of NO is promoted by the coordination of the Co-containing by-product to basic groups of the

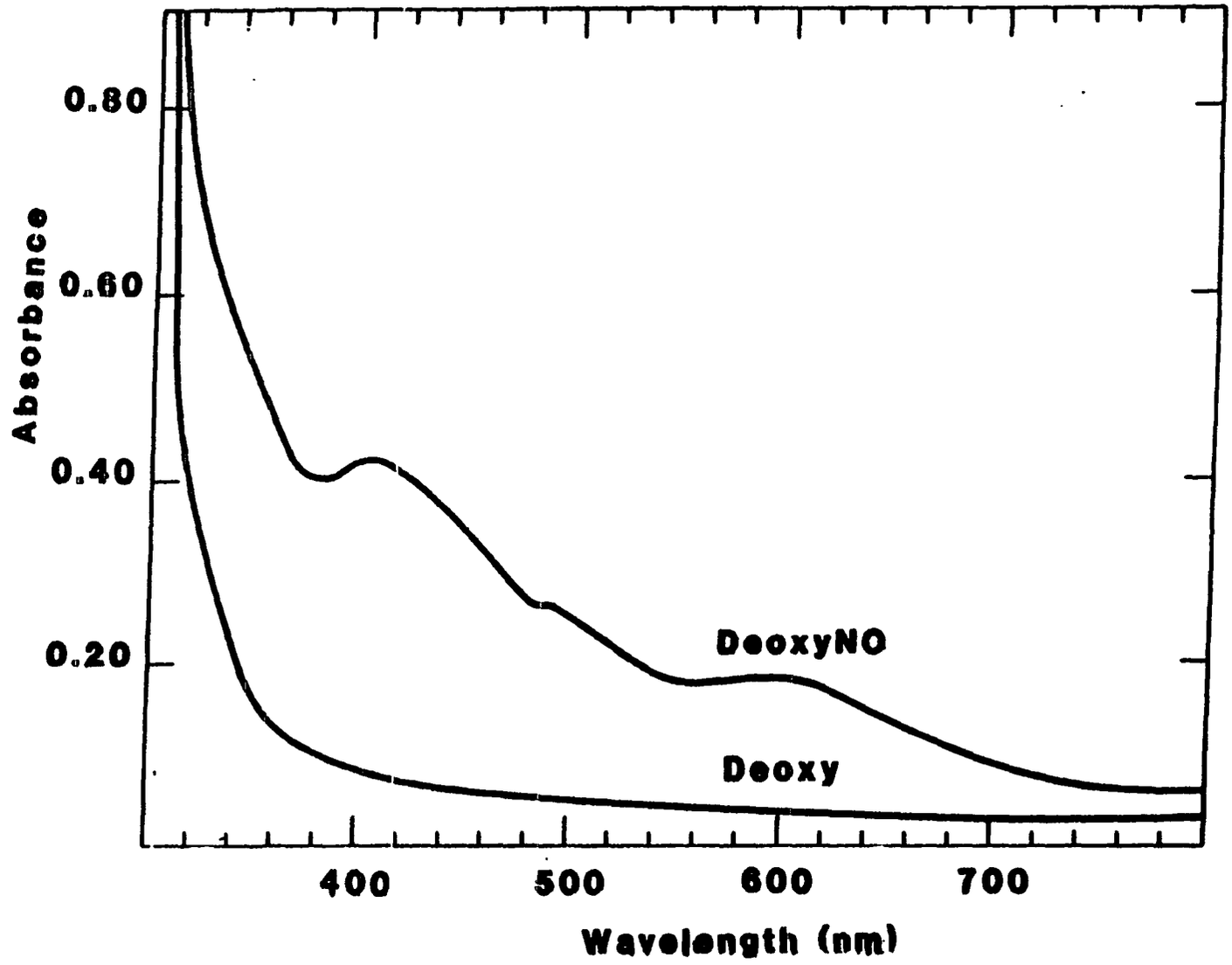

Figure 3.23. Optical spectrum of deoxyNO

0.54 mM Hr; [NO]/[Hr] ~4.0; 50 mM phosphate, pH 6.5

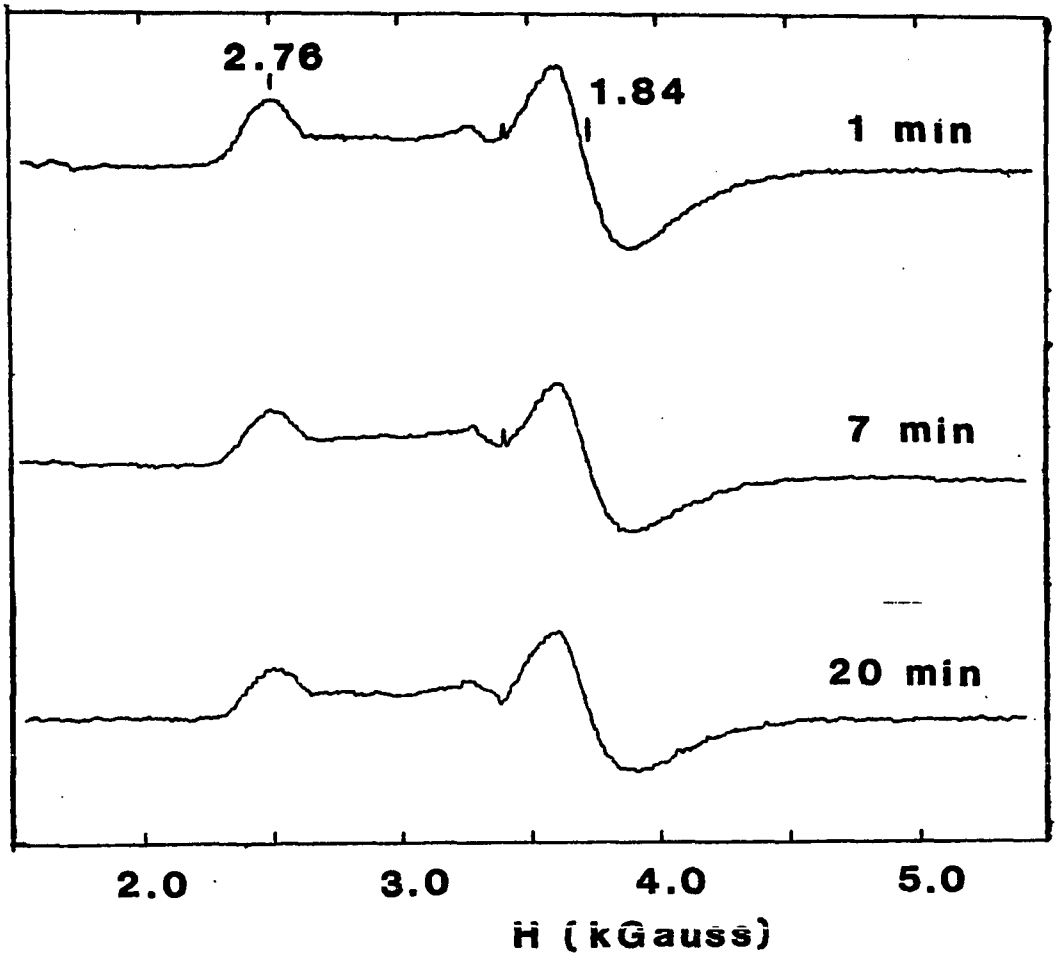

Figure 3.24. Preparation of deoxyNO using an aqueous stock solution of NO; EPR spectra resulting after varying the length of time for which the NO solution is incubated prior to adding deoxyHr

Spectral parameters: temperature, 4.2 K; frequency, 9.57 GHz; power, 100 μW; modulation, 16 G; gain, 1 x 10^5; time constant, 0.2 s; 0.712 mM Hr; 0.724 mM NO; 50 mm phosphate, pH 6.5

protein according to reactions 3.19-3.21.

$$Co(dmgH)_2NO \rightleftarrows Co(dmgH)_2 + NO \qquad (3.19)$$

$$Co(dmgH)_2 + B \rightarrow Co(dmgH)_2B \qquad B = His, Lys, Cys \qquad (3.20)$$

$$Co(dmgH)_2NO + L \rightarrow Co(dmgH)(L)NO \qquad L = Cys \qquad (3.21)$$

The fourth method utilized $(NO)BF_4$ as a source of NO. Nitric oxide was rapidly released upon addition of NO^+ to the pH 6.5 buffered protein solution. The color of the solution changed from colorless to pine-green, indicating binding of NO to deoxyHr. Unfortunately, the protein rapidly became gelatinous, making further characterization impossible.

Finally, when nitric oxide prepared from the one-electron reduction of sodium nitrite is added to deoxyHr, one obtains good yields of deoxyNO. While ascorbate, dithionite, hydroxylamine sulfate, or an acidic solution of ferrous sulfate all reduce nitrite to nitric oxide, further reduction (to N_2O) occurs to an appreciable extent for all but ascorbate. This method, using ascorbate as the reductant, was employed when preparing ^{15}NO from $Na^{15}NO_2$.

Overall, the best method found for preparing deoxyNO is the direct addition of gaseous nitric oxide to deoxyHr. At room temperature, the rate of reaction appears to be limited by the rate of dissolution of nitric oxide. For this reason and because of the instability of NO in aqueous solutions, nitric oxide is added gradually to the protein.

The reaction of deoxyHr with NO is not restricted to the species Phascolopsis gouldii. Figure 3.25 shows EPR spectra characteristic of deoxyNO obtained by addition of NO to either oxyHr (A) or deoxyHr (B) from Themiste dyscritum.

2. Characterization of deoxyNO

Four techniques were used to characterize this novel derivative: optical, EPR, Mossbauer, and resonance Raman spectroscopies.

The visible spectrum (Fig. 3.23) of deoxyNO has a moderately intense peak at 408 nm, a broad, weak feature at 600 nm, and a shoulder at 500 nm. Calculated extinction coefficients are shown in Table 3.12.

Unlike oxidized Hr derivatives (Table 1.4 and Fig. 1.10), the spectrum for deoxyNO lacks the characteristic bands between 300 and 400 nm. Features in this region are indicative of $O^{2-} \rightarrow Fe^{3+}$ charge transfer transitions of the μ-oxo bridge. Therefore, deoxyNO does not appear to contain an Fe(III)-O-Fe(III) moiety.

The electronic spectrum of deoxyNO shows a remarkable resemblance to the optical spectrum of Fe^{2+}(EDTA)NO (Fig. 3.14). Apparently, the two compounds have similar electronic environments. The similarity of the optical spectrum of deoxyNO to that of Fe^{2+}(EDTA)NO, a mononuclear compound, suggests that nitric oxide is coordinated to only one iron of the binuclear pair of deoxyNO. In addition, the optical transitions do not arise form $Fe\text{-}O_{oxo}$ LMCT transitions, since no such bridge is present in Fe^{2+}(EDTA)NO.

In the ^{57}Fe-Mossbauer spectrum of deoxyNO (Fig. 3.26B), occurrence of two distinct quadrupole doublets having nearly equal areas also shows

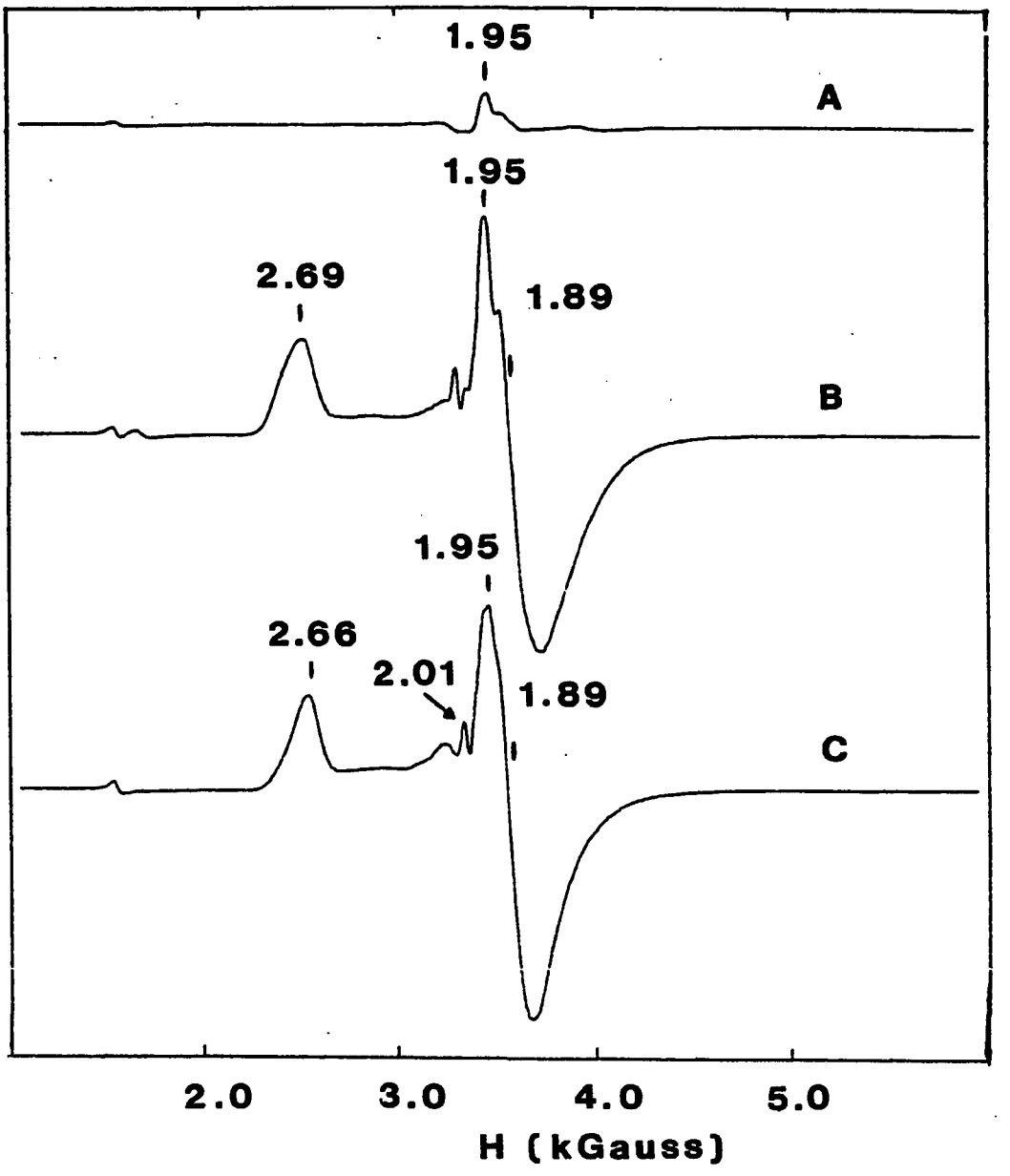

Figure 3.25. Preparation of deoxyNO with Hr from Themiste dyscritum

Spectra parameters: temperature, 4.2 K; frequency, 9.43 GHz; power, 40 μW; modulation, 40 G; gain, 2.5 x 10^4; time constant, 0.2 s; 1.53 mM Hr; [NO]/[Hr] = 2.61; 0.2 M Tris-sulfate, pH 8

A. deoxyHr
B. deoxyNO prepared from deoxyHr
C. deoxyNO prepared from oxyHr

Table 3.12. Extinction coefficients for deoxyNO[a]

[Hr] (mM)	[NO]/[Hr]	ε ($M^{-1}cm^{-1}$) 408 nm	500 nm	600 nm
0.534	3.2	949	562	407
0.537	3.6	958	572	411
0.203	4.5	1182	729	502
0.286	8.0	1164	731	514
0.233	4.9	1365	846	558[b]
0.182	1.4	1071	661	461
0.315	3.5	1292	813	578
0.362	2.0	1238	776	533[c]
	average =	1150	710	500
		±140	±100	±60

[a]pH 6.5; 50 mM phosphate; room temperature.

[b]0.1 M perchlorate.

[c]0.1 M nitrate.

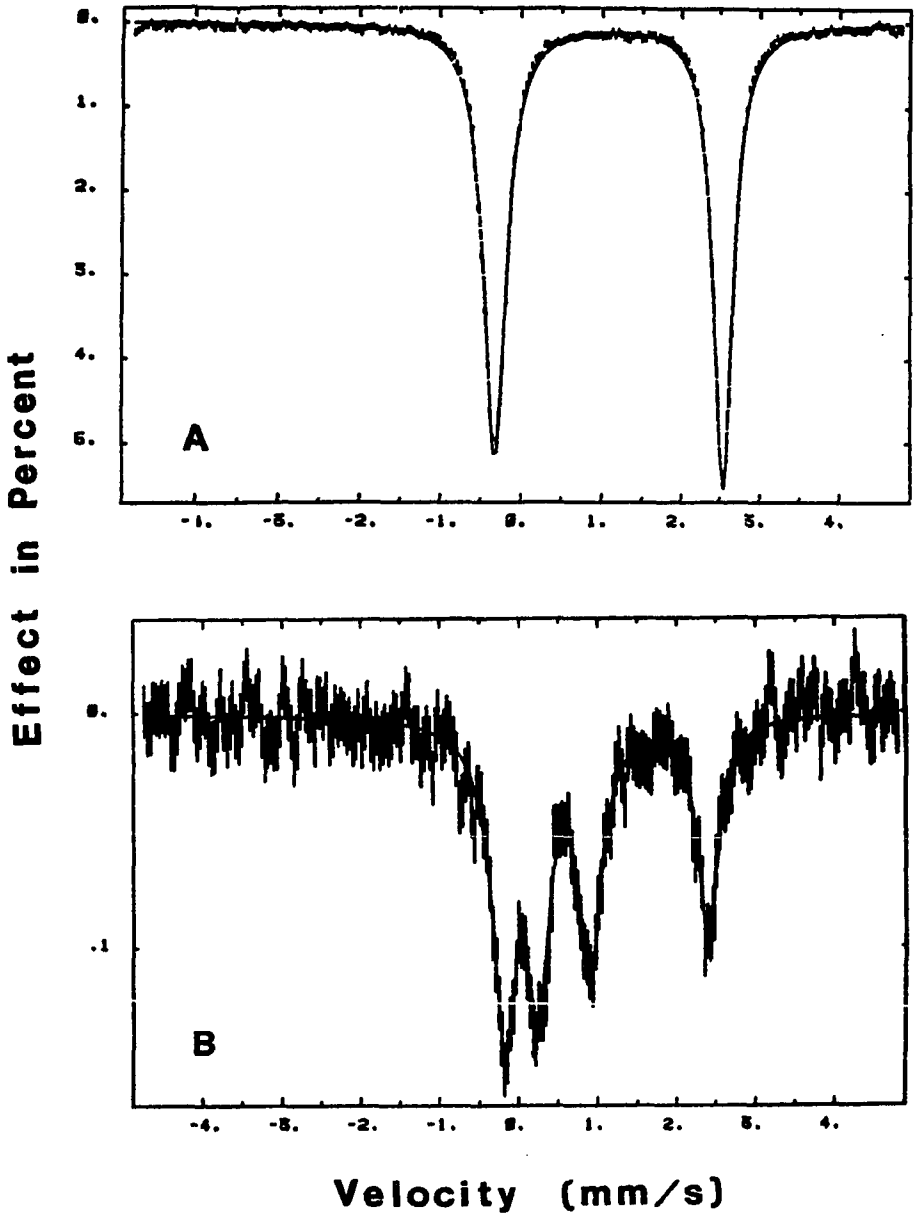

Figure 3.26. ^{57}Fe-Mössbauer spectra for deoxyHr (A) and deoxyNO (B)

Spectral parameters: zero applied field, 4.2 K
A. crystalline suspension of deoxyHr
B. solution of deoxyNO in 50 mM phosphate buffers at pH 6.5

that nitric oxide interacts predominantly with only one iron of the binuclear pair. The outermost doublet exhibits an isomer shift (δ) of 1.23 mm/s and quadrupole splitting (ΔE_q) of 2.64 mm/s at 100 K. These values are typical of high spin (S = 2) ferrous centers and are near the values for deoxyHr shown in Fig. 3.26A (δ = 1.19 mm/s; ΔE_q = 2.81 mm/s). Parameters for the innermost doublet (δ = 0.68 mm/s and ΔE_q = 0.65 mm/s) are unlike those for low-spin $\{FeNO\}^7$ but similar to those for monomeric S = 3/2 $\{FeNO\}^7$ (Table 1.22). Thus, NO appears to be bound as a terminal rather than bridging ligand in deoxyNO and coordination of NO does not cause high to low spin conversion of either iron.

Assuming that NO is not bridging, there are three possible formalisms for the oxidation states of the iron and NO within the $\{FeNO\}^7$ S = 3/2 unit: $Fe^{+}NO^{+}$, $Fe^{2+}NO$, $Fe^{3+}NO^{-}$. To distinguish NO^{+} from NO^{-}, the N-O stretching frequency is often used. Unfortunately, ν(N-O) was not observed by either resonance Raman spectroscopy or FTIR for deoxyNO (or deoxyF^{-}NO). Steric restrictions at the iron site are likely to favor a bent Fe-NO geometry as is the case for the FeO_2 moiety of oxyHr (82) and bent $\{FeNO\}^7$ moieties are formulated as $Fe^{3+}NO^{-}$.

At 4.2 K, all four components of the Mossbauer spectrum broaden (Fig. 3.27). Under similar conditions, the deoxyHr Mossbauer signal is not broadened (5). Thus, both sites contribute to the paramagnetic center. These results are consistent with a model in which high spin S = 2 Fe^{2+} is antiferromagnetically coupled to the S = 3/2 $\{FeNO\}^7$ site, leading to an S_{eff} = 1/2 ground state.

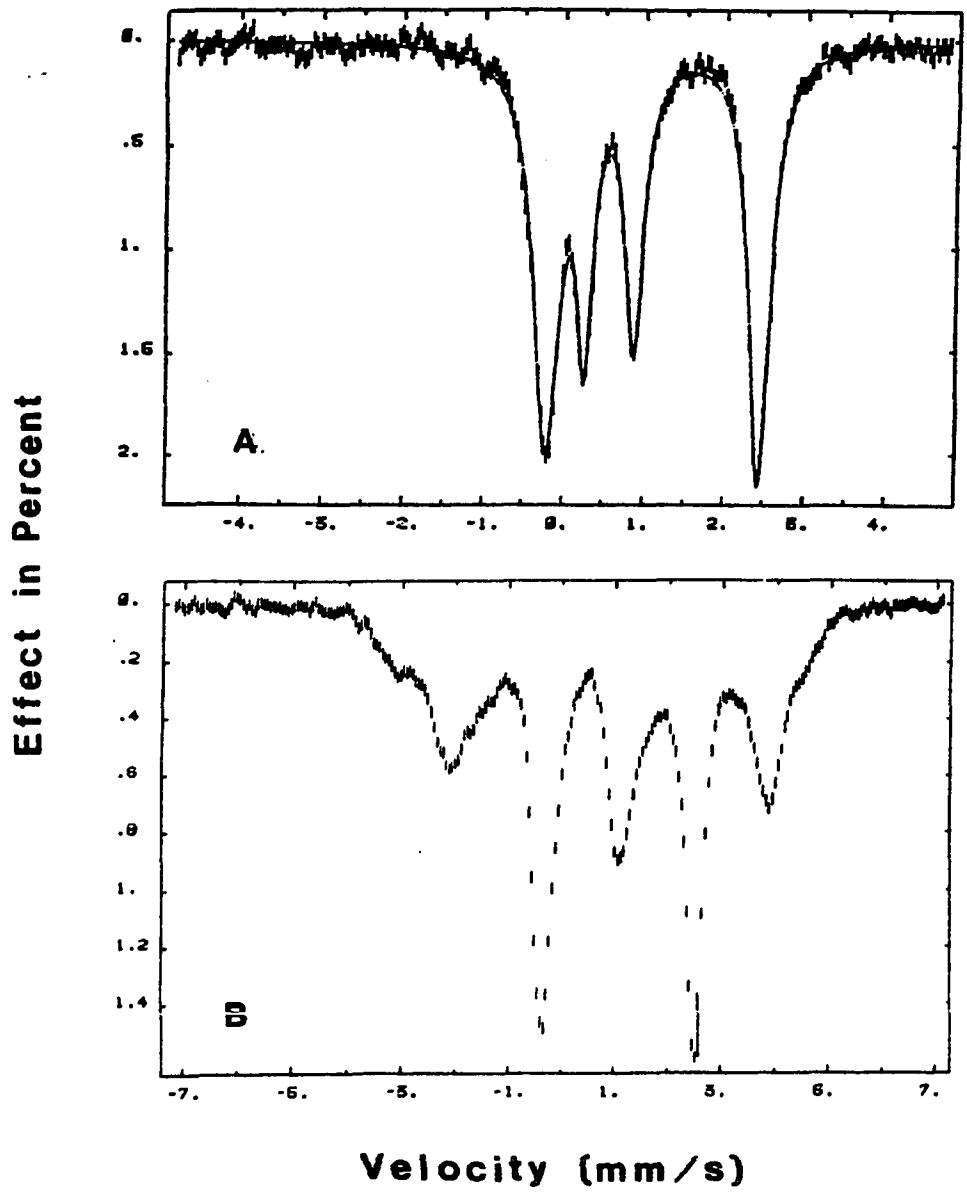

Figure 3.27. ^{57}Fe-Mössbauer spectra for a crystalline slurry of deoxyNO obtained in zero applied field (A) and in a 320 G parallel applied field (B)

Spectral parameters: 4.2 K. In spectrum A, the greater intensity of the outermost peaks relative to the innermost doublet and, in spectrum B, the sharp doublet (0.5 mm/s and 2.5 mm/s) result from the presence of deoxyHr in the sample

The low temperature Mossbauer data suggest that nitric oxide, in providing an additional electron, converts the EPR-silent deoxy into a paramagnetic state. This paramagnetism is verified by EPR spectroscopy. The X-band EPR signal obtained from frozen samples of deoxyNO is axial with g-values of 2.77 ± 0.02 and 1.84 ± 0.01 (Fig. 3.28 and Table 3.13).

This signal is unique in two respects. First of all, the observed g-values are not like those observed for monomeric $\{FeNO\}^7$ S = 3/2 units which have g-values at ~4.0 ($g_\perp$) and ~2.0 ($g_\parallel$) nor do they resemble low-spin, S = 1/2 units which have signals with $2.1 > g_x, g_y, g_z > 1.8$ (Table 1.21). Secondly, the signal is unusually broad both in comparison with monomeric $\{FeNO\}^7$ compounds and with other EPR-active Hr derivatives. Both of these features may be attributable to the proximity of a second paramagnetic center and support the idea that a ferrous site is antiferromagnetically coupled to the S = 3/2 $\{FeNO\}^7$ site. Since, at most, only one of the active site irons is formally oxidized, antiferromagnetic coupling of the irons occurs prior to formal oxidation of the second iron atom.

Double integration of the EPR signal for deoxyNO against $CuSO_4$ yields 0.913 ± 0.08 spins/2Fe (Table 3.13). Thus, conversion to the EPR-active center is quantitative.

The saturation behavior of the EPR signal for deoxyNO is also different from that of other Hr derivatives. At 4.2 K, the deoxyNO EPR signal saturates at lower powers than either $(semi\text{-}met)_O$ or $(semi\text{-}met)_R$ (Fig. 3.29).

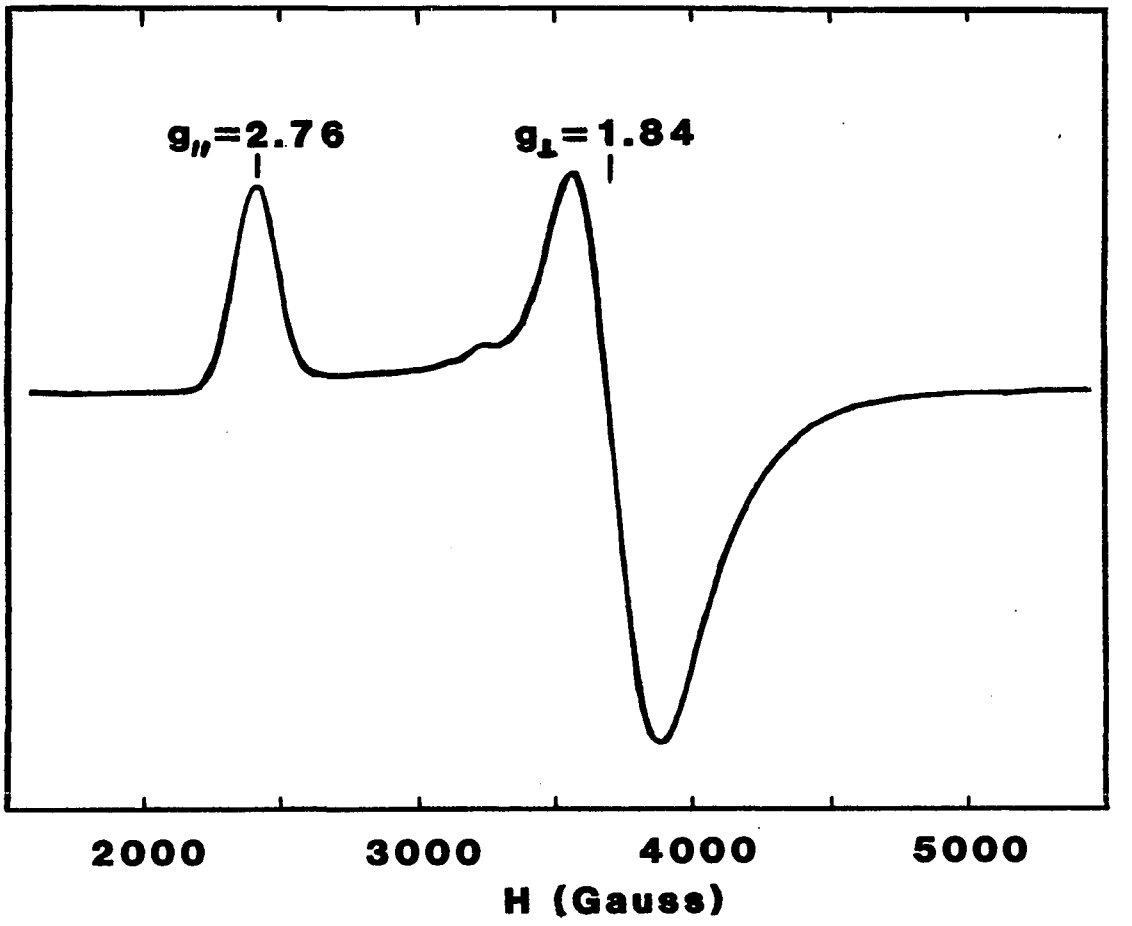

Figure 3.28. EPR spectrum for deoxyNO at 4.2 K

Spectral parameters: temperature, 4.2 K; frequency, 9.42 GHz; power, 40 μW; modulation, 40 G; gain, 2.5×10^4; time constant, 0.2 s; 3.40 mM oxyHr; [NO]/[Hr] = 10.0; 50 mM phosphate, pH 6.5

Table 3.13. Double integrations of the EPR signal for deoxyNO[a]

[Hr]	[NO]/[Hr]	$g_{\parallel}$	$g_{\perp}$	%pmag
1.88	3.6	2.791	1.828	82.0
2.11	3.15	2.763	1.849	90.8[b]
0.88	4.5	2.770	1.840	92.0
0.79	1.42	2.739	1.846	89.5
1.35	98.0	2.786	1.829	84.0[c]
9.30	6.69	2.754	1.837	101[d]
1.57	2.0	2.781	1.837	100[e]
	average =	2.77	1.84	91.3
		±0.017	±0.008	±6.7

[a]% pmag = [spins]/[Hr] x 100%; pH 6.5; 50 mM phosphate.

[b]0.59 M CN^-.

[c]Sample prepared from oxyHr; NO prepared from reduction of nitrite with ascorbate.

[d]0.3 M sulfate.

[e]0.1 M nitrate.

Figure 3.29. Power saturation of the EPR signals obtained at 4.2 K for deoxyNO (A), $(semi\text{-}met)_R$ (B), $(semi\text{-}met)_O$ (C), and deoxyF⁻NO (D)

Spectral parameters: frequency, 9.57 GHz (B and C) or 9.42 GHz (A and D); modulation 40 G (A and D) or 16 G (B and C); time constant, 0.2 s

A. 4.65 mM Hr; [NO]/[Hr] = 5.1; 50 mM phosphate, pH 6.5; 0.3 M sulfate
B. 8.24 mM Hr; 4.39 mm dithionite; 50 mM phosphate, pH 6.5
C. 1.90 mM Hr; 1.66 mM ferricyanide; 50 mM Tris-perchlorate, pH 8.0
D. 2.72 mM Hr; 127 mM NaF; [NO]/[Hr] = 4.8; 50 mM phosphate, pH 6.5; 0.3 M sulfate

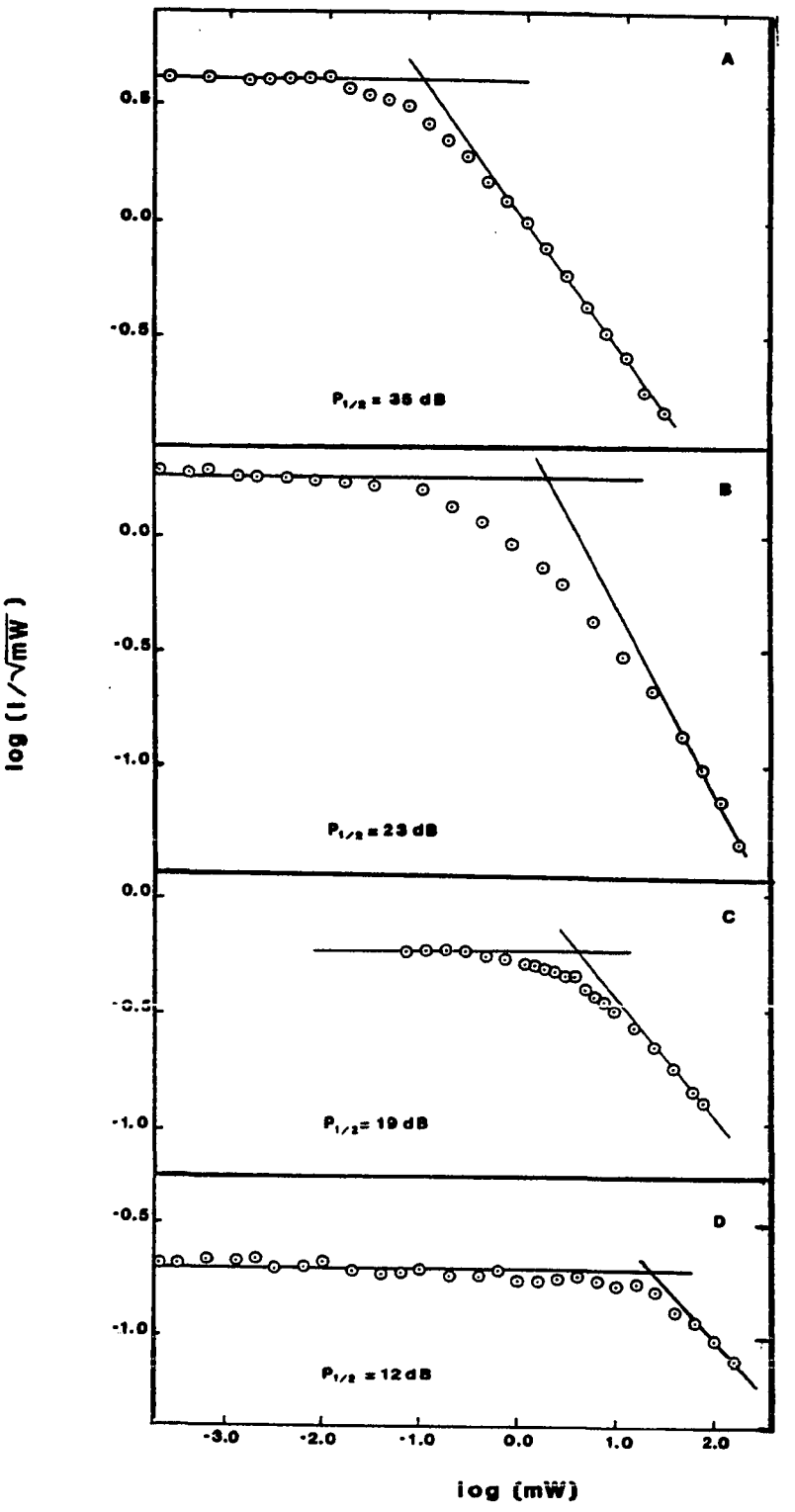
A
B
C
D
0.5
0.0
-0.5
-1.0
$P_{1/2}$ = 35 dB
$P_{1/2}$ = 23 dB
$P_{1/2}$ = 19 dB
$P_{1/2}$ = 12 dB
-3.0
-2.0
-1.0
0.0
1.0
2.0
log (1/√mW)
log (mW)

From the slope of a plot of the half-saturation power as a function of temperature^{-1}, the energy separation (Δ) between the S_{eff} = 1/2 ground state and the lowest energy excited state can be determined (Fig. 3.30). For deoxyNO, the value of Δ was found to be 70.3 ± 4.4 cm^{-1} (Table 3.14).

For binuclear compounds, the magnitude of Δ is a function of both the zero-field splitting energy (D) and the antiferromagnetic coupling energy (J). If either D >> J or D << J, the variable temperature data may be used to derive the values of D and J. Attempts to simulate the EPR spectra indicate that D ~ 0.32 J for deoxyNO and a straightforward separation of the values of D and J cannot be made. However, one calculation assuming isotropic exchange between the S = 3/2 and S' = 1/2 sites and including zero-field splittings for both sites (D = 17 cm^{-1} and D' = -3.75 cm^{-1}; E = 2 cm^{-1} and E' = -1.25 cm^{-1}) produced an S_{eff} = 1/2 ground state with g-values (1.838, 1.845, 2.762) close to the observed values. From this calculation, the antiferromagnetic exchange coupling constant is predicted to be 20 cm^{-1}.

Occasionally, a weak EPR signal is observed near g = 4.0 in preparations of deoxyNO. Such signals are observed for monomeric S = 3/2 {FeNO}^{7} compounds (Table 1.21). In deoxyNO, therefore, this signal could arise from a form of Hr in which the coupling between the S = 2 ferrous site and the S = 3/2 {FeNO}^{7} site has been eliminated, perhaps by the breakage of an Fe-O_{oxo} bond (Fig. 3.31).

Strong evidence that nitric oxide coordinates directly to iron comes from resonance Raman spectroscopy. The spectrum of deoxyNO col-

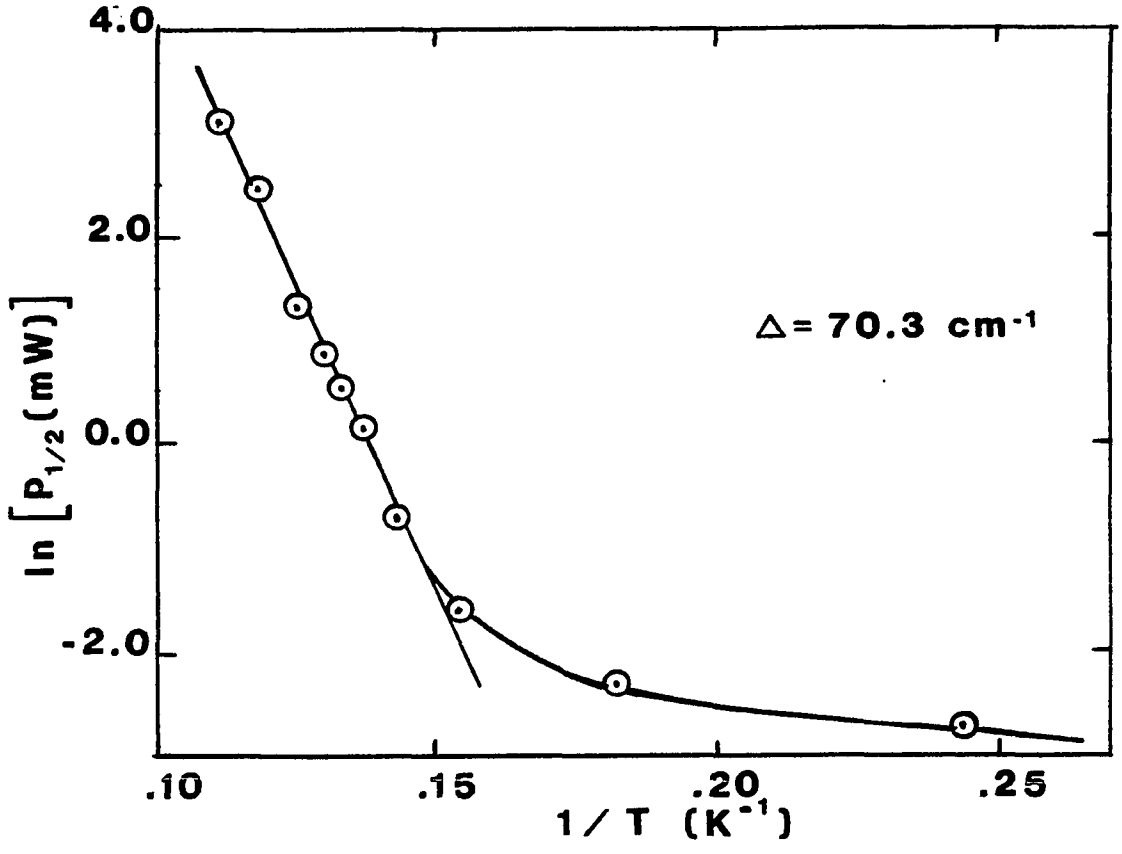

Figure 3.30. Temperature dependence of the half-saturation power for deoxyNO

Spectral parameters: frequency, 9.42 GHz; modulation, 40 G; time constant, 0.2 s; 4.65 mM Hr; [NO]/[Hr] = 5.1; 50 mM phosphate, pH 6.5; 0.3 M sulfate; g = 1.84

Table 3.14. Experimental determinations of Δ for deoxyNO[a]

Δ^b (cm^{-1})	γ	Δ^c (cm^{-1})	γ
	g = 1.84		
66.5	-0.997	76.4	-0.988
83.0	-0.997	68.3	-0.999
	g = 2.78		
71.5	-0.996	64.5	-0.968
85.0	-0.992	72.1	-0.995
average = 76.5 ± 7.7		average = 70.3 ± 4.4	

[a]pH 6.5; 50 mM phosphate; correlation coefficient (γ); Δ was determined using Eq. 2.2.

[b]The best lines were drawn through each saturation plot by visual inspection.

[c]Data in the nonsaturating region was averaged and data in the saturating region of the curves was fit by least-squares analysis to the best line.

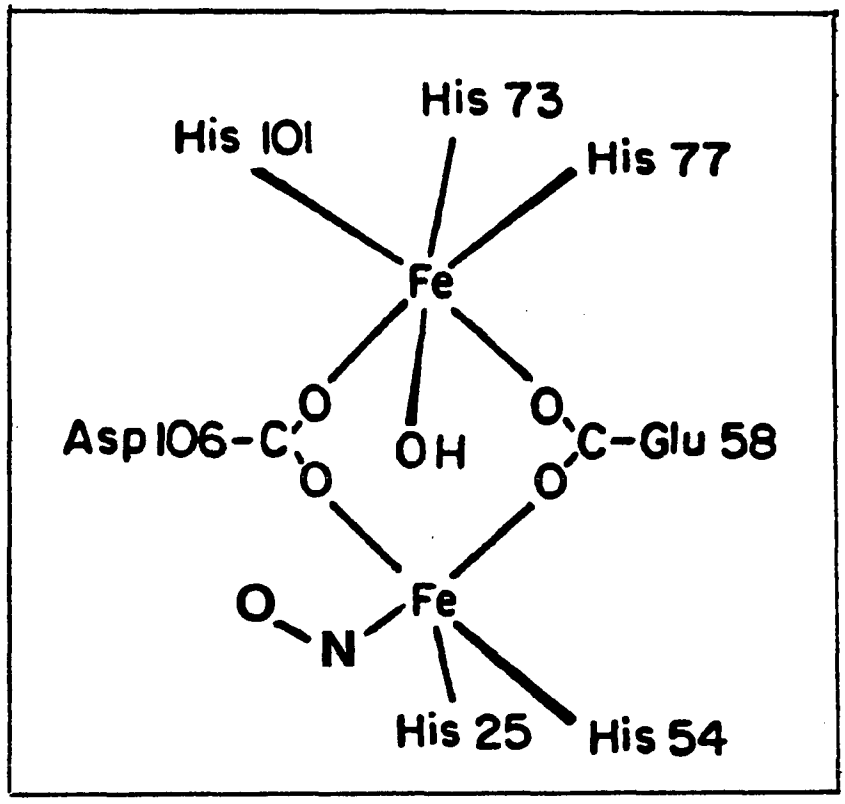

Figure 3.31. Proposed structure for an NO derivative having an uncoupled active site

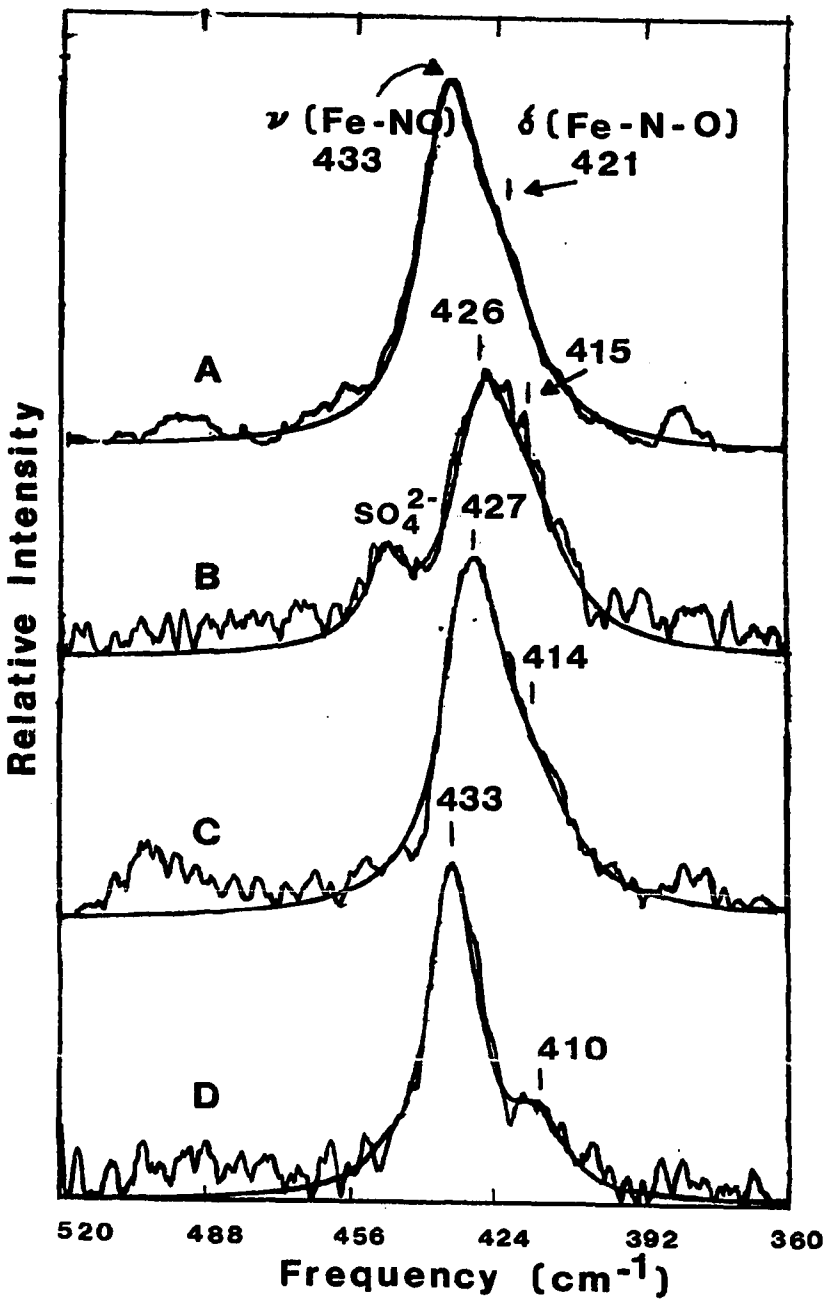

Figure 3.32. Resonance Raman spectra for deoxyNO prepared with $^{14}N^{16}O$ (A), $^{15}N^{16}O$ (B), $^{14}N^{18}O$ (C), and in D_2O (D)

Spectral parameters: excitation wavelength, 647.1 nm; temperature, 90 K; power, 70-80 mW; scan rate, 2 cm^{-1}/s; slit width, 8 cm^{-1}

lected at 90 K with an excitation frequency of 647.1 nm is shown in Fig. 3.32. The only salient feature of the spectrum not assignable to either solvent or internal reference bands is a broad mode centered at 433 cm^{-1}. Vibrational modes for N-O stretches, expected to occur between 1500 and 1900 cm^{-1} (71), were searched for intensively but not detected. Also absent were features assignable to oxyHr, the starting material, which verifies the completeness of the binding of NO.

At half-height, the 433 cm^{-1} band has a width of approximately 25 cm^{-1}. The width of this signal and the appearance of a shoulder on the low energy side of the peak, a feature that is most pronounced in the deuterated solvent, suggest that this feature has more than one component. Curve-fitting analysis showed two components (433 cm^{-1} and 421 cm^{-1}) in a 3.3:1.0 area ratio.

Table 3.15 and Fig. 3.32 display the effects of isotopic substitution on the two frequencies. Downward shifts are observed with either ^{15}NO or $N^{18}O$ for both modes. The shift with ^{15}NO indicates that the vibrations are affiliated with the exogenous ligand rather than with vibrations involving the metal-ligating amino acids. The two bands are affected differently by D_2O; the 421 cm^{-1} band is shifted downward by 11 cm^{-1} while the 433 cm^{-1} band does not shift.

The positions of ν_1 and ν_2 suggest assignments as ν(Fe-NO), δ(Fe-N-O), or ν_s(Fe-OH-Fe). The range where ν(Fe-NO) and δ(Fe-N-O) have been observed extends from ~720 cm^{-1} to ~290 cm^{-1} (Table 1.23) (142,146). Symmetric bridging mode vibrations for oxidized Hr derivatives appear

Table 3.15. Resonance Raman data for deoxyNO at 90 K using 647.1 nm excitation[a]

Isotope	ν_1 (cm^{-1})	ν_2 (cm^{-1})	Intensity Ratio
$^{14}N^{16}O$	433	421	3.3:1.0
$^{15}N^{16}O$	426	415	2.6:1.0[b]
$^{14}N^{18}O$	427	414	4.8:1.0[c]
	427	415	1.4:1.0[d]
$^{14}N^{16}O$ in D_2O	433	410	5.0:1.0[e]

[a]0.25 mm slit width; scan rate of 2 cm^{-1}/s; 50 mM phosphate, pH 6.5; 0.3 M sulfate; 10% Gaussian/90% Lorentzian fit; width at half height of 18 cm^{-1}.

[b]80% Gaussian/20% Lorentzian fit; width at half height of 20 cm^{-1}.

[c]^{18}O-bridged in $H_2{}^{18}O$.

[d]^{16}O-bridged in $H_2{}^{18}O$.

[e]30% Gaussian/70% Lorentzian fit; width at half height of 15 cm^{-1}.

between 486 and 516 cm^{-1} (Table 1.9) and it is expected that ν_s[Fe(II)-OH-Fe(II)] would appear at a somewhat lower frequency.

To test whether or not the assignment as ν_s(Fe-OH-Fe) was correct, samples were prepared in $H_2{}^{18}O$ from both ^{16}O-bridged deoxyHr (sample I) and ^{18}O-bridged deoxyHr (sample II). The frequencies for ν_1 and ν_2 are identical to each other (Figs. 3.33A and 3.33B and Table 3.15). To assure that ^{18}O had not been incorporated into the bridge during preparation of sample I, a portion of the sample was chemically oxidized with $Fe(CN)_6{}^{3-}$ and treated with sodium azide. The resonance Raman spectrum of the resulting $metN_3{}^-$ had ν_s(Fe-O-Fe) at 508 cm^{-1} (Fig. 3.33C). Published values are 507 cm^{-1} for ^{16}O-bridged $metN_3{}^-$ and 494 cm^{-1} for the ^{18}O-bridged derivative (80). In addition, both bands are shifted when deoxyNO is prepared with $^{15}N^{16}O$ indicating the involvement of NO in both vibrations. All of these results show that the peaks in the resonance Raman spectrum of deoxyNO are not due to a symmetric Fe-OH-Fe bridging mode.

With adducts of metmyoHr from Themiste zostericola, it was observed that incorporation of ^{18}O into the oxo bridge is induced by subjecting samples to irradiation (174). This process is presumed to involve cleavage of the $Fe\text{-}O_{oxo}$ bond. To show that such a photochemical transformation had not occurred with deoxyNO, the EPR spectrum of a portion of the deoxyNO sample was re-examined after being irradiated at 77 K for 65 min (λ_{ex} = 619.5 nm, 70 mW). The spectrum was found to be identical to that prior to laser irradiation (Fig. 3.34). Furthermore, there was

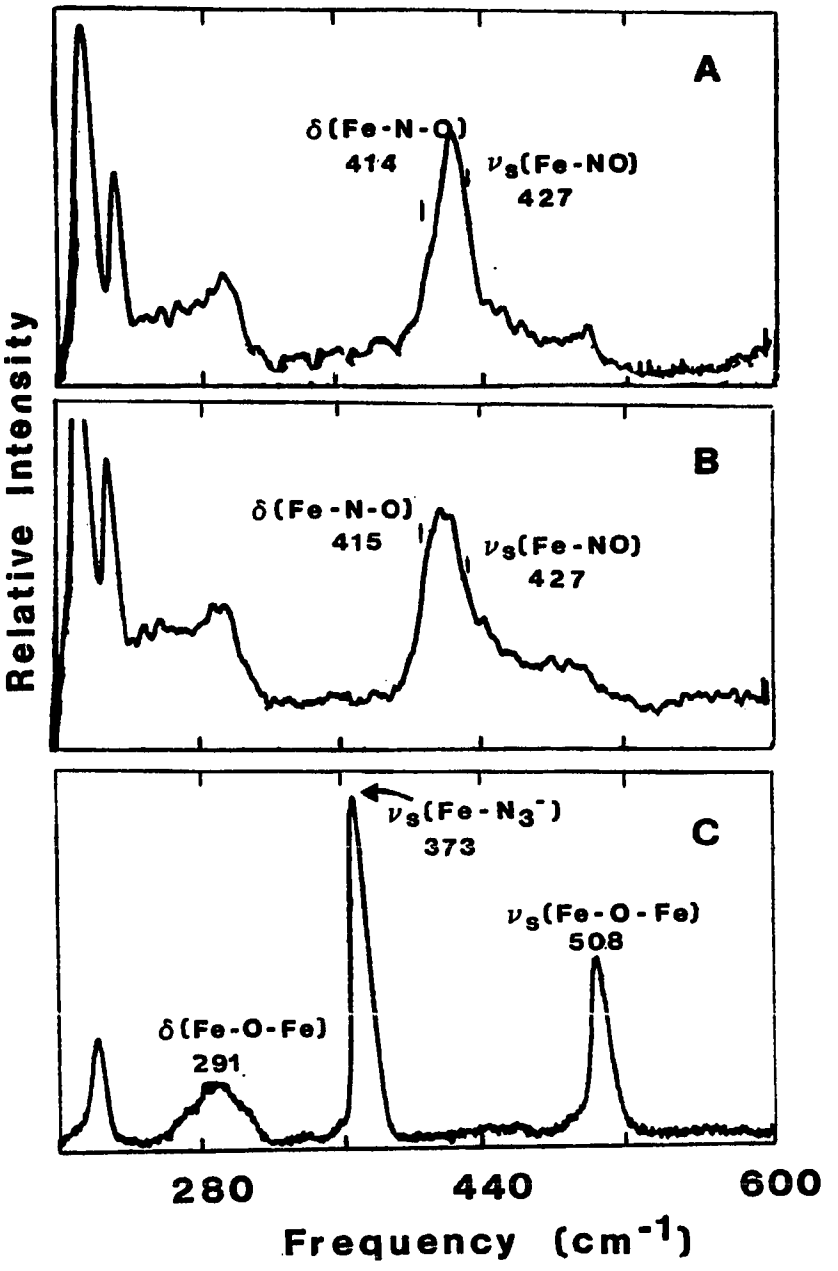

Figure 3.33. Resonance Raman spectra in $H_2{}^{18}O$ for ^{16}O-bridged deoxyNO (A), ^{18}O- bridged deoxyNO (B), and for $metN_3^-$ prepared from ^{16}O- bridged deoxyNO (C)

Spectral conditions: temperature, 77 K; excitation wavelength, 647.9 nm (A and B) and 514.5 nm (C); scan rate, 2 cm^{-1}/s (A and B) and 1 cm^{-1}/s (C); slit width, 8 cm^{-1} (A and B) and 4 cm^{-1} (C)

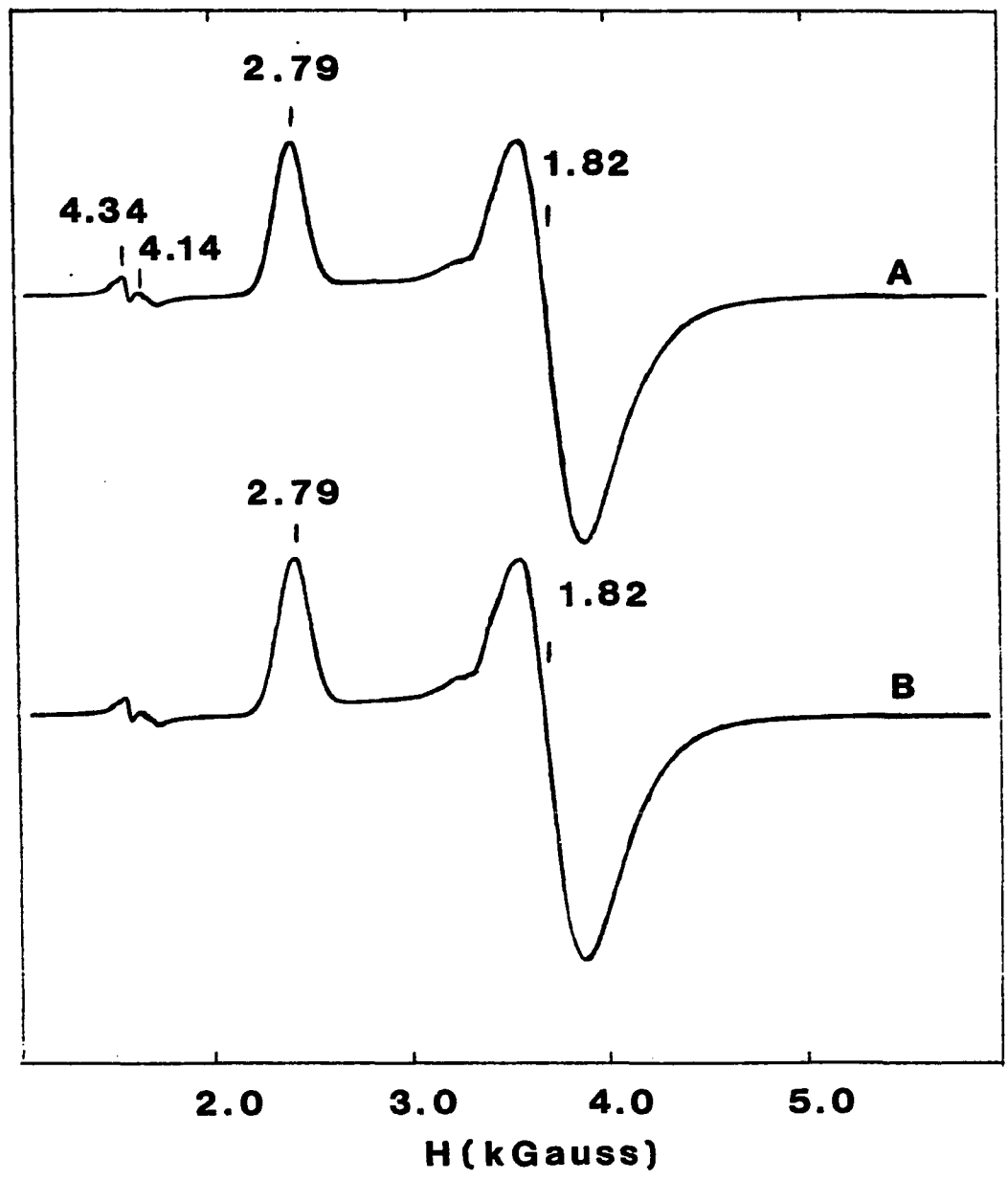

Figure 3.34. EPR spectra before and after irradiation (614.5 nm) of deoxyNO

Spectral conditions: temperature, 4.2 K; frequency, 9.42 GHz; power 40 μW; modulation, 40 G; gain, 1.25×10^4; time constant, 0.2 s; 4.65 mM Hr; [NO]/[Hr] = 5.09; 50 mM phosphate, pH 6.5; 0.3 M sulfate; irradiation at 77 K for 1 hr with 70 mW power of light (614.5 nm)

no increase in the intensity of the g = 4 feature. Thus, the photochemical treatment of the sample did not alter the sample.

Absence of resonance-enhancement of Fe-O-Fe bridging mode vibrations is in contrast to metHr derivatives but similar to deoxyHr and semi-metHrs. The Hr derivatives that exhibit resonance-enhanced bridging modes also exhibit $O^{2-} \rightarrow Fe^{3+}$ LMCT bands between 300 and 400 nm. Since the optical spectrum of deoxyNO lacks any Fe(III)-O_{oxo} bands, it is not surprising that resonance-enhancement of the bridging vibrations does not occur for deoxyNO. Thus, the optical bands arise from charge transfer between nitric oxide and iron rather than from charge transfer from either the hydroxo bridge or the endogenous ligands to iron.

Preparation of deoxyNO in $H_2{}^{18}O$ shifts both vibrations relative to their positions in $H_2{}^{16}O$. Since ^{18}O is not incorporated into the bridging group, exchange must have occurred with the oxygen of the nitrosyl group. Indeed, Bonner has shown that in the presence of traces of O_2 (and hence NO_2) facile exchange occurs between NO and $H_2{}^{18}O$ (171). It is likely that O_2 is initially present in the deoxyNO solutions since the samples were prepared by replacing O_2 from oxyHr with NO.

Having shown that the two bands arise from vibrations of the Fe-N-O group, two assignments are possible. Either the two bands arise from ν(Fe-NO) and δ(Fe-N-O) or else there are two conformations of the protein that are detectable at 90 K. Some possible structures for these two forms are shown in Table 3.16.

The occurrence of an equilibrium between two conformations has been suggested as an explanation for the temperature-dependent changes in the

Table 3.16. Possible structures leading to two Fe-NO stretching vibrations

		D_2O shifted	D_2O unshifted
1	Cis ⇄ trans	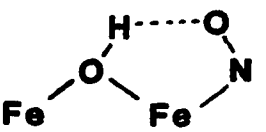	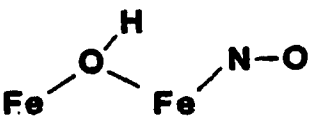
2	Deprotonation of the μ-oxo bridge	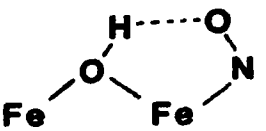	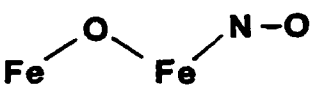
3	Uncoupling	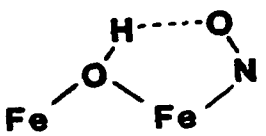	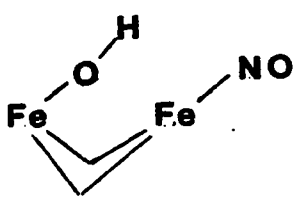
4	H_2O molecule	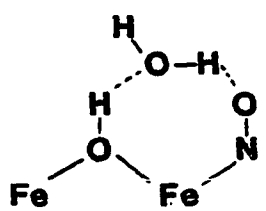	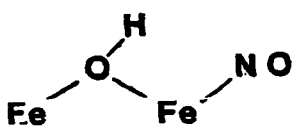

intensities of the ν_s(Fe-O-Fe) bands in the resonance Raman spectra of metOH$^-$ (175). Structural changes analogous to those of either case 1 or case 4 have been proposed as an explanation for these changes. For this reason, the resonance Raman spectrum of deoxyNO prepared in D_2O, which shows the clearest resolution of the two bands (Fig. 3.32D), was examined at several temperatures. The results obtained between 90 K and 249 K are summarized in Table 3.17. Within experimental error, there appears to be no temperature dependence. Although this does not eliminate the possibility that two forms of the protein may be present, it does show that if there are two species present, they are not in equilibrium between 90 K and 249 K. Consistent with the absence of two conformations for deoxyNO is the observation that the intensity ratio of the two frequencies is invariant, within experimental error, for three different preparations of deoxyNO in D_2O.

Assuming, then, that one vibration is a stretching mode and the other is a bending mode, one can attempt to assign ν_1 and ν_2. There are three ways in which one might differentiate between a stretching mode and a bending mode:

(i) For ^{15}N substituted derivatives, stretching modes exhibit smaller shifts than bending modes (Table 1.23).

(ii) The experimental frequency shift in ^{15}N for the stretching mode should compare favorably with the theoretical value calculated from the diatomic oscillator model while that for the bending mode should not.

Table 3.17. Variable temperature resonance Raman data for deoxyNO in D_2O[a]

T (K)	ν_1 (cm^{-1})	ν_2 (cm^{-1})	Intensity Ratio	Peak Widths (cm^{-1})
90	432	414	5.0:1.0	14, 14[b]
90	433	410	7.0:1.0	18, 15[c]
90	432	413	5.0:1.0	13, 14[d]
104	432	414	6.0:1.0	13, 13[d]
163	432	410	5.4:1.0	18, 15[c]
249	427	414	6.0:1.0	16, 16[d]

[a]Prepared from oxyHr; slit width of 0.25 mm; 1 cm^{-1}/s; 10% Gaussian/90% Lorentzian fit; excitation at 647.1 nm.

[b]2 cm^{-1}/s.

[c]30% Gaussian/70% Lorentzian fit.

[d]Prepared from deoxyHr.

(iii) If the NO ligand is protonated or hydrogen-bonded, then different shift patterns should occur in D_2O for the stretching and bending vibrations.

Stretching and bending vibrations have been observed for both {FeNO}^{6} and {FeNO}^{7} complexes (Table 1.23). For some compounds, the stretching mode appears at a higher frequency than the bending mode, while for other compounds the reverse ordering occurs. Quinby-Hunt and Feltham (142) observed that for ^{15}N-substituted derivatives, the stretching modes shifted downward by a lesser amount than the bending modes (3 to 6 cm^{-1} for the stretching modes vs. 9 to 15 cm^{-1} for the bending modes). Thus, one way to distinguish the stretching mode from the bending mode might be from the magnitude of the shift for the ^{15}N derivative. For deoxyNO, ν_1 and ν_2 shift downward by 7 and 6 cm^{-1}, respectively. Thus, an unambiguous assignment of ν_1 and ν_2 cannot be made for deoxyNO based on the magnitude of the ^{15}N-isotope shift.

A second way one might distinguish the stretching mode from the bending mode is by comparing the experimentally observed isotope shifts with those calculated from the diatomic oscillator model. If both ν_1 and ν_2 are assumed to be stretching modes, the frequency shifts calculated from the diatomic oscillator model for deoxy$^{14}N^{18}O$ are 424 cm^{-1} and 412 cm^{-1} for ν_1 and ν_2, respectively. The experimental values (Table 3.15) are <u>both</u> higher in frequency. The corresponding numbers for deoxy$^{15}N^{16}O$ are 428 cm^{-1} (ν_1) and 416 cm^{-1} (ν_2). Both of the observed vibrations appear at slightly lower frequencies. These calcula-

tions, thus, do not clearly distinguish which of the two modes is the stretching mode and which is the bending mode.

Thirdly, the stretching and bending modes should be affected differently by deuterium substitution. Indeed, for deoxyNO, only the less intense ν_2 is shifted by deuterium substitution. If the oxygen atom of the NO ligand is either protonated or hydrogen-bonded, the bending mode should be affected by deuterium substitution to a greater extent than the stretching mode. This suggests that ν_1 be assigned as ν(Fe-NO) and ν_2 as δ(Fe-N-O).

Finally, stretching vibrations are generally more intense than bending vibrations in resonance Raman spectra. The appearance of ν_1 and ν_2 in a ~3:1 ratio is consistent with the assignment of the higher frequency mode as the stretching vibration.

On the basis of the latter two observations, the best interpretation of the resonance Raman spectrum of deoxyNO, thus, assigns the two vibrations as ν(Fe-NO) (433 cm^{-1}) and δ(Fe-N-O) (421 cm^{-1}).

Two additional questions arise about the geometry of the Fe-NO site:

(i) Is the geometry of the FeNO moiety linear ($Fe^{+}NO^{+}$) or bent ($Fe^{3+}NO^{-}$)?

(ii) Is the NO ligand protonated or hydrogen-bonded?

The M-NO stretching mode is sensitive to the geometry of the M-NO interaction (Table 1.23). Compounds having a bent M-NO geometry have their stretching frequencies below 500 cm^{-1} [e.g., $Fe(DAS)_2(NO)Br^{+}$ and $Fe(DAS)_2(NO)(NCS)^{+}$ have ν(Fe-NO) at 463 and 455 cm^{-1}, respectively]. On

the other hand, for Fe(DMDTC)NO, a compound that has a linear M-NO geometry, ν(Fe-NO) occurs at 563 cm^{-1}. Occurrence of ν(Fe-NO) at 433 cm^{-1} for deoxyNO, thus, supports a structural model in which the M-NO unit is bent.

A second argument consistent with the MNO unit having a bent geometry is the absence of a reaction between CO and deoxyHr (176). For CO compounds, only linear coordination has been observed. The inability of deoxyHr to bind CO suggests that steric hindrance at the active site disfavors a linear coordination mode. Steric hindrance at the active site has been documented by x-ray crystallography for $metN_3^-$. Thus, for deoxyNO a bent coordination geometry (similar to that observed for oxyHr) is favored over a linear coordination geometry and an $Fe^{3+}NO^-$ formalism is appropriate.

It is not possible to provide a definite answer to the second question. However, by analogy to the oxyHr structure, it is likely that the D_2O shift arises from a hydrogen-bonding interaction. Because HNO-ligated model compounds are rare, the hydrogen atom is likely to be more tightly bound to the oxo bridge than to the nitrosyl ligand. On the basis of these studies, the structure shown in Fig. 3.35 is proposed for deoxyNO.

The resonance Raman spectra obtained for samples prepared by dissolving crystalline deoxyHr in D_2O give results identical to those prepared by diluting a concentrated solution of oxyHr with D_2O (Table 3.17). Scheme 3.2 shows a possible route for the incorporation of deuterium from the solvent into deoxyNO.

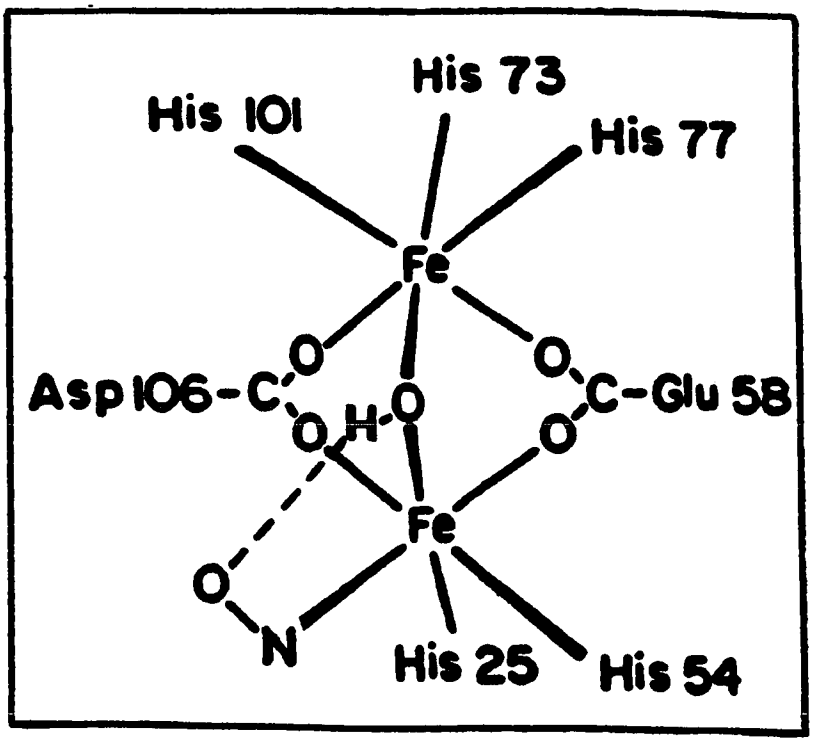

DeoxyNO
Fe(II)Fe(III)NO⁻

Figure 3.35. Proposed structure for deoxyNO

Scheme 3.2.

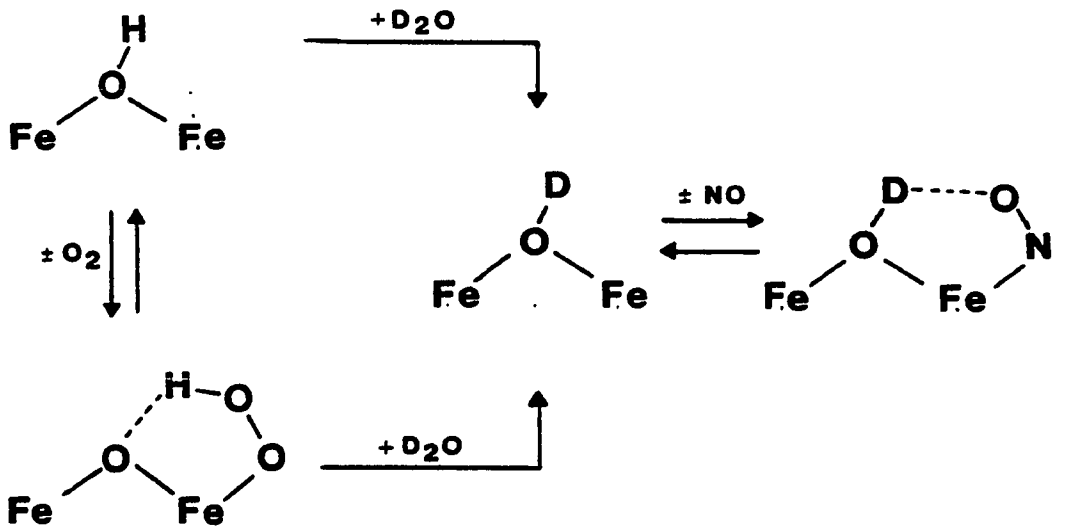

Since deuterium incorporation took only several hours and incorporation of solvent-derived ^{18}O into the μ-hydroxo bridge of deoxyHr takes several days, different mechanisms must be involved for the two processes. That is, rupture of an $Fe\text{-}O_{oxo}$ bond is involved with ^{18}O-incorporation into the μ-hydroxo bridge but not in the incorporation of deuterium into the bridge.

3. Preparation and characterization of deoxyF⁻NO

Addition of nitric oxide to deoxyHr in the presence of fluoride leads to formation of a highly stable green-colored product (deoxyF⁻NO). In the optical spectrum (Fig. 3.36) of deoxyF⁻NO, there are broad peaks at 450 and 590 nm along with a shoulder at 340 nm. These compare with transitions at 500 nm, 600 nm, and 408 nm, respectively, for deoxyNO. All three transitions appear at higher energies for deoxyF⁻NO than for the corresponding transitions in deoxyNO.

Estimates of the extinction coefficients for deoxyF⁻NO at 340 nm, 450 nm, and 590 nm are displayed in Table 3.18. The magnitudes of the extinction coefficients exceed those for the corresponding transitions in deoxyNO. Nevertheless, the extinction coefficients are appreciably less than those for either semi-metHrs or metHrs. Accordingly, it is likely that the reaction of nitric oxide with deoxyF⁻ results from binding of nitric oxide without oxidation of the binuclear center.

Addition of nitric oxide to deoxyF⁻ is expected to produce a paramagnetic derivative. The EPR spectrum of this new adduct (deoxyF⁻NO) is axial with $g_{\parallel} = 2.58 \pm 0.01$ and $g_{\perp} = 1.80 \pm 0.01$ (Fig. 3.37A) and extends from 2500 to 5000 G. At 4.2 K, the deoxyF⁻NO signal has a half-

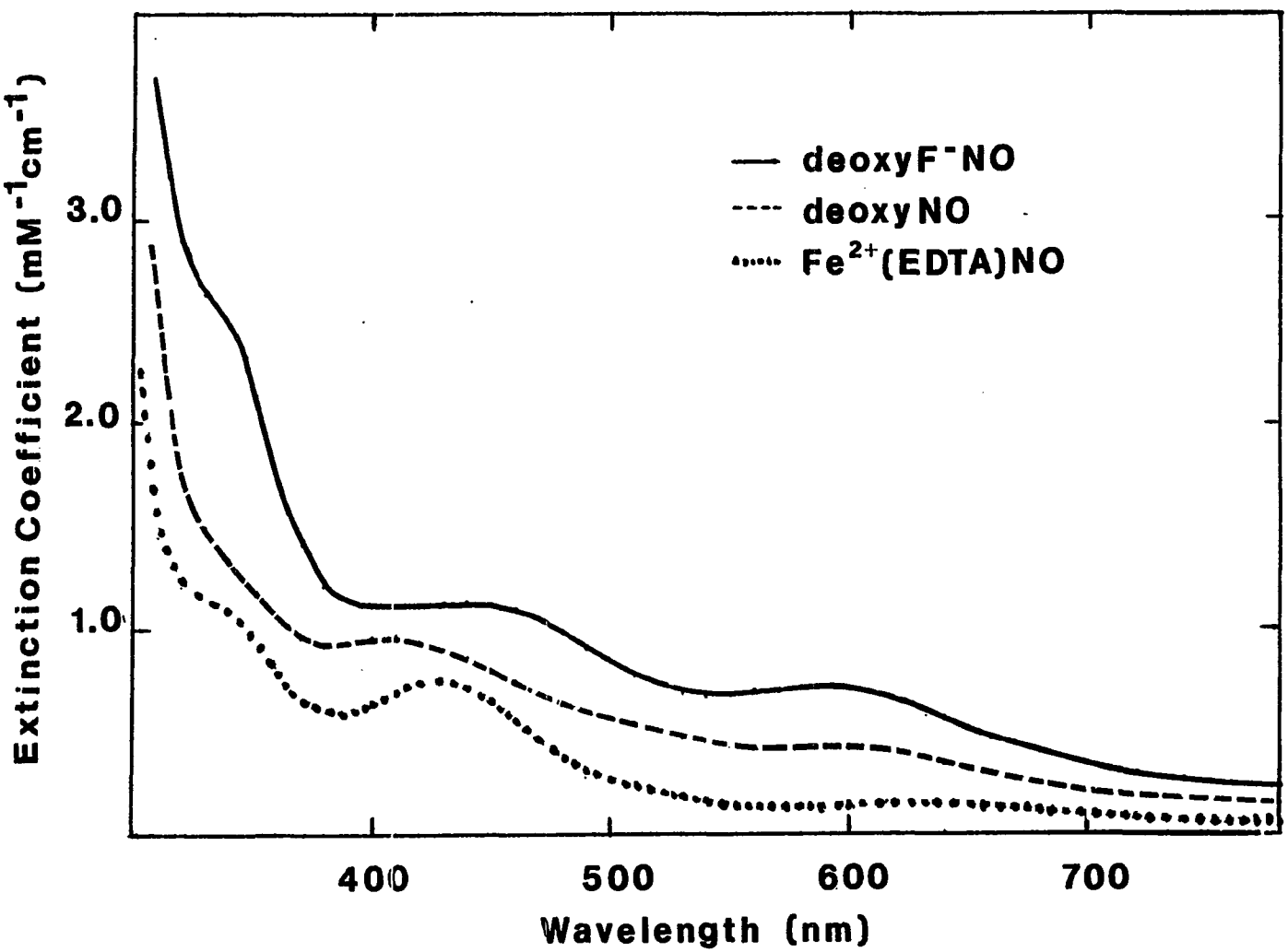

Figure 3.36. Optical spectra of deoxyNO, deoxyF⁻NO, and Fe^{2+}(EDTA)NO in 50 mM phosphate buffer at pH 6.5

Table 3.18. Estimated extinction coefficients for deoxyF$^-$NO[a]

[Hr] (mM)	[F$^-$]/[Hr]	[NO]/[Hr]		ε ($M^{-1}cm^{-1}$) 340 nm	450 nm	590 nm
0.283	45.8	12.7		2590	1150	731[b]
0.283	45.8	12.7		2710	1160	710[c]
0.190	628	2.34		3290	1430	900
0.254	62.3	3.10		2520	1220	768
0.453	46.7	4.83		2390	967	596
			average =	2700	1190	760
				±350	±166	±110

[a]50 mM phosphate; pH 6.5.

[b]^{15}NO.

[c]~24 hrs after preparation of deoxyF$^-$NO; sample stored at 4°C under argon.

Figure 3.37. EPR spectra for deoxyNO at 37 dB (A), deoxyF⁻NO at 37 dB (B), and deoxyF⁻NO at 15 dB (C) in 50 mM phosphate buffer at pH 6.5

Spectral conditions: temperature, 4.2 K; frequency, 9.42 GHz; modulation, 40 G; gain, 5×10^4 (A), 8×10^4 (B), or 8×10^3 (C); time constant, 0.2 s

A. 1.40 mM Hr; 2.01 mM NO
B. 3.11 mM Hr; 142 mM F^-; [NO]/[Hr] = 9.5; 0.3 M sulfate
C. 3.25 mM Hr; 644 mM NaF; [NO]/[Hr] = 4.6; 0.3 M sulfate

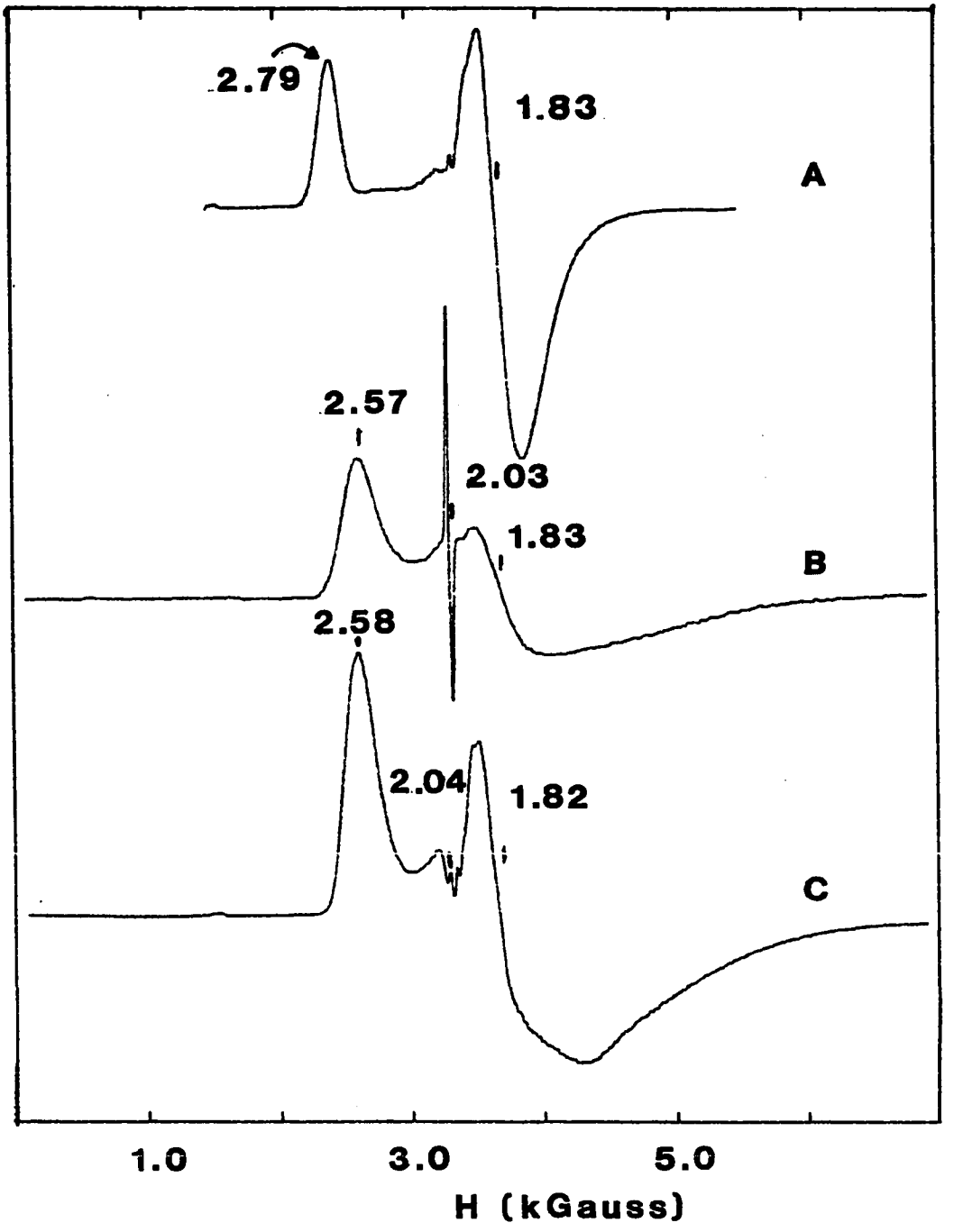
2.79
1.83
A
2.57
2.03
1.83
B
2.58
2.04
1.82
C
1.0
3.0
5.0
H (kGauss)

saturation power of 12 dB (Fig. 3.29). The g-values and the shape of this signal are similar to those of deoxyNO, which suggests that deoxyF⁻NO also contains a high-spin ferrous center that is antiferromagnetically coupled to an S = 3/2 $\{FeNO\}^7$ site.

A sharp radical signal with its main g-value at 2.03 is observed when low microwave power (37 dB) is used to record the EPR spectrum (Fig. 3.37B). In contrast to the signal for deoxyF⁻NO, the g = 2.03 signal is easily saturated ($P_{1/2}$ > 35 dB) and at higher powers (15 dB), the g = 2.03 signal is not observed (Fig. 3.37C). Both the sharpness of the signal and the readiness with which it is saturated suggest that the g = 2.03 signal is not a metal-derived signal.

The ^{57}Fe-Mössbauer spectrum for deoxyF⁻NO (Fig. 3.38) confirms that each subunit contains one high-spin Fe^{2+} (S = 2) site (δ = 1.23 mm/s; ΔE_q = 3.04 mm/s) and one S = 3/2 $\{FeNO\}^7$ site (δ = 0.75 mm/s; ΔE_q = 1.02 mm/s). The ratio of the area of the Fe^{2+} signal to the area of the S = 3/2 $\{FeNO\}^7$ doublet is 1.12, indicating that there are only two types of iron present. Because of the paramagnetic nature of deoxyF⁻NO and because the two iron sites are antiferromagnetically coupled to each other, both doublets are broadened in the low temperature (4.2 K) Mössbauer spectrum (Fig. 3.39).

Table 3.19 shows the double-integrations of the deoxyF⁻NO signal. The best results account for no more than 50% of the total protein. Because the saturation properties for the EPR signal of deoxyF⁻NO are quite different from the saturation properties of the standard, $CuSO_4$,

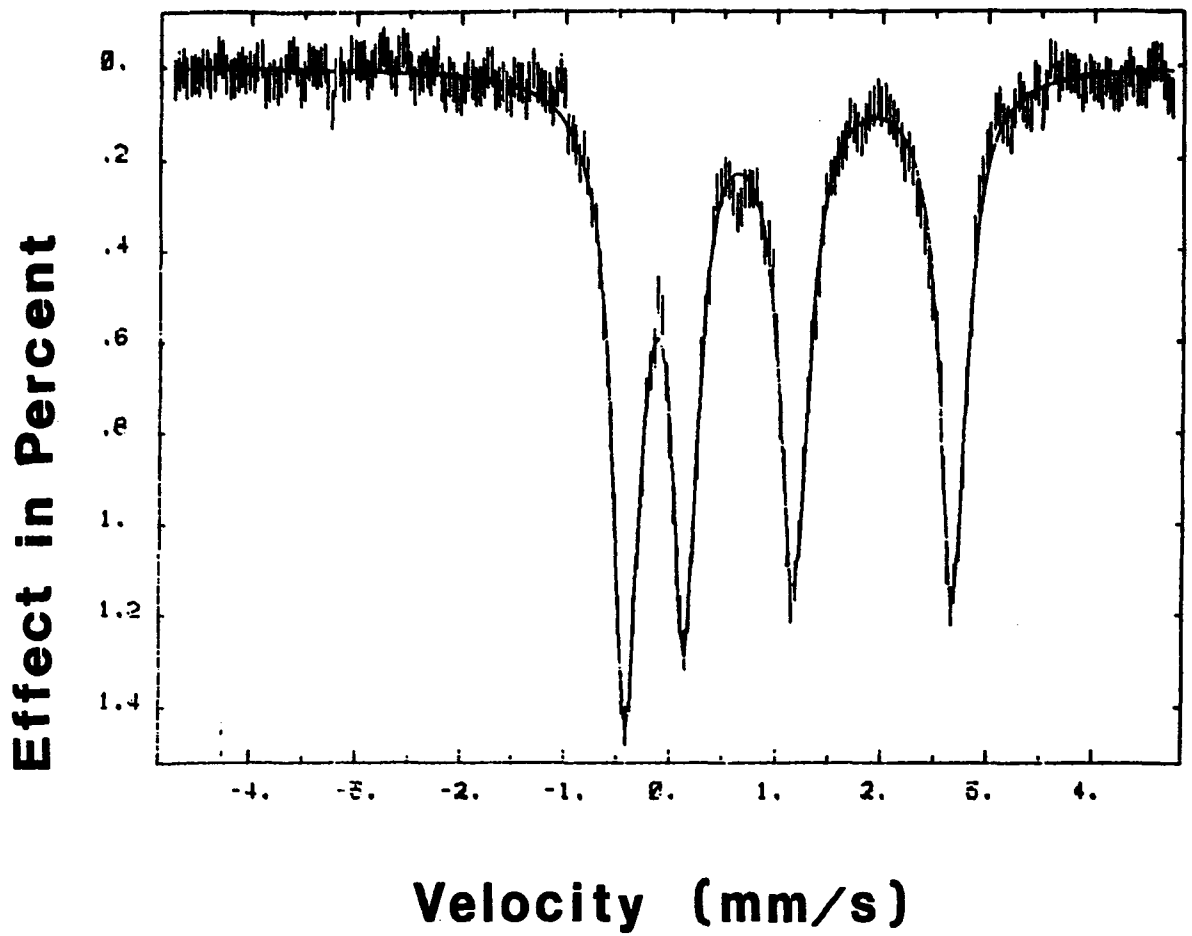

Figure 3.38. ^{57}Fe-Mössbauer spectrum for deoxyF-NO in zero field at 100 K

9.75 mM Hr; 644 mM fluoride; [NO]/[Hr] = 4.61; 50 mM phosphate, pH 6.5

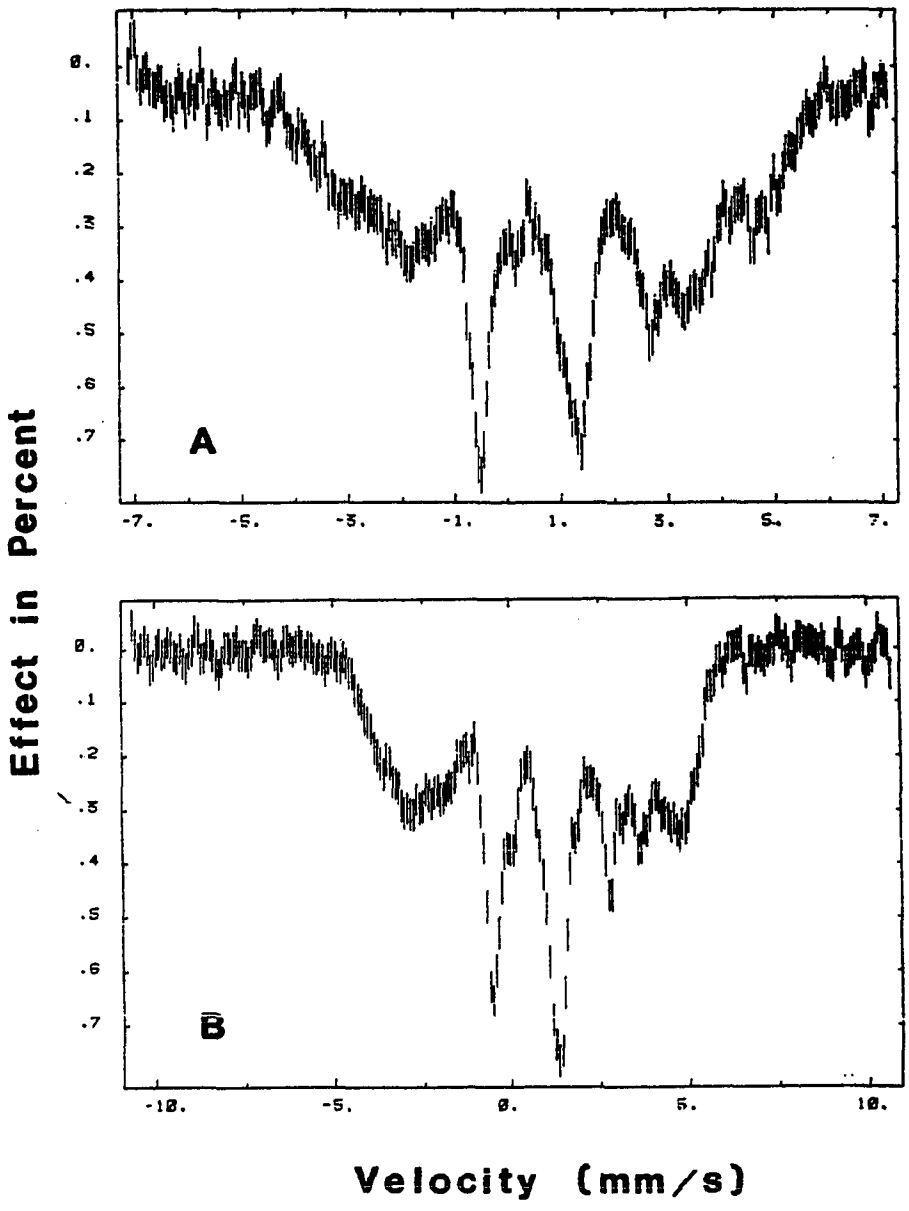

Figure 3.39. ^{57}Fe-Mössbauer spectra at 4.2 K for deoxyF$^-$NO in a 320 G parallel (A) or perpendicular (B) applied field

9.75 mM Hr; 644 mM fluoride; [NO]/[Hr] = 4.61; 50 mM phosphate, pH 6.5

Table 3.19. Double integrations of the EPR signal for deoxyF$^-$NO[a]

[Hr] (mM)	[F$^-$]/[Hr]	[NO]/[Hr]	Time[b] (min)	% pmag		$g_{\parallel}$	$g_{\perp}$
3.11	45.8	9.50	8	46.6		2.580	1.801
3.11	45.8	9.50	43	48.7		2.594	1.799
3.11	45.8	12.7	202	37.9		2.578	1.796[c]
3.25	198	4.61	38	39.1		2.572	1.822
					average =	2.58	1.80
						±0.008	±0.010

[a]pH 6.5; 50 mM phosphate; 0.3 M sulfate; % pmag = [spin]/[Hr] x 100%.

[b]Measured relative to the time at which fluoride was added to deoxyHr.

[c]^{15}NO.

the quantitations obtained from the double integration of the EPR signal are not very reliable.

Despite the results from the double integrations, several observations indicate that the formation of deoxyF$^-$NO is near quantitative. First of all, the extinction coefficients calculated assuming complete formation of deoxyF$^-$NO are similar in magnitude to those for deoxyNO. If the reaction were not complete, one would expect the extinction coefficients to be significantly less than those for deoxyNO. Secondly, only one metal-centered species is observed by EPR spectroscopy. Any other components in these solutions must be both colorless and EPR silent. Both deoxyHr and deoxyF$^-$ satisfy these criteria. However, the Mössbauer spectrum shows only the two components expected for deoxyF$^-$NO, and the ratio of the areas of the two doublets is very nearly 1.0. Clearly, there is only one species present in the deoxyF$^-$NO sample and the binding of NO to deoxyF$^-$ is near quantitative.

To further verify the completeness with which NO binds to deoxyF$^-$, attempts were made to increase the yield by varying the fluoride incubation time, the reaction time, or the amounts of either F$^-$ or NO. The binding of fluoride to deoxyHr is rapid and, thus, increasing the incubation time prior to NO addition did not enhance the yields of deoxyF$^-$NO (Table 3.19). Neither increasing the fluoride concentration from a 45-fold excess to a 200-fold excess nor increasing the amount of NO lead to greater yields of deoxyF$^-$NO (Table 3.19). Furthermore, a sample frozen nearly 24 hrs after adding NO accounts for as much Hr as that

frozen several minutes after NO was added (Table 3.18), indicating that the presence of fluoride has increased the stability of the NO adduct.

DeoxyF⁻NO was also characterized by resonance Raman spectroscopy (Fig. 3.40). Only one peak (ν = 420 cm^{-1}) is observed when the resonance Raman spectrum is obtained with 647.1 nm light. Neither vibrations for Fe-F-Fe, which should appear near 700 cm^{-1}, nor N-O stretching modes are resonance enhanced.

The results of isotope substitution experiments are summarized in Table 3.20. The frequency shift with ^{15}NO indicates that the band at 420 cm^{-1} involves the nitric oxide ligand and, by analogy to deoxyNO, nitric oxide is apparently coordinated terminally to one iron of the binuclear pair. Since stretching modes are generally more intense than bending modes, assignment of the band as ν_s(Fe-NO) is preferred to assignment as δ(Fe-N-O).

The presence of fluoride clearly produces a nitric oxide adduct of deoxyHr that is different from the adduct formed in the absence of fluoride. Because the optical, EPR, Mossbauer, and resonance Raman spectra for deoxyF⁻NO differ from the corresponding spectra of deoxyNO, fluoride must be coordinated at or near the binuclear center. Two possible structures are shown in Fig. 3.41. While structure II in which there is a hydrogen-bonding interaction between hydrogen fluoride and the hydroxo bridge cannot be disregarded, structure I, which proposes that a μ-fluoro bridge has replaced the μ-hydroxo bridge, is favored.

Two major differences between the EPR spectra of deoxyNO and deoxyF⁻NO support the proposed μ-fluoro bridged structure. First of

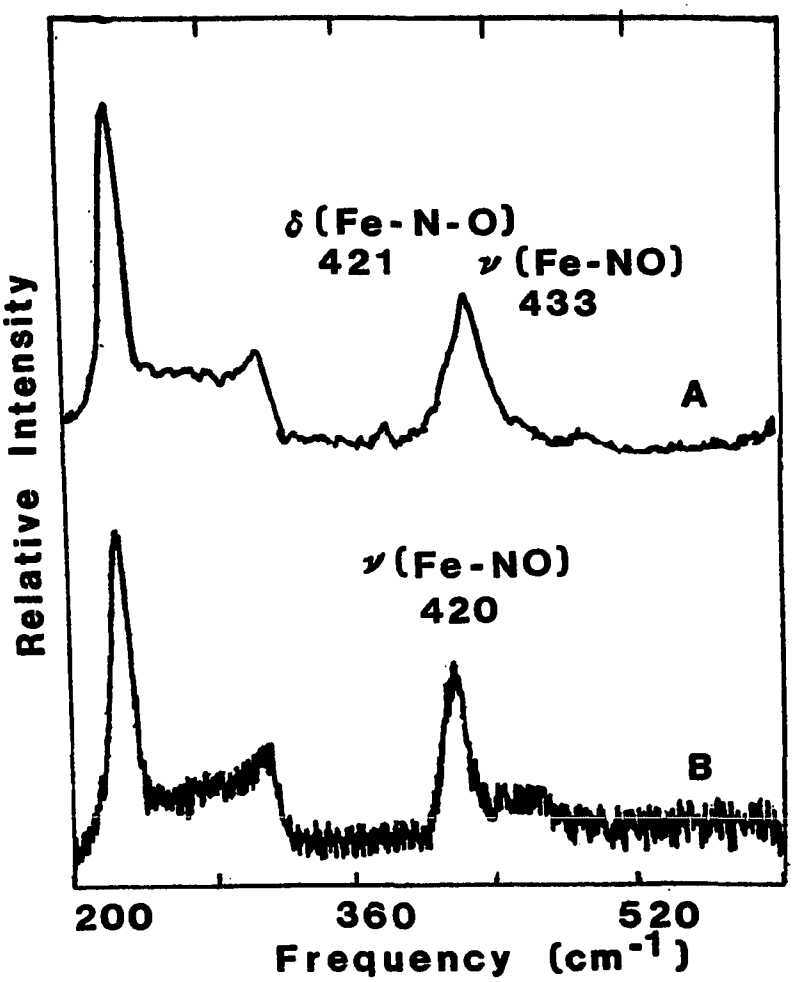

Figure 3.40. Resonance Raman spectra of deoxyNO (A) and deoxyF⁻NO (B) prepared with $^{14}N^{16}O$

Spectral conditions: temperature, 77 K; excitation wavelength, 647.1 nm; scan rate, 2 cm^{-1}/s; power, 100 mW; slit width, 8 cm^{-1}

Table 3.20. Resonance Raman data for deoxyF$^-$NO at 90 K using 647.1 nm excitation[a]

Isotope	Frequency (cm^{-1})
^{14}NO	420[b]
^{15}NO	416[c]
D_2O	421[d]

[a]50 mM phosphate; 0.3 M sulfate; pH 6.5; 2 cm^{-1}/s; 100 mW; 3.11 mM Hr; 142 mM F^-.

[b][NO]/[Hr] = 9.50.

[c][NO]/[Hr] = 12.7.

[d]5.52 mM Hr; 534 mM F^-; [NO]/[Hr] = 14.3.

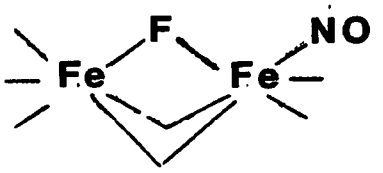

I

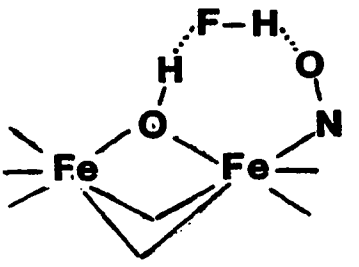

II

Figure 3.41. Possible structures of deoxyF⁻NO

all, the EPR signal for deoxyF⁻NO is significantly broadened relative to that of deoxyNO and secondly, the signal for deoxyF⁻NO is much more difficult to saturate ($P_{1/2}$ = 35 dB and 12 dB for deoxyNO and deoxyF⁻NO, respectively). Broadening could result from interaction of the iron center with a ^{19}F nucleus (I = 1/2). The ease with which the deoxyNO signal saturates compared to deoxyF⁻NO indicates that the energy separation between the ground state and the lowest-lying excited state is smaller for deoxyF⁻NO than for deoxyNO. This could result if the antiferromagnetic exchange coupling is weaker in deoxyF⁻NO than in deoxyNO, which is consistent with replacement of the hydroxo bridge of deoxyNO with a μ-fluoro bridge for deoxyF⁻NO.

$Fe_2F_5 \cdot 2H_2O$ provides a precedent for the occurrence of an Fe^{2+}-F-Fe^{3+} unit. X-ray crystallography (177) shows that the infinite array contains chains of fluoride bridged ferric ions [d(Fe^{3+}-F) = 1.94 Å; LFe^{3+}-F-Fe^{3+} = 145.7°] that are linked to ferrous ions via fluoride bridges [d(Fe^{2+}-F) = 2.05 Å; LFe^{2+}-F-Fe^{3+} = 136°]. These Fe-F distances do not differ significantly from those of Fe-O_{oxo} in metN_3^- (Table 1.1). Thus, it should be possible for there to be a μ-fluoro bridge in deoxyF⁻NO.

Magnetic susceptibility measurements for the discrete binuclear complexes having a monofluoro bridge, $[(TA)_2M_2F](BF_4)_3$ (M = Cu, Co), provide a gauge for determining the strength of the coupling through a μ-floro bridge (178). For the copper(II) and cobalt(II) complexes, antiferromagnetic coupling constants (-J) of 200 and 70 cm^{-1}, respectively, were reported (178). In both compounds, the MFM units are es-

sentially linear (LCu-F-CU = 178°). For deoxyF⁻NO, the Fe-F-Fe angle is likely to be significantly less than 180°. If one assumes an Fe-Fe separation that is comparable to that of $metN_3^-$ (3.30 Å) and uses the Fe^{2+}-F and Fe^{3+}-F bond distances for $Fe_2F_5 \cdot 2H_2O$, one obtains a value of 111° for the Fe^{2+}-F-Fe^{3+} angle. This decrease in the Fe-F-Fe angle is expected to result in significantly weaker coupling between the irons.

One further result that suggests that the iron atoms are bridged by fluoride in deoxyF⁻NO is the absence of a shift in the position of ν(Fe-NO) when deoxyF⁻NO is prepared in D_2O (Table 3.20). To verify that the lack of a shift in D_2O did not arise from failure of deuterium to exchange with the hydroxo bridge, the deoxyHr crystals were equilibrated in D_2O for 24 hours before they were used to prepare the deoxyF⁻NO sample. Since identical resonance Raman spectra were obtained for deoxyNO prepared from deoxy in D_2O (1 hr incubation time) and for deoxyNO prepared from oxy crystals dissolved in D_2O, 1 hr is a sufficient time for the deuterium exchange reaction to be completed. Thus, the absence of a D_2O affect on the frequency of ν(Fe-NO) is consistent with replacement of the μ-hydroxo bridge of deoxyNO with a μ-fluoro bridge for deoxyF⁻NO.

That fluoride and nitric oxide occupy different coordination sites is supported by the observation that the best route for preparation of deoxyF⁻NO involves addition of fluoride <u>before</u> the addition of NO. Addition of 0.1 M F^- to deoxyNO partially bleaches the color of the solution (Fig. 3.42A). Similarly, the intensity of the EPR signal for deoxyNO is diminished and replaced by that for deoxyF⁻NO (Fig. 3.42B).

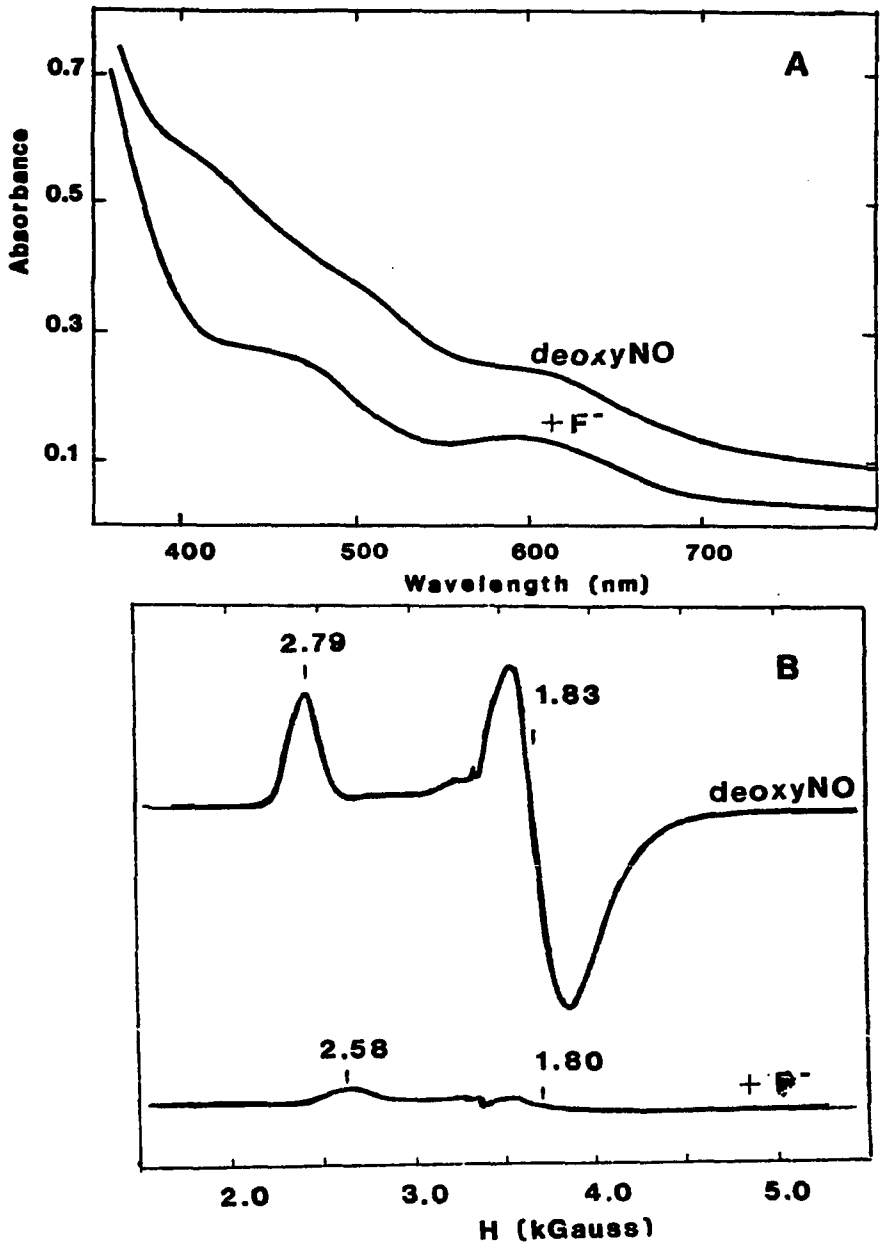

Figure 3.42. Optical (A) and EPR (B) spectra for the addition of excess NaF to deoxyNO

Spectral parameters: temperature, 4.2 K; frequency, 9.42 GHz; power, 40 μW; modulation, 40 G; gain, 5 x 10^4; time constant, 0.2 s

A. 0.375 mM Hr; 28.5 mM NaF; [NO]/[Hr] = 4.4; 50 mM phosphate, pH 7.0; 0.15 M sulfate

B. 1.40 mM Hr; 495 mM F^-; [NO]/[Hr] = 1.44; 50 mM phosphate, pH 6.5

Thus, the solution is a mixture of deoxyF$^-$ and deoxyF$^-$NO. This result implies that fluoride may replace NO at its terminal site when OH$^-$ is bridging. Based on these observations, a possible mechanism for formation of deoxyF$^-$NO is shown in Scheme 3.3.

Scheme 3.3:

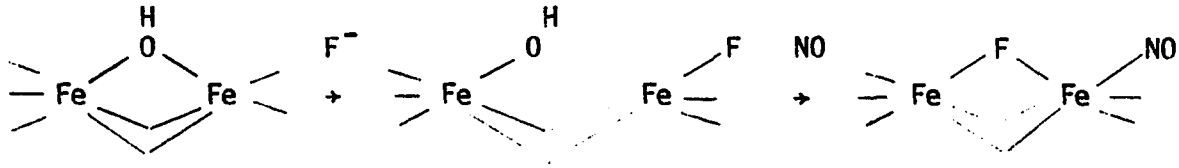

According to Scheme 3.3, fluoride ion effectively labilizes the hy-hydroxo bridge toward substitution. The strong tendency for the iron atoms to retain a bridging group favors formation of a μ-fluoro bridge. Nevertheless, one is lead to wonder whether or not a magnetically uncoupled derivative lacking a bridging group might be prepared using fluoride.

E. Attempts to Prepare a Nitric Oxide Adduct of Methemerythrin

The fully oxidized form of Hr, metHr, is unreactive toward molecular oxygen. Although nitric oxide adducts of iron(II) are more common than adducts with iron(III), the latter are not unknown. It is possible that the reaction of NO with semi-metHr occurs with the ferric site of the binuclear center. If this is the case, preparation of a nitric oxide adduct of metHr should be possible. Four approaches were used in attempting to prepare metNO.

(i) Direct addition of nitric oxide to an anaerobic solution of metHr.

(ii) Transfer of nitric oxide *in situ* from either $Co(NH_3)_5NO^{2+}$ or $Co(dmgH)_2NO$ to metHr.

(iii) Reduction of the bound nitrite ligand of $metNO_2^-$ without reduction of the metal site.

(iv) Oxidation of the metal center of semi-metNO without oxidation of the coordinated ligand.

In 50 mM phosphate (pH 6.5), no changes in the optical spectrum of metHr are observed upon addition of a 4.7-fold molar excess of nitric oxide to an anaerobic solution of metHr (Fig. 3.43A). After a 10 minute incubation period, a 67-fold molar excess of sodium azide was added. The optical spectrum that results (Fig. 3.43B) is that of $metN_3^-$. Quantitation of this spectrum shows that 89% of the protein is at the met oxidation level.

It was reported by Brudvig et al. (170) that a one-electron reduction of cytochrome oxidase occurs when both NO and N_3^- are added to the fully oxidized state of the protein (reaction 3.11).

$$Fe(III)Cu(II) + NO + N_3^- \rightarrow Fe(II)NO\ Cu(II) + N_2O + N_2 \qquad (3.22)$$

If an analogous reaction occurs with metHr, the Hr-containing product should be an EPR-silent NO adduct of semi-metHr (reaction 3.23).

$$Fe(III)_2 + NO + N_3^- \rightarrow Fe(II)NO\ Fe(III) + N_2O + N_2 \qquad (3.23)$$

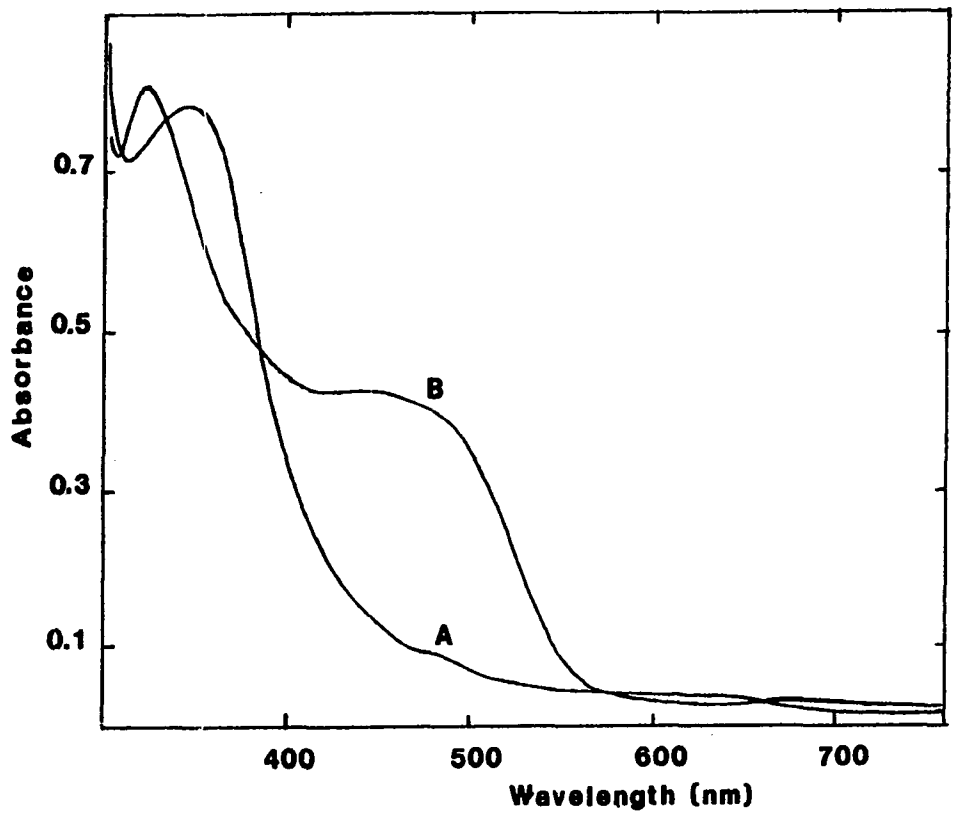

Figure 3.43. Optical spectra before (A) and after (B) the addition of excess azide to metHr incubated in NO for 5 min

0.133 mM Hr; 0.624 mM NO; 8.85 mM azide; 50 mM phosphate, pH 6.5

The EPR spectra obtained for samples frozen before and after addition of azide provide even more convincing evidence that there is no direct reaction between metHr and NO either before or after addition of azide. One would expect to observe an EPR signal for metNO, since the latter should possess an odd number of electrons. As Fig. 3.44 shows, no such signal is produced.

Either $Co(NH_3)_5NO^{2+}$ or $Co(dmgH)_2NO$ were used in an attempt to transfer NO to metHr. When $Co(dmgH)_2NO$ is added to an anaerobic solution of metHr (50 mM phosphate at pH 7.5), no optical changes occur.

Immediately upon addition of $Co(NH_3)_5NO^{2+}$ to 50 mM phosphate buffer (pH 7.5), vigorous bubbling is observed and a lilac precipitate forms. The colorless supernatant, which contains dissolved NO, does not react with an anaerobic solution of metHr. Furthermore, if metHr is added directly to the solid reagent, no reaction is observed when equimolar amounts of Hr and NO are present. With a 61-fold molar excess of $Co(NH_3)_5NO^{2+}$, the protein solution turns a deep brown color. Only a broad signal arising from Co(II) is observed by EPR spectroscopy. Since the brown-colored product is not EPR-active, it is probably semi-metNO rather than metNO. Reactions 3.24 to 3.26 show one route that could lead to production of semi-metNO.

$$Co(NH_3)_5NO^{2+} \rightarrow Co^{2+} + 5NH_3 + NO \qquad (3.24)$$

$$met + Co^{2+} \rightarrow semi\text{-}met + Co^{3+} \qquad (3.25)$$

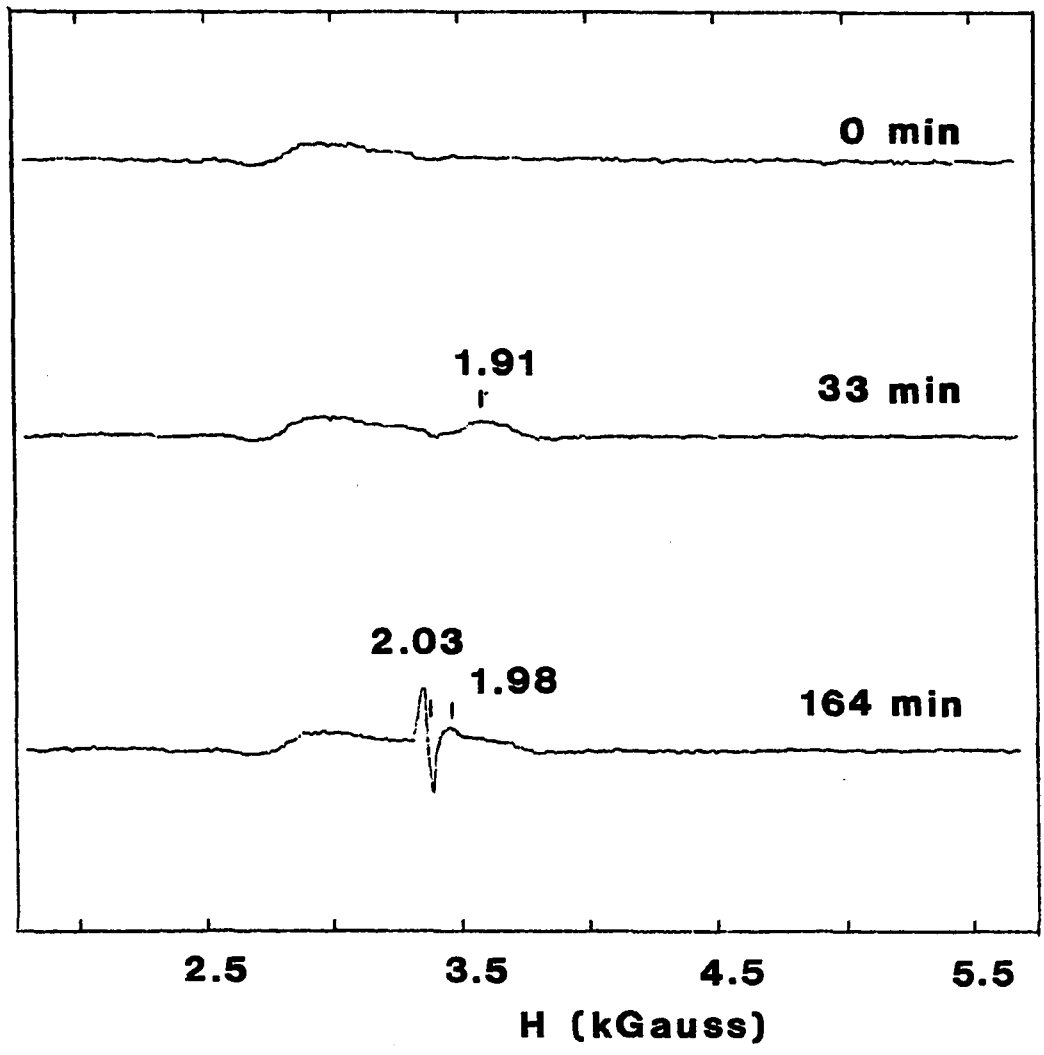

Figure 3.44. EPR spectra for the addition of excess NO to metHr

Spectral parameters: temperature, 4.2 K; frequency, 9.57 GHz; power, 100 μW; modulation, 16 G; gain, 8 x 10^4; time constant, 0.2 s; times measured relative to the addition of azide; samples were incubated with NO for 5 min before adding azide; 1.46 mM Hr; [NO]/[Hr] 4.7; 97.4 mM azide; 50 mM phosphate, pH 6.5; the zero time spectrum was obtained before the addition of azide

$$\text{semi-met} + NO \rightarrow \text{semi-metNO} \qquad (3.26)$$

The third preparative method was an attempt to preferentially reduce the coordinated nitrite ligand without altering the oxidation state of the metal site (reaction 3.27).

$$\text{metNO}_2^- + \text{Asc}^- \rightarrow \text{metNO} + \text{dehydroasc}^- \qquad (3.27)$$

Ascorbate, while it reacts with free nitrite to produce NO, will not reduce metHr when present in a 20-fold molar excess at pH 6.5. No reaction occurs when ascorbate is added to an anaerobic solution of metNO_2^- ([met]:[ascorbate]:[nitrite] = 1:10:20).

The fourth approach was an attempt to prepare metNO by oxidizing semi-metNO (reaction 3.28).

$$\text{semi-metNO} + Fe(CN)_6^{3-} \rightarrow \text{metNO} + Fe(CN)_6^{4-} \qquad (3.28)$$

Since semi-metNO and $Fe(CN_6)^{4-}$ are not detectable by EPR spectroscopy and metNO is expected to give rise to an EPR signal, EPR spectroscopy was used to determine whether a reaction occurred. Figure 3.45 shows the time course for the reaction of $(\text{semi-met})_0\text{NO}$ with ferricyanide. New EPR signals are not observed. Thus, once again, there is no evidence that a metNO derivative can be prepared.

Figure 3.45. EPR spectra for the reaction between $(semi\text{-}met)_0NO$ and ferricyanide

Spectral parameters: temperature, 4.2 K; frequency, 9.42 GHz; power, 100 μW; modulation, 16 G; gain, 4×10^4; time constant, 0.2 s; 1.58 mM Hr; 4.60 mM ferricyanide; [NO]/[Hr] = 4.7; 50 mM phosphate, pH 6.5; 0.2 M sulfate; signal at g = 2.72 belongs to ferricyanide

A. $(semi\text{-}met)_0$
B. spectrum immediately after addition of NO to $(semi\text{-}met)_0$
C. 2 minutes after addition of ferricyanide to $(semi\text{-}met)_0NO$
D. 360 minutes after addition of ferricyanide to $(semi\text{-}met)_0NO$
E. addition of NaN_3 (s) to a portion of the sample used to obtain spectrum D

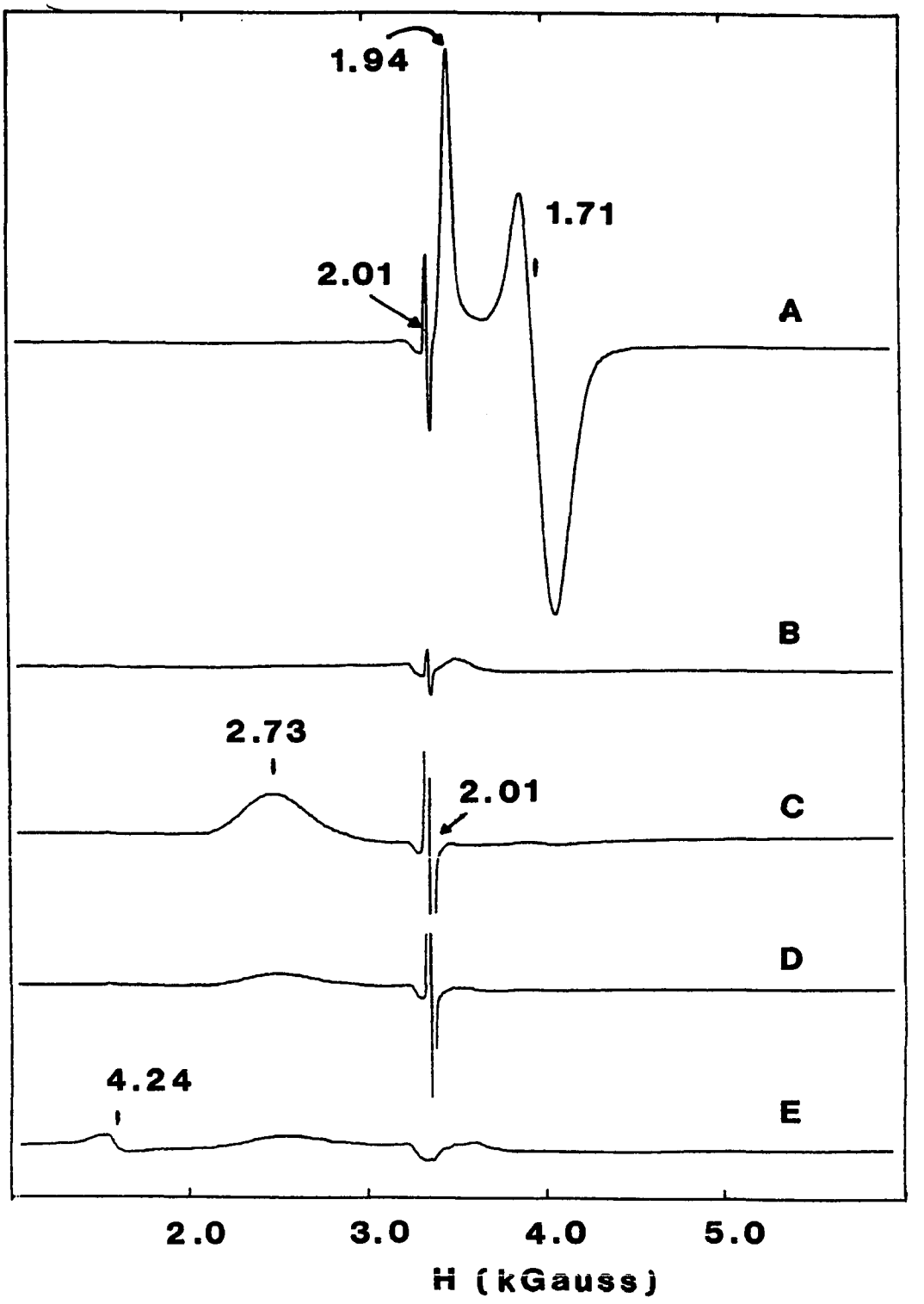
1.94
1.71
2.01
A
B
2.73
2.01
C
D
4.24
E
2.0
3.0
4.0
5.0
H (kGauss)

F. Reactions of DeoxyNO

Based on their proposed structural similarity, oxyHr and deoxyNO might be expected to exhibit similar reactivity patterns. By comparing the reactions of oxyHr and deoxyNO, an assessment can be made of the relevance of deoxyNO as an analog for the proposed superoxide intermediate of oxygenation. The reactions studied address four questions:

1. Is nitric oxide binding reversible?
2. Is deoxyNO stable with respect to auto-oxidation?
3. Is the bridge labile to substitution?
4. Is it possible to disrupt the magnetic coupling between the irons in deoxyNO?

1. Reversibility of NO binding

The physical characterization of deoxyNO is consistent with an $Fe(II)Fe(III)NO^-$ oxidation state formalism for deoxyNO. The reaction of deoxyHr with NO, like that with oxygen, may be viewed as an oxidative addition reaction (reaction 3.29).

$$Fe(II)Fe(II) + NO \rightleftarrows Fe(II)Fe(III)NO^- \qquad (3.29)$$

If NO binding results in the <u>irreversible</u> oxidation of one of the irons of the binuclear pair, then the reactivity of deoxyNO should parallel that of semi-metHr (Scheme 3.4A). This is the net reaction that should occur if deoxyNO undergoes an auto-oxidation process. However, if nitric oxide binds <u>reversibly</u> to the iron site, then the reactivity of deoxyNO should parallel that of deoxyHr (Scheme 3.4B).

Scheme 3.4A: Irreversible oxidation

$$Fe(II)Fe(III)NO^{-} \rightarrow Fe(II)Fe(III) + NO^{-}$$

Scheme 3.4B: Reversible oxidation

$$Fe(II)Fe(III)NO^{-} \rightleftarrows Fe(II)Fe(II) + NO$$

Five experiments were used to demonstrate that the binding of NO to deoxyHr is a reversible process:

(i) The reaction of deoxyNO with dithionite.

(ii) The reaction of deoxyNO with oxygen.

(iii) Oxidation of deoxyNO with ferricyanide.

(iv) Oxidation of deoxyNO with nitrite.

(v) The reaction of deoxyNO with monovalent anions.

The reaction of deoxyNO with sodium dithionite was used to show that NO can be removed from deoxyNO. After ~90 minutes, the green color of the solution of deoxyNO had almost completely disappeared (Fig. 3.46). The resulting solution was pale yellow and reacted with oxygen to produce oxyHr, the major product was identified as deoxyHr (Fig. 3.46C). Loss of the EPR signal of deoxyNO (Fig. 3.47) parallels the bleaching of the green color from the solution. The reaction between nitric oxide and dithionite occurs with a rate constant of 1.4×10^{3} $M^{-1}s^{-1}$ (20°C, pH 7.0, 50 mM phosphate) (153). Thus, this reaction can be viewed as a method for trapping NO rather than as a redox reaction between dithionite and the binuclear site.

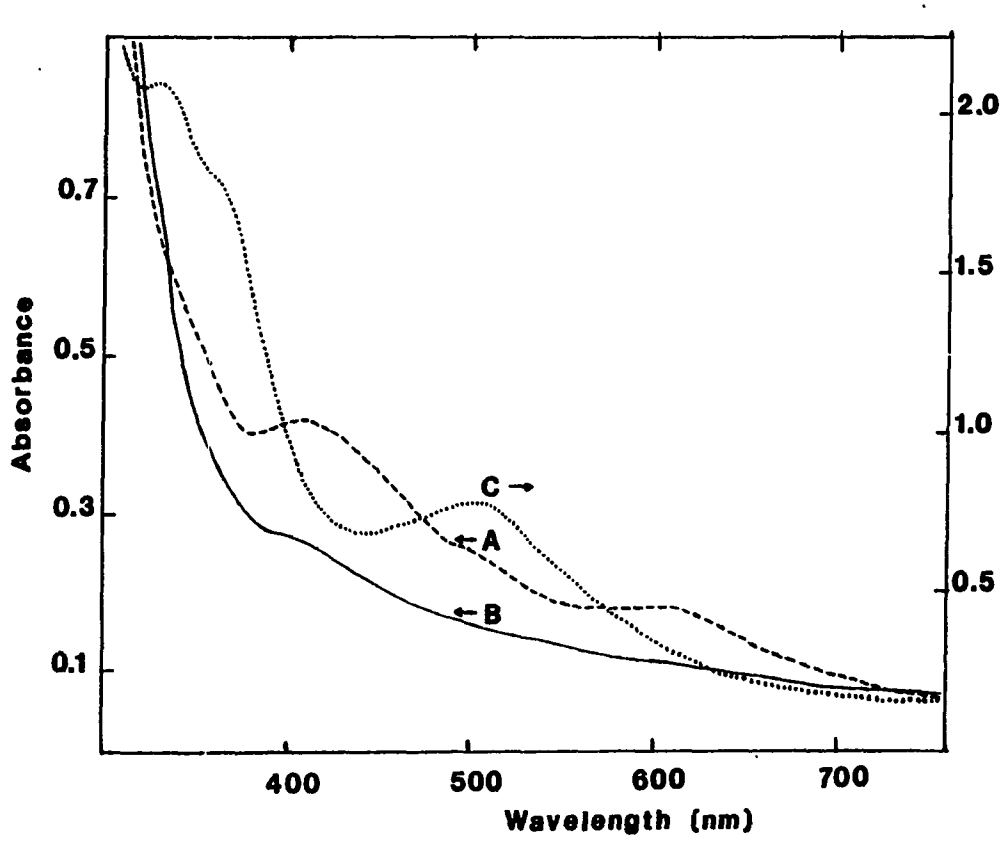

Figure 3.46. Optical spectra for the reaction of deoxyNO with sodium dithionite

0.535 mM Hr; 0.217 mM dithionite; [NO]/[Hr] = 3.6; 50 mM phosphate, pH 6.5; spectra recorded before addition of dithionite (A), 54 min after adding dithionite (B), and after bubbling oxygen into the solution for sample B (C)

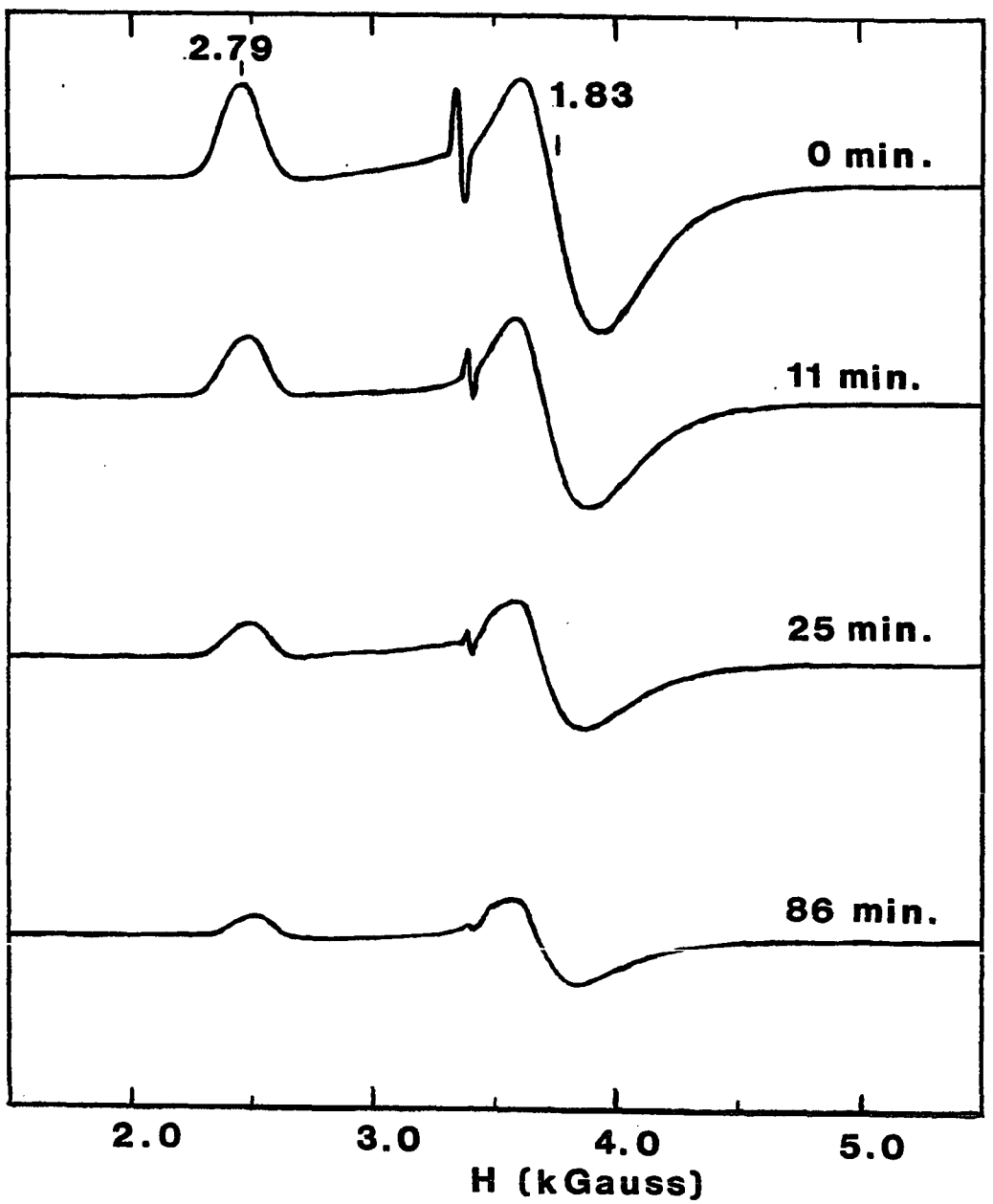

Figure 3.47. EPR spectra for the reaction between deoxyNO and sodium dithionite

Spectral conditions: temperature, 4.2 K; frequency, 9.56 GHz; power, 40 μW; modulation, 40 G; gain, 4 x 10^4; time constant, 0.2 s; 1.76 mM Hr; 3.18 mM dithionite; [NO]/[Hr] = 3.64; 50 mM phosphate, pH 6.5

For the latter four experiments, the reagents used undergo well-characterized reactions with deoxyHr. These further confirm that the binding of NO is a reversible process.

When oxygen is bubbled into a solution of deoxyNO, an 89% yield (based on quantitation of the optical spectrum) of oxyHr is obtained. This reaction also is consistent with dissociation of NO, the reversible pathway, rather than NO^- (reaction 3.30).

$$\text{DeoxyNO} \rightleftarrows \text{Deoxy} \rightleftarrows \text{Oxy} \qquad (3.30)$$

DeoxyNO and $Fe(CN)_6^{3-}$ were reacted in a 1:1 mole ratio for 2 1/2 hours, after which time the composition of the solution was analyzed by addition of a 29.4-fold excess of sodium azide. The shape of the optical spectrum indicates formation of $metN_3^-$ in a 63% yield. If deoxyNO were reacting by dissociation of NO^- (Scheme 3.4A), the yield of $metN_3^-$ should have been much higher since only one equivalent of ferricyanide would be needed for quantitative oxidation of semi-metHr to metHr. On the other hand, decomposition by loss of NO produces deoxyHr (Scheme 3.4B) and, therefore, a 50% yield of metHr is expected. The 63% yield is, therefore, consistent with the decomposition occurring predominantly according to Scheme 3.4B.

When the reaction of ferricyanide with deoxyNO is followed by EPR spectroscopy (Fig. 3.48), the EPR signal of deoxyNO is no longer observed after a 47 minute reaction period. Only a small amount of semi-

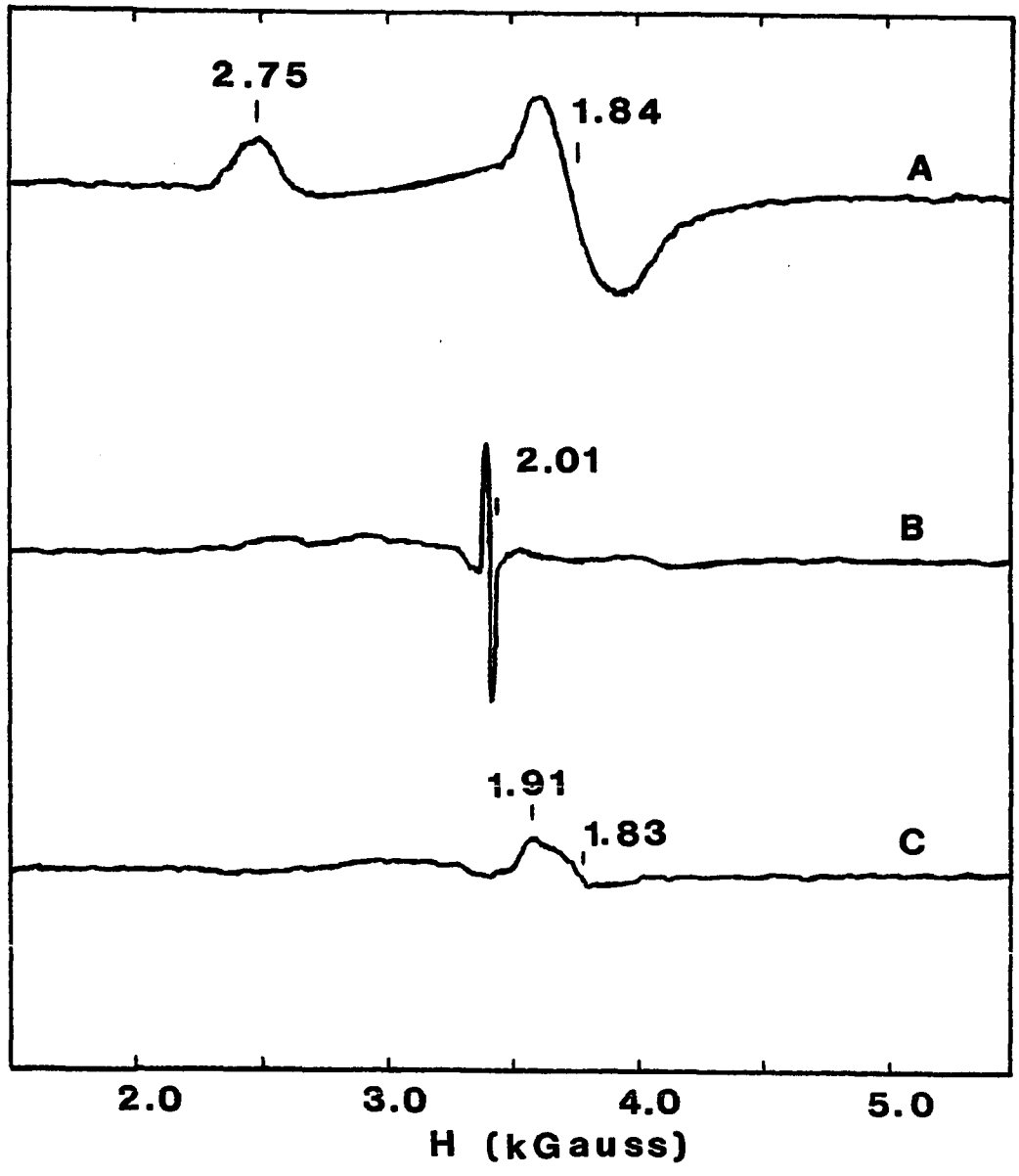

Figure 3.48. EPR spectra for the reaction of deoxyNO with one equivalent of ferricyanide

Spectral parameters: temperature, 4.2 K; frequency, 9.57 GHz; power, 40 μW; modulation, 40 G; gain, 8 x 10^4; time constant, 0.2 s; 1.11 mM Hr; 1.10 mM ferricyanide; [NO]/[Hr] = 6.92; 50 mM phosphate, pH 6.5

$metN_3^-$ is observed in an EPR sample frozen 77 minutes after the addition of sodium azide. Thus, the oxidation product is $metN_3^-$.

Within 20 minutes after the addition of a 50-fold molar excess of $NaNO_2$ to deoxyNO, the solution becomes a dark brown color. At this time, less than 10% of the protein is in a paramagnetic state (Fig. 3.49). These observations suggest that the immediate product of the oxidation of deoxyNO by nitrite is semi-metNO. This reaction is followed by the slow generation of an EPR signal that is identical to that of semi- $metNO_2^-$ (Fig. 3.49). Thus, the reaction of deoxyNO with nitrite parallels the reaction of deoxyHr with nitrite, suggesting that deoxyHr is an intermediate in the reaction between deoxyNO and nitrite.

Nitrite is the only monovalent iron-ligating anion that has been found to promote the auto-oxidation of deoxyNO. The ligands that were used fall into two groups based upon their reactivity with deoxyNO. Azide, cyanate, and fluoride (0.1 M for ~2.0 mM Hr), anions known to bind to deoxyHr, bleach the color of deoxyNO within minutes after being mixed (Fig. 3.50). Contained in the second group are anions that neither hinder formation of deoxyNO nor react with deoxyNO. Included in this group are Cl^-, Br^-, I^-, SCN^-, and CN^-. Figure 3.51 shows the EPR spectra obtained for ligands representative of both groups.

Within the first group of ligands, azide is unique in that in addition to bleaching the deoxyNO color, the product exhibits an EPR signal with g-value at 12.3. Such a signal was previously observed for $deoxyN_3^-$ (6). Thus, in the case of azide, cyanate, and fluoride, the colorless products are ligand adducts of deoxyHr. As suggested by Reem

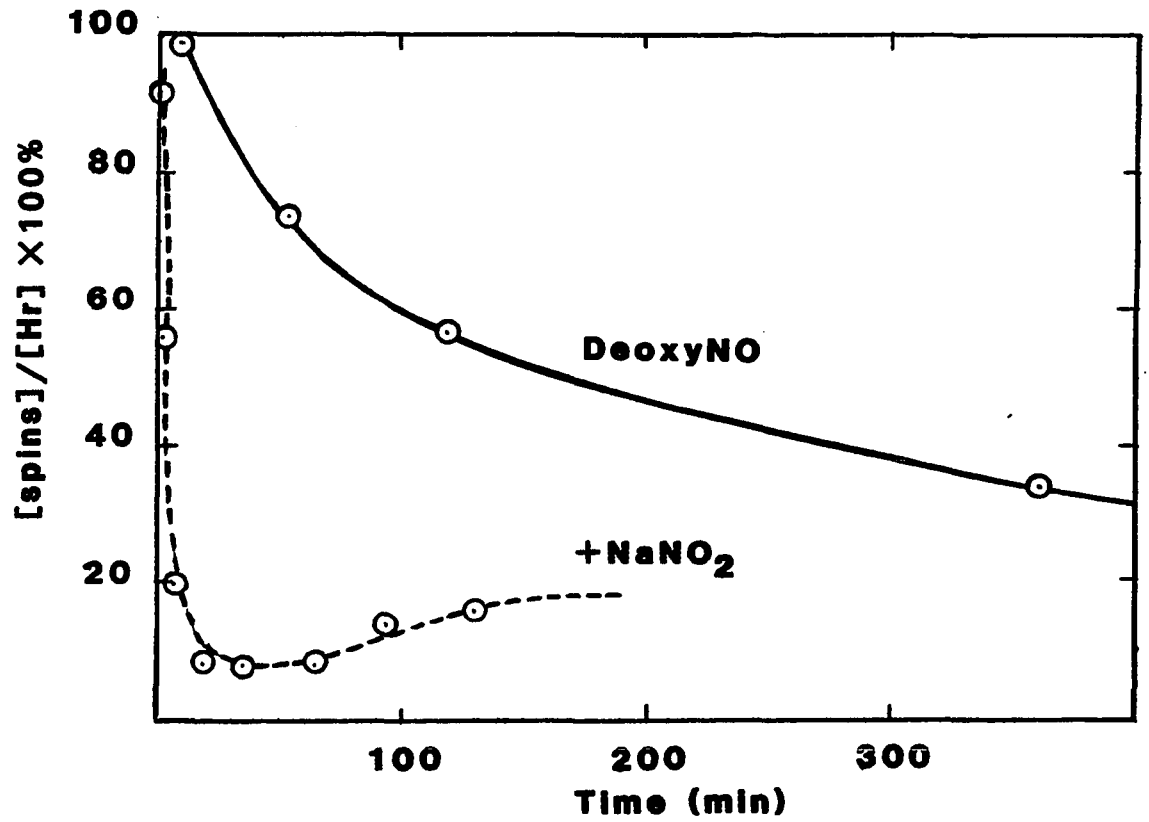

Figure 3.49. Time course for the decomposition of deoxyNO with and without excess nitrite

A. deoxyNO: 0.79 mM Hr; [NO]/[Hr] = 1.4; 50 mM phosphate, pH 6.5
B. deoxyNO + NO_2^-: 0.88 mM Hr; [NO]/[Hr] = 4.5; 45.6 mM nitrite; 50 mM phosphate, pH 6.5

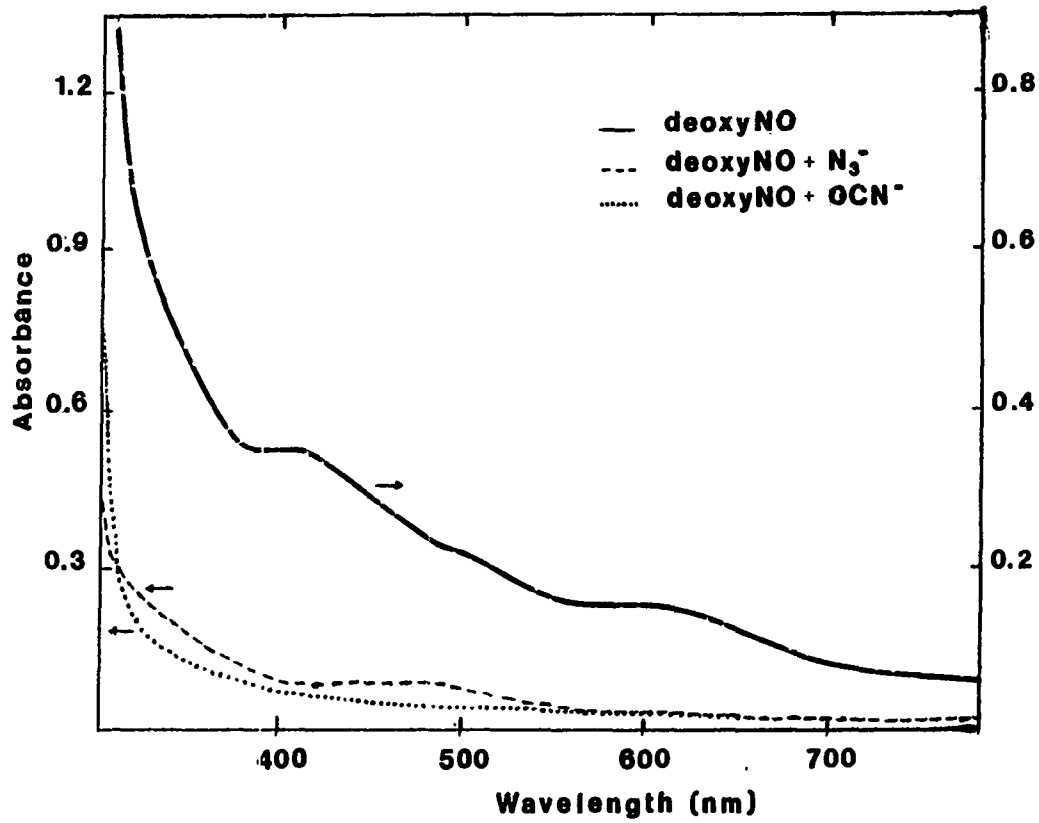

Figure 3.50. Optical spectra for the reaction of deoxyNO with excess azide (---) or cyanate (•••)

0.487 mM Hr; 114 mM NaN_3 or 114 mM KOCN; 50 mM phosphate; pH 6.5; spectra were recorded within 5 minutes after the addition of Hr to either NaN_3 or KOCN

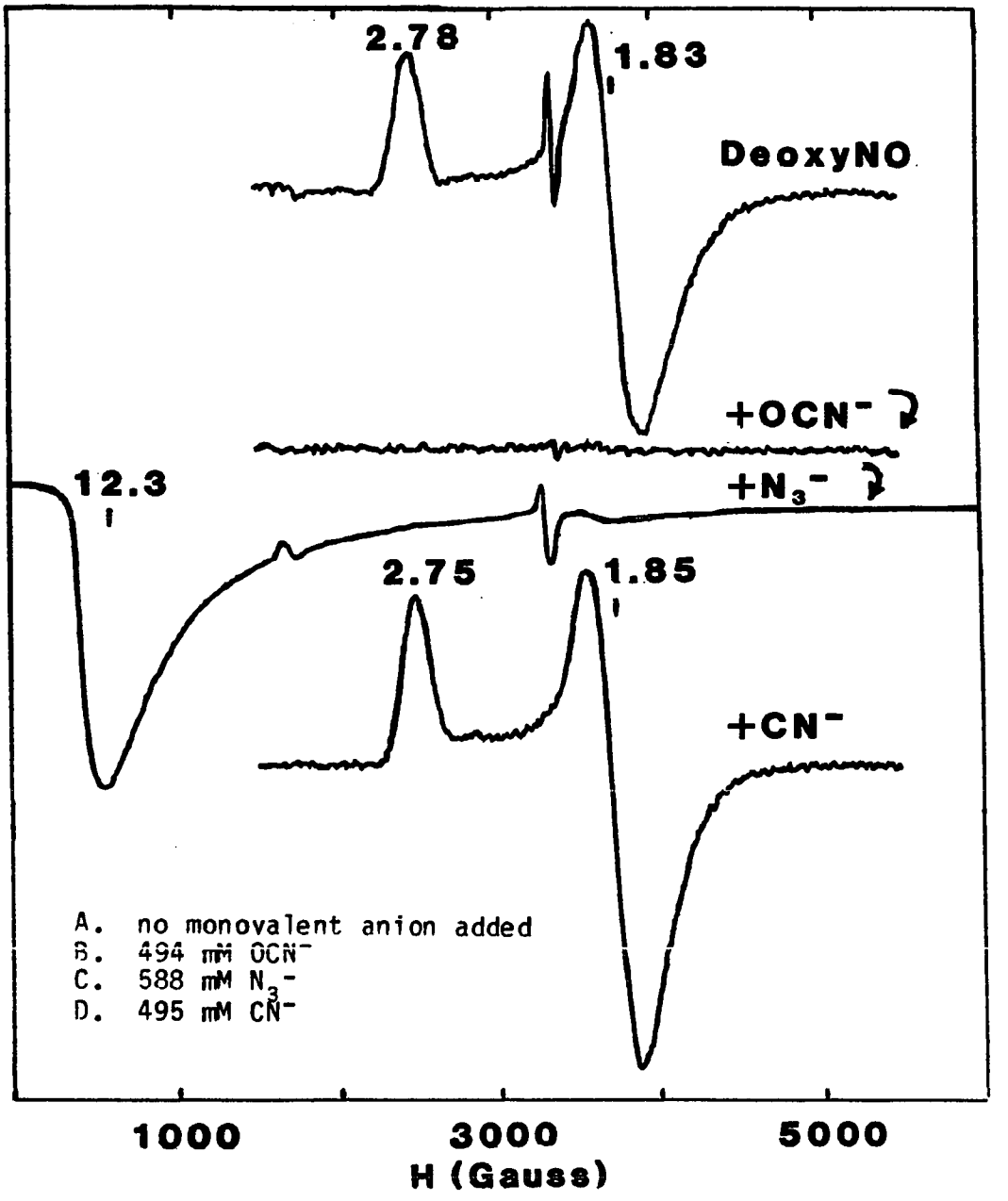

Figure 3.51. EPR spectra for the reaction of deoxyNO with monovalent anions

Spectral parameters: temperature, 4.1 K; frequency, 9.57 GHz; power, 40 μW (A, B, and D) and 100 μW (C); modulation, 40 G; gain, 8×10^4; time constant, 0.2 s; 2.11 mM Hr; [NO]/[Hr] = 3.1; 50 mM phosphate, pH 6.5

and Solomon (6), the structure of these adducts likely contains hydroxide bound to only one iron rather than as a bridging group (I).

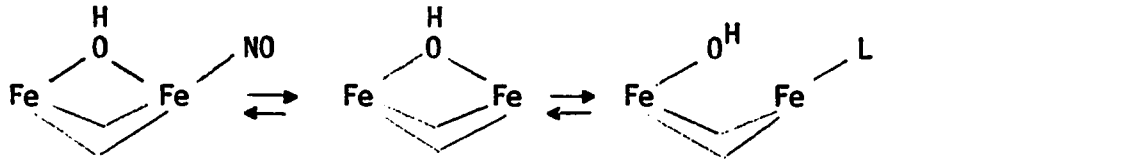

DeoxyNO Deoxy DeoxyL$^-$ L$^-$ = N_3^-, OCN^-, F^-

I

The reaction of deoxyN_3^- (prepared from deoxyHr with an 1800-fold excess of sodium azide) with oxygen is shown in Fig. 3.52. This reaction produces metN_3^- without the development of an isosbestic point as was observed during the reaction of oxyHr with azide (Fig. 3.53).

When nitric oxide is added to a solution of deoxyN_3^-, oxidation does not occur to a significant extent (Fig. 3.54). The weak signal near 3500 G arises from a small amount of semi-metN_3^-. Since the intensity of the EPR signal for deoxyN_3^- is not significantly altered, NO does not appear to react with deoxyN_3^-.

Thus, like oxygen-binding, the binding of nitric oxide is a reversible reaction.

2. Affinity constant for the binding of NO to deoxyHr

The affinity constant for the binding of NO to deoxyHr was estimated by equilibrium measurements in which various ratios of azide and nitric oxide were added to deoxyHr. The equilibrium between deoxyN_3^- and deoxyNO (reaction 3.31)

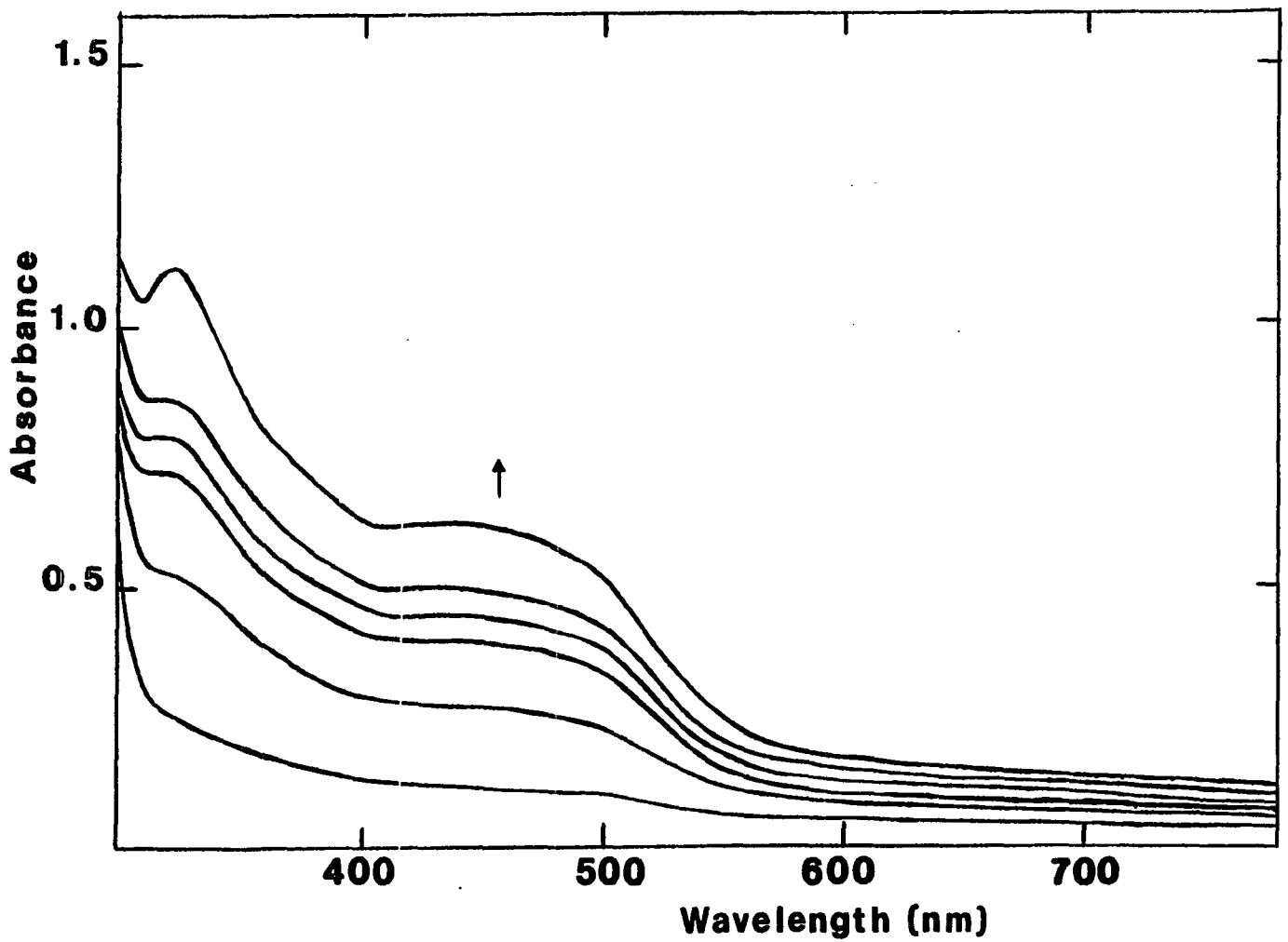

Figure 3.52. Optical time course for the reaction of deoxyN_3^- with oxygen

0.173 mM Hr; $[N_3^-]/[Hr]$ = 1780; 50 mM phosphate, pH 6.5; spectra recorded at 15 min intervals; last spectrum after 21 hours

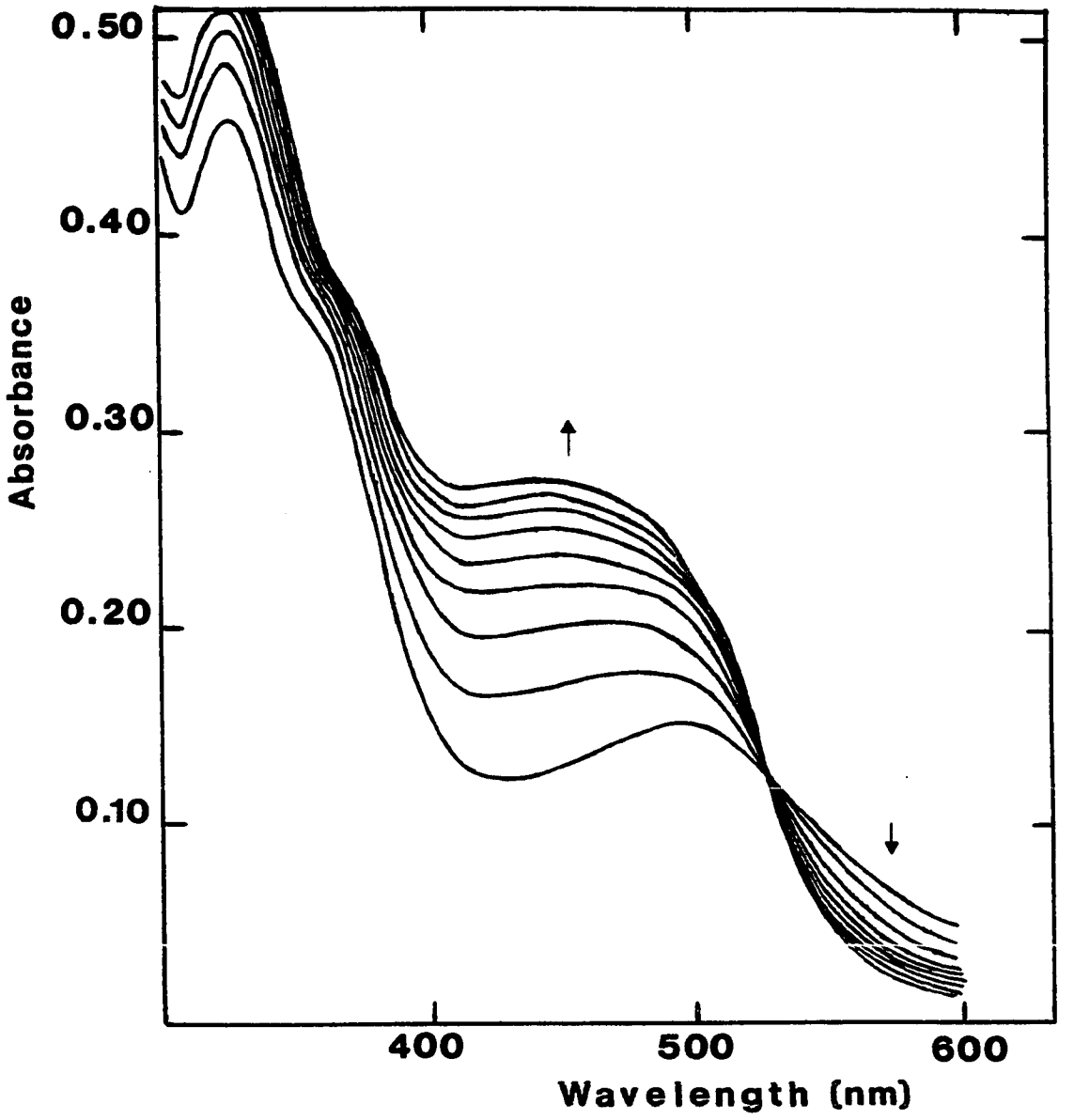

Figure 3.53. Optical time course for the reaction of oxyHr with sodium azide

0.0629 mM Hr; 4.68 mM azide; 50 mM phosphate, pH 7.5; spectra at 15 min intervals; isosbestic point at 525 nm

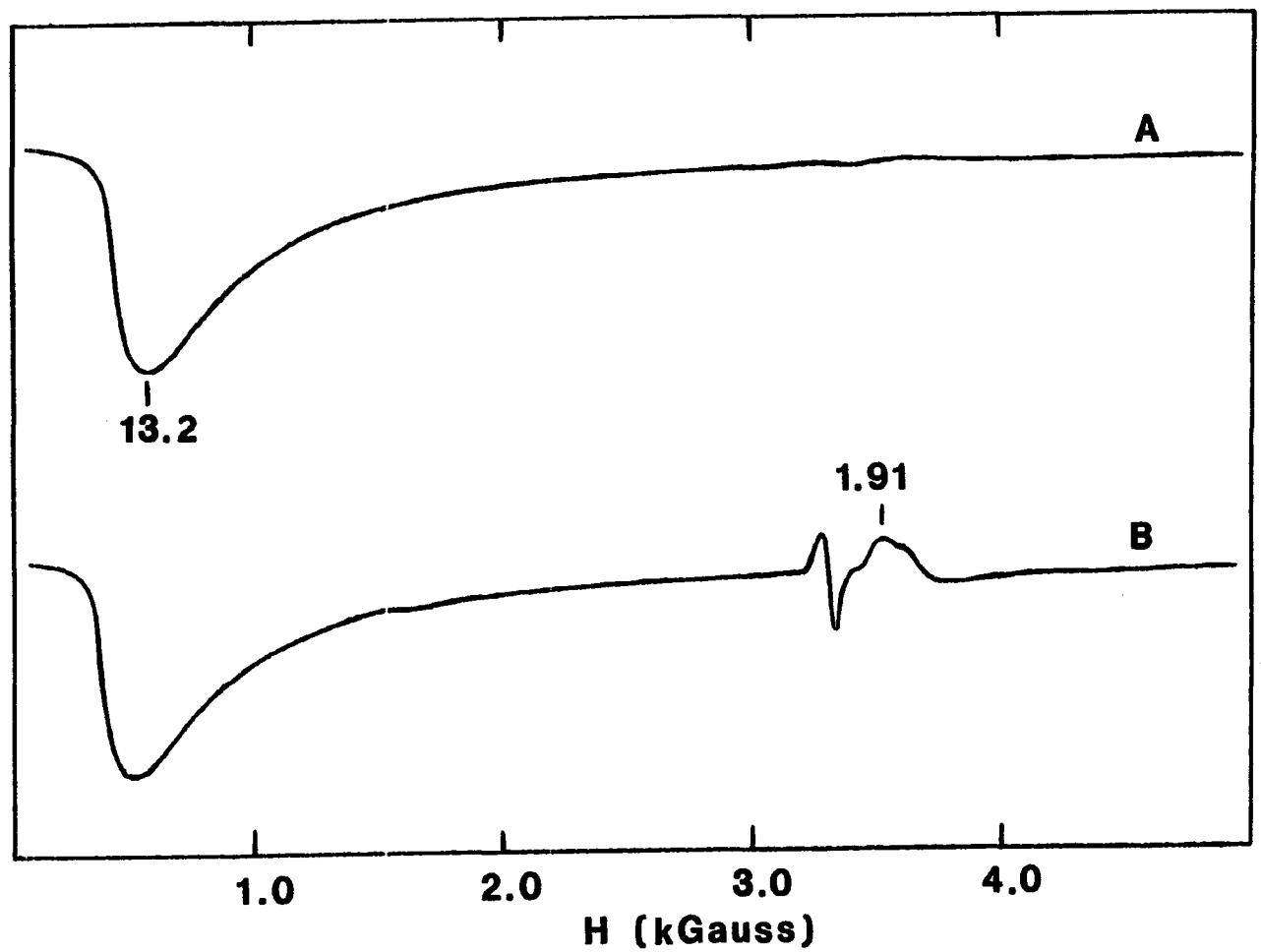

Figure 3.54. EPR spectra before and after addition of NO to deoxyN_3^-

Spectral parameters: temperature, 4.1 K; frequency, 9.42 GHz; power, 40 μW; modulation, 40 G; gain, 1 x 10^4; time constant, 0.2 s; 2.92 mM Hr; 0.76 M azide; [NO]/[Hr] = 2.7; 50 mM phosphate, pH 6.5; 0.3 M sulfate

$$deoxyN_3^- + NO \rightleftharpoons deoxyNO + N_3^- \quad (3.31)$$

may be expressed as the sum of reactions 3.32 and 3.33.

$$deoxy + NO \rightleftharpoons deoxyNO \quad (3.32)$$

$$deoxyN_3^- \rightleftharpoons deoxy + N_3^- \quad (3.33)$$

The equilibrium constant for the binding of azide to deoxyHr at pH 7.7 was reported to be 70 M^{-1} by Reem and Solomon (6) and 6700 M^{-1} at pH 6.0 (179). By interpolation, the equilibrium constant for the binding of azide to deoxyHr at pH 6.5 was determined to be 2120 M^{-1}. Using this value for $K_{DN_3^-}$ in Eq. 3.34, the value for the equilibrium constant for reaction 3.32 was calculated (see Appendix A).

$$K_{HrNO} = \frac{[DNO][N_3^-]}{[DN_3^-][NO]} K_{DN_3^-} \quad (3.34)$$

The results, summarized in Table 3.21, indicate that $K_{HrNO} = 5.5 \times 10^5$ M^{-1} at pH 6.5. Thus, the affinity of deoxyHr for NO is only ~4 times greater than the affinity of deoxyHr for oxygen.

3. Stability of deoxyNO

At 25°C and pH 7, oxyHr is auto-oxidized to metHr with a half-life of 18.5 hrs in 0.3 M Cl^- (19). This rate of auto-oxidation is enhanced when other monovalent anions are present. Figure 3.53 shows the optical

Table 3.21. Equilibrium constants for the binding of nitric oxide to deoxyHr[a]

$([N_3^-]/[NO])$	[Hr] (μM)	$[N_3^-]$ (mM)	[NO] (μM)	10^{-5} K_{HrNO} (M^{-1})
1280	84.3	212	165	6.2
257	84.3	42.4	165	7.1
128	88.2	22.2	173	5.4
38.5	91.1	6.87	178	3.4
				average = 5.5 ± 1.4

[a]50 mM phosphate; pH 6.5; 0.3 M sulfate.

spectra obtained when a 74-fold molar excess of sodium azide is added to a deaerated sample of oxyHr. Appearance of an isosbestic point at 530 nm signifies that two colored species are interconverting without the accumulation of significant amounts of colored intermediates.

If deoxyNO undergoes such an auto-oxidation reaction, semi-metHr would be the expected product (Scheme 3.4A). At room temperature, over the course of several hours, the green color of deoxyNO is replaced by a golden-brown color (Fig. 3.55). Along with this change, the intensity of the deoxyNO EPR signal decreases (Fig. 3.49). The color of the solution indicates that this EPR-silent species is not deoxyHr, but rather, the product was shown to be at the semi-met oxidation level from the EPR signal resulting from addition of an excess of sodium azide (Fig. 3.56). Quantitation by double integration of the initial EPR signal accounts for 100.2% of the protein. After 20 hours, 9.6% remains in a paramagnetic form and after azide is added, 80.2% of the protein is present as semi-metN_3^-. The lack of an EPR signal at 20 hours indicates that the product is a nitric oxide adduct of semi-metHr (section III.C).

The instability of deoxyNO may arise from the generation of nitrite in solutions of deoxyNO. The source of nitrite in the deoxyNO samples is believed to be the disproportionation of free NO (reaction 3.35), a reaction that Chalamet previously suggested occurs in aqueous solutions containing NO (114). Furthermore, N_2O was detected by GC/MS in buffered stock solutions of NO both in the presence and absence of Hr (see Appendix B).

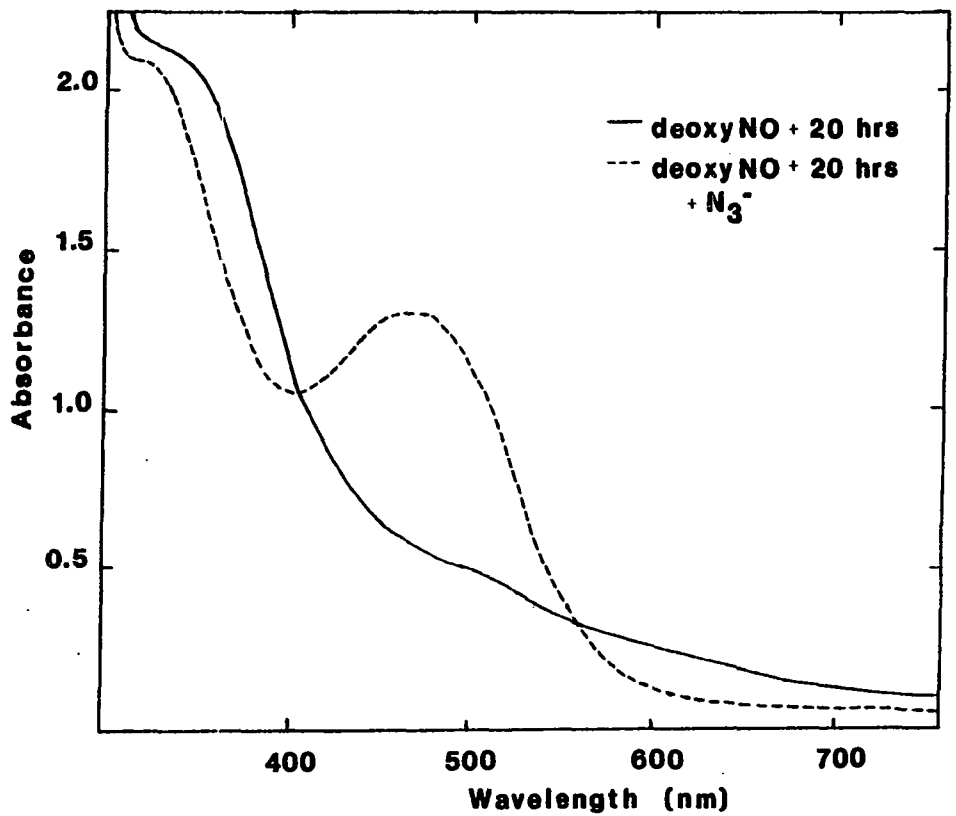

Figure 3.55. Optical spectra before (——) and after (---) the addition of NaN_3 to deoxyNO that had auto-oxidized for 20 hrs

0.563 mM Hr; [NO]/[Hr] = 4.6; 13.5 mM NO_3^-; 50 mM phosphate; pH 6.5; 0.2 M sulfate

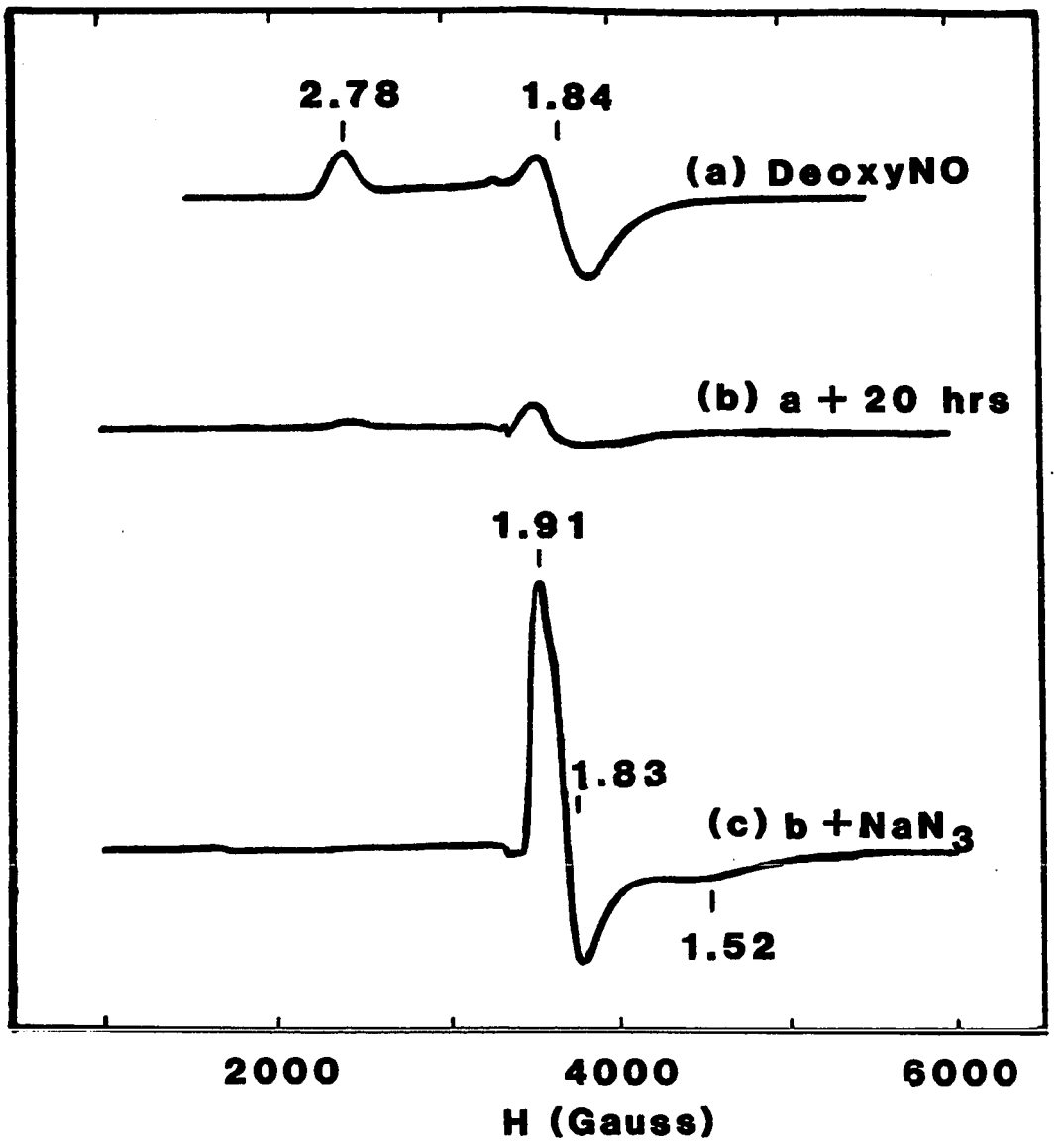

Figure 3.56. EPR spectra showing the oxidative decomposition of deoxyNO

Spectral parameters: temperature, 4.2 K; frequency, 9.42 GHz; power, 40 μW (A and B) and 100 μW (C); modulation, 40 G (A and B) and 16 G (C); gain, 1 x 10^4; time constant, 0.2 s

A. DeoxyNO: 1.57 mM Hr; 103 mM NO_3^-; [NO]/[Hr] = 1.96; 50 mM phosphate, pH 6.5
B. Sample A after 20 hours
C. Anaerobic addition of a few crystals of sodium azide to sample B

$$4NO + H_2O \rightarrow 2HNO_2 + N_2O \qquad (3.35)$$

Thus, both the oxidative decomposition of deoxyNO and the enhancement of decomposition by the deliberate addition of $NaNO_2$, are initiated by the dissociation of NO (Scheme 3.5).

An additional factor that influences the stability of deoxyNO is pH. Figure 3.57 shows the EPR spectrum of deoxyNO at pHs 6.5, 8.5, and 10. When the pH of a solution of deoxyNO is raised to pH 10, the solution gradually becomes pale yellow. The EPR spectrum of the pale yellow solution contains only a radical signal (g = 2.03). Because of the sharpness of this signal, it is probably not associated with the iron site. At intermediate pHs, the EPR spectrum resembles a mixture of deoxyNO and semi-metNO_2^-. Clean preparation of deoxyNO occurs below pH 7.5.

4. Attempts to prepare a magnetically uncoupled iron site

The questions about the lability of the hydroxo bridge of deoxyHr and the stability of a magnetically uncoupled iron site are related in that both processes involve breaking Fe-O_{oxo} bonds. It has been suggested that the lability of the bridging ligand might correlate with auto-oxidation; i.e., rupture of the oxo bridge might be a necessary step during auto-oxidation. Replacement of the hydroxo bridge with some other bridging species would clearly demonstrate that the hydroxo bridge is labile toward substitution. To stabilize a magnetically uncoupled site, one must prevent the reformation of the bridge.

While the major product of the reaction between deoxyHr and NO is a derivative in which the irons are antiferromagnetically coupled, small

SCHEME 3.5

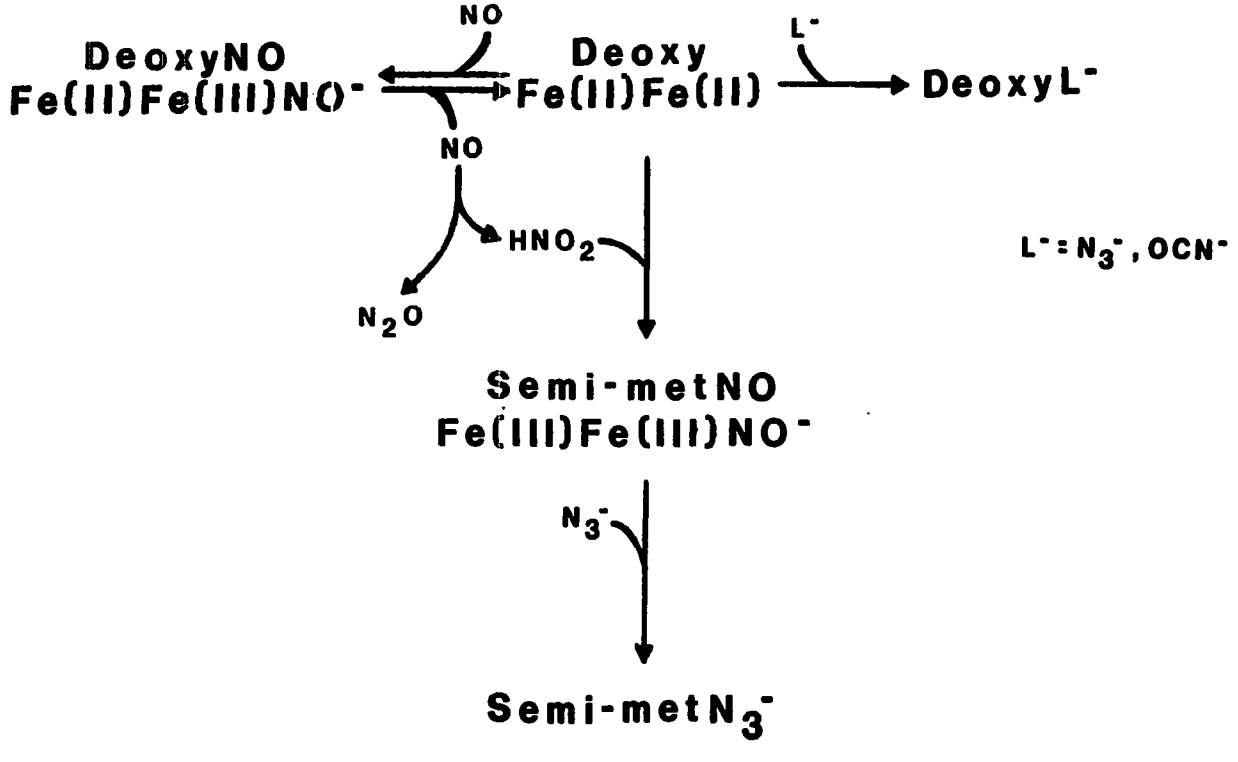
DeoxyNO
Fe(II)Fe(III)NO⁻
NO
Deoxy
Fe(II)Fe(II)
L⁻
DeoxyL⁻
NO
HNO₂
N₂O
L⁻ = N₃⁻, OCN⁻
Semi-metNO
Fe(III)Fe(III)NO⁻
N₃⁻
Semi-metN₃⁻

Figure 3.57. EPR spectra of deoxyNO prepared at pHs 6.5, 8.5, and 10

Spectral parameters: temperature, 4.2 K; frequency, 9.57 GHz (A) and 9.42 GHz (B, C, and D); power, 40 μW (A and B) and 200 μW (C); modulation, 40 G; gain, 4 x 10^4 (A), 1.25 x 10^4 (B), and 2 x 10^4 (C); time constant, 0.2 s

A. pH 6.5: 1.88 mM Hr; [NO]/[Hr] = 3.6; 50 mM phosphate
B. pH 8.5: 2.17 mM Hr; [NO]/[Hr] = 1.2; 50 mM Tris-sulfate
C. pH 10: 1.66 mM Hr; [NO]/[Hr] = 3.9; 0.2 ml of 1 M NaOH added to deoxyHr (50 mM phosphate)

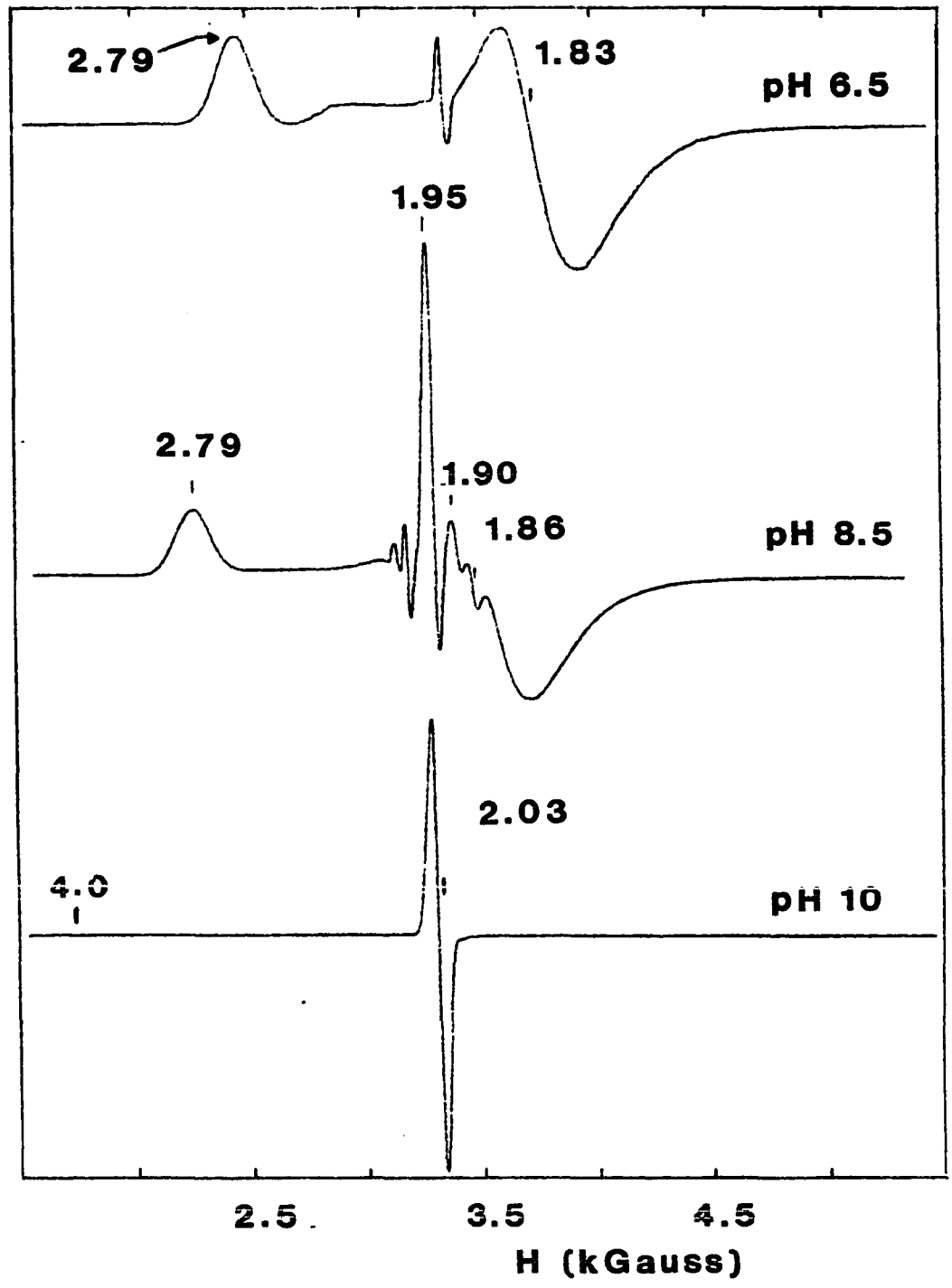
2.79
1.83
pH 6.5
1.95
2.79
1.90
1.86
pH 8.5
2.03
4.0
pH 10
2.5
3.5
4.5
H (kGauss)

quantities of a species having g = 4 are frequently detected by EPR spectroscopy in solutions of deoxyNO (Fig. 3.34). This signal could result from a form of the iron site in deoxyHr that lacks a hydroxo bridge (Fig. 3.31). It is expected that the iron atoms could then behave independently of each other. Thus, the high spin S = 2 iron should be EPR-silent while the iron atom having NO coordinated to it, being in the S = 3/2 spin state, should exhibit a rhombic EPR spectrum having $g_{\perp}$ = 4.0 and $g_{\parallel}$ = 2.0 similar to that observed for Fe^{2+}(EDTA)NO (Fig. 3.13A). Attempts to increase the yield of the uncoupled form were, thus, undertaken.

Two different approaches were used in attempting to produce a magnetically uncoupled iron site. In the first of these, the starting material for the uncoupling experiments was deoxyNO. Frequently, μ-oxo bridged ferric compounds have been observed to decompose to yield monomeric species under slightly acidic conditions (68). It was hoped that the hydroxo-bridged deoxyNO site would undergo an analogous reaction and that NO would not be released in the treatment. The second approach attempted to cleave the hydroxo bridge before NO was added to the sample. The reagents used for this approach included:

(i) protein denaturants (urea and guanidinium chloride).

(ii) sulfide.

(iii) ligands known to uncouple the iron site (azide, fluoride, and cyanate).

(iv) noncoordinating anions such as perchlorate.

(v) either acid or base.

The first approach was motivated by the observation that dimeric μ-oxo compounds convert to monomers at low pHs (68). Neither acidification of deoxyNO to pH 6.0 nor raising the pH to 10 by addition of aliquots of OH^- produced significant amounts of the uncoupled species (Fig. 3.57). At high pHs, where free NO is expected to be unstable, it appears that even metal-coordinated NO is unstable.

Among the reagents utilizing the second approach were the denaturing agents, urea, and guanidine hydrochloride. Here, it was hoped that the protein would be unfolded enough to rupture the hydroxo bridge without removing the metals.

When NO is added to deoxyHr prepared in either 1.5 M GdmCl or 1.5 M urea, formation of deoxyNO is unhindered and very little of the uncoupled derivative is detected (Fig. 3.58A). This is not surprising since Hr is not denatured under these conditions.

When NO is added to deoxyHr prepared in 6.0 M urea, however, the solution turned a brilliant yellow color instead of the pine green color that is associated with deoxyNO. The EPR spectrum of this sample (Fig. 3.58C) shows only a small amount of the deoxyNO signal, a very faint signal at g = 4.0, and an intense radical signal at g = 2.03. All of these signals are absent from the EPR spectrum of deoxyHr in 6.0 M urea (Fig. 3.58B). Addition of sodium azide to a portion of the yellow solution decreases the g = 2.03 signal and reveals new signals at g = 4.43 and 3.95 (Fig. 3.58D). These new signals may be attributed to isolated high spin Fe^{3+} and S = 3/2 $\{FeNO\}^7$, respectively. One possible explana-

Figure 3.58. Effect of urea on the preparation of deoxyNO

Spectral parameters: temperature, 4.2 K; frequency, 9.42 GHz; power, 40 μW; modulation, 40 G; gain, 5 x 10^4 (A and B) and 2.5 x 10^4 (C and D); time constant, 0.2 s; pH 6.5

A. deoxy + NO in 1.5 M urea: 1.48 mM Hr; [NO]/[Hr] = 3.1
B. deoxyHr in 6 M urea
C. Addition of 0.50 ml NO(g) to 2.0 ml deoxyHr in 6 M urea
D. Anaerobic addition of solid sodium azide to an aliquot of sample C

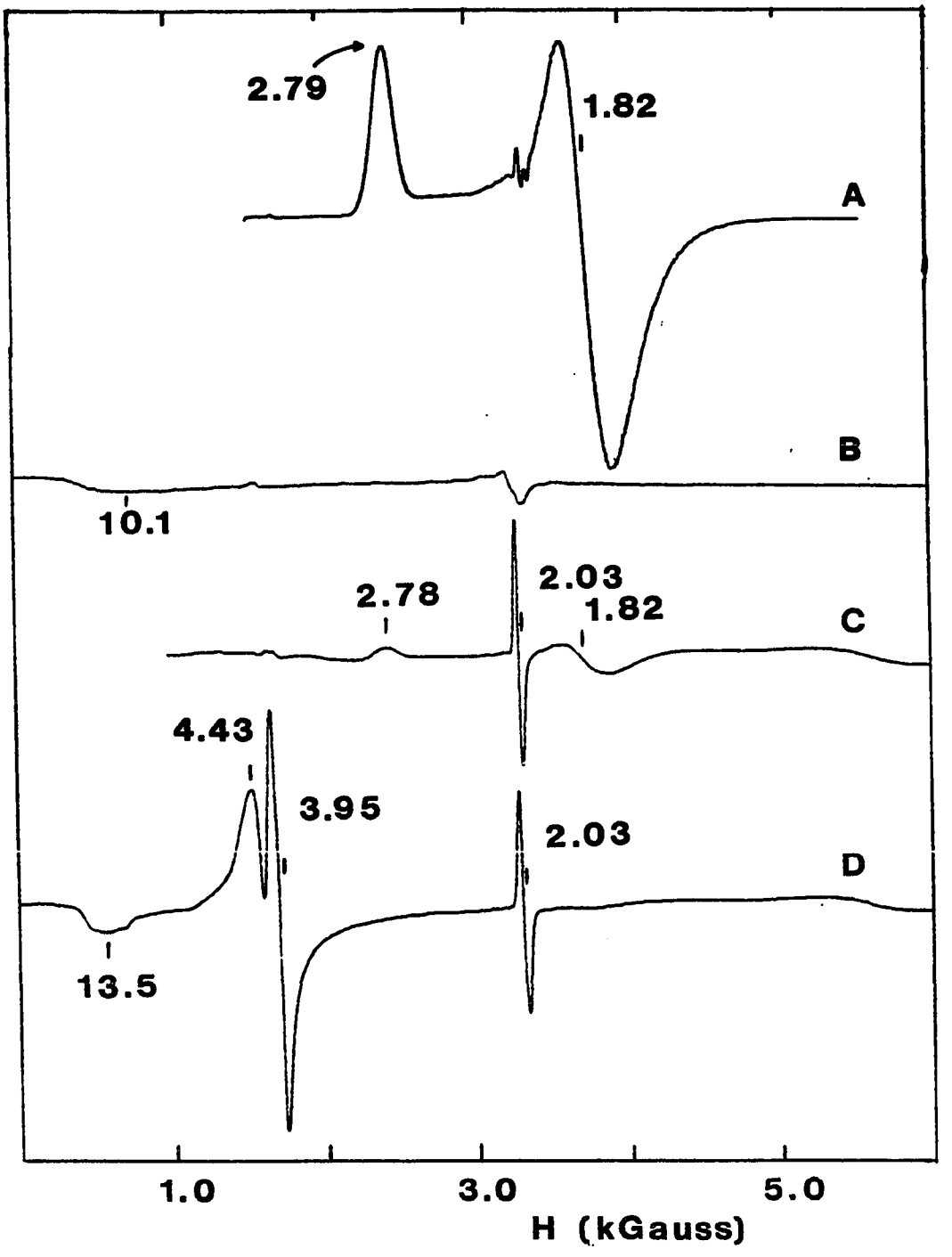
2.79
1.82
A
B
10.1
2.78
2.03
1.82
C
4.43
3.95
2.03
D
13.5
1.0
3.0
5.0
H (kGauss)

tion for these observations is that the yellow solution contains a magnetically uncoupled form of deoxyNO (Scheme 3.6).

Scheme 3.6:

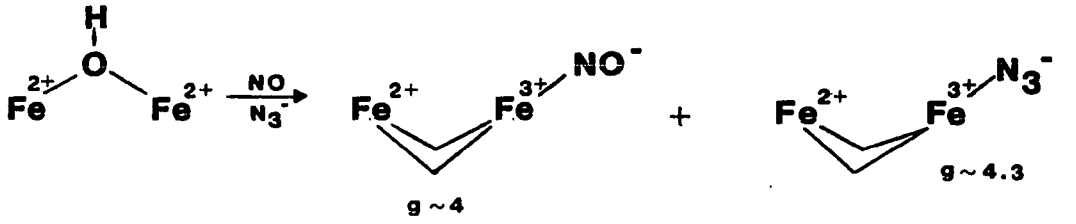

The results from the reaction of deoxyHr with NO in 6 M urea suggest that a magnetically uncoupled site is conceivable and that using denaturing agents might be a viable approach toward stabilizing such a site. Unfortunately, removal of the denaturant by dilution of the sample caused the protein to precipitate, since denaturation of Hr is not a reversible process.

For μ-sulfidosemi-met and μ-sulfidomet, it has been shown that sulfide replaces the oxo bridge (74). While it has been shown that sulfide interacts with deoxyHr (109), the nature of this interaction is not well-defined. It was hoped that this interaction would involve either replacement of the oxo bridge with sulfide or rupture of the bridge in a mode analogous to that occurring with the monovalent anions (azide, fluoride, and cyanate).

Figure 3.59 shows the effect of sulfide on the binding of NO. When NO is added after incubating deoxyHr in sulfide for minutes, incomplete conversion to deoxyNO results. If deoxyHr is incubated in sulfide for

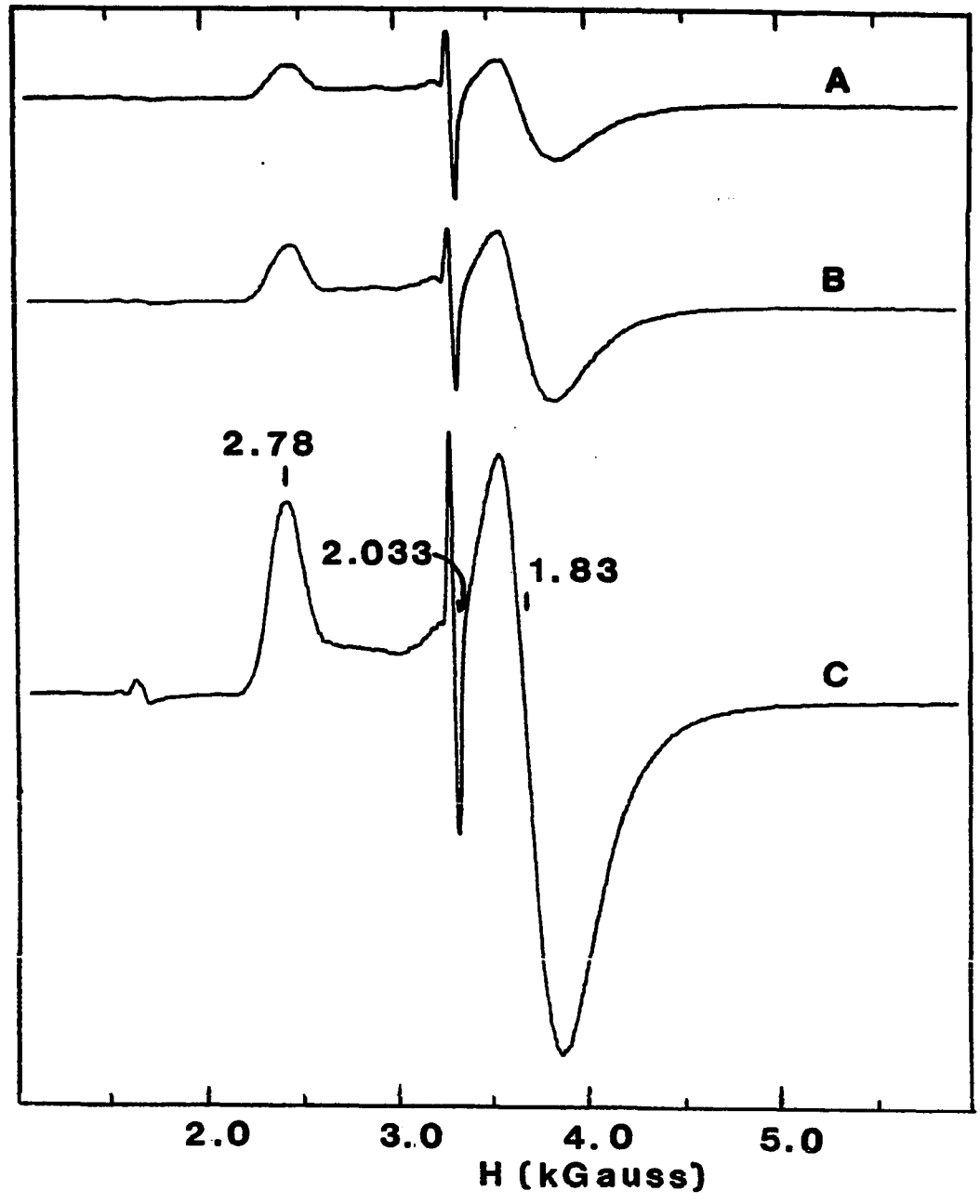

Figure 3.59. Effect of the length of time for which deoxyHr is incubated in sulfide on the preparation of deoxyNO

Spectral parameters: temperature, 7 K; frequency, 9.42 GHz; power, 40 μW; modulation, 40 G; gain, 5 x 10^4; time constant, 0.2 s; 1.32 mM Hr; 30.8 mM sulfide; [NO]/[Hr] = 15; 50 mM phosphate, pH 6.5; 0.3 M sulfate; incubation times: 15 min (A), 75 min (B), 277 min (C)

several hours before NO is added, a sharp radial signal at g = 2.03 is observed and increased amounts of deoxyNO are produced (Table 3.22). These results suggest that sulfide initially interacts with the iron site, preventing NO from binding. A slow conformational change can occur and this makes the sulfide more easily released such that deoxyNO can be formed (Scheme 3.7).

Scheme 3.7:

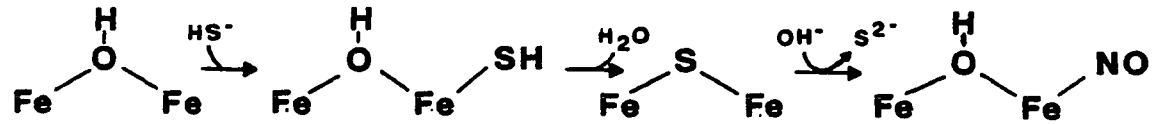

Since azide, cyanate, and fluoride were shown to form adducts with deoxyHr that apparently have the hydroxo bridge cleaved (6), it was anticipated that these anions might promote bridge substitutions. In a third experiment, NO was added in the presence of either azide, cyanate, or fluoride. As shown in section III.D, the presence of fluoride leads to production of a fluoride-bridged NO adduct. The other two anions inhibit the production of deoxyNO, but do not enhance formation of the g = 4.0 signal (Fig. 3.53).

The presence of noncoordinating anions such as perchlorate, also does not lead to stabilization of the uncoupled adduct. Similarly, the anions that do not interact with deoxyHr (Cl^-, Br^-, I^-, SCN^-, and CN^-) also do not produce the uncoupled NO adduct.

Table 3.22. Double integration of the EPR signal for deoxyNO as a function of the incubation period for sulfide[a]

Time (min)[b]	% pmag[c]
15	28.0
75	58.9
277	~100.0

[a]1.32 mM Hr; 123 mM sulfide; pH 6.5; 50 mM phosphate; 0.3 M sulfate.

[b]Measured relative to the time of the addition of sulfide to deoxyHr.

[c]% pmag = [spins]/[Hr] x 100%.

G. Reactions of DeoxyF$^-$NO

The most significant difference between the reactivity of deoxyNO and that of deoxyF$^-$NO is the enhanced stability of deoxyF$^-$NO relative to deoxyNO. Table 3.19 shows that the amount of deoxyF$^-$NO obtained immediately after preparing deoxyF$^-$NO is nearly identical to the amount present 24 hours after its preparation. The maximum value of the rate constant for the dissociation of NO, assuming a minimal half-life of 24 hours, is 8.0×10^{-6} s^{-1}. A solution of deoxyNO, on the other hand, would be nearly completely decomposed after the same period of time.

Competition experiments in which NO was added to a solution containing various ratios of deoxyMb and deoxyF$^-$Hr indicate that the affinity of deoxyF$^-$Hr for NO is similar in magnitude to the affinity of deoxyMb for NO [1.4×10^{11} M^{-1} (153)]. In these experiments, no more than a 2-fold molar excess of NO over Mb was added to mixtures of deoxyMb and deoxyF$^-$Hr. As increasing amounts of Hr were added, decreasing amounts of MbNO were formed. Absorbance readings at 420 nm and 434 nm, measured within 1-3 minutes after adding NO, were used to calculate the concentrations of Mb ([Mb]), MbNO ([MbNO]), deoxyF$^-$Hr ([DF$^-$]), and deoxyF$^-$NO ([DF$^-$NO]) following the procedure described in Appendix A. Since the rates for dissociation of NO from MbNO [1.2×10^{-4} s^{-1} (153)] and deoxyF$^-$NO ($<8.0 \times 10^{-6}$ s^{-1}) are small, the rate for the binding of NO to deoxyF$^-$Hr (k_{DFNO}) is proportional to the concentrations of Mb, MbNO, deoxyF$^-$Hr, and deoxyF$^-$NO (Eq. 3.36) and to the rate for the binding of NO to Mb (k_{MbNO}).

$$k_{DFNO} = \frac{[DF^-NO][Mb](k_{MbNO})}{[DF^-][MbNO]} \qquad (3.36)$$

The rate constants estimated using the published value for k_{MbNO} [1.7×10^7 $M^{-1}s^{-1}$ (153)] are summarized in Table 3.23. By combining the average value for the rate of binding of NO to deoxyF-Hr (6.7 ± 4.2) $\times 10^5$ $M^{-1}s^{-1}$ with the estimated value for the rate of dissociation of NO ($<8.0 \times 10^{-6}$ s^{-1}), the equilibrium constant for the binding of NO to deoxyF-Hr is estimated to be at least 8.4×10^{10} M^{-1}.

The reactivity of deoxyF-NO differs from the reactivity of deoxyNO in a second important way. Within a 24 hour period, there is no evidence suggesting that, in the absence of oxygen, deoxyF-NO undergoes auto-oxidation and, even in the presence of oxygen, deoxyF-NO reacts only very slowly to produce metF- (Fig. 3.60). There is no indication of the formation of oxyHr during this process.

Table 3.23. Rate constants estimated for the binding of NO to deoxyF[a]

[Hr]/[Mb]	[Hr] (μM)	[Mb] (μM)	[NO] (μM)	[F⁻] (mM)	10^{-5} K ($M^{-1}s^{-1}$)
2.15	15.0	6.98	9.22	5.64	3.2
4.31	29.8	6.91	9.13	11.2	14.7
5.39	37.1	6.88	9.09	13.9	8.1
6.47	44.3	6.85	9.05	16.6	8.7
10.8	72.4	6.72	8.88	27.1	11.4
15.4	120	7.77	17.7	13.4	5.8[b]
15.3	224	14.6	33.2	25.1	5.0[b]
15.4	120	7.77	17.7	13.4	2.4[b]
23.0	175	7.59	17.3	19.6	0.98[b]
					6.7 ± 4.2

[a]50 mM phosphate; 0.15 M sulfate; pH 7.0.

[b]50 mM phosphate; 0.3 M sulfate; pH 6.5.

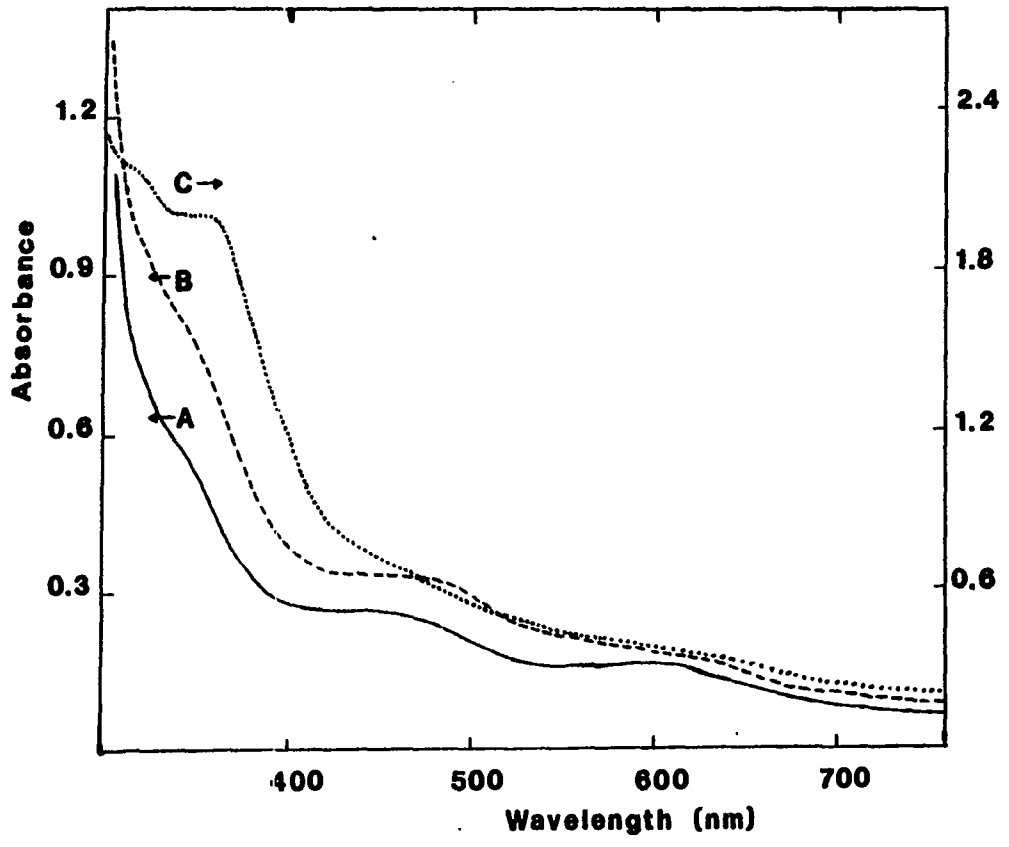

Figure 3.60. Optical changes accompanying the reaction of deoxyF-NO with oxygen

0.190 mM Hr; [F⁻]/[Hr] = 628; [NO]/[Hr] = 2.3; 50 mM phosphate, pH 6.5; spectra were recorded before addition of oxygen (A), ~60 min after adding oxygen (B), and after letting the reaction sit overnight (C)

IV. SUMMARY AND CONCLUSIONS

A. Preparation, Characterization and Reactivity of the Nitric Oxide and Nitrite Derivatives of Hemerythrin

Discovery has been presented of five new derivatives of Hr: deoxyNO, deoxyF$^-$NO, (semi-met)$_O$NO, (semi-met)$_R$NO, and semi-metNO$_2^-$. Tables 4.1 and 4.2 summarize the physical properties of these derivatives.

1. Adducts at the deoxy oxidation level

The salient features of the structures of the NO adducts of deoxyHr and deoxyF$^-$ are:

(i) Equal amounts of high spin ferrous and S = 3/2 {FeNO}^{7} are present and these are coupled antiferromagnetically to yield an effective spin of 1/2. No evidence was found for temperature-dependent spin-state changes.

(ii) Nitric oxide coordinates end-on via nitrogen to one iron atom of the binuclear center, most probably with a bent geometry.

(iii) In addition to the carboxylate bridges, there is a μ-hydroxo bridge in deoxyNO and a μ-fluoro bridge in deoxyF$^-$NO.

(iv) A hydrogen-bonding interaction, most likely between the NO ligand and a hydroxo bridge, occurs in deoxyNO. Such an interaction is absent in deoxyF$^-$NO. Thus, hydrogen bonding is not absolutely necessary for stabilization of NO binding to reduced Hrs.

(v) The appropriate formalism for the oxidation states of deoxyNO and deoxyF$^-$NO is Fe(II)Fe(III)NO$^-$.

Table 4.1. Physical properties of the nitric oxide adducts of deoxyHr and deoxyF$^-$

	deoxyNO	deoxyF$^-$NO
	Optical Spectra	
λ in nm	408 (1150)	340 (2700)
(ε in $M^{-1}cm^{-1}$)	500 (710)	450 (1190)
	600 (500)	590 (750)
	EPR Spectra	
$g_{\parallel}$	2.76	2.58
$g_{\perp}$	1.82	1.80
$P_{1/2}$ (dB)	35	12
Δ (cm^{-1})	70.3	-
	Mössbauer Spectra	
$\delta(\Delta E_q)$ in mm/s:		
S = 3/2 $\{FeNO\}^7$	0.68 (0.65)	0.75 (1.02)
S = 2 Fe^{+2}	1.23 (2.64)	1.23 (3.04)
	Resonance Raman Spectra	
ν(Fe-NO) (cm^{-1})	433	421
δ(Fe-N-O) (cm^{-1})	421	-
	Binding Constant	
K_{HrNO} (M^{-1})	5.5×10^5	$>8.4 \times 10^{10}$

Table 4.2. Physical properties of the nitric oxide and nitrite adducts of semi-metHr

	$(semi\text{-}met)_ONO$	$(semi\text{-}met)_RNO$	$semi\text{-}metNO_2^-$
	Optical Spectra		
λ in nm	350	330 (4800)	330
(ε in $M^{-1}cm^{-1}$)	620	380 (3300)	380
		510 (1220)	510
	EPR Spectra		
g-values	n.o.[a]	n.o.[a]	1.93
			1.87
			1.66
	Resonance Raman Spectra		
ν(Fe-NO) (cm^{-1})	431		433
δ(Fe-N-O) (cm^{-1})	423		422

[a] n.o. = none observed.

The reactivity of deoxyNO parallels that of oxyHr. Like oxygen, nitric oxide binds reversibly to deoxyHr (K_{HrNO} = 5.5 x 10^5 M^{-1}). Also, like oxyHr, deoxyNO undergoes auto-oxidation.

Four reactions demonstrate that nitric oxide binds reversibly to deoxyHr:

(i) Reaction of deoxyNO with dithionite produces deoxyHr.

(ii) Reaction of deoxyNO with oxygen produces oxyHr.

(iii) Reaction of deoxyNO with azide or cyanate produces the ligand adduct of deoxyHr.

(iv) Reaction of deoxyNO with nitrite initially produces semi-metNO and, more slowly, leads to build-up of semi-metNO_2^-.

Evidence suggesting that deoxyNO is auto-oxidized to semi-metNO includes:

(i) Within 20 hrs, the color of the solution changes from green to golden-brown and the resulting optical spectrum resembles the optical spectrum of semi-metNO.

(ii) After 20 hrs, only ~5% of the protein is observable by EPR spectroscopy. Similarly, no EPR signal is observed for solutions of semi-metNO.

(iii) Addition of azide after 20 hrs produces an optical spectrum and the EPR signal that are characteristic of semi-metN_3^-.

(iv) Addition of nitrite to deoxyNO promotes the color changes and the disappearance of the EPR signal. Ultimately, semi-metNO_2^- is produced.

Based on these observations, a mechanism was proposed for the autoxidation of deoxyNO (Scheme 3.5). According to this mechanism, dissociation of NO produces deoxyHr. Nitrite, produced from unligated NO, then oxidizes deoxyHr to semi-metNO.

2. Adducts at the semi-met oxidation level

The structures of the NO and nitrite adducts of the mixed-valence Hrs are less well-characterized. The following conclusions may be drawn about these derivatives:

(i) The EPR-silent nature of the NO adducts most probably arises from an $S_{eff} = 1$ ground state obtained from a high spin ferric center that is antiferromagnetically coupled to an S = 3/2 $\{FeNO\}^7$ center. Semi-metNO_2^- has an EPR-observable ground state (S=1/2) and is formally a nitrite adduct of Fe(II)Fe(III).

(ii) Resonance Raman data indicate that the exogeneous ligand is coordinated at the binuclear site via an iron-nitrogen link. Thus, semi-metNO_2^- is more clearly described as a nitro derivative than as a nitito derivative. Nitro-nitrito exchange was not observed.

(iii) Hydrogen-bonding interactions are observed for semi-metNO_2^-.

(iv) The oxidation states of the NO derivatives may be formally represented as Fe(III)Fe(III)NO^-. The apparent stability of the semi-metNO derivatives and the inability of NO to bind to metHr are consistent with this formalism.

(v) In contrast to the binding of monovalent anions to semi-metHrs, different derivatives result from the binding of NO to $(semi\text{-}met)_R$ and $(semi\text{-}met)_O$. The differences between these derivatives

suggest that (semi-met)$_0$NO is more "deoxy-like" whereas (semi-met)$_R$NO is more "met-like".

B. Comparisons to the Physiologically Occurring Reactions: Oxygenation and Auto-oxidation

1. Oxygenation reaction

The physical and chemical properties of the nitric oxide adducts of the fully reduced Hrs indicate that the binuclear center reversibly transfers one electron to the terminally-bound nitrosyl ligand. The formal representation of the oxidation states is, thus, Fe(II)Fe(III)NO$^-$. The formal transfer of only one electron onto the NO ligand suggests that a first step of the oxygenation reaction could be the formation of a semi-metO_2^- intermediate. Apparently, this intermediate has not been detected because the transfer of the second electron to oxygen is too facile.

Since the irons are coupled in deoxyNO, it is likely that the iron atoms are coupled prior to transfer of this second electron. Furthermore, the coupling in the putative superoxide intermediate is likely to be mediated by a μ-hydroxo bridge (rather than a μ-oxo bridge). Transfer of the proton onto the bound dioxygen ligand most probably occurs when the second electron is transferred onto oxygen.

Transfer of one electron onto the NO ligand when NO binds to semi-metHr leads to formal representation of the oxidation states for semi-metNO as $Fe^{3+}Fe^{3+}NO^-$. Thus, the binding of NO to semi-metHr could provide a model for the transfer of the second electron from the putative superoxide intermediate onto oxygen (reaction 4.1).

$$[Fe(II), Fe(III)O_2^-] \rightarrow Fe(III), Fe(III)O_2^{2-} \qquad (4.1)$$

2. Auto-oxidation reaction

Kinetic studies have shown that the oxidation of deoxyHr with nitrite is a biphasic reaction. The product of the first phase is an EPR-silent nitrosyl adduct of semi-metHr, and the second phase involves rate-limiting loss of NO, followed by binding of NO_2^-. The final product is the nitrite adduct of semi-metHr.

Oxidation of deoxyHr by excess nitrite differs from oxidation by excess ferricyanide in three ways. First of all, the products of the two reactions differ. MetHr results from the oxidation by ferricyanide, while semi-metNO_2^- results from the oxidation with nitrite. Secondly, the two oxidants react differently with semi-metHr. With ferricyanide, further oxidation to metHr occurs, whereas with nitrite a ligand adduct is produced. Thirdly, the rate constant for the first phase of the nitrite reaction ($k = 2.10\ M^{-1}s^{-1}$ at pH 6.58) is nearly 500 times slower than that for the first phase of oxidation by ferricyanide ($k = 1.2 \times 10^3\ M^{-1}s^{-1}$ at pH 6.3). All of these observations suggest that the two reactions are occurring by different mechanisms. Since the active site cavity of Hr is inaccessible to reagents containing more than three nonhydrogen atoms, it is likely that ferricyanide does not react directly with the binuclear center. Rather, oxidation with ferricyanide occurs by an outer-sphere route. Nitrite, in contrast, is small enough to react directly with the binuclear center.

The reduction potential for the $Fe(CN)_6^{3-/4-}$ couple (0.43 V at pH 8.0) is nearly identical to the reduction potential for the NO_2^-/NO couple (0.366 V at pH 7.0). Thus, the different behavior of the two oxidants with deoxyHr is not a function of differences in their reduction potentials. A more likely explanation is that binding of nitrite to the iron center stabilizes semi-metHr. Figure 4.1 shows that the stability gained by the binding of nitrite to semi-metHr makes it more difficult to further oxidize the protein to metHr (or $metNO_2^-$). The reduction potential for the $metNO_2^-/semi\text{-}metNO_2^-$ couple should be more positive than the reduction potential for the $met/(semi\text{-}met)_R$ couple.

Auto-oxidation of oxyHr in the presence of nitrite was reported to occur by a uniphasic process with a rate constant of 0.31 $M^{-1}s^{-1}$ (pH 6.3, 25°C) (2). The two mechanistic schemes that were proposed are shown in Scheme 1.1. The reaction of nitrite with deoxyHr occurs nearly 10 times faster than the auto-oxidation of oxyHr by nitrite. Thus, it is possible that deoxyHr is an intermediate in auto-oxidation (Scheme 1.1A). Furthermore, both reactions exhibit a unimolecular dependence upon $[H^+]$.

Two mechanisms leading to the direct formation of $(semi\text{-}met)_RNO$ from the reaction between nitrous acid and deoxyHr are shown in Fig. 4.2 (Schemes I and IIb). According to the first of these, oxidation occurs without rupture of the hydroxo bridge. The second scheme, in which the hyroxo bridge is replace by a bridging nitrite ligand, provides a convenient rationale for the oxidation of the iron to which NO is not bound. The recent isolation and characterization of a discrete binu-

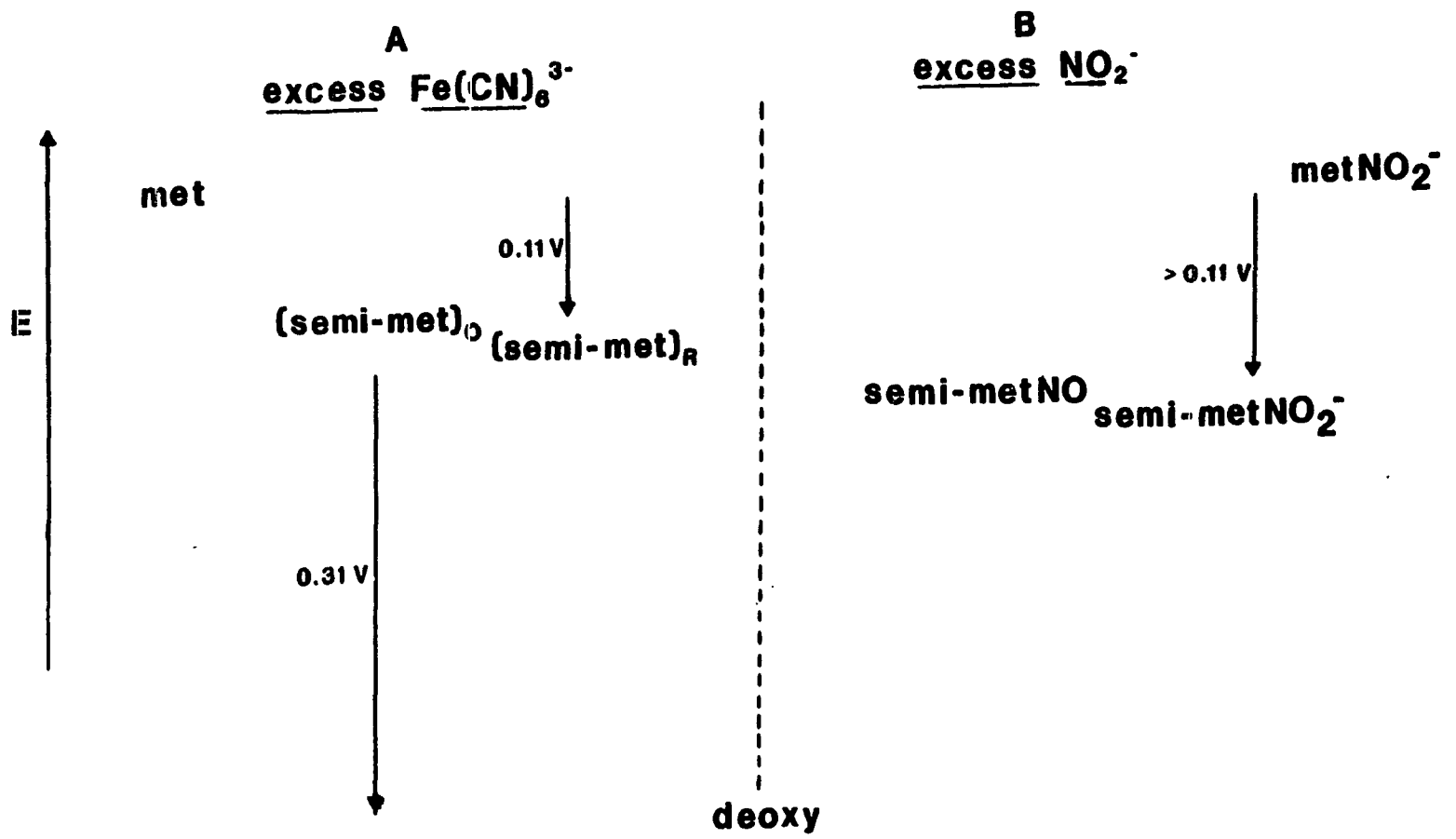

Figure 4.1. Energy diagram for the oxidation of deoxyHr by ferricyanide (A) and by nitrous acid (B)

clear copper cluster (see section I.C) containing an unsymmetrically bridged nitrite ligand lends credence to this proposal.

The results of resonance Raman studies with $H_2{}^{18}O$ have shown that solvent-derived ^{18}O may be incorporated into the hydroxo bridge of deoxyHr. Furthermore, for azide, cyanide, and cyanate, ^{18}O is incorporated into the oxo bridge during auto-oxidation. These results suggest that the hydroxo (or oxo) bridge is ruptured during auto-oxidation. The mechanism shown in Fig. 4.2 (Scheme IIa) suggests that auto-oxidation occurs by replacement of the hydroxo bridge with a dioxo bridge. Production of both semi-metNO_2^- and metNO_2^- from auto-oxidation in the presence of nitrite suggests that there are two competing reactions occurring and could reflect the relative stabilities of dioxo-bridged and NO_2^--bridged derivatives of Hr.

C. Comparisons to the Reactions of Nitrite and Nitric Oxide with Hemoglobin

1. Binding of NO

Most significant is the difference in the relative affinities that Hb (Mb) and Hr have for nitric oxide, oxygen, and carbon monoxide (Table 4.3). While the oxygen affinities of all three proteins are similar, both NO and CO bind more strongly to Hb and Mb than to Hr.

The difference in the CO affinities of Hb and Hr may be attributed, in part, to the ability of the heme cavity to accommodate a linear M-X-O geometry. The steric interference with linear coordination in Hb is offset by a slight change in the heme tilt (180). Apparently, the binuclear active site of Hr can not adjust to overcome the steric restraints

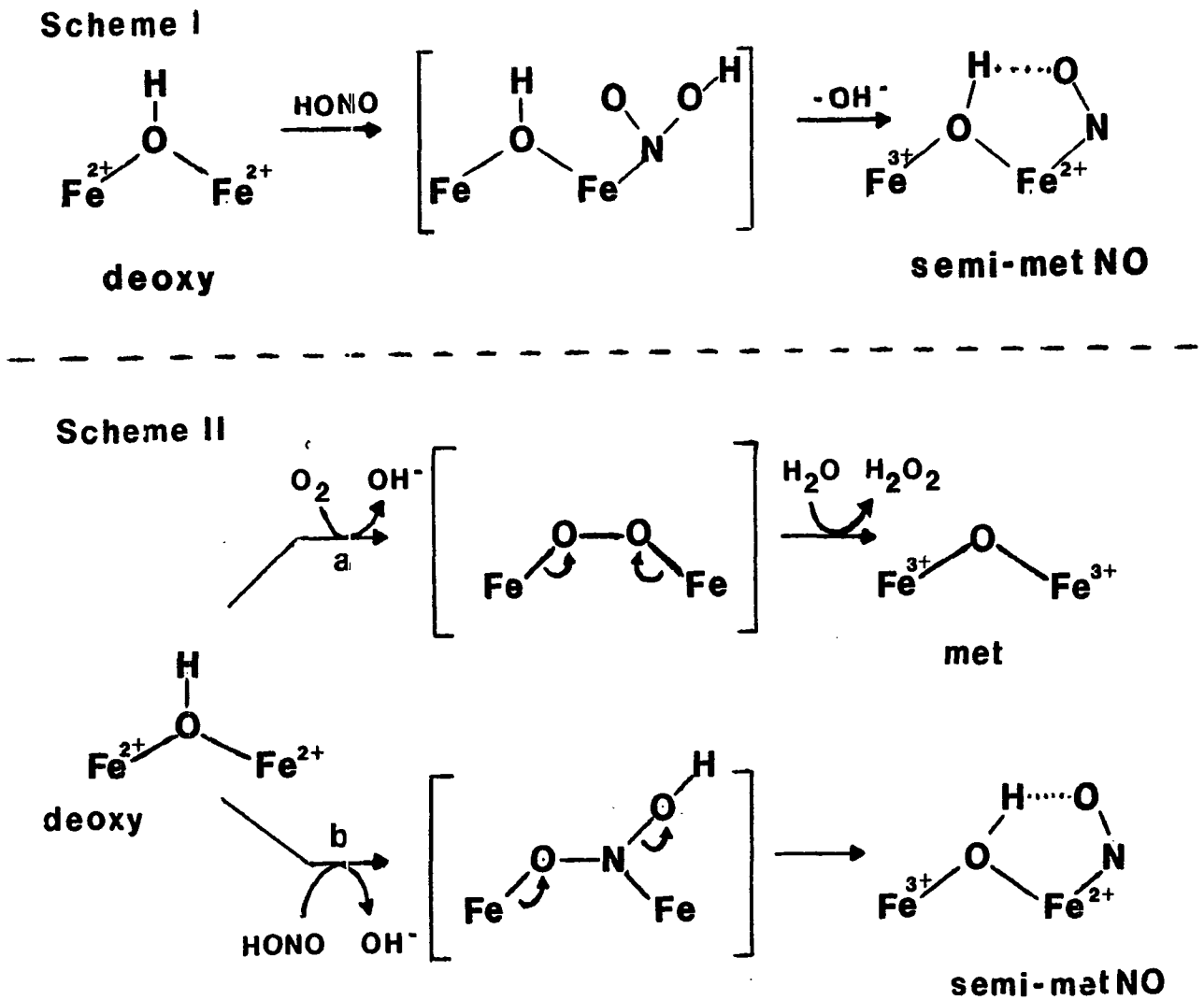

Figure 4.2. Proposed mechanisms for the oxidation of deoxyHr by nitrous acid and for auto-oxidation

Table 4.3. Affinity constants (M^{-1}) for the binding of XO (X = N, O, C) to Hb[a], Mb[a], and Hr

	Hb	Mb	Hr
NO	3.0×10^{10}	1.4×10^{11}[b]	5.5×10^{5}
CO	2.0×10^{7}	2.9×10^{7}	not known
O_2	1.3×10^{5}	1.9×10^{6}	1.5×10^{5}[c]

[a]Reference 169.

[b]Reference 153.

[c]Reference 58.

posed by linear coordination. Carbon monoxide, which prefers linear coordination, does not appear to bind to Hr.

Bent coordination modes are possible for both oxygen and nitric oxide. Indeed, from x-ray crystallography angles of 115° and 145° were determined for MbO_2 (181) and HbNO (180), respectively. These bent geometries favor assignment of the formal oxidation states for MbO_2 and HbNO as $Fe^{3+}O_2^-$ and $Fe^{3+}NO^-$, respectively. Such formalisms are in accord with the notion that there is significant polarization of the M-XO group. Foremost among the factors that may contribute to stabilizing such polar bonds is the proposed hydrogen-bonding of the ligand to either a solvent water molecule or a distal histidine residue (182).

In contrast to Hb and Mb, Hr appears to have nearly equal affinities for NO and O_2. As with Hb and Mb, both ligands are likely to adopt bent coordination geometries in Hr. The M-N-N_2^- angle determined by x-ray crystallographic studies with $metN_3^-$ is 111° and the M-O-O angle for oxyHr is likely to be similar to this. For Hr, the presence of a second iron atom at the active site leads to even more extreme polarization of the Fe-O_2 group. Formally, the Fe-O_2 group is an $Fe^{3+}O_2^{2-}$ unit. As with Hb and Mb, hydrogen-bonding may play a vital role in stabilizing the Fe-O_2 link in oxyHr. Since crystallography indicates that there are no amino acid residues within hydrogen-bonding distance of the bound ligand, it was suggested that the hydroxo bridge is the source of hydrogen-bonding. Resonance Raman spectroscopy supports this hypothesis.

Since NO binds more strongly to deoxyF^- (where fluoride rather than hydroxide bridges the iron atoms) than to deoxyHr, it appears that hydrogen-bonding is not the only factor involved in stabilizing the NO adducts of Hr. The stabilization arising from the presence of a μ-fluoro bridge could be due to the absence of hydrogen-bonding to the NO ligand or to differing steric effects near the binuclear cluster.

The M-N-X angle observed for metN_3^- is 111° (45,60). This angle is significantly less than the MNO angles adopted by bent monomeric iron-nitrosyl compounds (see section I.C and Table 1.23). Absence of hydrogen-bonding could allow the MNO angle to be nearer to 120°-140°. Hydrogen-bonding to the hydroxo bridge could be restraining the MNO angle in deoxyNO. By replacing the hydroxo bridge with a fluoro bridge, the MNO angle is less restrained, leading to a more stable derivative.

Alternatively, replacement of the bridging hydroxide with fluoride will alter the geometry at the active site. Based on electron density difference maps with Hr, the binding of ligands to Hr results in minimal changes at the active site. In particular, there is very little change in the Fe--Fe separation. Assuming an Fe--Fe separation of 3.30 Å (45,60) and using the Fe-F bond distances for the Fe-F-Fe bridges of $Fe_2F_5 \cdot 2H_2O$ [$d(Fe^{2+}\text{-}F)$ = 2.05 Å and $d(Fe^{3+}\text{-}F)$ = 1.94 Å (177)], one obtains a value of 111° for the Fe^{2+}-F-Fe^{3+} angle. This is not significantly less than the Fe^{2+}-OH-Fe^{2+} angle [113.2° (63)] in Wieghardt's model compound, $[(tacn)_2(Fe^{2+})_2(OH)(CH_3CO_2)_2](ClO_4) \cdot H_2O$, suggesting that the geometric changes resulting from the replacement of hydroxide with fluoride contribute only minimally to the stability of the NO adducts.

In addition to the steric factors, dynamic factors might also contribute to the stabilization of deoxyF⁻NO with respect to deoxyNO. It is possible that the protein backbone is more flexible in deoxyNO than in deoxyF⁻NO. If the protein backbone engulfing the active site is less flexible, one would expect the rate of dissociation of NO to be hindered. Similarly, a less flexible environment would be less accessible to incoming nucleophiles (e.g., nitrite) that might promote autoxidation.

2. Oxidation by nitrite

The mechanism proposed for the oxidation of deoxyHb by nitrite is presented in Schemes 1.8 and 1.9. For both proteins, the one-electron oxidation occurs by an "inner sphere" mechanism. At pH 7.0, the reaction with Hb is approximately twice as fast as that with Hr (Table 4.4).

The oxidation of Hb by nitrite differs from the oxidation of Hr by nitrite in two ways. First of all, the reaction with Hr results in quantitative oxidation of deoxyHr, while with Hb only 72% of the protein is oxidized. (The remaining 28% is HbNO.) The incomplete oxidation of Hb may be a reflection of the observation that NO binds more strongly (and probably more rapidly) to deoxyHb than to deoxyHr. Secondly, deoxyHb is oxidized by alkyl nitrites as well as nitrous acid. DeoxyHr, in contrast, is not oxidized directly by alkyl nitrites. Rather, deoxyHr reacts with the hydrolysis product (nitrous acid). This indicates that the active site cavity in Hr is more sterically hindered than that in Hb, making the active site of Hr inaccessible to the larger alkyl nitrites.

Table 4.4. Rate constants for reactions with nitrite[a]

Reactant	Products	k ($M^{-1}s^{-1}$)	Reference
deoxyHr	semi-metNO	1.20	this work
oxyHr	$metNO_2^-$	0.31	7[b]
deoxyHb	metHb; HbNO	2.69	123
metMb	$metMbNO_2^-$	470	169

[a]pH 7.0; 50 mM phosphate; 25°C.

[b]pH 6.3.

In addition, nitrite reacts with the oxygenated forms of both proteins. For HbO_2, the reaction with nitrite is auto-catalytic. Nitrogen dioxide and peroxide are the proposed products of the slow initiation step (reaction 4.2).

$$HbO_2 + NO_2^- \rightarrow Hb^+ + O_2^{2-} + NO_2 \qquad (4.2)$$

Nitrite is, then, regenerated from the subsequent reaction of HbO_2 with nitrogen dioxide and oxidative decomposition of the peroxynitrate intermediate (Fig. 4.3). For oxyHr, the mechanism of oxidation with nitrite is not nearly as complex. Under aerobic conditions, only a single product ($metNO_2^-$) results. Kinetic studies have shown this to be a uniphasic reaction. It is only when free oxygen is removed from solution that build-up of semi-$metNO_2^-$ is observed.

D. Implications About Nitrite Metabolism

While a vast supply of nitrogen exists in the atmosphere, most organisms are not able to metabolize dinitrogen. For these organisms, nitrate and ammonia are the more common sources of nitrogen. Nitrite and possibly nitric oxide are involved in the interconversion of nitrate and ammonia (Fig. 4.4) and, hence, reactions leading to production of nitrite and to its subsequent conversion to more reduced forms of nitrogen have biological significance.

Nitrate is reduced to nitrite by the molybdoenzyme, nitrate reductase. In addition, nitrate reductases contain iron in the form of either Fe-S centers or as hemes (Table 4.5).

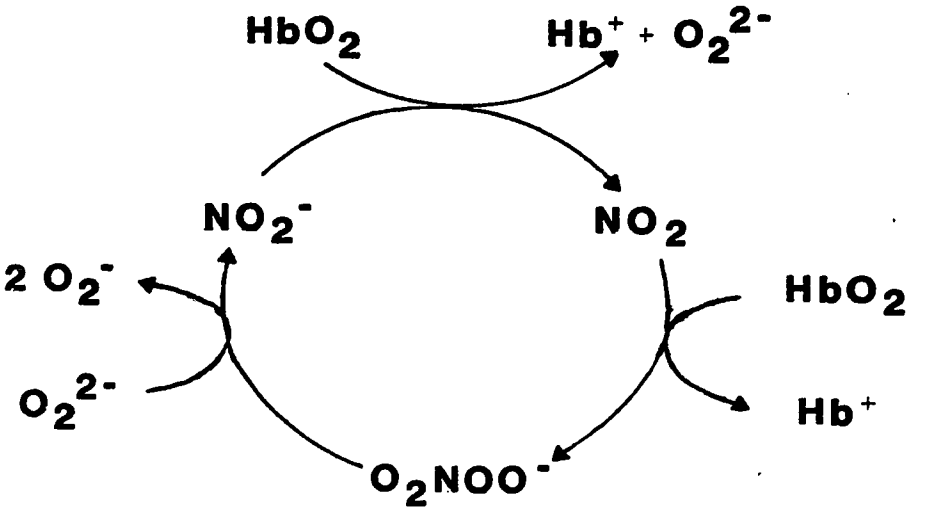

Figure 4.3. Auto-catalytic cycle proposed for the oxidation of oxyHb by nitrite

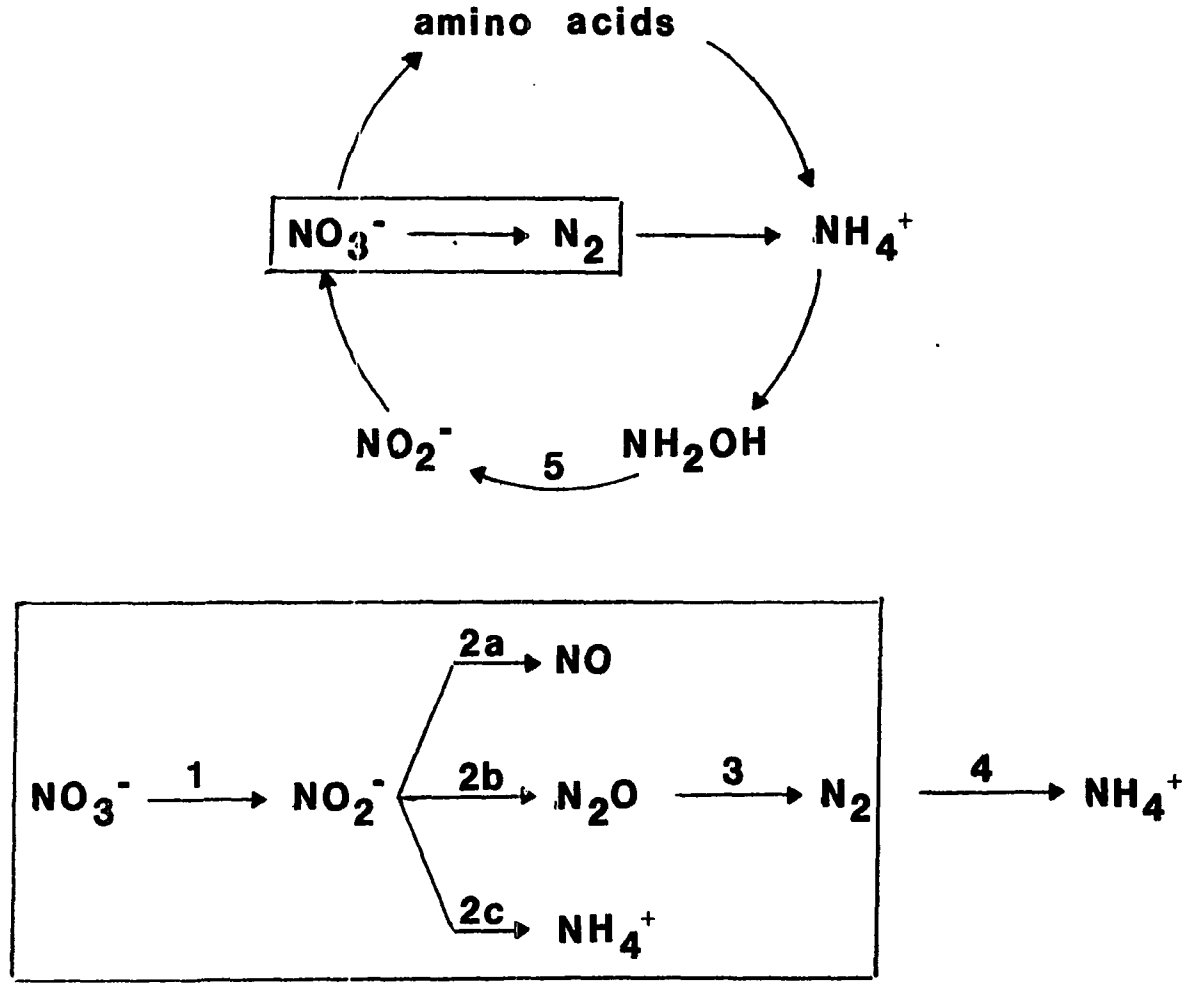

Figure 4.4. The nitrogen cycle and the reactions catalyzed by nitrite reductases

Table 4.5. Enzymes of the N_2 cycle and their prosthetic group content

	Enzyme	Catalytic Reaction Reactant	Product	Prosthetic Groups
1	Nitrate reductase	NO_3^-	NO_2^-	Mo cyt c FAD
	Nitrate reductase			Mo [3Fe] 3-4 [4Fe-4S]
2a	Nitrite reductase	NO_2^-	NO	heme c heme d_1
2b	Nitrite reductase	NO_2^-	N_2O	2 Cu
2c	Nitrite reductase	NO_2^-	NH_4^+	siroheme [4Fe-4S]
3	N_2O reductase	N_2O	N_2	7-8 Cu
4	Nitrogenase	N_2	NH_4^+	2 Mo (30 ± 2)Fe (30 ± 2)S
5	Hydroxylamine oxidoreductase	NH_2OH	NO_2^-	7-8 hemes cyt P_{460}

Nitrite reductases are of three types. The first of these, assimilatory nitrite reductase, catalyze the six electron reduction of nitrite to ammonia and contain iron bound to a siroheme and a single [4Fe-4S] center. Dissimilatory nitrite reductases reduce nitrite to nitric oxide. Heme c and one heme d_1 are the prosthetic groups of this type of enzyme. The third type of nitrite reductase converts 2 mol of nitrite to nitrous oxide by a 4-electron reduction. Two atoms of copper (I) are involved. Remarkable diversity, thus, exists for the types of biologically occurring metal sites that undergo reactions with nitrite.

It is interesting to note that reduction to nitric oxide may be achieved with a protein that, like hemerythrin, contains two atoms of iron per active center. Unfortunately, release of NO from hemerythrin is a slow process, making hemerythrin an unlikely candidate for biological catalysis of the reduction of nitrite to ammonia. The two-heme system in which the two iron centers are probably not coupled appears to be the more efficient system for one-electron reduction of nitrite.

V. REFERENCES

1. Klotz, I. M.; Klotz, T. A. Science 1955, 121, 477-480.

2. Klotz, I. M.; Kurtz, D. M., Jr. Acc. Chem. Res. 1984, 17, 16-22.

3. Stenkamp, R. E.; Sieker, L. C.; Jensen, L. H.; McCallum, J. D.; Sanders-Loehr, J. Proc. Natl. Acad. Sci. USA 1985, 82, 713-716.

4. Dawson, J. W.; Gray, H. B.; Hoenig, H. E.; Rossman, G. R.; Schredder, J. M.; Wang, R. Biochemistry 1972, 11(3), 461-465.

5. Garbett, K.; Johnson, C. E.; Klotz, I. M.; Okamura, M. Y.; Williams, R. J. P. Arch. Biochem. Biophys. 1971, 142, 574-583.

6. Reem, R. C.; Solomon, E. I. J. Am. Chem. Soc. 1984, 106, 8323-8325.

7. Bradic, Z.; Conrad, R.: Wilkins, R. G. J. Biol. Chem. 1977, 252(17), 6069-6075.

8. Doyle, M. P.; Pickering, R. A.; DeWeert, T. M.; Hoekstra, J. W.; Pater, D. J. Biol. Chem. 1981, 256(23), 12393-12398.

9. York, J. L.; Bearden, A. J. Biochemistry 1970, 9(23), 4549-4554.

10. Sjoberg, B.; Loehr, T. M.; Sanders-Loehr, J. Biochemistry 1982, 21, 96-102.

11. Woodland, M. P.; Dalton, H. J. Biol. Chem. 1984, 259(1), 53-59.

12. Davis, J. C.; Averill, B. A. Proc. Natl. Acad. Sci. USA 1982, 79, 4623-4627.

13. Debrunner, P. B.; Hendrich, M. P.; DeJersey, J.; Keough, D. T.; Sage, J. T.; Zerner, B. Biochim. Biophys. Acta 1983, 745, 103-106.

14. Mockler, G. M.; deJersey, J.; Zerner, B.; O'Connor, C. J.; Sinn, E. J. Am. Chem. Soc. 1983, 105, 1891-1893.

15. Antanaitis, B. C.; Aisen, P.; Lilienthal, H. R. J. Biol. Chem. 1983, 258(5), 3166-3172.

16. Lauffer, R. B.; Antanaitis, B. C.; Aisen, P.; Que, L., Jr. J. Biol. Chem. 1983, 258(23), 14212-14218.

17. Gaber, B. P.; Sheridan, J. P.; Bazer, F. W.; Roberts, R. M. J. Biol. Chem. 1979, 254(17), 8340-8342

18. Chiaie, S. D. "Memorie sulla storie enotomia degli animali del Regno di Napoli" Stamperia dei Frat. Fernandes; Naples, Italy, 1823, 444.

19. Wilkins, R. G.; Harrington, P. C. Adv. Inorg. Biochem. 1983, 5, 51-85.

20. Manwell, C. Comp. Biochem. Physiol. 1960, 1, 277-285.

21. Lankester, E. R. Proc. Roy. Soc. 1873, 21, 70-81.

22. Andrews, E. A. J. Johns Hopkins Univ. 1890, 4, 389.

23. Griffiths, A. B. Compt. Rend. Acad. Sci. 1892, 115, 669.

24. Resnick, R. A.; Klotz, I. M. Biol. Bull. 1951, 101, 227.

25. Brill, A. S.; Olsen, J. M. Biol. Bull. 1953, 105, 371.

26. Klotz, I. M.; Keresztes-Nagy, S. Biochemistry 1963, 2(3), 445-452.

27. Manwell, C. Comp. Biochem. Physiol. 1977, 58B, 331-338.

28. Klotz, I. M.; Keresztes-Nagy, S. Nature 1962, 195, 900-901.

29. Keresztes-Nagy, S.; Klotz, I. M. Biochemistry 1963, 2, 923-927.

30. Klippenstein, G. L. Biochem. Biophys. Res. Commun. 1972, 49, 1474-1479.

31. Rill, R. L.; Klotz, I. M. Arch. Biochem. Biophys. 1971, 147, 226-241.

32. Langerman, N. R.; Klotz, I. M. Biochemistry 1969, 8, 4746-4752.

33. Klippenstein, G. L.; Van Riper, D. A.; Oosterom, E. A. J. Biol. Chem. 1972, 247(18), 5959-5963.

34. Liberatore, F. A.; Truby, M. F.; Klippenstein, G. L. Arch. Biochem. Biophys. 1974, 160, 223-229.

35. Addison, A. W.; Dougherty, P. L. Comp. Biochem. Physiol. 1982, 72B, 433-438.

36. Manwell, C. Science 1960, 132, 550-551.

37. Richardson, D. E.; Reem, R. C.; Solomon, E. K. J. Am. Chem. Soc. 1983, 105, 7780-7781.

38. Boeri, E.; Ghiretti-Magaldi, A. Biochim. Biophys. Acta 1957, 23, 489-493.

39. Klippenstein, G. L.; Holleman, J. W.; Klotz, I. M. Biochemistry 1968, 7(11), 3868-3878.

40. Loehr, J. S.; Lammers, P. J.; Brimhall, B.; Hermodson, M. A. J. Biol. Chem. 1978, 253(16), 5726-5731.

41. Klippenstein, G. L.; Cote, J. L.; Ludlam, S. E. Biochemistry 1976, 15(5), 1128-1136.

42. Klippenstein, G. L. Amer. Zool. 1980, 20, 39-51.

43. Garbett, K.; Darnall, D. W.; Klotz, I. M.; Williams, R. J. P. Arch. Biochem. Biophys. 1969, 135, 419-434.

44. Klotz, I. M.; Klippenstein, G. L.; Hendrickson, W. A. Science 1976, 192, 335-344.

45. Stenkamp, R. E.; Sieker, L. C.; Jensen, L. H. J. Am. Chem. Soc. 1984, 106, 618-622.

46. Hendrickson, W. A.; Smith, J. L. In "Invertebrate Oxygen-Binding Proteins: Structure, Active Site, and Function"; Lamy, J.; Lamy, J., Eds.; Marcel Dekker: New York, 1981; pp. 343-352.

47. Sieker, L. C.; Bolles, L.; Stenkamp, R. E.; Jensen, L. H.; Appleby, C. A. J. Mol. Biol. 1981, 148, 493-494.

48. Smith, J. L.; Hendrickson, W. A. Acta Crystallogr. 1981, A37, C-11.

49. Smith, J. L.; Hendrickson, W. A.; Addison, A. W. Nature 1983, 303, 86-88.

50. Love, W. E. Biochim. Biophys. Acta 1957, 23, 465-471.

51. Ward, K. B.; Hendrickson, W. A.; Klippenstein, G. L. Nature 1975, 257, 818-821.

52. Stenkamp, R. E.; Sieker, L. C.; Jensen, L. H.; McQueen, J. E., Jr. Biochemistry 1978, 17(13), 2499-2504.

53. Subramanian, A. R.; Holleman, J. W.; Klotz, I. M. Biochemistry 1978, 7, 3859-3867.

54. Hendrickson, W. A.; Ward, K. B. J. Biol. Chem. 1977, 252(9), 3012-3018.

55. Stenkamp, R. E.; Sieker, L. C.; Jensen, L. H. J. Mol. Biol. 1978, 126, 457-466.

56. Stenkamp, R. E.; Sieker, L. C.; Jensen, L. H.; Loehr, J. S. J. Mol. Biol. 1976, 100, 23-34.

57. DePhillips, H. A., Jr. Arch. Biochem. Biophys. 1971, 144, 122-126.

58. deWaal, D. J. A.; Wilkins, R. G. J. Biol. Chem. 1976, 251(8), 2339-2343.

59. Stenkamp, R. E.; Sieker, L. C.; Jensen, L. H.; Sanders-Loehr, J. Nature 1981, 291, 263-264.

60. Armstrong, W. H.; Lippard, S. J. J. Am. Chem. Soc. 1983, 105, 4837-4838.

61. Armstrong, W. H.; Lippard, S. J. J. Am. Chem. Soc. 1984, 106, 4632-4633.

62. Wieghardt, K.; Pohl, K.; Gebert, W. Angew. Chem. Int. Ed. Eng. 1983, 22(9), 727.

63. Chaudhuri, P.; Wieghardt, K.; Nuber, B.; Weiss, J. Angew. Chem. Int. Ed. Eng. 1985, 24(9), 778-779.

64. Hendrickson, W. A.; Co, M. S.; Smith, J. L.; Hodgson, K. O.; Klippenstein, G. L. Proc. Natl. Acad. Sci. USA 1982, 79, 6255-6259.

65. Sieker, L. C.; Stenkamp, R. E.; Jensen, L. H. In "The Biological Chemistry of Iron"; Dunford, H. B.; Dolphin, D.; Raymond, K. N.; Sieker, L., Eds.; D. Reidel Publishing Company: New York, 1982, pp. 161-175.

66. Elam, W. T.; Stern, E. A.; McCallum, J. D.; Sanders-Loehr, J. J. Am. Chem. Soc. 1982, 104, 6369-6373.

67. Elam, W. T.; Stern, E. A.; McCallum, J. D.; Sanders-Loehr, J. J. Am. Chem. Soc. 1983, 105, 1919-1923.

68. Murray, K. S. Coor. Chem. Rev. 1974, 12, 1-35.

69. Bradic, Z.; Wilkins, R. G. Biochemistry 1983, 22(23), 5396-5401.

70. Loehr, J. S.; Loehr, T. M.; Mauk, A. G.; Gray, H. B. J. Am. Chem. Soc. 1980, 102, 6992-2996.

71. Harrington, P. C.; Wilkins, R. G. J. Am. Chem. Soc. 1981, 103, 1550-1556.

72. Gay, R. R.; Solomon, E. I. J. Am. Chem. Soc. 1978, 100(6), 1972-1973.

73. Okamura, M. Y.; Klotz, I. M.; Johnson, C. E.; Winter, M. R. C.; Williams, R. J. P. Biochemistry 1969, 8(5), 1951-1958.

74. Lukat, G. S.; Kurtz, D. M., Jr.; Shiemke, A. K.; Loehr, T. M.; Sanders-Loehr, J. Biochemistry 1984, 23(26), 6416-6422.

75. Kurtz, D. M., Jr.; Sage, J. T.; Hendrich, M.; Debrunner, P. G.; Lukat, G. S. J. Biol. Chem. 1983, 258, 2115-2117.

76. Armstrong, W. H.; Spool, A.; Papaefthymiou, G. C.; Frankel, R. B.; Lippard, S. J. J. Am. Chem. Soc. 1984, 106, 3653-3667.

77. Muhoberac, B. B.; Wharton, D. C.; Babcock, L. M.; Harrington, P. C.; Wilkins, R. G. Biochim. Biophys. Acta 1980, 626, 337-345.

79. Harrington, P. C.; Wilkins, R. G.; Muhoberac, B. B.; Wharton, D. C. In "The Biological Chemistry of Iron", Dunford, H. B.; Dolphin, D.; Raymond, K. N.; Sieker, L., Eds.; D. Reidel Publishing Company: New York, 1982, pp. 145-160.

78. Babcock, L. M.; Bradic, Z.; Harrington, P. C.; Wilkins, R. G.; Yoneda, G. S. J. Am. Chem. Soc. 1980, 102(8), 2849-2850.

80. Shiemke, A. K.; Loehr, T. M.; Sanders-Loehr, J. J. Am. Chem. Soc. 1984, 106, 4951-4956.

81. Freier, S. M.; Duff, L. L.; Shriver, D. F.; Klotz, I. M. Arch. Biochem. Biophys. 1980, 205(2), 449-463.

82. Kurtz, D. M., Jr.; Shriver, D. F.; Klotz, I. M. J. Am. Chem. Soc. 1976, 98(16), 5033-5035.

83. Dunn, J. B. R.; Shriver, D. F.; Klotz, I. M. Proc. Natl. Acad. Sci. USA 1973, 70(9), 2582-2584.

84. Irwin, M. J.; Duff, L. L.; Shriver, D. F.; Klotz, I. M. Arch. Biochem. Biophys. 1983, 224(2), 473-478.

85. Plowman, J. E.; Loehr, T. M.; Schauer, C. K.; Anderson, O. P. Inorg. Chem. 1985, in press.

86. Solbrig, R. M.; Duff, L. L.; Shriver, D. F.; Klotz, I. M. J. Inorg. Biochem. 1982, 17, 69-74.

87. Sitter, A. J.; Reczak, C. M.; Terner, J. J. Biol. Chem. 1985, 260, 7515-7522.

88. Shiemke, A. K.; Sanders-Loehr, J.; Loehr, T. M. Rev. Port. Quim. 1985, 27, 159-160.

89. Maroney, M. J.; Lauffer, R. B.; Que, L., Jr.; Kurtz, D. M., Jr. J. Am. Chem. Soc. 1984, 106, 6445-6446.

90. York, J. L.; Millett, F. S.; Minor, L. B. Biochemistry 1980, 19(12), 2583-2588.

91. Lauffer, R. B.; Antanaitis, B. C.; Aisen, P.; Que, L., Jr. J. Biol. Chem. 1983, 258(23), 14212-14218.

92. Hodges, K. D.; Wollmann, R. G.; Barefield, E. K.; Hendrickson, D. N. Inorg. Chem. 1977, 16(11), 2746-2751.

93. Eisman, G. A.; Reiff, W. M. Inorg. Chim. Acta 1981, 50, 239-242.

94. Champion, P. M.; Sievers, A. J. J. Chem. Phys. 1977, 66(5), 1819-1825.

95. DePhillips, H., Jr. Arch. Biochem. Biophys. 1971, 144, 122-126.

96. Bates, G.; Brunori, M.; Amiconi, G.; Antonini, E.; Wyman, J. Biochemistry 1968, 7(8), 3016-3020.

97. Alberding, N.; Lavalette, D.; Austin, R. H. Proc. Natl. Acad. Sci. USA 1981, 78(4), 2307-2309.

98. Petrou, A. L.; Armstrong, F. A.; Sykes, A. G.; Harrington, P. C.; Wilkins, R. G. Biochim. Biophys. Acta 1981, 670, 377-384.

99. Hay, R. W. "Bio-inorganic Chemistry", Halsted Press: New York, 1984, p. 105.

100. Bradic, Z.; Harrington, P. C.; Wilkins, R. G.; Yoneda, G. Biochemistry 1980, 19, 4149-4155.

101. Wilkins, R. G.; Harrington, P. C. Adv. Inorg. Biochem. 1983, 5, 51-85.

102. Bradic, Z.; Harington, P. C.; Wilkins, R. G. Biochemistry 1979, 18(5), 889-893.

103. Harrington, P. C.; deWaal, D. J. A.; Wilkins, R. G. Arch. Biochem. Biophys. 1978, 191(2), 444-451.

104. Armstrong, G. D.; Ramasami, T.; Sykes, A. G. J. Chem. Soc., Chem. Commun. 1984, 15, 1017-1019.

105. Armstrong, F. A.; Harrington, P. C.; Wilkins, R. G. J. Inorg. Biochem. 1983, 18, 83-91.

106. Harrington, P. C.; Wilkins, R. G. J. Inorg. Biochem. 1983, 19, 339-344.

107. Meloon, D. R.; Wilkins, R. G. Biochemistry 1976, 15(6), 1284-1290.

108. Olivas, E.; deWaal, D. J. A.; Wilkins, R. G. J. Inorg. Biochem. 1979, 11, 205-212.

109. Lukat, G. S.; Kurtz, D. M., Jr. Biochemistry 1985, 24, 3464-3472.

110. Grajower, R.; Jortner, J. J. Am. Chem. Soc. 1963, 85, 512-516.

111. Stevens, T. H.; Brudvig, G. W.; Bocian, D. F.; Chan, S. I. Proc. Natl. Acad. Sci. USA 1979, 76(7), 3320-3324.

112. Ram, M. S.; Stanbury, D. M. J. Am. Chem. Soc. 1984, 106, 8136-8142.

113. Hay, R. W. "Bio-inorganic Chemistry", Halsted Press: New York, 1984, p. 102.

114. Chalamet, A. Ann. Chim. 1973, 8, 353-358.

115. Strickler, S. J.; Kasha, M. J. Am. Chem. Soc. 1963, 85, 2899-2901.

116. Smith, R. M.; Martell, A. E. "Critical Stability Constants", Plenum Press: New York, 1976, Vol. 4, p. 47.

117. Stedman, G. Adv. Inorg. Chem. Radiochem. 1979, 22, 113-170.

118. "Handbook of Chemistry and Physics", 62nd ed.; Weast, R. C.; Astle, M. J., Eds.; CRC Press, Inc.: Boca Raton, FL, 1982, pp. D133-D135.

119. Bates, J. C.; Reveco, P.; Stedman, G. J. Chem. Soc., Dalt. Trans. 1980, 1487-1488.

120. Reveco, P.; Stedman, G. Fresenius Z. Anal. Chem. 1979, 295, 252-255.

121. Bonner, F. T.; Pearsall, K. A. Inorg. Chem. 1982, 21(5), 1973-1978.

122. Bonner, F. T.; Pearsall, K. A. Inorg. Chem. 1982, 21(5), 1978-1985.

123. Doyle, M. P.; Pickering, R. A.; DeWeert, T. M.; Hoekstra, J. W.; Pater, D. J. Biol. Chem. 1981, 256(23), 12393-12398.

124. Enemark, J. H.; Feltham, R. D. Coord. Chem. Rev. 1974, 13, 339-406.

125. Rich, P. R.; Salerno, J. C.; Leigh, J. S.; Bonner, W. D., Jr. F. E. B. S. Lett. 1978, 93(2), 323-326.

126. Bernhardt, F.; Gersonde, K.; Twilfer, H.; Wende, P.; Bill, E.; Trautwein, A. X.; Pfleger, K. In "Oxygenases and Oxygen Metabolism", Academic Press: New York, 1982, pp. 63-77.

127. Arciero, D. M.; Lipscomb, J. D.; Huynh, B. H.; Kent, T. A.; Munck, E. J. Biol. Chem. 1983, 258(24), 14981-14991.

128. Salerno, J. C.; Siedow, J. N. Biochim. Biophys. Acta 1979, 579, 246-251.

129. Sugiura, Y.; Ishizu, K. J. Inorg. Biochem. 1979, 11, 171-180.

130. Kon, H. J. Biol. Chem. 1968, 243, 4350-4357.

131. O'Keeffe, D. H.; Ebel, R. E.; Peterson, J. A. J. Biol. Chem. 1978, 253, 3509-3516.

132. Yonetani, T.; Yamamoto, J.; Erman, J. E.; Leigh, J. S., Jr.; Reed, G. H. J. Biol. Chem. 1972, 2447-2455.

133. Chiang, R.; Makino, R.; Spomer, W. E.; Hager, L. P. Biochemistry 1975, 14, 4166-4171.

134. Wells, F. V.; McCann, S. W.; Wickman, H. H.; Kessel, S. L.; Hendrickson, D. N.; Feltham, R. D. Inorg. Chem. 1982, 21, 2306-2311.

135. Hodges, K. D.; Wollmann, R. G.; Kessel, S. L.; Hendrickson, D. N.; VanDerveer, D. G.; Barefield, E. K. J. Am. Chem. Soc. 1979, 101(4), 906-917.

136. Bill, E.; Bernhardt, F.; Trautwein, A. X.; Winkler, H. Eur. J. Biochem. 1985, 147, 177-182.

137. Greenwood, N. N.; Gibb, T. C. "Mössbauer Spectroscopy", Chapman and Hall, Ltd.: London, 1971, pp. 214-218.

138. Riley, D. P.; Busch, D. H. Inorg. Chem. 1984, 23, 3235-3241.

139. Oosterhuis, W. T.; Lang, G. J. Chem. Phys. 1969, 50(10), 4381-4387.

140. Greenwood, N. N.; Earnshaw, A. "Chemistry of the Elements", Pergamon Press: New York, 1984, pp. 514-521.

141. Schoonover, M. W.; Baker, E. C.; Eisenberg, R. J. Am. Chem. Soc. 1979, 101(7), 1880-1882.

142. Quinby-Hunt, M.; Feltham, R. D. Inorg. Chem. 1978, 17(9), 2515-2520.

143. Enemark, J. H.; Feltham, R. D.; Huie, B. T.; Johnson, P. L.; Swedo, K. B. J. Am. Chem. Soc. 1977, 99(10), 3285-3292.

144. Benko, B.; Yu, N. Proc. Natl. Acad. Sci. USA 1983, 80, 7042-7046.

145. Maxwell, J. C.; Caughey, W. S. Biochemistry 1976, 15(2), 388-396.

146. Adams, D. M. "Metal-Ligand and Related Vibrations: A Critical Survey of the Infrared and Raman Spectra of Metallic and Organometallic Compounds", St. Martin's Press: New York, 1968, pp. 268-315.

147. Inanaga, J.; Sasaki, S.; Grieco, P. A.; Kim, H. J. Am. Chem. Soc. 1985, 107, 4800-4802.

148. Enemark, J. H.; Feltham, R. D. Coor. Chem. Rev. 1974, 13, 339-406.

149. Karlin, K. D.; Lewis, D. L.; Rabinowitz, H. N.; Lippard, S. J. J. Am. Chem. Soc. 1974, 96(20), 6519-6521.

150. Rabinowitz, H. N.; Karlin, K. D.; Lippard, S. J. J. Am. Chem. Soc. 1977, 99(5), 1420-1426.

151. Calderon, J. L.; Fontana, S.; Frauendorfer, E.; Day, V. W.; Iske, S. D. A. J. Organomet. Chem. 1974, 64, C16-C18.

152. Chu, C. T.; Dahl, L. F. Inorg. Chem. 1977, 16(12), 3245-3251.

153. Moore, E. G.; Gibson, Q. H. J. Biol. Chem. 1976, 251(9), 2788-2794.

154. Greenwood, N. N.; Earnshaw, A. "Chemistry of the Elements", Pergamon Press: New York, 1984, pp. 531-536.

155. Goodgame, D. M.L.; Hitchman, M. A. Inorg. Chem. 1966, 5(8), 1303-1307.

156. Ileperuma, O. A.; Feltham, R. D. J. Am. Chem. Soc. 1976, 98(19), 6039-6040.

157. Gleizes, A.; Meyer, A.; Hitchman, M. A.; Kahn, O. Inorg. Chem. 1982, 21, 2257-2263.

158. Meyer, A.; Gleizes, A.; Girerd, J.; Verdaguer, M.; Kahn, O. Inorg. Chem. 1982, 1729-1739.

159. Averill, B. A.; Bale, J. R.; Orme-Johnson, W. H. J. Am. Chem. Soc. 1978, 100, 3034-3043.

160. Rutter, R.; Hager, L. P.; Dhonau, H.; Hendrich, M.; Valentine, M.; Debrunner, P. Biochemistry 1984, 23, 6809-6816.

161. Yim, M. B.; Kuo, L. C.; Makinen, M. W. J. Magn. Res. 1982, 46, 247-256.

162. Blumberg, W. E.; Peisach, J. Ann. N. Y. Acad. Sci. 1973, 222, 539-560.

163. Gayda, J.; Gibson, J. F.; Cammack, R.; Hall, D. O.; Mullinger, R. Biochim. Biophys. Acta 1976, 434, 154-163.

164. Aasa, R.; Vanngard, T. J. Magn. Res. 1975, 19, 308-315.

165. Drago, R. S. "Physical Methods in Chemistry", W. B. Saunders Company: Philadelphia, 1977, pp. 135-136.

166. Moeller, T.; King, G. L. Inorg. Synth. 1963, IV, 168-171.

167. Klotz, I. M.; Klotz, T. A.; Fiess, H. A. Arch. Biochem. Biophys. 1957, 68, 284-299.

168. Keresztes-Nagy, S.; Klotz, I. M. Biochemistry 1965, 4(5), 919-931.

169. Antonini, A.; Brunori, M. "Hemoglobin and Myoglobin in Their Reactions with Ligands", Neuberger, A.; Tatum, E. L., Eds., North Holland Publishing Company: Amsterdam-London, 1971.

170. Brudvig, G. W.; Stevens, T. H.; Chan, S. I. Biochemistry 1980, 19, 5275-5285.

171. Bonner, F. T. Inorg. Chem. 1970, 9(1), 190-193.

172. Shiemke, A. K.; Loehr, T. M.; Sanders-Loehr, J. J. Am. Chem. Soc. 1986, submitted for publication.

173. Doyle, M. P.; Pickering, R. A.; Dykstra, R. L.; Cook, B. R. J. Am. Chem. Soc. 1982, 104, 3392-3397.

174. Duff, L. L.; Klippenstein, G. L.; Shriver, D. F.; Klotz, I. M. Proc. Natl. Acad. Sci. USA 1981, 78(7), 4138-4140.

175. Sanders-Loehr, J. submitted to "Bioinorg. Chem", 5, A. V. Xavier, Ed., VCH Publishers: Weinheim, 1985.

176. Florkin, M. Arch. Intern. Physiol. 1933, 36, 247.

177. Hall, W.; Kim, S.; Zubieta, J.; Walton, E. G.; Brown, D. B. Inorg. Chem. 1977, 16(18), 1884-1887.

178. Chaudhuri, A. P.; Singh, A. N.; Hendrix, D. C.; Holtman, D. A.; Sinn, E.; Butcher, R. J.; Jameson, G. B.; Teo, B. K.; Averill, B. A. "Abstracts of Papers", 189th National Meeting of the American Chemical Society, Miami Beach, FL, April 1985; American Chemical Society: Washington, DC, 1985, INOR 36.

179. Wilkins, R. G.; Wilkins, P. C., New Mexico State University, Las Cruces, NM, personal communication.

180. Deatherage, J. F.; Moffat, K. J. Mol. Biol. 1979, 134, 401-417.

181. Phillips, S. E. V. J. Mol. Biol. 1980, 142, 531-554.

182. Jameson, G. B.; Drago, R. S. J. Am. Chem. Soc. 1985, 107, 3017-3020.

VI. ACKNOWLEDGEMENTS

Of all the people who have played a part in the preparation of this dissertation, I am most grateful to two - my mother and my father. I am indebted to them for instilling in me a thirst for knowledge and am grateful for the freedom they have given me to pursue my education.

Secondly, I wish to thank the many instructors who have sought to develop my scientific skills. In particular, I am grateful to Dr. Donald M. Kurtz, Jr. for his inspirations and for the insights that he provided during my studies. I also appreciate the expertise availed to me through collaborations with Drs. Peter Debrunner, Joann Sanders-Loehr, Tom Loehr, Mike Doyle, and Larry Que, and the experimental assistance provided in these efforts by Tim Sage, Drew Shiemke, Ruth Pickering, and Mike Maroney.

A special thank you is given to the many friends who have been my second family these past years. Foremost, I want to thank Gudrun Lukat for many hours of helpful discussions, for her constant encouragement, for her good nature, and most of all for her friendship. To my classmates and co-workers, I say thanks for all the good memories we've created and shared. And, finally, to my brothers and sisters - John, Jerry, Jackie, Joe, and Jeanne - I extend my thanks for all your love and support.

VII. APPENDIX A

Equation 3.36 was used to determine the rate constant for the binding of NO to deoxyF$^-$. Mixtures containing Mb, MbNO, deoxyF$^-$, and deoxyF$^-$NO were prepared by adding NO (2:1 ratio of NO to Mb) to solutions containing various ratios of Mb and deoxyF$^-$. Since Mb and MbNO have much greater extinction coefficients in the visible region than either deoxyF$^-$ or deoxyNO, the relative concentrations of Mb and MbNO were obtained from the absorbance readings at 420 and 434 nm using Eqs. 7.1 and 7.2.

$$A_{420} = \varepsilon_{420,Mb}[Mb] + \varepsilon_{420,MbNO}[MbNO] \qquad (7.1)$$

$$A_{434} = \varepsilon_{434,Mb}[Mb] + \varepsilon_{434,MbNO}[MbNO] \qquad (7.2)$$

The values for $\varepsilon_{434,Mb}$ and $\varepsilon_{420,MbNO}$ are 115 mM^{-1} cm^{-1} and 127 mM^{-1} cm^{-1}, respectively (131,169). The values for $\varepsilon_{420,Mb}$ and $\varepsilon_{434,MbNO}$ were calculated from solutions containing known amounts of Mb and MbNO, respectively. The average values obtained were: $\varepsilon_{420,Mb}$ = 103 mM^{-1} cm^{-1} and $\varepsilon_{434,MbNO}$ = 64.5 mM^{-1} cm^{-1}.

To solve for the [HrNO], Eq. 7.3 was used.

$$[NO]_{TOT} = [MbNO] + [HrNO] \qquad (7.3)$$

Here, [MbNO] is the value obtained from the simultaneous solution to Eqs. 7.1 and 7.2, and $[NO]_{TOT}$ is determined from the volume of NO(aq)

injected into the protein sample. The concentration of the saturated stock solution of NO was 1.9 mM.

Finally, the [Hr] was determined with Eq. 7.4.

$$[Hr]_{TOT} = [Hr] + [HrNO] \tag{7.4}$$

Here, [HrNO] is the value determined from Eq. 7.3 and $[Hr]_{TOT}$ is the total amount of Hr present in the solution.

A similar procedure was used to determine the equilibrium constant for the binding of NO to deoxyHr. Here, competitive binding of N_3^- and NO to deoxyHr was utilized. Conditions were such that the absorbance readings at 500 and 600 nm resulted from only deoxyNO and deoxyN_3^-; absorbance due to deoxyHr was negligible. Simultaneous solution of Eqs. 7.5 and 7.6 yields values for [deoxyNO] and [deoxyN_3^-].

$$A_{500} = \varepsilon_{500,DNO}[DNO] + \varepsilon_{500,DN_3^-}[DN_3^-] \tag{7.5}$$

$$A_{600} = \varepsilon_{600,DNO}[DNO] + \varepsilon_{600,DN_3^-}[DN_3^-] \tag{7.6}$$

Since no literature values are available for the extinction coefficients for either deoxyNO or deoxyN_3^-, values were estimated by preparing deoxyN_3^- and deoxyNO from solutions containing a known amount of Hr. Typical values were: $\varepsilon_{500,DN_3^-} = 1040\ M^{-1}cm^{-1}$; $\varepsilon_{600,DN_3^-} = 500\ M^{-1}cm^{-1}$; $\varepsilon_{500,DNO} = 710\ M^{-1}cm^{-1}$; $\varepsilon_{600,DNO} = 500\ M^{-1}cm^{-1}$. From Eqs. 7.7 and 7.8, [NO] and $[N_3^-]$ were obtained, respectively.

$$[NO]_{TOT} \doteq [NO] + [DNO] \tag{7.7}$$

$$[N_3^-]_{TOT} = [N_3^-] + [DN_3^-] \tag{7.8}$$

VIII. APPENDIX B

Table 8.1 summarizes the results of the GC/MS analysis of the head-space gas above stock solutions of NO and deoxyNO. For all three samples, N_2O was detected.

The amount of N_2O present in the head-space above the stock solution of NO was invariant within a 2 1/2 hr reaction period (compare readings 1-5 and 6-8 in Table 8.1). Since readings for this solution were obtained within 45 minutes after the preparation of the NO stock solution, the conversion of NO to N_2O is more rapid than the auto-oxidation of deoxyNO (nearly complete within 20 hrs).

Lesser amounts of N_2O were found in the protein samples than in the stock solution of NO. Furthermore, a 3.5-fold increase in the amount of N_2O was observed when $NaNO_2$ was added to the solution of deoxyNO. The observation that $NaNO_2$ promotes the auto-oxidation of deoxyNO (see section III.5) suggested that nitrite is a likely oxidant. The detection of N_2O both in the presence and absence of $NaNO_2$ supports the proposal that nitrite is formed in aqueous solutions via the disproportionation of NO, as suggested by Scheme 3.5.

Table 8.1. Intensity of the m/e = 44.001 peak (in cm) for a saturated buffered solution of NO and for deoxyNO in the presence and absence of $NaNO_2$[a]

Reading Number	NO(aq)[b]	deoxyNO[c]	deoxyNO + NO_2^-[d]
1	4.7	0.6	2.9
2	2.9	0.86	2.8
3	4.2	0.66	2.3
4	3.3	0.80	2.7
5	3.8	0.83	2.2
6	3.9	0.75 ± 0.10	2.6 ± 0.3
7	3.0		
8	3.8		
	average = 3.7 ± 0.6		

[a] N_2O and NO were separated on a 30 m ΔB1 capillary column (0.25 mm i.d. and 25 μ film thickness) and detected with a Kratos MS-50 TC mass spectrometer. Aliquots (200 μl) of the head-space gas were injected at 220°C with a split ratio of 25:1. For detection, a decade box ratio of $N_2O:CO_2$ of 0.9997448 was used.

[b] NO(g) was bubbled into 15 ml of 50 mM phosphate buffer (pH 6.5) that had been degassed with helium for 30 min. Readings 1-5 were obtained within 45 minutes and readings 6-8 were obtained ~2 1/2 hrs after preparing the stock solution.

[c] 200 μl of NO(g) was injected into 4.0 ml of 1.92 mM deoxyHr. Readings were measured 1-2 hrs after preparing the solution of deoxyNO.

[d] 3.0 ml of deoxyNO was added to 10.4 mg $NaNO_2$ (50.2 mM) under helium. The deoxyNO stock solution was prepared ~2 hrs before the addition of $NaNO_2$, and readings were obtained no more than 30 min later.